ANALYSIS OF TEMPERATURE, PRESSURE AND DENSITY OF THE ATMOSPHERE EXTENDING TO EXTREME ALTITUDES

G. GRIMMINGER

NOVEMBER, 1948

The RAND Corporation
1500 FOURTH ST. • SANTA MONICA • CALIFORNIA

Price $2.85

610574

This monograph has been prepared under the sponsorship of the United States Air Force. Parts I and II were issued previously for limited distribution in February 1947. Part III was completed in January 1948. With the cooperation of the Air Force, this publication is being made generally available at a nominal charge to cover printing costs.

CONTENTS

SUMMARY xi

LIST OF SYMBOLS xiii

INTRODUCTION 1

SECTIONS

I. THE ATMOSPHERE UP TO THE F_2 LAYER 3

A. The Temperature Distribution 4

B. The Composition 16

C. Effect of Composition on the Determination of the Temperature in an Ionized Layer 20

D. The Calculations 21

II. THE ATMOSPHERE ABOVE THE F_2 LAYER - MODELS I AND II 52

A. The Temperature Distribution and the Interstellar Gas 52

B. The Distribution of Angular Velocity 54

C. The Composition 56

D. The Limit of the Atmosphere 61

E. The Calculations for Atmospheric Model I 69

F. The Calculations for Atmospheric Model II 86

III. THE ATMOSPHERE ABOVE THE F_2 LAYER - MODEL III 104

A. The Maximum Temperature of the Upper Atmosphere (Exosphere) 105

B. The Height of the Base of the Exosphere (Dynamical Orbit Region) 111

C. Diffusion Equilibrium 116

D. Density Calculation for the Region Between the F_2 Layer and the Level of Diffusion Equilibrium 116

E. Density Calculation for the Region Between the Level of Diffusion Equilibrium and the Base of the Exosphere 119

F. Density Calculation for the Exosphere 121

IV. CONCLUSIONS 122

REFERENCES 143

LIST OF TABLES

1 Temperature of Troposphere and Stratosphere, Latitude 45° 4
2 Temperature of Troposphere and Stratosphere, Latitude 0° 4
3 Tentative Standard Temperature Values for the Region 20 - 120 km, Latitude 45° 5
4 Ionosphere Temperatures 9
5 Temperature in the F-Region at the Equator According to Fuchs 9
6 Composition of Tropospheric Air 16
7 Composition of the Atmosphere up to the F_2 Layer at the Equator 18
8 Composition of the Atmosphere up to the F_2 Layer, Latitude 45° 18
9 Temperatures in the E and F_2 Layers, Latitude 45° 20
10 Radius of the Earth and the Acceleration of Gravity 22
11 Values of Temperature, Pressure, and Density up to the F_2 Layer, Latitude 0°. (Engr. Units) 26
12 Values of Temperature, Pressure, and Density up to the F_2 Layer, Latitude 0°. (Metric Units) 29
13 Values of Temperature, Pressure, and Density up to the F_2 Layer, Latitude 45°. (Engr. Units) 32
14 Values of Temperature, Pressure, and Density up to the F_2 Layer, Latitude 45°. (Metric Units) 35
15 Atmospheric Model I. Possible Composition States 58
16 Assumed Composition of the Interstellar Gas in the Vicinity of the Planet Earth 60
17 Maximum Possible Height of Limit of Atmosphere Based on Escape Velocity for a Constant Speed Gas 62
18 Atmospheric Model I. Limit of the Atmosphere at Latitude 0° Based on Continuity of Pressure with the Interstellar Gas 67
19 Atmospheric Model I. Limit of the Atmosphere at Latitude 0° Based on Continuity of Density with Interstellar Gas 67
20 Atmospheric Model I. Values of Temperature, Pressure, and Density Above the F_2 Layer, Based on M_L = 0.5, Latitude 0°. (Engr. Units) 70
21 Atmospheric Model I. Values of Temperature, Pressure, and Density Above the F_2 Layer, Based on M_L = 7, Latitude 0°. (Engr. Units) 71
22 Atmospheric Model I. Values of Temperature, Pressure, and Density Above the F_2 Layer, Based on M_L = 14, Latitude 0°. (Engr. Units) 72
23 Atmospheric Model I. Values of Temperature, Pressure, and Density Above the F_2 Layer, Based on M_L = 0.5, Latitude 0°. (Metric Units) 73
24 Atmospheric Model I. Values of Temperature, Pressure, and Density Above the F_2 Layer, Based on M_L = 7, Latitude 0°. (Metric Units) 74
25 Atmospheric Model I. Values of Temperature, Pressure, and Density Above the F_2 Layer, Based on M_L = 14, Latitude 0°. (Metric Units) 75
26 Atmospheric Model I. Values of Temperature, Pressure, and Density Above the F_2 Layer, Based on M_L = 7.0, Latitude 45°. (Engr. Units) 76
27 Atmospheric Model I. Values of Temperature, Pressure, and Density Above the F_2 Layer, Based on M_L = 7.0, Latitude 45°. (Metric Units) 77

LIST OF TABLES (*Cont'd*)

28 Atmospheric Model II. Total Number of Particles N_* to give the Collision Probability P. Based on $d = 2 \times 10^{-8}$ cm 87
29 Atmospheric Model II. Total Number of Particles N_1 Above the Height h_1, Latitude 0° 93
30 Atmospheric Model II. Values of the Height h_*, Latitude 0° 93
31 Atmospheric Model II. Conditions at the Height h_*, Latitude 0° 94
31a Atmospheric Model II. Total Number of Particles N_1 Above the Height h_1, Latitude 45° 94
32 Atmospheric Model II. Values of Height h_*, Latitude 45° 95
33 Atmospheric Model II. Conditions at the Height h_*, Latitude 45° 95
34 Atmospheric Model II. Values of Temperature, Pressure, and Density Above the F_2 Layer, Latitude 0°. (Engr. Units) 96
35 Atmospheric Model II. Values of Temperature, Pressure, and Density Above the F_2 Layer, Latitude 0°. (Metric Units) 97
36 Atmospheric Model II. Values of Temperature, Pressure, and Density Above the F_2 Layer, Latitude 45°. (Engr. Units) 98
37 Atmospheric Model II. Values of Temperature, Pressure, and Density Above the F_2 Layer, Latitude 45°. (Metric Units) 99
38 Atmospheric Model III. Possible Values for the Temperature T_* in the Exosphere 111
39 Atmospheric Model III. Possible Values for the Height h_* of the Base of the Exosphere 115
40 Atmospheric Model III. Composition Assumed at the Beginning of the Region of Diffusion Equilibrium, $h = h_d$ 125
41 Atmospheric Model III. Conditions at the Base of the Exosphere, $h = h_*$ 126
42 Atmospheric Model III. Values of Temperature, Pressure, and Density Above the F_2 Layer, Latitude 0° (Engr. Units) 127
43 Atmospheric Model III. Values of Temperature, Pressure, and Density Above the F_2 Layer, Latitude 0° (Metric Units) 128
44 Atmospheric Model III. Values of Temperature, Pressure, and Density Above the F_2 Layer, Latitude 45° (Engr. Units) 129
45 Atmospheric Model III. Values of Temperature, Pressure, and Density Above the F_2 Layer, Latitude 45° (Metric Units) 130

LIST OF FIGURES

1 Vertical Distribution of Temperature at the Equator from Sea Level up to 120 km. (Metric Units) 7
2 Vertical Distribution of Temperature at the Equator from Sea Level up to 75 Miles. (Engr. Units) 7
3 Vertical Distribution of Temperature at Latitude 45° from Sea Level up to 120 km. (Metric Units) 8
4 Vertical Distribution of Temperature at Latitude 45° from Sea Level up to 75 Miles. (Engr. Units) 8
5 Vertical Distribution of Temperature in the *F* Region at the Equator. (Metric Units) 10
6 Vertical Distribution of Temperature in the *F* Region at the Equator. (Engr. Units) 11
7 Vertical Distribution of Temperature in the *F* Region at Latitude 45°. (Metric Units) 14
8 Vertical Distribution of Temperature in the *F* Region at Latitude 45°. (Engr. Units) 15
9 Degree of Ionization in the *E* and *F* Regions 19
10(a) Vertical Distribution of the Density Ratio σ from Sea Level up to the F_2 Layer, Latitude 0°. (Engr. Units) 38
10(b) Vertical Distribution of the Density Ratio σ from Sea Level up to the F_2 Layer, Latitude 0°. (Engr. Units) 39
10(c) Vertical Distribution of the Density Ratio σ from Sea Level up to the F_2 Layer, Latitude 0°. (Engr. Units) 40
11(a) Vertical Distribution of the Density Ratio σ from Sea Level up to the F_2 Layer, Latitude 0°. (Metric Units) 41
11(b) Vertical Distribution of the Density Ratio σ from Sea Level up to the F_2 Layer, Latitude 0°. (Metric Units) 42
11(c) Vertical Distribution of the Density Ratio σ from Sea Level up to the F_2 Layer, Latitude 0°. (Metric Units) 43
12(a) Vertical Distribution of the Density Ratio σ from Sea Level up to the F_2 Layer, Latitude 45°. (Engr. Units) 44
12(b) Vertical Distribution of the Density Ratio σ from Sea Level up to the F_2 Layer, Latitude 45°. (Engr. Units) 45
13(a) Vertical Distribution of the Density Ratio σ from Sea Level up to the F_2 Layer, Latitude 45°. (Metric Units) 46
13(b) Vertical Distribution of the Density Ratio σ from Sea Level up to the F_2 Layer, Latitude 45°. (Metric Units) 47
14 Vertical Distribution of the Sonic Velocity from Sea Level up to 100 Miles, Latitude 0°. (Engr. Units) 48
15 Vertical Distribution of the Sonic Velocity from Sea Level up to 160 km, Latitude 0°. (Metric Units) 49
16 Vertical Distribution of the Sonic Velocity from Sea Level up to 100 Miles, Latitude 45°. (Engr. Units) 50

LIST OF FIGURES (*Cont'd*)

17 Vertical Distribution of the Sonic Velocity from Sea Level up to 160 km, Latitude 45°. (Metric Units) 51
18 Solutions of Equation (50) Corresponding to Conditions at Latitude 0° 68
19 Adopted Values of Temperature for Atmospheric Model I from the F_2 Layer up to 1000 Miles, Latitude 0°. (Engr. Units) 78
20 Adopted Values of Temperature for Atmospheric Model I from the F_2 Layer up to 1600 km, Latitude 0°. (Metric Units) 79
21 Adopted Values of the Density Ratio σ for Atmospheric Model I from the F_2 Layer up to 1000 Miles, Latitude 0°. (Engr. Units) 80
22 Adopted Values of the Density Ratio σ for Atmospheric Model I from the F_2 Layer up to 1600 km, Latitude 0°. (Metric Units) 81
23 Adopted Values of Temperature for Atmospheric Model I from the F_2 Layer up to 1000 Miles, Latitude 45°. (Engr. Units) 82
24 Adopted Values of Temperature for Atmospheric Model I from the F_2 Layer up to 1600 km, Latitude 45°. (Metric Units) 83
25 Adopted Values of the Density Ratio σ for Atmospheric Model I from the F_2 Layer up to 1000 Miles, Latitude 45°. (Engr. Units) 84
26 Adopted Values of the Density Ratio σ for Atmospheric Model I from the F_2 Layer up to 1600 km, Latitude 45°. (Metric Units) 85
27 Atmospheric Model II. Total Number of Particles Above the Height h_1 Contained in a Column of Unit Cross Section, Latitude 0° 92
28 Atmospheric Model II. Total Number of Particles Above the Height h_1 Contained in a Column of Unit Cross Section, Latitude 45° 92
29 Adopted Values of the Density Ratio σ for Atmospheric Model II from h_* up to 1000 Miles, Latitude 0°. (Engr. Units) 100
30 Adopted Values of the Density Ratio σ for Atmospheric Model II from h_* up to 1000 Miles, Latitude 0°. (Metric Units) 101
31 Adopted Values of the Density Ratio σ for Atmospheric Model II from h_* up to 1000 Miles, Latitude 45°. (Engr. Units) 102
32 Adopted Values of the Density Ratio σ for Atmospheric Model II from h_* up to 1000 Miles, Latitude 45°. (Metric Units) 103
33 Atmospheric Model III. Vertical Distribution of the Density Ratio σ From the F_2 Layer up to 1000 Miles at Latitude 0° (Engr. Units) 131
34 Atmospheric Model III. Vertical Distribution of the Density Ratio σ From the F_2 Layer up to 1600 km at Latitude 0° (Metric Units) 132
35 Atmospheric Model III. Vertical Distribution of the Density Ratio σ From the F_2 Layer up to 1000 Miles at Latitude 45° (Engr. Units) 133
36 Atmospheric Model III. Vertical Distribution of the Density Ratio σ From the F_2 Layer up to 1600 km at Latitude 45° (Metric Units) 134
37 Atmospheric Model III. Vertical Distribution of the Temperature and Composition From the F_2 Layer up to 1000 Miles (Engr. Units) 135
38 Atmospheric Model III. Vertical Distribution of the Temperature and Composition From the F_2 Layer up to 1600 km (Metric Units) 136
39 Vertical Distribution of the Density Ratio σ From Sea Level up to 120 km, Latitude 45° 137
40 Vertical Distribution of Mean Molecular Weight From Sea Level up to the F_2 Layer, Latitude 45° 138

LIST OF FIGURES (*Cont'd*)

41 Vertical Distribution of Temperature Above the F_2 Layer for Models I, II, and III at Latitude 45° (Metric Units) 139

42 Vertical Distribution of Mean Molecular Weight Above the F_2 Layer for Models I, II, and III at Latitude 45° 140

43 Vertical Distribution of the Density Ratio σ Above the F_2 Layer for Models I, II, and III at Latitude 45° 141

44 Plot Showing the Small Effect of the Value Used for M_L in Determining the Vertical Density Distribution for Model I, Latitude 0° 142

SUMMARY

Values giving the vertical distribution of temperature, pressure, and density in the atmosphere from sea level up to extreme heights of the order of 5000 miles or more have been derived for the atmosphere both at the equator and at middle latitudes. In view of the rather complete lack of knowledge concerning atmospheric conditions in regions above the F_2 layer of the ionosphere, calculations for these regions have been carried out on the basis of three different atmospheric models or concepts. The atmospheric model I is based on the hypothesis or concept that there is an outer atmospheric limit far beyond the F_2 layer where the atmosphere is in thermal equilibrium with the interstellar gas at a kinetic temperature of 10,000°K. This demands that the temperature continue to increase beyond the F_2 layer. The mean molecular weight is assumed to decrease with height in a specified manner. Typical results derived on this basis are given in Tables 21 and 26.

The atmospheric model II is based on the concept that above a certain height, situated somewhere above the F_2 layer, the mean free path of the gas particles becomes so large, and the collision frequency becomes so small, that the particles move over dynamical orbits under essentially free flight conditions in a gravitational field, and those moving fast enough would be able to rise to great distances with but little chance of collision with other particles. If the effects of radiation are negligible, the temperature distribution in this region will be isothermal. Typical results derived on this basis, when the composition (molecular weight) is assumed constant, are contained in Tables 34 and 36.

Atmospheric model III is similar to model II inasmuch as it is based upon a free-flight dynamical orbit region ("exosphere") which is isothermal. In model III, further consideration is given to the question of the temperature of the exosphere and the height where it may be considered to begin; and, unlike model II, the composition is variable with height — the variation with height being determined by the assumption of diffusion equilibrium. In this model the effects of diffusion equilibrium are treated on a more rational basis than was the case for model I. Typical results are contained in Tables 42 and 44.

Through an oversight, the formula $g' = g_a (a/r)^2 - r\Omega^2 \cos\theta$ was used for the apparent gravity instead of the correct formula $g' = g_a (a/r)^2 - r\Omega^2 \cos^2\theta$. As far as the results for latitude 0° are concerned, this introduces no error. At latitude 45° the values for g' (and ϕ) are slightly too low, but the error is extremely small. The corresponding error produced in the pressure and density, etc., is entirely negligible and is insignificant in comparison with the uncertainties which exist in the temperature and molecular weight. From the hydrostatic relation

$$\log \frac{p}{p_1} = -\int_{h_1}^{h} \frac{1}{H} dh \equiv -\int_{h_1}^{h} \frac{Mg'}{R_u T} dh$$

it is seen that if new values for g' are introduced, the calculated values of pressure and density, etc., remain unchanged if they are interpreted as corresponding to slightly different temperatures (T_{new}), which are related to the temperatures given in the tables (T_{old}) by the ratio $T_{new}/T_{old} = g'_{correct}/g'_{old}$. The correct values of g' at latitude 45° and the ratios which they form with the old values are shown in the tables attached.

SYMBOLS

a = radius of the earth.

c = adiabatic speed of sound.

C_x = percent composition by volume of element x.

C_O = percent composition of oxygen.

C_N = percent composition of nitrogen.

C_H = percent composition of hydrogen.

C_{He} = percent composition of helium.

d = mean particle diameter.

E = kinetic energy.

e = electron, electronic charge.

g' = apparent acceleration of gravity at any height.

g_a = absolute value of gravity at sea level.

g'_a = apparent gravity at sea level.

g'_* = apparent gravity at the height h_*.

$\overline{g}'$ = mean apparent acceleration of gravity in the interval, $h - h_1$.

H = scale height = $R_u T/Mg'$.

H_* = scale height at the base of the exosphere (dynamical-orbit region).

h = height above sea level.

h_d = height above sea level where diffusion equilibrium begins.

h_L = height above sea level of the limit of the earth's atmosphere.

h_0 = height above sea level of the F_2 layer.

h_* = height above sea level at the base of the exosphere (dynamical-orbit region).

k = Boltzmann's constant = 1.381×10^{-16} cm dyne/°K.

L = mean free path of atmospheric gas particle.

M = mean molecular weight of gas mixture.

M_0 = mean molecular weight at the F_2 layer.

M_L = mean molecular weight at the limit of the earth's atmosphere.

M_x = mean molecular weight of constituent x.

M_* = mean molecular weight at the height h_*.

m = mean particle mass of gas mixture.

m_e = mass of electron.

m_O = mass of oxygen atom.

m_1 = mass of atom of unit atomic weight = 1.6489×10^{-24} grams.

m_* = mean particle mass at the height h_*.

N_* = total number of particles above h_* contained in a column of 1 cm^2 cross section.

n = number of particles per unit volume.

n_e = number of free electrons.

n_n = number of neutral particles.

n_+ = number of positive ions.

n_O = number of oxygen atoms per unit volume.

n_x = number density of constituent x.

n_0 = number of particles per unit volume at the F_2 layer.

n_* = number of particles per unit volume at the height h_*.

P = collision probability for a particle.

p = pressure.

p_a = pressure at sea level.

p_L = pressure at the limit of the earth's atmosphere.

p_0 = pressure at the F_2 layer.

p_1 = pressure at the height h_1.

p_* = pressure at the height h_*.

R_u = universal gas constant = 49677 ft-lb/slug-mole °R = 8.314×10^7 erg/gram-mole °K.

r = distance from the center of the earth to a point in the earth's atmosphere = $a + h$.

r_d = distance from the earth's center to the height where diffusion equilibrium begins.

r_L = distance from the earth's center to the limit of the earth's atmosphere = $a + h_L$.

r_0 = distance from the earth's center to the F_2 layer.

r_* = distance from the earth's center to the height h_*.

S = collision cross section.

T = absolute temperature.

T_L = absolute temperature at the limit of the earth's atmosphere = 10,000°K = 18,000°R.

T_0 = absolute temperature at the F_2 layer.

T_* = absolute temperature at the height h_*.

V_i = ionization potential.

v = mean particle velocity.

α = vertical gradient of temperature, dT/dh.

β = vertical gradient of molecular weight, dM/dh.

γ = ratio of specific heats = C_p/C_v.

θ = latitude.

ν = mean collision frequency of gas particles.

ρ = nm = mass density.

ρ_a = density at sea level.

ρ_L = density at the limit of the earth's atmosphere.

ρ_x = partial density contributed by constituent x.

ρ_{He} = density of helium.

ρ_H = density of hydrogen.

ρ_N = density of nitrogen.

ρ_O = density of oxygen.

ρ_{x*} = partial density contributed by constituent x at the height h_*.

ρ_* = density at the height h_*.

σ = the density ratio = ρ/ρ_a.

ϕ = apparent gravity potential function.

ϕ_* = apparent gravity potential function at the height h_*.

ϕ_L = apparent gravity potential at the limit of the earth's atmosphere.

Ω = constant angular velocity of rotation of the earth's atmosphere = 7.29211×10^{-5} radians/sec.

ω = variable angular velocity of rotation of the atmosphere.

ANALYSIS OF TEMPERATURE, PRESSURE, AND DENSITY OF THE ATMOSPHERE EXTENDING TO EXTREME ALTITUDES

INTRODUCTION

Owing to the recent important developments in the field of high-speed, high-altitude rockets and jet-propelled missiles, more and more demand has arisen for information concerning the temperature, pressure, and density of the atmosphere up to altitudes of the order of 100 to 300 miles or more. The pressure and density at such heights are extremely small, corresponding to conditions of a highly rarefied gas. Nevertheless, there may still be sufficient atmosphere to affect the motion of a long-range rocket travelling at high supersonic speeds. This would be especially true, for example, if one should consider the dynamical effects of the atmosphere on the motion of a high-speed body (speeds of the order of 25,000 ft/sec) travelling about the earth on a circular orbit as a satellite. Here the rarefied gas effects, although small in themselves, operate over a sufficiently long time interval to give an integrated effect which may be appreciable. It is also conceivable that estimates of the physical state of the atmosphere at extreme altitudes might be of some use — in various ways as yet unforeseen — in connection with certain problems which might arise in the study of interplanetary rockets.

At an altitude of about 100 miles where the mean free path of the molecules of the atmospheric gas becomes comparable to the dimensions of a rocket, the drag of the rocket in the rarefied gas must be computed on the basis of gas kinetics or free molecule flow rather than from the gas-dynamical laws of a continuous medium. In this case the drag coefficient is quite large, having a value of at least 2.0[(1),(1a),(2)]. The gas-dynamical laws based on a continuous medium probably begin to break down at even lower altitudes where the mean free path of the gas particles takes on values equivalent to the thickness of the boundary layer. Furthermore, since the thickness of a shock wave must be at least as large as the mean free path[±], it follows that in the highly rarefied atmosphere at high altitudes where the laws of free molecule flow apply, shock wave phenomena can no longer take place, at least not in any sharply defined fashion as is the case under conditions of normal temperature and pressure.

Thus, in evaluating the performance of very-high-speed, high-altitude rockets, it becomes necessary to have values for the physical properties of the upper atmosphere up to altitudes which heretofore were of little interest to the meteorologist or the aeronautical engineer. Values for the state of the atmosphere up to 100 km have

---

For references see p. 143.

± Cf Thomas, L.H., "Note on Becker's Theory of the Shock Front," *Jour. Chem. and Physics*, Vol.12, No.11, p.449, November, 1944.

been fairly well established. Above this level, the knowledge becomes more and more uncertain and speculative with increasing altitude. In spite of these uncertainties, a preliminary attempt will be made here to calculate the physical properties of the atmosphere out to great distances beyond the F_2 layer and to determine, for example, what might be considered as the "limit" of the atmosphere (atmospheric model I). Although the results derived for the region above the F_2 layer are more or less open to question, they may at least be considered as a basis for extrapolating to the regions beyond the F_2 layer up to heights of the order of 500-1000 miles (800-1600 km).

For the purpose of discussion, the atmosphere is usually divided into three main regions. The atmosphere from sea level to 10-15 km is referred to as the troposphere, and that above this up to about 30 km is called the stratosphere. The region above the stratosphere extending outward to interplanetary space may be called the upper atmosphere.

The atmosphere above about 80 km is strongly ionized and hence this region of the upper atmosphere, from 80 km outwards, is known as the ionosphere. The ionosphere is of fundamental importance in radio-wave propagation since it is owing to the reflection of radio waves by the ionosphere that long distance radio communication is possible. It seems to be established that the ionization of the ionosphere, and therefore its electrical conductivity, is caused primarily by the ultra-violet solar radiation.

The ionosphere itself is divided into three main regions or layers which are stratified on the basis of electron or ion density[3],[4]. The lower of these regions, known as the E layer, is moderately ionized and is situated in the vicinity of the 100-km level. The next higher layer, the F_1 layer, is more strongly ionized and is situated in the vicinity of 200 km. Still higher and still more strongly ionized is the F_2 layer at about 300 km. There is recent evidence[73] which strongly suggests the presence of an additional ionized layer, called the G layer, situated above the F_2 layer somewhere in the region from 400 to 700 km. The upper region of ionization comprising the F_1 and F_2 layers is referred to in its entirety as the F region. The regular E layer and the F_1 layer are present only during the day and are most intensely ionized during the hours of local noon. A sporadic E layer may be present at any time.

Diurnal changes also occur in the F region. The concept and terminology used in the older literature was that during the night there was a merging of the F_1 and F_2 layers to form a single layer, referred to simply as the F layer. In the newer terminology it is more clearly recognized that the F_2 layer maintains its identity throughout the night while undergoing diurnal variations. The regular E layer and the F_1 layer are not present during the night, and it is unnecessary to use the term F layer in this connection. The term F region is applied to the upper region of ionization regardless of time of day; it comprises the F_1 and F_2 layers during the day and the F_2 layer during the night.

Since the main aim of this study is to arrive at tentative working values for a "standard" upper atmosphere, no attempt will be made at an especially critical discussion; but rather the various data which are available will be presented, and what appear to be the most reasonable deductions from them will serve as a basis

for the calculations. The calculations will be carried out for the atmosphere at the equator and also at latitude 45°. Although many gaps and uncertainties still exist in the knowledge of the upper atmosphere, it is believed that the results presented here, at least up to the F_2 layer, represent about the best that can be done considering the data which are available at the present time (see footnote 3, page 12), and that the values given for the temperature, pressure, and density up to the F_2 layer may be accepted with considerable confidence. It must be emphasized that the calculations for the atmosphere beyond the F_2 layer, where there are no data available and where the atmospheric models considered here are based on rather speculative reasoning, must be regarded as representing little more than possible values. However, there seem to be no other calculations of this nature available, and the values derived here should at least give some indication of the limits within which the actual values would lie.

The writer asks to be excused for frequently using mixed systems of units. This happens because all the literature on the subject is based on the c.g.s. system, while the values used in aeronautical applications are always desired in the engineering system.

I - THE ATMOSPHERE UP TO THE F_2 LAYER

The exact calculation of the variation of atmospheric pressure and density with altitude requires a knowledge of the following quantities as a function of altitude above the earth's surface.

1. Temperature.

2. Composition. This includes not only the kind of constituent gases, but also the degree of dissociation and also of ionization, since these effects can be important in determining the value of the molecular weight which is used in the equation of state. For example, consider a gas composed initially of molecular oxygen having the molecular weight 32. If this gas undergoes complete dissociation into the atomic state the molecular weight is reduced to 16. If, further, the gas is not only completely dissociated but also completely ionized, the mean molecular weight is reduced to 8 owing to the presence of positive ions and free electrons in equal number. Finally, a knowledge of the composition presupposes a knowledge of the degree of diffusion equilibrium which is present; that is, the degree to which the constituent gases are distributed in the vertical according to their molecular weights, with the lighter gases situated above those which are heavier.

3. The Angular Velocity of Rotation of the Atmosphere about the Axis of the Earth. The angular velocity determines the value of apparent gravity and thus has an effect in determining the distribution of pressure.

I-A. THE TEMPERATURE DISTRIBUTION

The temperature conditions in the troposphere and stratosphere are well known from direct measurements by means of sounding balloons and form the basis for the standard atmosphere used in aeronautics as given by Diehl[7]. These values will be used to represent conditions at latitude 45°. The stratosphere at a temperature of 218°K is extended from 20 km to 32 km in accordance with a recent recommendation of the NACA Subcommittee on Upper Atmosphere[13]. The significant levels for this atmosphere are shown in Table 1.

Table 1

TEMPERATURE OF TROPOSPHERE AND STRATOSPHERE, LATITUDE 45°.			
Altitude, km	0	10.77	32
Temperature, °C	15	-55	-55
Temperature, °K	288	218	218

Pressure at sea level = 760 mm of Hg

The troposphere and stratosphere temperatures at the equator will be based on the Batavia data[8]. Values taken from the mean annual curve (Fig. 102, Ref. 8), with linear extrapolation from 25 to 30 km, are given in Table 2.

Table 2

TEMPERATURE OF TROPOSPHERE AND STRATOSPHERE, LATITUDE 0°.					
Altitude, km	0	5	10	16	30
Temperature, °C	26	-2	-37.5	-82	-42
Temperature, °K	299	271	235.5	191	231

Pressure at sea level = 1012 millibars

Between the significant levels the temperature is assumed to vary linearly with altitude, which represents a close approximation to actual mean conditions. It will be noted that in the tropics the stratosphere does not have well-defined isothermal properties as in middle latitudes, but rather is characterized by temperature increasing with height.

Above about 35 km there are no direct measurements of temperature and the only values available are those which result from indirect methods[1]. Thus the available values for the temperature of the upper atmosphere are based on the study of

[1] For footnote see p.5.

the ozone absorption of solar radiation, the anomalous propagation of sound, atmospheric tides, the luminosity and speed of meteors, the spectrum of the aurora, and the reflection of radio waves in the ionosphere[2] by the E, F_1, and F_2 layers. An account of these studies and their results has been given by Haurwitz(9), Penndorf(10),(11), and Gutenberg(12).

The results of these studies indicate that above the stratosphere the temperature increases to a maximum value in the neighborhood of 50 km, decreases to a minimum value at around 80 km, and then increases again to a high value at 120 km. The tentative standard values of temperature for this region as adopted by the NACA Subcommittee on Upper Atmosphere(13) are given in Table 3.

Table 3

TENTATIVE STANDARD TEMPERATURE VALUES
FOR THE REGION 20 - 120 km, LATITUDE 45°

Altitude km	Probable Minimum Temp., °K	Tentative Standard Temp., °K	Probable Maximum Temp., °K
20	---	218	250
25	---	---	250
32	---	218	---
45	200	---	380
50	---	355*	---
55	300	---	---
60	---	355*	---
70	---	---	380
78	---	240	---
80	170	---	300
83	---	240	---
120	300	375	600

* The value 355°K has been inadvertently used here instead of the intended value 350°K. However, in view of the small value of this difference, and also the uncertainty concerning the exact value which should be used, the effect is entirely inconsequential.

Although these values refer mainly to middle latitudes, they will also be used for the equatorial atmosphere above 32 km, mainly because corresponding figures for the equatorial regions seem to be lacking, and also because they would per-

[1] However, the vertical distribution of density up to 100 km has been measured recently by using a V2 rocket. The measured values of density are in good agreement with those calculated by using the temperature distribution of Table 3. See *Physical Review*, Vol.70, p.985, December, 1946, "Pressure and Temperature Measurements in the Upper Atmosphere." Also, see "Upper Atmosphere Temperatures from the Helgoland *Big Bang*," Bulletin American Meteorological Society, Vol.29, No.2, p.78, Feb., 1948.

[2] Extended discussions of the ionosphere and the upper atmosphere have been presented by Berkner(3), Chapman (15), Hulburt(4), Mitra(5),(85), and Millington(6).

haps not differ greatly from the values used. The values adopted for the vertical distribution of temperature from sea level up to 120 km at the equator and in middle latitudes are plotted in Figs. 1-4.

It will be noted that there is no isothermal stratospheric region shown for the equatorial atmosphere in Fig. 1. Although a very thin isothermal layer could have been deduced from the data used (Ref. 8), this was not very clearly indicated and the neglect of such a layer will be of no practical significance for the calculations.

The temperatures used for the atmosphere above 120 km will be those values deduced from the reflection of radio waves by the F_1 and F_2 layers. There are two methods by which the temperature may be deduced from the ionosphere measurements. In one of these, Appleton[14], it is possible to evaluate in the reflecting layer a quantity H called the scale height, which is closely related to the thickness of the ionized layer, and which is defined by

$$H = \frac{kT}{mg'} = \frac{R_u T}{Mg'} \quad , \tag{1}$$

where k is Boltzmann's constant, m is the mean mass of the molecules, R_u is the universal gas constant, M is the mean molecular weight, and g' is the apparent acceleration of gravity. Thus, when the value of H is known from ionosphere measurements and M is known from the composition, the value of T is then determined. The scale height H is discussed by Chapman[15], and is derived later in Section II-F†. The thickness of an ionized layer is usually considered to be roughly about four times the scale height H[74]. In the other method, Appleton[16], Eckersley[17], Farmer and Ratcliffe[18],[19], it is possible to estimate in the reflecting layer the average electron collision frequency ν_e defined by‡

$$\nu_e = 4nd^2\sqrt{\frac{\pi kT}{m}} \equiv 4nd^2\sqrt{\frac{\pi R_u T}{M}} \, , \tag{2}$$

where n is the number of particles per unit volume and d their mean diameter. By either method, it is seen that it is necessary to know the composition (i.e., the mean molecular weight M or the mean molecular mass m) in order to estimate the temperature in the ionosphere from radio-wave soundings.

---

† Also see Section III-B.

‡ Also see Chapman, S., and Cowling, T.G., Ref.65a, p.146.

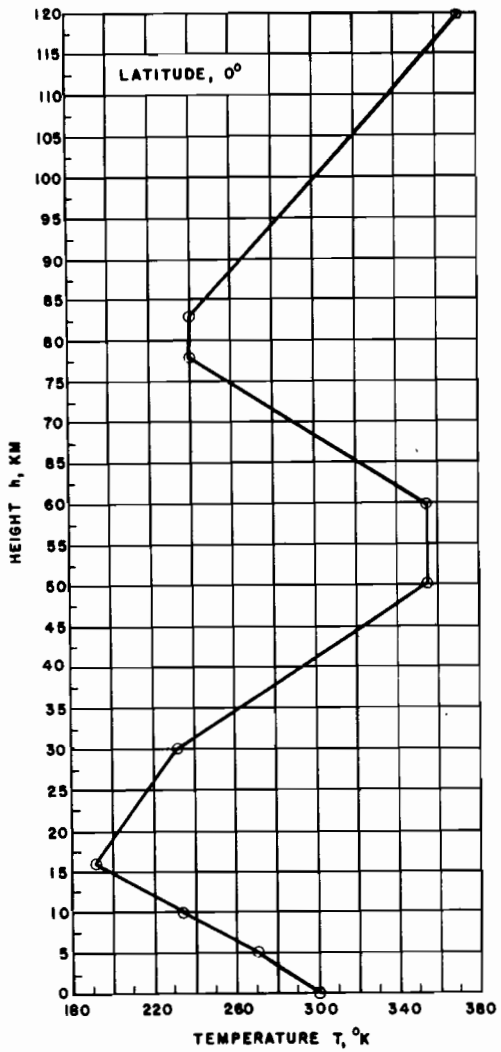

VERTICAL DISTRIBUTION OF TEMPERATURE AT THE EQUATOR FROM SEA LEVEL UP TO 120 KM. METRIC UNITS.

FIG. 1

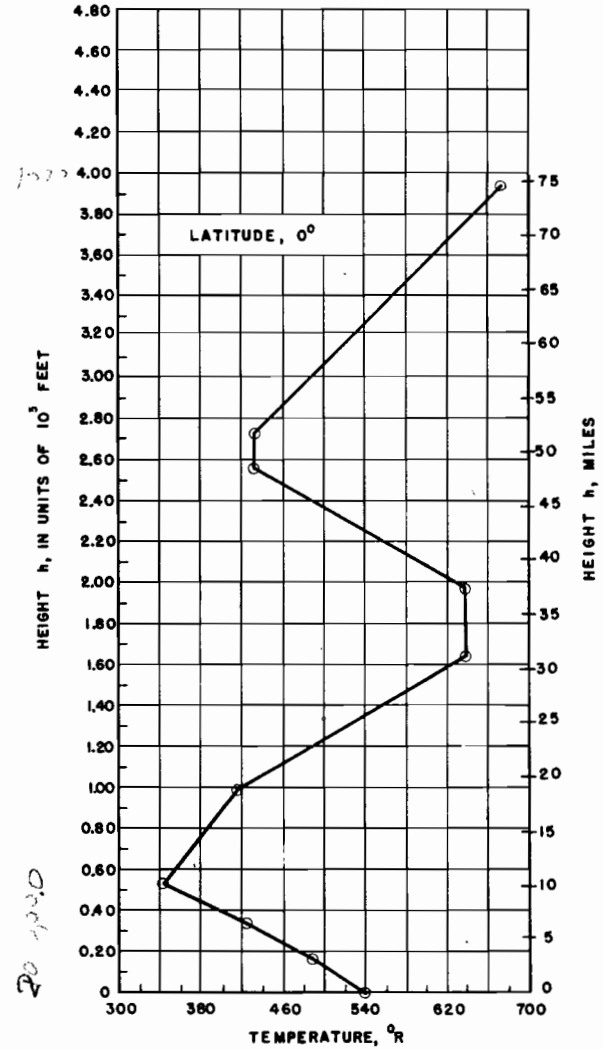

VERTICAL DISTRIBUTION OF TEMPERATURE AT THE EQUATOR FROM SEA LEVEL UP TO 75 MILES. ENGINEERING UNITS.

FIG. 2

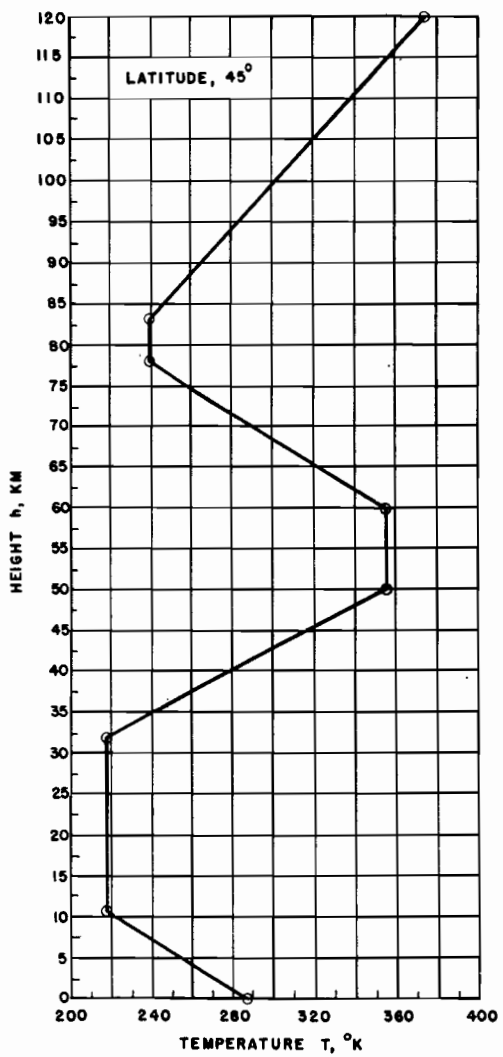

VERTICAL DISTRIBUTION OF TEMPERATURE AT LATITUDE 45° FROM SEA LEVEL UP TO 120 KM. METRIC UNITS.

FIG. 3

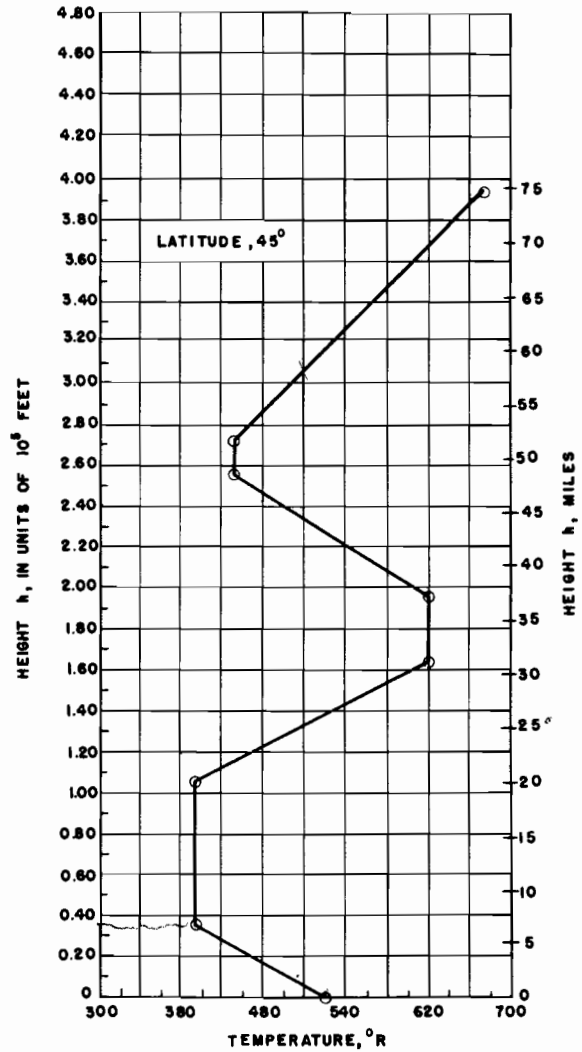

VERTICAL DISTRIBUTION OF TEMPERATURE AT LATITUDE 45° FROM SEA LEVEL UP TO 75 MILES. ENGINEERING UNITS.

FIG. 4

Practically all the deductions of temperature from ionosphere measurements indicate a considerable increase in temperature above 100 km (the E layer), as shown in Table 4, and the evidence in favor of high temperature in the F_2 layer is very considerable. Although the determination of the value for the temperature in the F_2 layer is not one of great accuracy, it is generally recognized that a high temperature must prevail in this region of the order of 1000°K.

Table 4

IONOSPHERE TEMPERATURES (TAKEN FROM PENNDORF[10])

	100 km	200-300 km	350-400 km
Maris (1936)	---	373°K	---
Müller (1935)	370°K	---	---
Fuchs[20] (1936)	---	400°-1000°K	1400°-1900°K
Martyn and Pulley[21] (1936)	300°K	1200°K	---
Appleton (1936)	100°K	1200°K	---
Godfrey and Price[22] (1937)	---	1200°K	---
Das[23] (1938)	1000°K	1000°K	---
Senda[24] (1938)	---	1400°-2000°K	---
Bhar[25] (1938)	300°K	600°K	---
Appleton (1939)	385°K	700°-1300°K	---
Penndorf[26] (1940)	308°-375°K	437°- 936°K	---

As far as ionosphere temperatures at the equator are concerned, the only values available are those given by Fuchs[20], which are based on observations of the ionosphere at Huancayo, Peru, latitude 12° south, as given by Berkner and Wells[27]. The temperatures derived by Fuchs are shown in Table 5.

Table 5

TEMPERATURE IN THE F REGION AT THE EQUATOR ACCORDING TO FUCHS[20]

Altitude, km	190	220	350	420
Temperature, °K	400	1000	1400	1900

These values are plotted in Fig. 5 together with the point T = 375°K at 120 km from Table 3. Except for the point T = 400°K at 190 km, which has been discounted, the values are represented with sufficient accuracy by the straight line shown in the figure, and this is the linear relationship which will be used for the temperature distribution in the F region at the equator. Thus it will be assumed that the temperature in this region is defined by the straight line connecting the points T = 375°K at 120 km and T = 1800°K at 400 km. The corresponding curve in engineering units is plotted in Fig. 6.

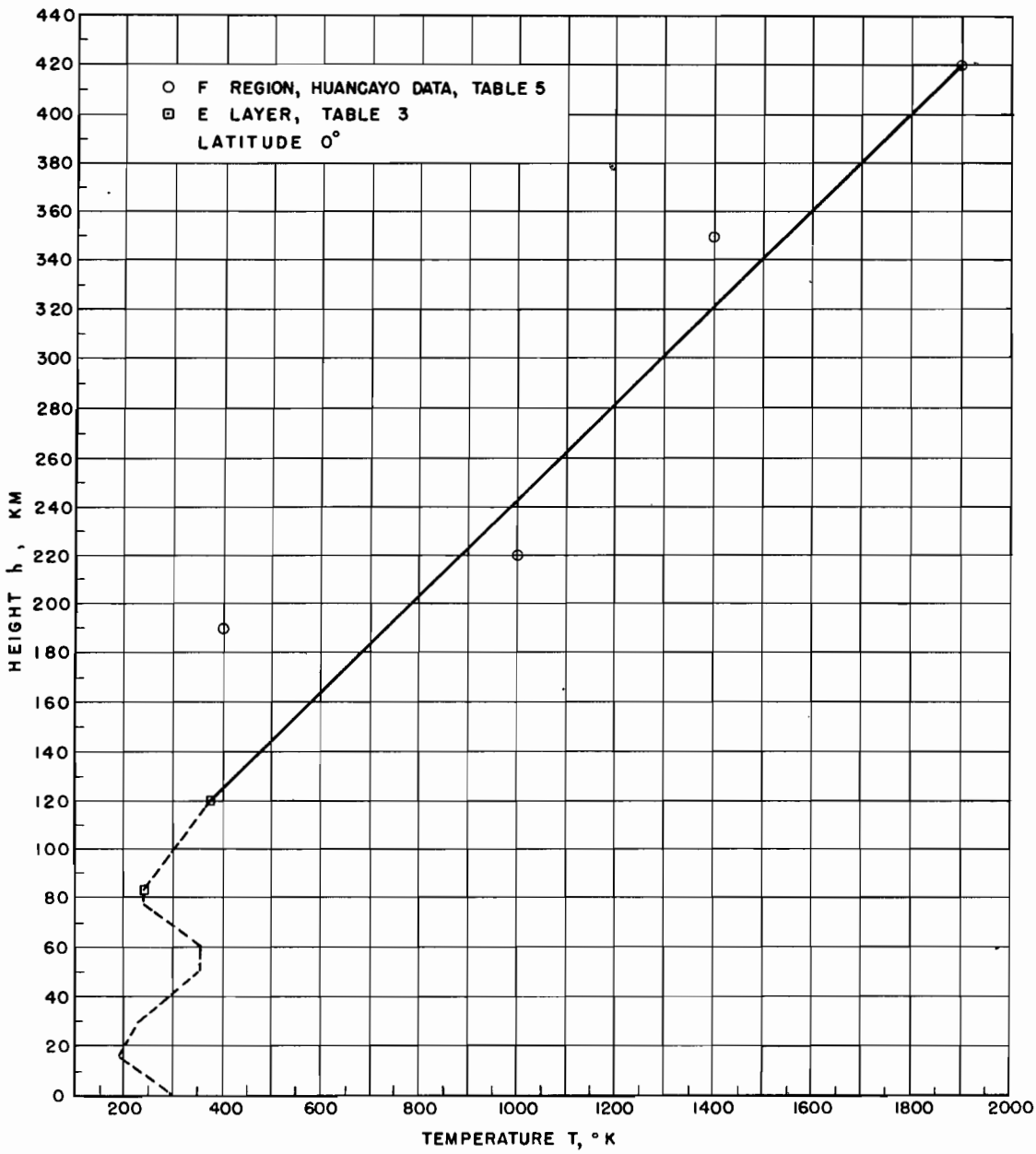

VERTICAL DISTRIBUTION OF TEMPERATURE IN THE F REGION AT THE EQUATOR. METRIC UNITS. (BASED ON HUANCAYO DATA, REFS. 20 AND 27)

FIG. 5

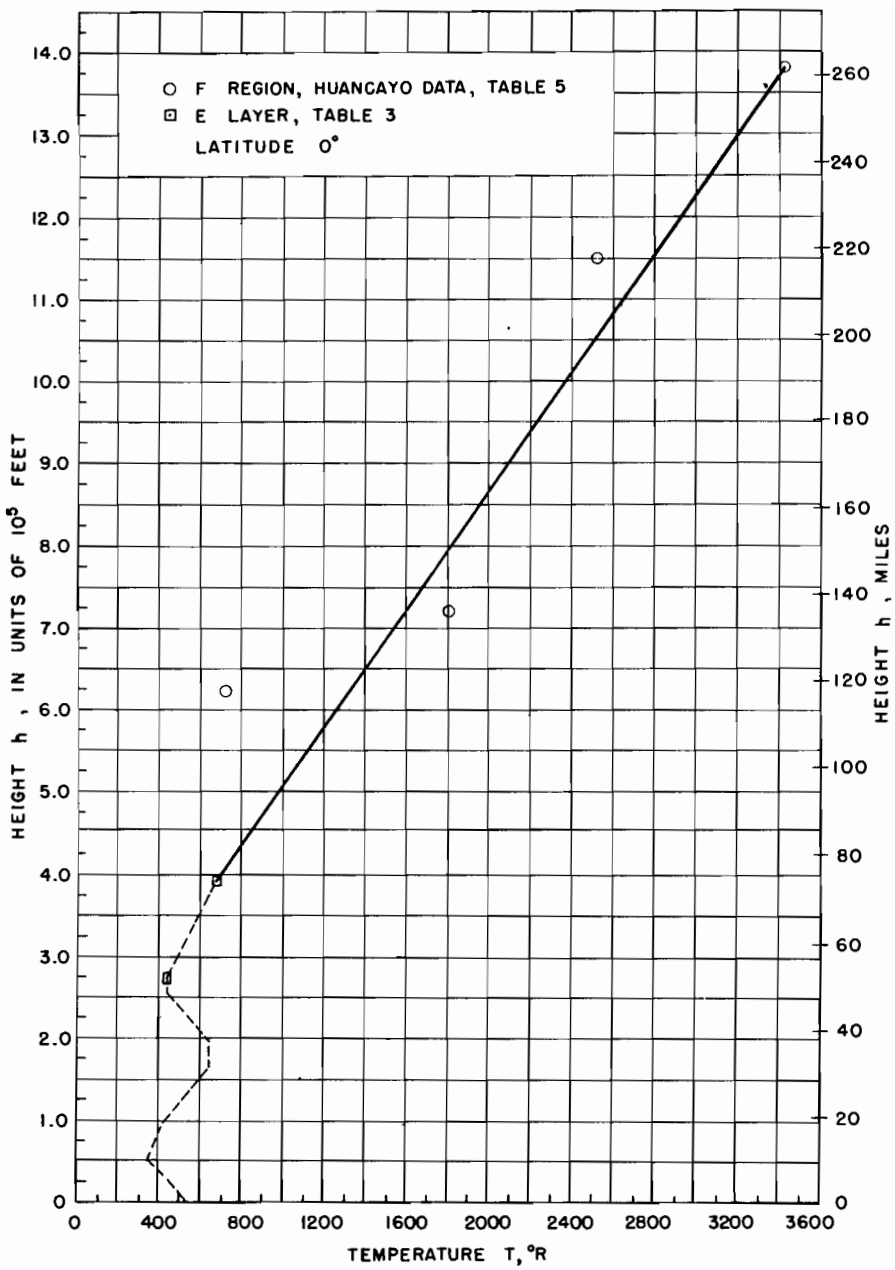

VERTICAL DISTRIBUTION OF TEMPERATURE IN THE F REGION AT THE EQUATOR. ENGINEERING UNITS. (BASED ON HUANCAYO DATA, REFS. 20 AND 27)

FIG. 6

In the middle latitudes it is seen from Table 4 that considerable choice exists in the temperatures to be used in the F region. It has been decided here to adopt a value of 1100°K at 300 km which, from data given by Martyn and Pulley[21] (see Fig. 5 of Ref. 21), represents a probable mean diurnal value. The distribution of temperature is assumed to be linear between this value and the value 375°K at 120 km, since there is no information available to specify the exact nature of the temperature curve in this region. It is well known that there is a distinct diurnal variation in the properties of the F region. During the day this contains the F_1 as well as the F_2 layer, with the F_2 layer situated at about 300 km and at a temperature of the order of 1200°K. During the night only the F_2 layer remains, and in middle latitudes this is usually at a lower height and temperature than during the day. From the data of Martyn and Pulley it is considered that the mean diurnal condition of the F_2 layer is represented by the value 1100°K at 300 km. No attempt is made here to take into account any seasonal variations which occur, mainly because there seem to be very few data in usable form (height and temperature) available in this respect. The vertical distribution of temperature adopted to represent conditions in the F region in middle latitudes is presented in Figs.7 and 8 (pp.14 and 15).

The temperature values used for the F region at the equator are not mean diurnal values but are based on noon observations, and are therefore probably higher than the mean diurnal values would be. So far, no deduced temperature data for Huancayo which could be used to determine mean diurnal conditions have come to the attention of the writer, and although it would no doubt be possible to make such deductions from original Huancayo data, no attempt will be made to do this here[3].

In the calculations by Fuchs using the Huancayo data, it was assumed that both the oxygen and the nitrogen were completely dissociated. As pointed out in Section I-C, the effect of assuming an O + N-atmosphere is to give lower temperatures than would be the case for an O + N_2-atmosphere.

As pointed out by Zenneck[28], considering the high values deduced for the temperature of the F_2 layer together with the rarefied gas conditions existing there, the concept of temperature requires a few remarks by way of explanation. In the rarefied gas of the upper atmosphere it is convenient and perhaps even necessary to think of temperature in terms of "kinetic" temperature. Consider a unit volume of gas, assumed homogeneous for simplicity, containing n particles each of mass m. It is shown in the kinetic theory of gases that the pressure p of the gas may be expressed in the form

$$p = \frac{1}{3} nm\overline{v^2} = \frac{2}{3} n \times \frac{1}{2} m\overline{v^2} = \frac{2}{3} \times \frac{\rho}{2} \overline{v^2} , \qquad (3)$$

[3] In view of the great mass of world-wide ionosphere data that has been accumulated during the war years and which is becoming available, this would seem to be a very appropriate time to start a critical survey and study of these data from the meteorological standpoint, since the result of such a study should add greatly to the knowledge of the physical state of the upper atmosphere. Thus the results would give well-established mean values for the diurnal, seasonal, and geographical variations of the height and temperature of the ionized layers. In the published data available at the present time, such information is either scarce or lacking entirely. As a result of the emphasis being placed at present on high-altitude, high-speed rocket research, the results described above could be used to great advantage if they were available. Recent world-wide ionosphere data will be found in the CRPL-F series (Central Radio Propagation Laboratory) publications of the National Bureau of Standards.

where $\overline{v^2}$ is the mean square particle velocity and $\rho = nm$ is the mass density. Thus the pressure is directly proportional to the mean kinetic energy of translation of the gas particles.

The equation of state for a perfect gas

$$p = \rho \frac{R_u}{M} T = \rho \frac{k}{m} T = nkT \quad , \tag{4}$$

where R_u is the universal gas constant, M is the molecular weight, and k is Boltzmann's constant, may be derived from purely thermodynamical reasoning based only on the assumption of thermodynamic equilibrium, i.e., space and time derivatives equal to zero. In this case the temperature T is the absolute thermodynamic temperature as defined through the second law of thermodynamics.

The equation of state (4) may also be regarded as an empirical relation derived from the laws of Boyle and Gay-Lussac[†], and temperature may be independently defined by means of this relation. This, for example, would be the temperature indicated by a gas thermometer, which depends for its operation on the concept of pressure as expressed by relations (3). In fact, by comparing (3) and (4), it follows that

$$\frac{1}{2} m\overline{v^2} = \frac{3}{2} kT \quad , \tag{5}$$

which shows the relationship between the mean kinetic energy of translation of the gas particles and the temperature.

In view of this relation, Eq. (5) may be made the basis for the definition of temperature and may be said to define a "kinetic" temperature rather than a thermodynamic scale of temperature[‡]. From this point of view it would be possible to speak of the temperature of a single particle if it is so desired and to define this by the relation

$$\frac{1}{2} mv^2 = kT \quad , \tag{5a}$$

where v and T are the instantaneous values for a single particle. From the way in which it is defined, it is seen that the kinetic temperature satisfies the perfect gas equation and is therefore precisely the temperature which is used in calculating the pressure or density. Thus, when a temperature of 1000°K or more is specified in the F_2 layer, for example, this is to be interpreted in terms of Eq. (5), that is, in terms of the mean kinetic energy of the gas particles.

---

† Cf Poynting, J.H., and Thompson, J.J., *A Textbook of Physics - Heat*, London: Griffin, Chap.4, 1928.

‡ Cf Chapman, S., and Cowling, T.G., Ref.65a, p.37.

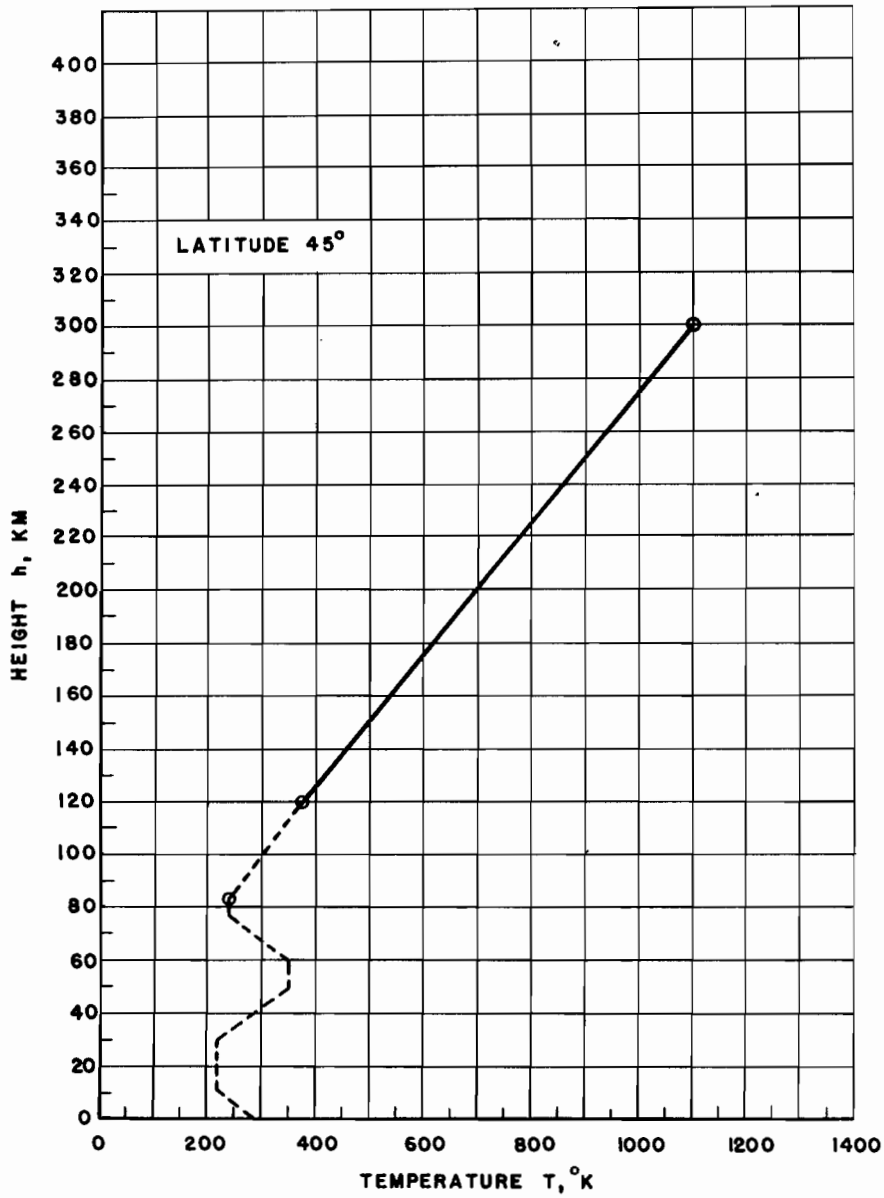

VERTICAL DISTRIBUTION OF TEMPERATURE IN THE F REGION AT LATITUDE 45°. METRIC UNITS.

FIG. 7

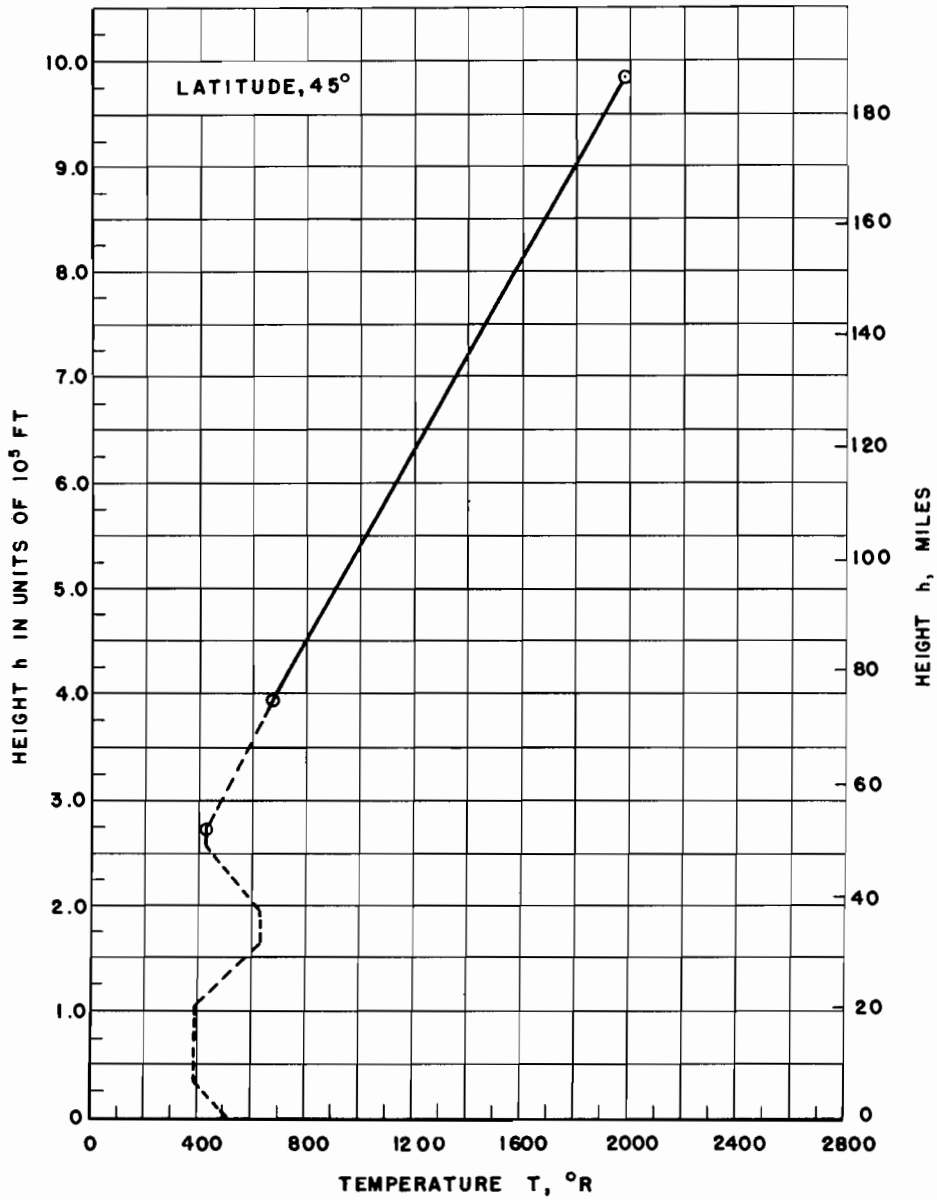

VERTICAL DISTRIBUTION OF TEMPERATURE IN THE F REGION AT LATITUDE 45°. ENGINEERING UNITS.

FIG. 8

It is shown in statistical mechanics[29] that when the gas particles have a Maxwellian velocity distribution and the temperature is defined thermodynamically, the equation of state of a perfect gas can be derived. Thus, when the kinetic and thermodynamic temperatures are equal, the gas will have a Maxwellian distribution; or, stated more appropriately in the converse form, the equation of state (4) defines a gas having a Maxwellian velocity distribution if the kinetic temperature is identical with the thermodynamic temperature. This will be the case, provided a time interval can be chosen to correspond to a mean steady state condition, as far as external influences are concerned, and provided this time interval is large compared to the relaxation time, or the time interval between collisions.

Although high kinetic temperatures exist in the *F* region of the ionosphere, it must not be inferred that a body situated in this region would come into thermal equilibrium with the gas at these temperatures. Owing to the extremely rarefied nature of the gas at these heights, the temperature of the body would be determined solely by radiation processes, any heat transfer resulting from the presence of the gas particles being entirely negligible. If the body is moving at extremely high speeds, there would also be a small amount of heat transfer resulting from the impacts of the free gas particles with the skin of the body, in which the gas particles lose all of their directed kinetic energy upon striking the surface of the body.

I-B. THE COMPOSITION

As far as the composition of the atmosphere is concerned, it is found that the tropospheric values are maintained with little change up to about 80 km. The composition of tropospheric air, as given by Paneth[30], is shown in Table 6.

Table 6

COMPOSITION OF TROPOSPHERIC AIR

Gas	Formula	Volume %	Mass %	Molecular Wt (O = 16.000)
Nitrogen	N_2	78.09	75.53	28.016
Oxygen	O_2	20.95	23.14	32.000
Argon	Ar	0.93	1.28	39.944
Carbon Dioxide	CO_2	0.03	.046	44.00
Helium	He	5.24×10^{-4}	7.24×10^{-5}	4.002
Hydrogen	H_2	5.10×10^{-5}	3.55×10^{-6}	2.016

From the table it is seen that N_2 and O_2 account for 99 per cent of the composition, by volume, of the tropospheric air. As pointed out by Chapman[31] and Penndorf[32], the results of auroral spectroscopy indicate that even from 100 km to 1000 km, oxygen and nitrogen are still the main constituents of the atmosphere, and it will be assumed here that the upper atmosphere, at least up to 1000 km, is a nitrogen-oxygen atmosphere. However, due to the absorption of ultra-violet solar radiation,

the molecular oxygen undergoes dissociation in the vicinity of the 100-km level, Chapman[31], Wulf and Deming[33], and the oxygen in the remainder of the upper atmosphere is generally regarded as existing mainly in the atomic state. It will be assumed here that the dissociation of oxygen begins at 83 km, becoming complete at 120 km (i.e., the E layer). The question of the dissociation of nitrogen is quite controversial and not nearly so clear; it will be assumed that the nitrogen remains in the molecular state at least up to the F_2 layer [3a].

From the measurements of the reflection of radio waves, it is known that the upper atmosphere is ionized and that the electron density (number of electrons per unit volume) reaches a maximum in the F_2 layer. The degree of ionization x of a gas is defined by the ratio

$$x = \frac{n_e}{n_n + n_+} = \frac{n_e}{n_0} \tag{6}$$

where

$n_0 = n_n + n_+$ = initial number of particles before ionization,

n_e = number of free electrons,

n_n = number of neutral atoms or molecules, and

n_+ = number of positive ions,

all referred to a given mass of gas. Thus for complete ionization, $x = 1$. This formula presupposes that there are no negative ions and therefore that $n_e = n_+$. If n denotes the total number of particles in thermal equilibrium (ions, electrons, neutral atoms or molecules) in a given volume of gas, the total pressure p is given from kinetic theory by

$$p = nkT , \tag{7}$$

where T is the absolute temperature and k is the Boltzmann constant. This may be written

$$p = (n_e + n_+ + n_n)\ kT = n_0\ (1 + x)\ kT , \tag{8}$$

which shows how the ionization can increase the pressure simply by adding free electrons to the gas without changing its mass.

However, from data given by Cowling[34] for the E, F_1, and F_2 layers, it is found that x is of the order of 10^{-5} or smaller, and may therefore be neglected compared to unity in Eq. (7). Typical values of the degree of ionization in the E and

[3a] Although Vassy and Vassy[80] believe that the evidence indicates the complete dissociation of nitrogen in the F_2 layer, this view had not been widely accepted as yet and requires further substantiation. It seems more likely that the dissociation of nitrogen occurs in the G layer - see Section III-D.

F regions are shown in Fig. 9. Thus, as far as the atmosphere up to the F_2 layer is concerned, the degree of ionization may be entirely neglected as far as its effect on the calculation of the pressure is concerned. The composition which will be used to represent conditions in the equatorial atmosphere up to the F_2 layer is given in Table 7.

Table 7

COMPOSITION OF THE ATMOSPHERE UP TO THE F_2 LAYER AT THE EQUATOR

Altitude km	Composition, % Volume	Molecular Weight of Mixture, M	Ratio of Specific Heats, γ
0	21% O_2, 78% N_2, 0.93% Ar	28.9	1.405
83	20% O_2, 80% N_2	28.8	1.405
120	33% O , 67% N_2	24.0	1.46
400 (F_2 layer)	33% O , 67% N_2	24.0	1.46

It will be noted that the composition is assumed to remain unchanged from 120 km up to and including the F_2 layer; that is, the constituent gases in this region are assumed to be completely mixed, giving an atmosphere of uniform composition. This agrees more or less with the results of Mitra and Rakshit[35] who found that, for an N_2– O atmosphere with temperature increasing with height, diffusive equilibrium would exist only above 350 km. The values 33% O and 67% N_2 are based on a gas which corresponds to 20% O_2 and 80% N_2 when there is no dissociation of oxygen. Essentially it is assumed that the dissociation occurs at constant pressure, but that the volume may change.

In middle latitudes it appears likely, Penndorf[11], Regener[36], that there is a slight change in composition at about 50 km to the values 18% O_2 and 82% N_2. Using these figures the values in Table 8 are obtained as representative of the composition of the atmosphere up to the F_2 layer in middle latitudes.

Table 8

COMPOSITION OF THE ATMOSPHERE UP TO THE F_2 LAYER. LATITUDE 45°

Altitude km	Composition, % Volume	Molecular Weight of Mixture, M	Ratio of Specific Heats, γ
0	21% O_2, 78% N_2, 0.93% Ar	28.9	1.405
50	18% O_2, 82% N_2	28.66	1.405
83	18% O_2, 82% N_2	28.66	1.405
120	30.5% O, 69.5% N_2	24.35	1.46
300 (F_2 layer)	30.5% O, 69.5% N_2	24.35	1.46

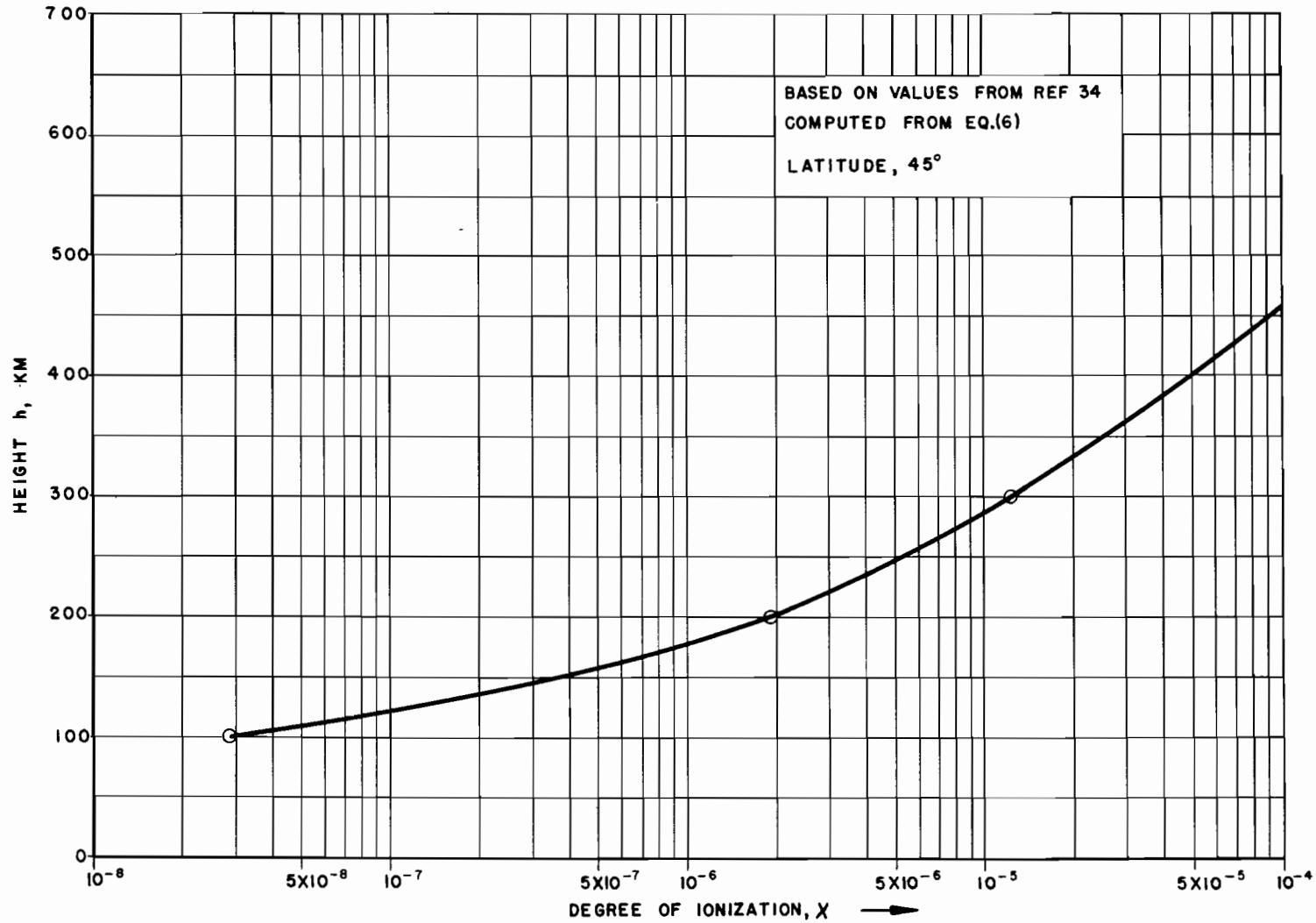

DEGREE OF IONIZATION IN THE E AND F REGIONS

FIG. 9

I-C. EFFECT OF COMPOSITION ON THE DETERMINATION OF THE TEMPERATURE IN AN IONIZED LAYER

It was pointed out in connection with Eq. (1) that the values derived for the ionosphere temperatures depend on the values used for the mean molecular weight M. It should also be mentioned that the value of H depends on the vertical distribution of the electron density†. This has been subjected to a detailed analysis by Pekeris[37] who finds values of H which are less than those previously used as given by Appleton[14]. If this result is accepted, this effect alone will give lower ionosphere temperatures than those derived previously. Using the H-values of Pekeris, Penndorf[10], [26] has calculated new values for the temperature in the E and F_2 layers for various assumed values of composition M. The results given by Penndorf are shown in Table 9.

Table 9

TEMPERATURES IN THE E AND F_2 LAYERS BASED ON PENNDORF[26] AND PEKERIS[37]. LATITUDE 45°.

	Designation	Composition	Mean Molecular Weight, M	H = 11.4 km Temperature	
E Layer ~100 km	A_1	81%N_2, 19%O_2	28.78	374°K	
	A_2	81%N_2, 19%O	25.74	330°K	
	A_3	67%N_2, 32%O	23.87	308°K	
	A_4^*	75.8%N_2, 9%O_2, 15.3%O	26.52	346°K	
	Designation	**Composition**	**Mean Molecular Weight, M**	**H = 20 km Temperature**	**H = 30 km Temperature**
F_2 Layer ~220 km**	B_1	81%N_2, 19%O_2	28.78	625°K	936°K
	B_2	93%N_2, 6%O_2	27.92	608°K	912°K
	B_3	81%N_2, 19%O	25.74	557°K	834°K
	B_4	36%N_2, 64%O	20.30	442°K	662°K
	B_5	41%N_2, 40%N, 19%O	20.12	437°K	655°K
	B_6^*	67%N_2, 33%O	24.03	530°K	795°K

* Computed from Eqs. (1) and (11).

** The value 220 km for the height of the F_2 layer is rather low and is about equal to the height ordinarily found for the F_1 layer.

† For some concepts, at least, the value of H will also depend upon the vertical distribution of dissociation. See footnote 8, p.113.

The rather large differences between these values show the importance of an accurate knowledge of M and H in deducing the ionosphere temperatures. From the data given by Pekeris[37] it is inferred that the E layer values correspond to a height of about 100 to 110 km and the F_2 layer values to about 220 km. Thus the E layer values correspond approximately to the height of the middle of the E layer. Using the values in Table 7 the composition in the middle of the E layer will be that of A_4 (see Table 9), which gives a temperature of 346°K. This is in good agreement with the value 340°K according to the adopted curve, Fig. 7, at 110-km height.

In the F_2 layer the values B_6 have been computed to correspond to the composition assumed in Table 7. From Fig. 7 a temperature of 780°K is indicated at 220 km, which is in good agreement with the higher of the B_6 values.

The temperatures used here for the F_2 region at the equator, as computed by Fuchs, Fig. 5, were based on the assumption that the nitrogen and oxygen were completely dissociated, giving a value for the molecular weight of the atmosphere of about 15. This is much lower than the value $M = 24$, which is used here to represent the composition of the F_2 region, and if Fuchs' values were to be corrected to be consistent with the composition $M = 24$, much higher temperatures would result. In fact, the values shown in Table 5 would have to be increased by the factor $24/15 = 1.6$. However, in view of the fact that the more exact analysis of Pekeris would lead to values of H which are lower by a factor of about the same order, it is considered that the temperatures adopted according to Fig. 5 are probably quite representative of actual conditions as they stand.

I-D. THE CALCULATIONS

The calculation of the pressure and density is based upon the hydrostatic equation

$$dp = -\rho g' dh , \tag{9}$$

and the equation of state for unit mass

$$p = \rho \frac{R_u}{M} T , \tag{10}$$

where

p = pressure

ρ = mass density

h = height above sea level

g' = apparent acceleration of gravity

R_u = universal gas constant

M = mean molecular weight

T = absolute temperature

In the engineering gravitational system of units, $R_u = 1544 \times 32.174 = 49677$ ft-lb/slug-mole°R, ρ is in slugs/ft^3, p is in lbs/ft^2, T is in degrees Rankine, and h is in feet. In the c.g.s. absolute system of units, $R_u = 83.15 \times 10^6$ erg/gram-mole°K, ρ is in grams/cm^3, p is in dynes/cm^2, T is in degrees Kelvin, and h is in centimeters.

It will be assumed that the atmosphere between sea level and the F_2 layer rotates with the earth as a solid so that the apparent gravity is given by

$$g' = g_a \left(\frac{a}{r}\right)^2 - r\Omega^2 \cos^2\theta , \tag{11}$$

where g_a is the absolute value of gravity at sea level at the latitude θ and a is the radius of the earth at this latitude. The angular velocity of rotation of the earth is denoted by Ω, and r is the distance from the center of the earth to a point in the earth's atmosphere; i.e., $r = a + h$. The value $\Omega = 7.29211 \times 10^{-5}$ radians/sec is used for the rotational speed of the earth; values for the earth's radius and acceleration of gravity are given in Table 10.

Table 10

RADIUS OF THE EARTH AND THE ACCELERATION OF GRAVITY

$\Omega = 7.29211 \times 10^{-5}$ radians/sec

Latitude, θ	Radius of the Earth, a			Apparent Gravity g'_a		Absolute Gravity g_a	
degrees	miles	ft	cm	ft/sec^2	cm/sec^2	ft/sec^2	cm/sec^2
0°	3963.34	2.09264×10^7	6.37839×10^8	32.088	978.04	32.199	981.43
45°	3956.59	2.08908×10^7	6.36751×10^8	32.174	980.66	32.253	983.07
90°	3949.92	2.08556×10^7	6.35691×10^8	32.258	983.22	32.258	983.22

Combining Eqs. (9) and (10) yields

$$\log \frac{p}{p_1} = -\frac{Mg'}{R_u} \int_{h_1}^{h} \frac{dh}{T} , \tag{12}$$

which gives the pressure p at a vertical distance $\Delta h = h - h_1$ above the level h_1 where the pressure is p_1. The molecular weight M and the apparent gravity g' are taken outside the integral here, since the interval Δh is taken small enough that it is permissible to use the mean values of M and g' appropriate to the interval in question.

Since the vertical distribution of temperature up to the F_2 layer has been represented by straight line segments, we always have a temperature-height relationship of the form

$$T = T_1 + \alpha\,(h - h_1)\,, \tag{13}$$

where $\alpha = dT/dh = (T_2 - T_1)/(h_2 - h_1)$ is the slope of any straight line segment. Thus α is positive for temperature increasing with height and negative for temperature decreasing with height. Introducing this relation, Eq. (12) becomes

$$\log\frac{p}{p_1} = -\frac{Mg'}{R_u}\int_{h_1}^{h}\frac{dh}{T_1 + \alpha\,(h - h_1)}\,, \tag{14}$$

which may be integrated [3b] giving

$$p = \frac{p_1}{\left[1 + \frac{\alpha}{T_1}(h - h_1)\right]^{\frac{Mg'}{\alpha R_u}}}\,. \tag{15}$$

[3b] When M is constant in the interval h-h_1, Eq. (14) may be integrated taking into account the variation of gravity. For an atmosphere which rotates with the earth as a solid, $g' = g_a(a/r)^2 - r\Omega^2\cos^2\theta$ and the pressure relation may be written

$$\log\frac{p}{p_1} = -\frac{M}{R_u}\int_{h_1}^{h}\frac{g_a\left(\frac{a}{r}\right)^2 - r\Omega^2\cos^2\theta}{T_1 + \alpha(r - r_1)}\,dr\,. \tag{14a}$$

This is readily integrated yielding the result

$$\log\frac{p}{p_1} = -\frac{M}{R_u}\left\{(r-r_1)\left[\frac{\Omega^2\cos\theta}{\alpha} - \frac{g_a a^2}{rr_1(T_1-\alpha r)}\right]\right.$$

$$\left. + \left[\frac{\alpha g_a a^2}{(T_1-\alpha r_1)^2} + \frac{(T_1-\alpha r_1)\Omega^2\cos^2\theta}{\alpha^2}\right]\log\left[\frac{T_1}{T_1+\alpha(r-r_1)}\right] + \left[\frac{\alpha}{(T_1-\alpha r_1)^2}\,g_a a^2\log\frac{r}{r_1}\right]\right\}. \tag{14b}$$

This is the formula used for calculating the pressures. From the values of pressure obtained in this way the corresponding density is obtained immediately from the equation of state,

$$\rho = \frac{MP}{R_u T} . \tag{16}$$

The values of temperature, pressure, and density for a standard atmosphere up to the F_2 layer at the equator and at latitude 45° are tabulated in Tables 11 to 14. The results are given in both the engineering and c.g.s. systems of units. The density ratio $\sigma = \rho/\rho_a$, where ρ_a is the density at sea level, is plotted in Figs. 10 to 13. The values in Tables 13 and 14 up to 20 km may differ very slightly from those given by Diehl [7] owing to the use of a slightly different value for the molecular weight.

Other quantities of interest which have been included in the tables are the molecular density, the mean free path, the mean molecular speed, the collision frequency, and the speed of sound. The molecular density n (also called the number density or particle density) is the number of gas particles per unit volume and is given by the expression,

$$n = \frac{\rho}{m} , \tag{17}$$

where m is the mean mass of the gas particles. An equivalent form which is perhaps more convenient is

$$n = \frac{\rho}{M\, m_1} , \tag{18}$$

where M is the mean molecular weight and m_1 is the mass of the atom of unit atomic weight ($m_1 = 1.6489 \times 10^{-24}$ gram). The mean free path L is given by

$$L = \frac{1}{\pi \sqrt{2}\, n\, d^2} , \tag{19}$$

where d is the mean diameter of the gas particles. From sea level up to 83 km, where all of the particles are molecular, the value $d = 3 \times 10^{-8}$ cm is considered appropriate. Above 120 km, where electrons, atoms, and molecules are present, it is conceivable that the value $d = 2 \times 10^{-8}$ cm might be more appropriate. In view of this uncertainty concerning the value for d, L and ν are given in the tables for both values — $d = 3 \times 10^{-8}$ cm and $d = 2 \times 10^{-8}$ cm.

The mean molecular speed v in a Maxwellian gas is found from

$$v = \sqrt{\frac{8\, k\, T}{\pi m}} , \tag{20}$$

where k is Boltzmann's constant. In view of the relation $k/m = R_u/M$, this may be written more conveniently as

$$v = \sqrt{\frac{8\,R_u T}{\pi\,M}} \quad . \tag{21}$$

For a constant speed gas the corresponding expression is

$$v_s = \sqrt{3\,\frac{R_u T}{M}} \quad , \tag{22}$$

which differs but very little from the Maxwellian case. The mean collision frequency ν is connected with L and v by the relation $\nu = v/L$, and thus may be computed from the relation,

$$\nu = \frac{v}{L} = 4\,n\,d^2 \sqrt{\pi\,\frac{R_u T}{M}} \quad . \tag{23}$$

The equation for the adiabatic speed of sound c in a perfect gas is

$$c = \sqrt{\gamma\,\frac{R_u T}{M}} \equiv \sqrt{\frac{\gamma\,p}{\rho}} \quad , \tag{24}$$

where γ is the ratio of the specific heats ($\gamma = C_p/C_v$). The speed of sound is plotted in Fig. 14 where it will be noticed that this quantity is not given beyond a height of 100 miles. This is because the ordinary laws of sound propagation probably begin to break down under the same rarefied gas conditions at which the gas dynamical laws become invalid and the gas kinetic laws take over. This probably occurs at some height less than 100 miles. The propagation of sound waves in rarefied gases has been discussed recently by Tsien and Schamberg[38]. Their results indicate that with regard to rarefied gas effects there is very little change in the speed of sound up to heights of about 60 miles, which represents about the limit of their curves as far as height is concerned. The damping of the sound, however, becomes appreciable at such heights. The sonic velocities are plotted in Figs. 14 to 17.

Warfield's[13] results giving the properties of the atmosphere up to 120 km appeared at about the same time as those presented here. Both studies — although carried out independently — are based on the same vertical temperature distribution, Table 3.

Table 11

VALUES OF TEMPERATURE, PRESSURE, AND DENSITY UP TO THE F_2 LAYER

Latitude, 0°. Engineering Units. p_a = 2115 lb/ft², ρ_a = 2.286 × 10⁻³ slug/ft³

Height h ft	Height h mi	Apparent Gravity g' ft/sec²	Mean Mol Wt M	Temp T °R	Scale Height H ft	Pressure p lb/ft²	Pressure Ratio p/p_a	Density ρ slug/ft³	Density Ratio σ ρ/ρ_a	Number Density n particles/ft³	Mean Particle Speed v ft/sec	$d = 3 \times 10^{-8}$ cm Mean Free Path L ft	$d = 3 \times 10^{-8}$ cm Mean Collision Freq ν 1/sec	$d = 2 \times 10^{-8}$ cm Mean Free Path L ft	$d = 2 \times 10^{-8}$ cm Mean Collision Freq ν 1/sec	Speed of Sound c ft/sec
0	0	32.088	28.90	538.2	2.883×10^4	2115	1.0000	2.286×10^{-3}	1.0000	7.000×10^{23}	1.535×10^3	3.321×10^{-7}	4.622×10^9	7.472×10^{-7}	2.054×10^9	1.141×10^3
5,000	.947	32.072	28.90	522.8	2.802×10^4	1774	.8389	1.974×10^{-3}	.8636	6.045×10^{23}	1.513×10^3	3.845×10^{-7}	3.934×10^9	8.652×10^{-7}	1.748×10^9	1.124×10^3
10,000	1.894	32.057	28.90	507.5	2.721×10^4	1481	.7002	1.698×10^{-3}	.7426	5.198×10^{23}	1.490×10^3	4.472×10^{-7}	3.333×10^9	1.006×10^{-6}	1.481×10^9	1.071×10^3
15,000	2.841	32.041	28.90	492.1	2.640×10^4	1229	.5813	1.453×10^{-3}	.6357	4.450×10^{23}	1.468×10^3	5.224×10^{-7}	2.810×10^9	1.175×10^{-6}	1.249×10^9	1.090×10^3
16,404	3.107	32.037	28.90	487.8	2.617×10^4	1166	.5511	1.390×10^{-3}	.6081	4.257×10^{23}	1.461×10^3	5.461×10^{-7}	2.676×10^9	1.229×10^{-6}	1.189×10^9	1.085×10^3
20,000	3.788	32.026	28.90	473.8	2.543×10^4	1014	.4795	1.245×10^{-3}	.5447	3.813×10^{23}	1.440×10^3	6.096×10^{-7}	2.362×10^9	1.372×10^{-6}	1.050×10^9	1.070×10^3
25,000	4.735	32.011	28.90	454.3	2.440×10^4	830.1	.3925	1.063×10^{-3}	.4649	3.254×10^{23}	1.410×10^3	7.143×10^{-7}	1.974×10^9	1.607×10^{-6}	8.775×10^8	1.047×10^3
30,000	5.682	31.996	28.90	434.8	2.336×10^4	673.6	.3185	9.012×10^{-4}	.3942	2.759×10^{23}	1.380×10^3	8.425×10^{-7}	1.638×10^9	1.896×10^{-6}	7.278×10^8	1.025×10^3
32,808	6.214	31.987	28.90	423.9	2.278×10^4	596.6	.2821	8.187×10^{-4}	.3581	2.507×10^{23}	1.362×10^3	9.273×10^{-7}	1.469×10^9	2.086×10^{-6}	6.529×10^8	1.012×10^3
35,000	6.629	31.980	28.90	415.0	2.230×10^4	541.4	.2560	7.589×10^{-4}	.3320	2.324×10^{23}	1.348×10^3	1.000×10^{-6}	1.347×10^9	2.251×10^{-6}	5.988×10^8	1.001×10^3
40,000	7.576	31.965	28.90	394.6	2.122×10^4	430.6	.2036	6.348×10^{-4}	.2777	1.944×10^{23}	1.314×10^3	1.196×10^{-6}	1.099×10^9	2.691×10^{-6}	4.884×10^8	9.762×10^2
45,000	8.523	31.950	28.90	374.3	2.014×10^4	338.2	.1599	5.256×10^{-4}	.2299	1.609×10^{23}	1.280×10^3	1.444×10^{-6}	8.861×10^8	3.250×10^{-6}	3.938×10^8	9.508×10^2
50,000	9.470	31.934	28.90	353.9	1.905×10^4	262.2	.1240	4.309×10^{-4}	.1885	1.319×10^{23}	1.245×10^3	1.762×10^{-6}	7.065×10^8	3.964×10^{-6}	3.140×10^8	9.246×10^2
52,493	9.942	31.926	28.90	343.8	1.851×10^4	229.7	.1086	3.887×10^{-4}	.1700	1.190×10^{23}	1.227×10^3	1.953×10^{-6}	6.280×10^8	4.395×10^{-6}	2.791×10^8	9.112×10^2
55,000	10.417	31.919	28.90	347.7	1.873×10^4	200.8	9.494×10^{-2}	3.359×10^{-4}	.1469	1.029×10^{23}	1.234×10^3	2.260×10^{-6}	5.459×10^8	5.085×10^{-6}	2.426×10^8	9.164×10^2
60,000	11.364	31.904	28.90	355.6	1.916×10^4	154.3	7.296×10^{-2}	2.525×10^{-4}	.1104	7.730×10^{22}	1.248×10^3	3.007×10^{-6}	4.149×10^8	6.766×10^{-6}	1.844×10^8	9.267×10^2
65,000	12.311	31.888	28.90	363.4	1.959×10^4	119.3	5.640×10^{-2}	1.910×10^{-4}	8.352×10^{-2}	5.847×10^{22}	1.261×10^3	3.976×10^{-6}	3.172×10^8	8.946×10^{-6}	1.410×10^8	9.368×10^2
70,000	13.258	31.873	28.90	371.2	2.002×10^4	92.74	4.385×10^{-2}	1.453×10^{-4}	6.356×10^{-2}	4.450×10^{22}	1.275×10^3	5.224×10^{-6}	2.440×10^8	1.176×10^{-5}	1.084×10^8	9.469×10^2
75,000	14.205	31.858	28.90	379.1	2.045×10^4	72.50	3.428×10^{-2}	1.113×10^{-4}	4.867×10^{-2}	3.407×10^{22}	1.288×10^3	6.824×10^{-6}	1.888×10^8	1.535×10^{-5}	8.390×10^7	9.568×10^2
80,000	15.152	31.842	28.90	386.9	2.089×10^4	56.97	2.694×10^{-2}	8.567×10^{-5}	3.747×10^{-2}	2.623×10^{22}	1.301×10^3	8.862×10^{-6}	1.468×10^8	1.994×10^{-5}	6.527×10^7	9.667×10^2
85,000	16.098	31.827	28.90	394.8	2.133×10^4	45.03	2.129×10^{-2}	6.636×10^{-5}	2.903×10^{-2}	2.032×10^{22}	1.314×10^3	1.144×10^{-5}	1.149×10^8	2.574×10^{-5}	5.106×10^7	9.764×10^2
90,000	17.045	31.812	28.90	402.6	2.175×10^4	35.72	1.689×10^{-2}	5.162×10^{-5}	2.258×10^{-2}	1.580×10^{22}	1.328×10^3	1.471×10^{-5}	9.025×10^7	3.310×10^{-5}	4.011×10^7	9.860×10^2
95,000	17.992	31.797	28.90	410.4	2.219×10^4	28.48	1.347×10^{-2}	4.037×10^{-5}	1.766×10^{-2}	1.236×10^{22}	1.340×10^3	1.880×10^{-5}	7.128×10^7	4.231×10^{-5}	3.168×10^7	9.956×10^2
98,424	18.641	31.786	28.90	415.8	2.249×10^4	24.46	1.156×10^{-2}	3.422×10^{-5}	1.497×10^{-2}	1.048×10^{22}	1.349×10^3	2.218×10^{-5}	6.081×10^7	4.992×10^{-5}	2.703×10^7	1.002×10^3
100,000	18.939	31.782	28.90	421.2	2.278×10^4	22.82	1.079×10^{-2}	3.152×10^{-5}	1.378×10^{-2}	9.650×10^{21}	1.358×10^3	2.409×10^{-5}	5.636×10^7	5.420×10^{-5}	2.505×10^7	1.009×10^3
105,000	19.886	31.766	28.90	438.2	2.371×10^4	18.41	8.703×10^{-3}	2.449×10^{-5}	1.071×10^{-2}	7.500×10^{21}	1.385×10^3	3.100×10^{-5}	4.468×10^7	6.974×10^{-5}	1.986×10^7	1.029×10^3
110,000	20.833	31.751	28.90	455.2	2.464×10^4	14.97	7.080×10^{-3}	1.914×10^{-5}	8.371×10^{-3}	5.860×10^{21}	1.412×10^3	3.967×10^{-5}	3.558×10^7	8.926×10^{-5}	1.581×10^7	1.048×10^3
115,000	21.780	31.736	28.90	472.2	2.557×10^4	12.28	5.804×10^{-3}	1.512×10^{-5}	6.616×10^{-3}	4.631×10^{21}	1.438×10^3	5.020×10^{-5}	2.864×10^7	1.129×10^{-4}	1.273×10^7	1.068×10^3
120,000	22.727	31.721	28.90	489.2	2.651×10^4	10.14	4.793×10^{-3}	1.206×10^{-5}	5.273×10^{-3}	3.691×10^{21}	1.463×10^3	6.297×10^{-5}	2.324×10^7	1.417×10^{-4}	1.033×10^7	1.087×10^3
125,000	23.674	31.706	28.90	506.2	2.744×10^4	8.428	3.985×10^{-3}	9.686×10^{-6}	4.237×10^{-3}	2.966×10^{21}	1.488×10^3	7.838×10^{-5}	1.899×10^7	1.764×10^{-4}	8.441×10^6	1.106×10^3
130,000	24.621	31.691	28.90	523.2	2.838×10^4	7.051	3.334×10^{-3}	7.840×10^{-6}	3.429×10^{-3}	2.401×10^{21}	1.513×10^3	9.683×10^{-5}	1.563×10^7	2.179×10^{-4}	6.946×10^6	1.124×10^3
135,000	25.568	31.671	28.90	540.2	2.932×10^4	5.934	2.806×10^{-3}	6.390×10^{-6}	2.795×10^{-3}	1.957×10^{21}	1.538×10^3	1.188×10^{-4}	1.294×10^7	2.673×10^{-4}	5.752×10^6	1.142×10^3
140,000	26.515	31.660	28.90	557.2	3.025×10^4	5.021	2.374×10^{-3}	5.243×10^{-6}	2.293×10^{-3}	1.605×10^{21}	1.562×10^3	1.448×10^{-4}	1.078×10^7	3.258×10^{-4}	4.793×10^6	1.160×10^3
145,000	27.462	31.645	28.90	574.2	3.118×10^4	4.271	2.020×10^{-3}	4.327×10^{-6}	1.893×10^{-3}	1.325×10^{21}	1.585×10^3	1.754×10^{-4}	9.037×10^6	3.947×10^{-4}	4.016×10^6	1.178×10^3
150,000	28.409	31.630	28.90	591.2	3.213×10^4	3.651	1.726×10^{-3}	3.592×10^{-6}	1.571×10^{-3}	1.100×10^{21}	1.609×10^3	2.113×10^{-4}	7.612×10^6	4.755×10^{-4}	3.383×10^6	1.195×10^3
155,000	29.356	31.615	28.90	608.2	3.307×10^4	3.135	1.482×10^{-3}	2.999×10^{-6}	1.312×10^{-3}	9.182×10^{20}	1.632×10^3	2.532×10^{-4}	6.445×10^6	5.696×10^{-4}	2.864×10^6	1.212×10^3
160,000	30.303	31.600	28.90	625.3	3.401×10^4	2.704	1.279×10^{-3}	2.516×10^{-6}	1.101×10^{-3}	7.705×10^{20}	1.654×10^3	3.017×10^{-4}	5.484×10^6	6.788×10^{-4}	2.437×10^6	1.229×10^3
164,040	31.068	31.588	28.90	639.0	3.477×10^4	2.407	1.138×10^{-3}	2.191×10^{-6}	9.584×10^{-4}	6.709×10^{20}	1.672×10^3	3.465×10^{-4}	4.827×10^6	7.796×10^{-4}	2.145×10^6	1.242×10^3
165,000	31.250	31.585	28.90	639.0	3.478×10^4	2.341	1.107×10^{-3}	2.132×10^{-6}	9.324×10^{-4}	6.527×10^{20}	1.672×10^3	3.562×10^{-4}	4.696×10^6	8.013×10^{-4}	2.087×10^6	1.242×10^3
170,000	32.197	31.570	28.90	639.0	3.479×10^4	2.028	9.590×10^{-4}	1.846×10^{-6}	8.077×10^{-4}	5.654×10^{20}	1.672×10^3	4.112×10^{-4}	4.068×10^6	9.251×10^{-4}	1.808×10^6	1.242×10^3
175,000	33.144	31.555	28.90	639.0	3.481×10^4	1.757	8.295×10^{-4}	1.600×10^{-6}	6.998×10^{-4}	4.899×10^{20}	1.672×10^3	4.745×10^{-4}	3.524×10^6	1.068×10^{-3}	1.566×10^6	1.242×10^3
180,000	34.091	31.540	28.90	639.0	3.483×10^4	1.523	7.200×10^{-4}	1.386×10^{-6}	$6.06[illegible] \times 10^{-4}$	4.245×10^{20}	1.672×10^3	5.476×10^{-4}	3.054×10^6	1.232×10^{-3}	1.357×10^6	1.242×10^3
185,000	35.038	31.525	28.90	639.0	3.484×10^4	1.320	6.239×10^{-4}	1.201×10^{-6}	5.255×10^{-4}	3.679×10^{20}	1.672×10^3	6.319×10^{-4}	2.646×10^6	1.422×10^{-3}	1.176×10^6	1.242×10^3
190,000	35.985	31.510	28.90	639.0	3.486×10^4	1.144	5.408×10^{-4}	1.041×10^{-6}	4.555×10^{-4}	3.188×10^{20}	1.672×10^3	7.291×10^{-4}	2.294×10^6	1.640×10^{-3}	1.020×10^6	1.242×10^3
195,000	36.932	31.495	28.90	639.0	3.488×10^4	.9914	4.688×10^{-4}	9.026×10^{-7}	3.948×10^{-4}	2.764×10^{20}	1.672×10^3	8.411×10^{-4}	1.988×10^6	1.892×10^{-3}	8.837×10^5	1.242×10^3

Table 11 *(Cont'd)*

Latitude, 0°. Engineering Units. p_a = 2115 lb/ft², ρ_a = 2.286 × 10⁻³ slug/ft³

Height h ft	Height h mi	Apparent Gravity g' ft/sec²	Mean Mol Wt M	Temp T °R	Scale Height H ft	Pressure p lb/ft²	Pressure Ratio p/p_a	Density ρ slug/ft³	Density Ratio σ ρ/ρ_a	Number Density n particles/ft³	Mean Particle Speed v ft/sec	$d = 3 \times 10^{-8}$cm Mean Free Path L ft	$d = 3 \times 10^{-8}$cm Mean Collision Freq ν 1/sec	$d = 2 \times 10^{-8}$cm Mean Free Path L ft	$d = 2 \times 10^{-8}$cm Mean Collision Freq ν 1/sec	Speed of Sound c ft/sec
196,848	37.282	31.489	28.90	639.0	3.488×10^4	.9405	4.447×10^{-4}	8.562×10^{-7}	3.745×10^{-4}	2.622×10^{20}	1.672×10^3	8.867×10^{-4}	1.886×10^6	1.995×10^{-3}	8.383×10^5	1.242×10^3
200,000	37.879	31.480	28.90	628.0	3.429×10^4	.8586	4.060×10^{-4}	7.955×10^{-7}	3.480×10^{-4}	2.436×10^{20}	1.658×10^3	9.544×10^{-4}	1.737×10^6	2.147×10^{-3}	7.720×10^5	1.232×10^3
205,000	38.826	31.465	28.90	610.4	3.335×10^4	.7408	3.502×10^{-4}	7.060×10^{-7}	3.088×10^{-4}	2.162×10^{20}	1.635×10^3	1.075×10^{-3}	1.520×10^6	2.419×10^{-3}	6.756×10^5	1.214×10^3
210,000	39.773	31.450	28.90	592.9	3.241×10^4	.6365	3.009×10^{-4}	6.245×10^{-7}	2.732×10^{-4}	1.912×10^{20}	1.611×10^3	1.216×10^{-3}	1.325×10^6	2.735×10^{-3}	5.890×10^5	1.197×10^3
215,000	40.720	31.435	28.90	575.4	3.146×10^4	.5444	2.574×10^{-4}	5.505×10^{-7}	2.408×10^{-4}	1.686×10^{20}	1.587×10^3	1.379×10^{-3}	1.151×10^6	3.103×10^{-3}	5.114×10^5	1.179×10^3
220,000	41.667	31.420	28.90	557.9	3.052×10^4	.4635	2.192×10^{-4}	4.834×10^{-7}	2.114×10^{-4}	1.480×10^{20}	1.563×10^3	1.571×10^{-3}	9.948×10^5	3.534×10^{-3}	4.422×10^5	1.161×10^3
225,000	42.614	31.405	28.90	540.3	2.957×10^4	.3927	1.857×10^{-4}	4.228×10^{-7}	1.849×10^{-4}	1.294×10^{20}	1.538×10^3	1.796×10^{-3}	8.564×10^5	4.040×10^{-3}	3.806×10^5	1.142×10^3
230,000	43.561	31.390	28.90	522.8	2.863×10^4	.3309	1.564×10^{-4}	3.682×10^{-7}	1.611×10^{-4}	1.127×10^{20}	1.513×10^3	2.062×10^{-3}	7.336×10^5	4.639×10^{-3}	3.261×10^5	1.124×10^3
235,000	44.508	31.375	28.90	505.3	2.768×10^4	.2772	1.311×10^{-4}	3.192×10^{-7}	1.396×10^{-4}	9.774×10^{19}	1.487×10^3	2.378×10^{-3}	6.253×10^5	5.351×10^{-3}	2.779×10^5	1.105×10^3
240,000	45.455	31.360	28.90	487.7	2.673×10^4	.2309	1.092×10^{-4}	2.754×10^{-7}	1.205×10^{-4}	8.433×10^{19}	1.461×10^3	2.757×10^{-3}	5.301×10^5	6.202×10^{-3}	2.356×10^5	1.085×10^3
245,000	46.402	31.346	28.90	470.2	2.579×10^4	.1910	9.033×10^{-5}	2.364×10^{-7}	1.034×10^{-4}	7.237×10^{19}	1.435×10^3	3.212×10^{-3}	4.466×10^5	7.227×10^{-3}	1.985×10^5	1.066×10^3
250,000	47.348	31.331	28.90	452.7	2.484×10^4	.1570	7.421×10^{-5}	2.017×10^{-7}	8.823×10^{-5}	6.176×10^{19}	1.408×10^3	3.764×10^{-3}	3.740×10^5	8.469×10^{-3}	1.662×10^5	1.046×10^3
255,000	48.295	31.316	28.90	435.2	2.389×10^4	.1280	6.051×10^{-5}	1.711×10^{-7}	7.484×10^{-5}	5.239×10^{19}	1.380×10^3	4.437×10^{-3}	3.110×10^5	9.984×10^{-3}	1.382×10^5	1.025×10^3
255,902	48.466	31.313	28.90	432.0	2.371×10^4	.1233	5.828×10^{-5}	1.660×10^{-7}	7.260×10^{-5}	5.082×10^{19}	1.375×10^3	4.574×10^{-3}	3.006×10^5	1.029×10^{-2}	1.336×10^5	1.021×10^3
260,000	49.242	31.301	28.90	432.0	2.372×10^4	.1037	4.902×10^{-5}	1.397×10^{-7}	6.110×10^{-5}	4.277×10^{19}	1.375×10^3	5.435×10^{-3}	2.530×10^5	1.223×10^{-2}	1.124×10^5	1.021×10^3
265,000	50.189	31.286	28.90	432.0	2.373×10^4	8.405×10^{-2}	3.972×10^{-5}	1.132×10^{-7}	4.951×10^{-5}	3.466×10^{19}	1.375×10^3	6.707×10^{-3}	2.050×10^5	1.509×10^{-2}	9.112×10^4	1.021×10^3
270,000	51.136	31.271	28.90	432.0	2.374×10^4	6.813×10^{-2}	3.220×10^{-5}	9.174×10^{-8}	4.013×10^{-5}	2.809×10^{19}	1.375×10^3	8.276×10^{-3}	1.662×10^5	1.862×10^{-2}	7.385×10^4	1.021×10^3
272,306	51.573	31.264	28.90	432.0	2.375×10^4	6.184×10^{-2}	2.922×10^{-5}	8.327×10^{-8}	3.642×10^{-5}	2.550×10^{19}	1.375×10^3	9.117×10^{-3}	1.508×10^5	2.051×10^{-2}	6.704×10^4	1.021×10^3
275,000	52.083	31.256	28.79	437.3	2.414×10^4	5.528×10^{-2}	2.612×10^{-5}	7.326×10^{-8}	3.205×10^{-5}	2.252×10^{19}	1.386×10^3	1.032×10^{-2}	1.343×10^5	2.323×10^{-2}	5.968×10^4	1.030×10^3
280,000	53.030	31.242	28.59	447.2	2.487×10^4	4.511×10^{-2}	2.132×10^{-5}	5.807×10^{-8}	2.540×10^{-5}	1.798×10^{19}	1.407×10^3	1.293×10^{-2}	1.088×10^5	2.910×10^{-2}	4.834×10^4	1.046×10^3
285,000	53.977	31.227	28.39	457.0	2.561×10^4	3.703×10^{-2}	1.750×10^{-5}	4.630×10^{-8}	2.025×10^{-5}	1.443×10^{19}	1.427×10^3	1.611×10^{-2}	8.861×10^4	3.624×10^{-2}	3.938×10^4	1.062×10^3
290,000	54.924	31.212	28.19	466.9	2.636×10^4	3.057×10^{-2}	1.445×10^{-5}	3.715×10^{-8}	1.625×10^{-5}	1.166×10^{19}	1.448×10^3	1.993×10^{-2}	7.263×10^4	4.484×10^{-2}	3.228×10^4	1.078×10^3
295,000	55.871	31.197	27.98	476.8	2.713×10^4	2.538×10^{-2}	1.199×10^{-5}	2.998×10^{-8}	1.312×10^{-5}	9.482×10^{18}	1.468×10^3	2.452×10^{-2}	5.988×10^4	5.516×10^{-2}	2.661×10^4	1.094×10^3
300,000	56.818	31.182	27.78	486.6	2.790×10^4	2.117×10^{-2}	1.001×10^{-5}	2.434×10^{-8}	1.064×10^{-5}	7.751×10^{18}	1.488×10^3	2.999×10^{-2}	4.963×10^4	6.748×10^{-2}	2.206×10^4	1.111×10^3
305,000	57.765	31.168	27.58	496.5	2.869×10^4	1.776×10^{-2}	8.391×10^{-6}	1.986×10^{-8}	8.685×10^{-6}	6.371×10^{18}	1.509×10^3	3.649×10^{-2}	4.136×10^4	8.210×10^{-2}	1.838×10^4	1.127×10^3
310,000	58.712	31.153	27.38	506.3	2.949×10^4	1.496×10^{-2}	7.071×10^{-6}	1.629×10^{-8}	7.124×10^{-6}	5.264×10^{18}	1.530×10^3	4.416×10^{-2}	3.464×10^4	9.936×10^{-2}	1.539×10^4	1.143×10^3
315,000	59.659	31.138	27.18	516.2	3.030×10^4	1.267×10^{-2}	5.986×10^{-6}	1.342×10^{-8}	5.872×10^{-6}	4.371×10^{18}	1.550×10^3	5.318×10^{-2}	2.915×10^4	1.196×10^{-1}	1.296×10^4	1.159×10^3
320,000	60.606	31.123	26.97	526.1	3.113×10^4	1.077×10^{-2}	5.089×10^{-6}	1.112×10^{-8}	4.862×10^{-6}	3.646×10^{18}	1.571×10^3	6.375×10^{-2}	2.464×10^4	1.434×10^{-1}	1.095×10^4	1.176×10^3
325,000	61.553	31.109	26.77	535.9	3.197×10^4	9.196×10^{-3}	4.346×10^{-6}	9.248×10^{-9}	4.045×10^{-6}	3.057×10^{18}	1.591×10^3	7.605×10^{-2}	2.092×10^4	1.711×10^{-1}	9.300×10^3	1.192×10^3
330,000	62.500	31.094	26.57	545.8	3.282×10^4	7.886×10^{-3}	3.727×10^{-6}	7.728×10^{-9}	3.380×10^{-6}	2.574×10^{18}	1.612×10^3	9.032×10^{-2}	1.785×10^4	2.032×10^{-1}	7.932×10^3	1.208×10^3
335,000	63.447	31.079	26.37	555.6	3.368×10^4	6.789×10^{-3}	3.208×10^{-6}	6.485×10^{-9}	2.837×10^{-6}	2.176×10^{18}	1.633×10^3	1.068×10^{-1}	1.528×10^4	2.403×10^{-1}	6.794×10^3	1.225×10^3
340,000	64.394	31.065	26.17	565.5	3.456×10^4	5.867×10^{-3}	2.773×10^{-6}	5.465×10^{-9}	2.390×10^{-6}	1.848×10^{18}	1.654×10^3	1.258×10^{-1}	1.314×10^4	2.830×10^{-1}	5.842×10^3	1.242×10^3
345,000	65.341	31.050	25.97	575.4	3.545×10^4	5.089×10^{-3}	2.405×10^{-6}	4.623×10^{-9}	2.022×10^{-6}	1.575×10^{18}	1.674×10^3	1.476×10^{-1}	1.135×10^4	3.320×10^{-1}	5.043×10^3	1.258×10^3
350,000	66.288	31.035	25.76	585.2	3.636×10^4	4.430×10^{-3}	2.093×10^{-6}	3.926×10^{-9}	1.717×10^{-6}	1.348×10^{18}	1.695×10^3	1.724×10^{-1}	9.832×10^3	3.879×10^{-1}	4.370×10^3	1.275×10^3
355,000	67.235	31.020	25.56	595.1	3.728×10^4	3.870×10^{-3}	1.829×10^{-6}	3.346×10^{-9}	1.464×10^{-6}	1.158×10^{18}	1.716×10^3	2.007×10^{-1}	8.550×10^3	4.516×10^{-1}	3.800×10^3	1.292×10^3
360,000	68.182	31.006	25.36	604.9	3.822×10^4	3.391×10^{-3}	1.603×10^{-6}	2.862×10^{-9}	1.252×10^{-6}	9.986×10^{17}	1.737×10^3	2.328×10^{-1}	7.460×10^3	5.238×10^{-1}	3.316×10^3	1.308×10^3
365,000	69.129	30.991	25.16	614.8	3.917×10^4	2.982×10^{-3}	1.409×10^{-6}	2.456×10^{-9}	1.074×10^{-6}	8.640×10^{17}	1.758×10^3	2.691×10^{-1}	6.535×10^3	6.054×10^{-1}	2.904×10^3	1.325×10^3
370,000	70.076	30.977	24.96	624.7	4.014×10^4	2.630×10^{-3}	1.243×10^{-6}	2.115×10^{-9}	9.252×10^{-7}	7.500×10^{17}	1.779×10^3	3.099×10^{-1}	5.741×10^3	6.974×10^{-1}	2.552×10^3	1.342×10^3
375,000	71.023	30.962	24.75	634.5	4.113×10^4	2.327×10^{-3}	1.100×10^{-6}	1.828×10^{-9}	7.994×10^{-7}	6.533×10^{17}	1.801×10^3	2.558×10^{-1}	5.060×10^3	8.006×10^{-1}	2.249×10^3	1.360×10^3
380,000	71.970	30.947	24.55	644.4	4.213×10^4	2.065×10^{-3}	9.758×10^{-7}	1.584×10^{-9}	6.927×10^{-7}	5.708×10^{17}	1.822×10^3	4.073×10^{-1}	4.474×10^3	9.164×10^{-1}	1.988×10^3	1.377×10^3
385,000	72.917	30.933	24.35	654.2	4.315×10^4	1.837×10^{-3}	8.687×10^{-7}	1.377×10^{-9}	6.021×10^{-7}	5.002×10^{17}	1.844×10^3	4.647×10^{-1}	3.967×10^3	1.046	1.763×10^3	1.394×10^3
390,000	73.864	30.918	24.15	664.1	4.418×10^4	1.639×10^{-3}	7.751×10^{-7}	1.200×10^{-9}	5.249×10^{-7}	4.397×10^{17}	1.865×10^3	5.287×10^{-1}	3.528×10^3	1.190	1.568×10^3	1.412×10^3
393,696	74.564	30.907	24.00	671.4	4.496×10^4	1.469×10^{-3}	6.944×10^{-7}	1.057×10^{-9}	4.622×10^{-7}	3.896×10^{17}	1.881×10^3	5.966×10^{-1}	3.153×10^3	1.342	1.401×10^3	1.424×10^3
395,000	74.811	30.904	24.00	675.0	4.521×10^4	1.427×10^{-3}	6.746×10^{-7}	1.021×10^{-9}	4.466×10^{-7}	3.688×10^{17}	1.886×10^3	6.174×10^{-1}	3.055×10^3	1.389	1.358×10^3	1.428×10^3
400,000	75.758	30.889	24.00	689.0	4.617×10^4	1.279×10^{-3}	6.047×10^{-7}	8.968×10^{-10}	3.923×10^{-7}	3.372×10^{17}	1.906×10^3	7.030×10^{-1}	2.711×10^3	1.582	1.205×10^3	1.443×10^3

Table 11 *(Cont'd)*

Latitude, 0°. Engineering Units. p_a = 2115 lb/ft², ρ_a = 2.286 × 10⁻³ slug/ft³

Height h ft	Height h mi	Apparent Gravity g' ft/sec²	Mean Mol Wt M	Temp T °R	Scale Height H ft	Pressure p lb/ft²	Pressure Ratio p/p_a	Density ρ slug/ft³	Density Ratio σ ρ/ρ_a	Number Density n particles/ft³	Mean Particle Speed v ft/sec	$d = 3 \times 10^{-8}$cm Mean Free Path L ft	$d = 3 \times 10^{-8}$cm Mean Collision Freq ν 1/sec	$d = 2 \times 10^{-8}$cm Mean Free Path L ft	$d = 2 \times 10^{-8}$cm Mean Collision Freq ν 1/sec	Speed of Sound c ft/sec
4.500×10^5	85.23	30.744	24.00	828.8	5.580×10^4	4.80×10^{-4}	2.27×10^{-7}	2.80×10^{-10}	1.22×10^{-7}	1.03×10^{17}	2.090×10^3	2.25	9.28×10^2	5.07	4.13×10^2	1.583×10^3
5.000×10^5	94.70	30.600	24.00	968.6	6.552×10^4	2.12×10^{-4}	1.00×10^{-7}	1.06×10^{-10}	4.64×10^{-8}	3.91×10^{16}	2.260×10^3	5.95	3.80×10^2	1.34×10	1.69×10^2	1.711×10^3
5.280×10^5	100.0	30.520	24.00	1047	7.100×10^4	1.40×10^{-4}	6.62×10^{-8}	6.45×10^{-11}	2.82×10^{-8}	2.38×10^{16}	2.349×10^3	9.77	2.40×10^2	2.20×10	1.07×10^2	1.779×10^3
5.500×10^5	104.2	30.457	24.00	1108	7.533×10^4	1.04×10^{-4}	4.92×10^{-8}	4.53×10^{-11}	1.98×10^{-8}	1.67×10^{16}	2.417×10^3	1.39×10	1.74×10^2	3.13×10	7.72×10	
6.000×10^5	113.6	30.315	24.00	1248	8.523×10^4	5.57×10^{-5}	2.63×10^{-8}	2.15×10^{-11}	9.41×10^{-9}	7.93×10^{15}	2.565×10^3	2.93×10	8.75×10	6.60×10	3.89×10	
6.500×10^5	123.1	30.174	24.00	1388	9.522×10^4	3.20×10^{-5}	1.51×10^{-8}	1.11×10^{-11}	4.86×10^{-9}	4.09×10^{15}	2.705×10^3	5.68×10	4.76×10	1.28×10^2	2.12×10	
7.000×10^5	132.6	30.033	24.00	1528	1.053×10^5	1.94×10^{-5}	9.17×10^{-9}	6.13×10^{-12}	2.68×10^{-9}	2.26×10^{15}	2.838×10^3	1.03×10^2	2.76×10	2.31×10^2	1.23×10	
7.500×10^5	142.0	29.894	24.00	1668	1.155×10^5	1.24×10^{-5}	5.86×10^{-9}	3.59×10^{-12}	1.57×10^{-9}	1.32×10^{15}	2.965×10^3	1.76×10^2	1.69×10	3.95×10^2	7.50	
8.000×10^5	151.5	29.756	24.00	1807	1.257×10^5	8.16×10^{-6}	3.86×10^{-9}	2.18×10^{-12}	9.54×10^{-10}	8.04×10^{14}	3.087×10^3	2.89×10^2	1.07×10	6.51×10^2	4.74	
8.500×10^5	161.0	29.619	24.00	1947	1.361×10^5	5.57×10^{-6}	2.63×10^{-9}	1.38×10^{-12}	6.04×10^{-10}	5.09×10^{14}	3.204×10^3	4.57×10^2	7.01	1.03×10^3	3.12	
9.000×10^5	170.4	29.482	24.00	2087	1.465×10^5	3.91×10^{-6}	1.85×10^{-9}	9.05×10^{-13}	3.96×10^{-10}	3.34×10^{14}	3.317×10^3	6.97×10^2	4.76	1.57×10^3	2.12	
9.500×10^5	179.9	29.347	24.00	2227	1.571×10^5	2.81×10^{-6}	1.33×10^{-9}	6.09×10^{-13}	2.66×10^{-10}	2.25×10^{14}	3.426×10^3	1.04×10^3	3.31	2.33×10^3	1.47	
1.000×10^6	189.4	29.212	24.00	2367	1.677×10^5	2.07×10^{-6}	9.79×10^{-10}	4.23×10^{-13}	1.85×10^{-10}	1.56×10^{14}	3.532×10^3	1.49×10^3	2.37	3.35×10^3	1.05	
1.050×10^6	198.9	29.079	24.00	2507	1.784×10^5	1.55×10^{-6}	7.33×10^{-10}	2.99×10^{-13}	1.31×10^{-10}	1.10×10^{14}	3.635×10^3	2.11×10^3	1.72	4.74×10^3	7.66×10^{-1}	
1.056×10^6	200.0	29.063	24.00	2523	1.797×10^5	1.50×10^{-6}	7.09×10^{-10}	2.87×10^{-13}	1.26×10^{-10}	1.06×10^{14}	3.647×10^3	2.20×10^3	1.66	4.94×10^3	7.38×10^{-1}	
1.100×10^6	208.3	28.946	24.00	2646	1.892×10^5	1.18×10^{-6}	5.58×10^{-10}	2.15×10^{-13}	9.41×10^{-11}	7.93×10^{13}	3.735×10^3	2.93×10^3	1.27	6.60×10^3	5.66×10^{-1}	
1.150×10^6	217.8	28.814	24.00	2786	2.001×10^5	9.12×10^{-7}	4.31×10^{-10}	1.58×10^{-13}	6.91×10^{-11}	5.83×10^{13}	3.832×10^3	3.99×10^2	9.60×10^{-1}	8.98×10^3	4.27×10^{-1}	
1.200×10^6	227.3	28.684	24.00	2926	2.111×10^5	7.15×10^{-7}	3.38×10^{-10}	1.18×10^{-13}	5.16×10^{-11}	4.35×10^{13}	3.927×10^3	5.34×10^3	7.35×10^{-1}	1.20×10^4	3.27×10^{-1}	
1.250×10^6	236.7	28.554	24.00	3066	2.222×10^5	5.68×10^{-7}	2.69×10^{-10}	8.95×10^{-14}	3.92×10^{-11}	3.30×10^{13}	4.020×10^3	7.04×10^3	5.71×10^{-1}	1.58×10^4	2.54×10^{-1}	
1.300×10^6	246.2	28.424	24.00	3206	2.334×10^5	4.56×10^{-7}	2.16×10^{-10}	6.87×10^{-14}	3.01×10^{-11}	2.53×10^{13}	4.110×10^3	9.18×10^3	4.48×10^{-1}	2.06×10^4	1.99×10^{-1}	
1.312×10^6	248.6	28.393	24.00	3240	2.362×10^5	4.33×10^{-7}	2.05×10^{-10}	6.45×10^{-14}	2.82×10^{-11}	2.38×10^{13}	4.132×10^3	9.77×10^3	4.23×10^{-1}	2.20×10^4	1.88×10^{-1}	

1 lb/ft² = 0.3591 mm of Hg

Table 12

VALUES OF TEMPERATURE, PRESSURE, AND DENSITY UP TO THE F_2 LAYER

Latitude, 0°. Metric Units. p_a = 1013 mb, $\rho_a = 1.178 \times 10^{-3}$ gm/cm³

Height h km	Height h mi	Apparent Gravity g' cm/sec²	Mean Mol Wt M	Temp T °K	Scale Height H km	Pressure p millibars	Pressure Ratio p/p_a	Density ρ gm/cm³	Density Ratio σ ρ/ρ_a	Number Density n particles/cm³	Mean Particle Speed v cm/sec	$d = 3 \times 10^{-8}$cm Mean Free Path L cm	$d = 3 \times 10^{-8}$cm Mean Collision Freq ν 1/sec	$d = 2 \times 10^{-8}$cm Mean Free Path L cm	$d = 2 \times 10^{-8}$cm Mean Collision Freq ν 1/sec	Speed of Sound c cm/sec
0	0	978.03	28.90	299.0	8.787	1.013×10^{3}	1.0000	1.178×10^{-3}	1.0000	2.472×10^{19}	4.678×10^{4}	1.012×10^{-5}	4.622×10^{9}	2.277×10^{-5}	2.054×10^{9}	3.477×10^{4}
1.524	.947	977.56	28.90	290.5	8.540	8.496×10^{2}	.8389	1.018×10^{-3}	.8636	2.135×10^{19}	4.611×10^{4}	1.172×10^{-5}	3.934×10^{9}	2.637×10^{-5}	1.748×10^{9}	3.425×10^{4}
3.048	1.894	977.09	28.90	281.9	8.294	7.092×10^{2}	.7002	8.750×10^{-4}	.7426	1.836×10^{19}	4.543×10^{4}	1.363×10^{-5}	3.333×10^{9}	3.067×10^{-5}	1.481×10^{9}	3.374×10^{4}
4.572	2.841	976.62	28.90	273.4	8.047	5.888×10^{2}	.5813	7.491×10^{-4}	.6357	1.572×10^{19}	4.474×10^{4}	1.592×10^{-5}	2.810×10^{9}	3.582×10^{-5}	1.249×10^{9}	3.323×10^{4}
5.000	3.107	976.46	28.90	271.0	7.977	5.583×10^{2}	.5511	7.166×10^{-4}	.6081	1.503×10^{19}	4.454×10^{4}	1.665×10^{-5}	2.676×10^{9}	3.745×10^{-5}	1.189×10^{9}	3.308×10^{4}
6.096	3.788	976.16	28.90	263.2	7.751	4.856×10^{2}	.4795	6.419×10^{-4}	.5447	1.347×10^{19}	4.389×10^{4}	1.858×10^{-5}	2.362×10^{9}	4.181×10^{-5}	1.050×10^{9}	3.260×10^{4}
7.620	4.735	975.69	28.90	252.4	7.437	3.975×10^{2}	.3925	5.478×10^{-4}	.4649	1.149×10^{19}	4.298×10^{4}	2.177×10^{-5}	1.974×10^{9}	4.898×10^{-5}	8.775×10^{8}	3.193×10^{4}
9.144	5.682	975.22	28.90	241.6	7.120	3.226×10^{2}	.3185	4.645×10^{-4}	.3942	9.744×10^{18}	4.205×10^{4}	2.568×10^{-5}	1.638×10^{9}	5.778×10^{-5}	7.278×10^{8}	3.124×10^{4}
10.000	6.214	974.96	28.90	235.5	6.943	2.857×10^{2}	.2821	4.220×10^{-4}	.3581	8.853×10^{18}	4.152×10^{4}	2.826×10^{-5}	1.469×10^{9}	6.359×10^{-5}	6.529×10^{8}	3.084×10^{4}
10.668	6.629	974.75	28.90	230.5	6.797	2.593×10^{2}	.2560	3.912×10^{-4}	.3320	8.206×10^{18}	4.108×10^{4}	3.049×10^{-5}	1.347×10^{9}	6.861×10^{-5}	5.988×10^{8}	3.051×10^{4}
12.192	7.576	974.29	28.90	219.2	6.468	2.062×10^{2}	.2036	3.272×10^{-4}	.2777	6.864×10^{18}	4.006×10^{4}	3.645×10^{-5}	1.099×10^{9}	8.202×10^{-5}	4.884×10^{8}	2.976×10^{4}
13.716	8.523	973.82	28.90	207.9	6.139	1.619×10^{2}	.1599	2.709×10^{-4}	.2299	5.683×10^{18}	3.901×10^{4}	4.403×10^{-5}	8.861×10^{8}	9.906×10^{-5}	3.938×10^{8}	2.898×10^{4}
15.240	9.470	973.35	28.90	196.6	5.803	1.256×10^{2}	.1240	2.221×10^{-4}	.1885	4.660×10^{18}	3.794×10^{4}	5.370×10^{-5}	7.065×10^{8}	1.208×10^{-4}	3.140×10^{8}	2.818×10^{4}
16.000	9.942	973.12	28.90	191.0	5.642	1.100×10^{2}	.1086	2.003×10^{-4}	.1700	4.203×10^{18}	3.739×10^{4}	5.954×10^{-5}	6.280×10^{8}	1.340×10^{-4}	2.791×10^{8}	2.777×10^{4}
16.764	10.417	972.88	28.90	193.2	5.709	9.617×10	9.494×10^{-2}	1.732×10^{-4}	.1469	3.633×10^{18}	3.760×10^{4}	6.888×10^{-5}	5.459×10^{8}	1.550×10^{-4}	2.426×10^{8}	2.793×10^{4}
18.288	11.364	972.42	28.90	197.5	5.840	7.390×10	7.296×10^{-2}	1.301×10^{-4}	.1104	2.730×10^{18}	3.803×10^{4}	9.166×10^{-5}	4.149×10^{8}	2.062×10^{-4}	1.844×10^{8}	2.824×10^{4}
19.812	12.311	971.96	28.90	201.9	5.971	5.713×10	5.640×10^{-2}	9.842×10^{-5}	8.352×10^{-2}	2.065×10^{18}	3.844×10^{4}	1.212×10^{-4}	3.172×10^{8}	2.727×10^{-4}	1.410×10^{8}	2.855×10^{4}
21.336	13.258	971.49	28.90	206.2	6.102	4.441×10	4.385×10^{-2}	7.490×10^{-5}	6.356×10^{-2}	1.571×10^{18}	3.886×10^{4}	1.592×10^{-4}	2.440×10^{8}	3.583×10^{-4}	1.084×10^{8}	2.886×10^{4}
22.860	14.205	971.02	28.90	210.6	6.233	3.472×10	3.428×10^{-2}	5.735×10^{-5}	4.867×10^{-2}	1.203×10^{18}	3.926×10^{4}	2.080×10^{-4}	1.888×10^{8}	4.680×10^{-4}	8.390×10^{7}	2.916×10^{4}
24.384	15.152	970.56	28.90	215.0	6.367	2.729×10	2.694×10^{-2}	4.416×10^{-5}	3.747×10^{-2}	9.263×10^{17}	3.967×10^{4}	2.701×10^{-4}	1.468×10^{8}	6.078×10^{-4}	6.527×10^{7}	2.946×10^{4}
25.908	16.098	970.10	28.90	219.3	6.501	2.156×10	2.129×10^{-2}	3.420×10^{-5}	2.903×10^{-2}	7.175×10^{17}	4.007×10^{4}	3.487×10^{-4}	1.149×10^{8}	7.846×10^{-4}	5.106×10^{7}	2.976×10^{4}
27.432	17.045	969.63	28.90	223.7	6.629	1.711×10	1.689×10^{-2}	2.660×10^{-5}	2.258×10^{-2}	5.581×10^{17}	4.046×10^{4}	4.483×10^{-4}	9.025×10^{7}	1.009×10^{-3}	4.011×10^{7}	3.005×10^{4}
28.956	17.992	969.17	28.90	228.0	6.764	1.364×10	1.347×10^{-2}	2.081×10^{-5}	1.766×10^{-2}	4.366×10^{17}	4.085×10^{4}	5.731×10^{-4}	7.128×10^{7}	1.290×10^{-3}	3.168×10^{7}	3.035×10^{4}
30.000	18.641	968.85	28.90	231.0	6.855	1.171×10	1.156×10^{-2}	1.764×10^{-5}	1.497×10^{-2}	3.700×10^{17}	4.112×10^{4}	6.762×10^{-4}	6.081×10^{7}	1.521×10^{-3}	2.703×10^{7}	3.054×10^{4}
30.480	18.939	968.71	28.90	234.0	6.943	1.093×10	1.079×10^{-2}	1.624×10^{-5}	1.378×10^{-2}	3.408×10^{17}	4.138×10^{4}	7.342×10^{-4}	5.636×10^{7}	1.652×10^{-3}	2.505×10^{7}	3.074×10^{4}
32.004	19.886	968.24	28.90	243.4	7.227	8.815	8.703×10^{-3}	1.262×10^{-5}	1.071×10^{-2}	2.649×10^{17}	4.221×10^{4}	9.447×10^{-4}	4.468×10^{7}	2.126×10^{-3}	1.986×10^{7}	3.135×10^{4}
33.528	20.833	967.78	28.90	252.9	7.510	7.171	7.080×10^{-3}	9.864×10^{-6}	8.371×10^{-3}	2.069×10^{17}	4.302×10^{4}	1.209×10^{-3}	3.558×10^{7}	2.721×10^{-3}	1.581×10^{7}	3.196×10^{4}
35.052	21.780	967.32	28.90	262.3	7.794	5.879	5.804×10^{-3}	7.796×10^{-6}	6.616×10^{-3}	1.635×10^{17}	4.382×10^{4}	1.530×10^{-3}	2.864×10^{7}	3.442×10^{-3}	1.273×10^{7}	3.255×10^{4}
36.576	22.727	966.86	28.90	271.8	8.080	4.855	4.793×10^{-3}	6.214×10^{-6}	5.273×10^{-3}	1.304×10^{17}	4.460×10^{4}	1.919×10^{-3}	2.324×10^{7}	4.319×10^{-3}	1.033×10^{7}	3.313×10^{4}
38.100	23.674	966.40	28.90	281.2	8.364	4.037	3.985×10^{-3}	4.993×10^{-6}	4.237×10^{-3}	1.047×10^{17}	4.537×10^{4}	2.389×10^{-3}	1.899×10^{7}	5.375×10^{-3}	8.441×10^{6}	3.370×10^{4}
39.624	24.621	965.93	28.90	290.7	8.650	3.377	3.334×10^{-3}	4.041×10^{-6}	3.429×10^{-3}	8.478×10^{16}	4.613×10^{4}	2.951×10^{-3}	1.563×10^{7}	6.641×10^{-3}	6.946×10^{6}	3.426×10^{4}
41.148	25.568	965.47	28.90	300.1	8.937	2.842	2.806×10^{-3}	3.294×10^{-6}	2.795×10^{-3}	6.910×10^{16}	4.687×10^{4}	3.621×10^{-3}	1.294×10^{7}	8.148×10^{-3}	5.752×10^{6}	3.481×10^{4}
42.673	26.515	965.01	28.90	309.6	9.220	2.405	2.374×10^{-3}	2.702×10^{-6}	2.293×10^{-3}	5.669×10^{16}	4.760×10^{4}	4.414×10^{-3}	1.078×10^{7}	9.932×10^{-3}	4.793×10^{6}	3.536×10^{4}
44.197	27.462	964.55	28.90	319.0	9.504	2.046	2.020×10^{-3}	2.230×10^{-6}	1.893×10^{-3}	4.679×10^{16}	4.832×10^{4}	5.347×10^{-3}	9.037×10^{6}	1.203×10^{-2}	4.016×10^{6}	3.589×10^{4}
45.721	28.409	964.09	28.90	328.5	9.793	1.749	1.726×10^{-3}	1.852×10^{-6}	1.571×10^{-3}	3.884×10^{16}	4.903×10^{4}	6.442×10^{-3}	7.612×10^{6}	1.449×10^{-2}	3.383×10^{6}	3.642×10^{4}
47.245	29.356	963.63	28.90	337.9	10.08	1.502	1.482×10^{-3}	1.546×10^{-6}	1.312×10^{-3}	3.243×10^{16}	4.973×10^{4}	7.717×10^{-3}	6.445×10^{6}	1.736×10^{-2}	2.864×10^{6}	3.694×10^{4}
48.769	30.303	963.17	28.90	347.4	10.37	1.295	1.279×10^{-3}	1.297×10^{-6}	1.101×10^{-3}	2.721×10^{16}	5.043×10^{4}	9.196×10^{-3}	5.484×10^{6}	2.069×10^{-2}	2.437×10^{6}	3.745×10^{4}
50.000	31.068	962.80	28.90	355.0	10.60	1.153	1.138×10^{-3}	1.129×10^{-6}	9.584×10^{-4}	2.369×10^{16}	5.097×10^{4}	1.056×10^{-2}	4.827×10^{6}	2.376×10^{-2}	2.145×10^{6}	3.787×10^{4}
50.293	31.250	962.71	28.90	355.0	10.60	1.121	1.107×10^{-3}	1.099×10^{-6}	9.324×10^{-4}	2.305×10^{16}	5.097×10^{4}	1.086×10^{-2}	4.696×10^{6}	2.442×10^{-2}	2.087×10^{6}	3.787×10^{4}
51.817	32.197	962.25	28.90	355.0	10.60	9.714×10^{-1}	9.590×10^{-4}	9.517×10^{-7}	8.077×10^{-4}	1.997×10^{16}	5.097×10^{4}	1.253×10^{-2}	4.068×10^{6}	2.820×10^{-2}	1.808×10^{6}	3.787×10^{4}
53.341	33.144	961.79	28.90	355.0	10.61	8.416×10^{-1}	8.295×10^{-4}	8.246×10^{-7}	6.998×10^{-4}	1.730×10^{16}	5.097×10^{4}	1.446×10^{-2}	3.524×10^{6}	3.254×10^{-2}	1.566×10^{6}	3.787×10^{4}
54.865	34.091	961.34	28.90	355.0	10.62	7.293×10^{-1}	7.200×10^{-4}	7.145×10^{-7}	6.064×10^{-4}	1.499×10^{16}	5.097×10^{4}	1.669×10^{-2}	3.054×10^{6}	3.756×10^{-2}	1.357×10^{6}	3.787×10^{4}
56.389	35.038	960.88	28.90	355.0	10.62	6.320×10^{-1}	6.239×10^{-4}	6.192×10^{-7}	5.255×10^{-4}	1.299×10^{16}	5.097×10^{4}	1.926×10^{-2}	2.646×10^{6}	4.334×10^{-2}	1.176×10^{6}	3.787×10^{4}
57.913	35.985	960.42	28.90	355.0	10.63	5.477×10^{-1}	5.408×10^{-4}	5.367×10^{-7}	4.555×10^{-4}	1.126×10^{16}	5.097×10^{4}	2.222×10^{-2}	2.294×10^{6}	5.000×10^{-2}	1.020×10^{6}	3.787×10^{4}
[illegible]	[illegible]	959.96	28.90	355.0	10.63	4.748×10^{-1}	4.688×10^{-4}	4.653×10^{-7}	3.948×10^{-4}	9.760×10^{15}	5.097×10^{4}	2.564×10^{-2}	1.988×10^{6}	5.768×10^{-2}	8.837×10^{5}	3.787×10^{4}

Table 12 *(Cont'd)*

Latitude, 0°. Metric Units. p_a = 1013 mb, ρ_a = 1.178 × 10^{-3} gm/cm³

Height h km	Height h mi	Apparent Gravity g' cm/sec²	Mean Mol Wt M	Temp T °K	Scale Height H km	Pressure p millibars	Pressure Ratio p/p_a	Density ρ gm/cm³	Density Ratio σ ρ/ρ_a	Number Density n particles/cm³	Mean Particle Speed v cm/sec	$d = 3 \times 10^{-8}$ cm: Mean Free Path L cm	$d = 3 \times 10^{-8}$ cm: Mean Collision Freq ν 1/sec	$d = 2 \times 10^{-8}$ cm: Mean Free Path L cm	$d = 2 \times 10^{-8}$ cm: Mean Collision Freq ν 1/sec	Speed of Sound c cm/sec
60.000	37.282	959.80	28.90	355.0	10.63	4.504×10^{-1}	4.447×10^{-4}	4.413×10^{-7}	3.745×10^{-4}	9.258×10^{15}	5.097×10^{4}	2.703×10^{-2}	1.886×10^{6}	6.081×10^{-2}	8.383×10^{5}	3.787×10^{4}
60.961	37.879	959.51	28.90	348.9	10.45	4.112×10^{-1}	4.060×10^{-4}	4.100×10^{-7}	3.480×10^{-4}	8.602×10^{15}	5.053×10^{4}	2.909×10^{-2}	1.737×10^{6}	6.545×10^{-2}	7.720×10^{5}	3.754×10^{4}
62.485	38.826	959.05	28.90	339.1	10.17	3.548×10^{-1}	3.502×10^{-4}	3.639×10^{-7}	3.088×10^{-4}	7.634×10^{15}	4.982×10^{4}	3.278×10^{-2}	1.520×10^{6}	7.374×10^{-2}	6.756×10^{5}	3.701×10^{4}
64.009	39.773	958.60	28.90	329.4	9.879	3.048×10^{-1}	3.009×10^{-4}	3.219×10^{-7}	2.732×10^{-4}	6.753×10^{15}	4.910×10^{4}	3.705×10^{-2}	1.325×10^{6}	8.337×10^{-2}	5.890×10^{5}	3.647×10^{4}
65.533	40.720	958.14	28.90	319.7	9.589	2.607×10^{-1}	2.574×10^{-4}	2.837×10^{-7}	2.408×10^{-4}	5.952×10^{15}	4.837×10^{4}	4.204×10^{-2}	1.151×10^{6}	9.459×10^{-2}	5.114×10^{5}	3.593×10^{4}
67.057	41.667	957.68	28.90	309.9	9.302	2.220×10^{-1}	2.192×10^{-4}	2.491×10^{-7}	2.114×10^{-4}	5.227×10^{15}	4.763×10^{4}	4.788×10^{-2}	9.948×10^{5}	1.077×10^{-1}	4.422×10^{5}	3.538×10^{4}
68.581	42.614	957.23	28.90	300.2	9.013	1.881×10^{-1}	1.857×10^{-4}	2.179×10^{-7}	1.849×10^{-4}	4.571×10^{15}	4.688×10^{4}	5.473×10^{-2}	8.564×10^{5}	1.232×10^{-1}	3.806×10^{5}	3.482×10^{4}
70.105	43.561	956.77	28.90	290.4	8.726	1.585×10^{-1}	1.564×10^{-4}	1.898×10^{-7}	1.611×10^{-4}	3.981×10^{15}	4.611×10^{4}	6.285×10^{-2}	7.336×10^{5}	1.414×10^{-1}	3.261×10^{5}	3.425×10^{4}
71.629	44.508	956.32	28.90	280.7	8.437	1.328×10^{-1}	1.311×10^{-4}	1.645×10^{-7}	1.396×10^{-4}	3.452×10^{15}	4.533×10^{4}	7.249×10^{-2}	6.253×10^{5}	1.631×10^{-1}	2.779×10^{5}	3.367×10^{4}
73.153	45.455	955.86	28.90	271.0	8.147	1.106×10^{-1}	1.092×10^{-4}	1.420×10^{-7}	1.205×10^{-4}	2.978×10^{15}	4.454×10^{4}	8.402×10^{-2}	5.301×10^{5}	1.890×10^{-1}	2.356×10^{5}	3.308×10^{4}
74.677	46.402	955.41	28.90	261.2	7.861	9.149×10^{-2}	9.033×10^{-5}	1.218×10^{-7}	1.034×10^{-4}	2.556×10^{15}	4.373×10^{4}	9.790×10^{-2}	4.466×10^{5}	2.203×10^{-1}	1.985×10^{5}	3.248×10^{4}
76.201	47.348	954.96	28.90	251.5	7.571	7.517×10^{-2}	7.421×10^{-5}	1.040×10^{-7}	8.823×10^{-5}	2.181×10^{15}	4.291×10^{4}	1.147×10^{-1}	3.740×10^{5}	2.581×10^{-1}	1.662×10^{5}	3.187×10^{4}
77.725	48.295	954.51	28.90	241.8	7.282	6.129×10^{-2}	6.051×10^{-5}	8.818×10^{-8}	7.484×10^{-5}	1.850×10^{15}	4.207×10^{4}	1.353×10^{-1}	3.110×10^{5}	3.043×10^{-1}	1.382×10^{5}	3.125×10^{4}
78.000	48.466	954.42	28.90	240.0	7.227	5.903×10^{-2}	5.828×10^{-5}	8.555×10^{-8}	7.260×10^{-5}	1.795×10^{15}	4.191×10^{4}	1.394×10^{-1}	3.006×10^{5}	3.137×10^{-1}	1.336×10^{5}	3.113×10^{4}
79.249	49.242	954.06	28.90	240.0	7.230	4.967×10^{-2}	4.902×10^{-5}	7.200×10^{-8}	6.110×10^{-5}	1.510×10^{15}	4.191×10^{4}	1.657×10^{-1}	2.530×10^{5}	3.728×10^{-1}	1.124×10^{5}	3.113×10^{4}
80.773	50.189	953.61	28.90	240.0	7.233	4.026×10^{-2}	3.972×10^{-5}	5.834×10^{-8}	4.951×10^{-5}	1.224×10^{15}	4.191×10^{4}	2.044×10^{-1}	2.050×10^{5}	4.600×10^{-1}	9.112×10^{4}	3.113×10^{4}
82.279	51.136	953.16	28.90	240.0	7.239	3.263×10^{-2}	3.220×10^{-5}	4.729×10^{-8}	4.013×10^{-5}	9.920×10^{14}	4.191×10^{4}	2.522×10^{-1}	1.662×10^{5}	5.675×10^{-1}	7.385×10^{4}	3.113×10^{4}
83.000	51.573	952.95	28.90	240.0	7.239	2.962×10^{-2}	2.922×10^{-5}	4.292×10^{-8}	3.642×10^{-5}	9.005×10^{14}	4.191×10^{4}	2.779×10^{-1}	1.508×10^{5}	6.252×10^{-1}	6.704×10^{4}	3.113×10^{4}
83.821	52.083	952.70	28.79	243.0	7.358	2.648×10^{-2}	2.612×10^{-5}	3.776×10^{-8}	3.205×10^{-5}	7.952×10^{14}	4.225×10^{4}	3.146×10^{-1}	1.343×10^{5}	7.080×10^{-1}	5.968×10^{4}	3.140×10^{4}
85.343	53.030	952.25	28.59	248.4	7.580	2.160×10^{-2}	2.132×10^{-5}	2.993×10^{-8}	2.540×10^{-5}	6.348×10^{14}	4.287×10^{4}	3.942×10^{-1}	1.088×10^{5}	8.869×10^{-1}	4.834×10^{4}	3.189×10^{4}
86.869	53.977	951.80	28.39	253.9	7.806	1.774×10^{-2}	1.750×10^{-5}	2.387×10^{-8}	2.025×10^{-5}	5.097×10^{14}	4.350×10^{4}	4.909×10^{-1}	8.861×10^{4}	1.105	3.938×10^{4}	3.238×10^{4}
88.393	54.924	951.35	28.19	259.4	8.035	1.464×10^{-2}	1.445×10^{-5}	1.915×10^{-8}	1.625×10^{-5}	4.119×10^{14}	4.412×10^{4}	6.075×10^{-1}	7.263×10^{4}	1.367	3.228×10^{4}	3.287×10^{4}
89.917	55.871	950.90	27.98	264.9	8.269	1.215×10^{-2}	1.199×10^{-5}	1.546×10^{-8}	1.312×10^{-5}	3.348×10^{14}	4.475×10^{4}	7.473×10^{-1}	5.988×10^{4}	1.681	2.661×10^{4}	3.336×10^{4}
90.441	56.818	950.45	27.78	270.3	8.504	1.014×10^{-2}	1.001×10^{-5}	1.254×10^{-8}	1.064×10^{-5}	2.737×10^{14}	4.537×10^{4}	9.141×10^{-1}	4.963×10^{4}	2.057	2.206×10^{4}	3.385×10^{4}
92.965	57.765	950.00	27.58	275.8	8.745	8.504×10^{-3}	8.391×10^{-6}	1.023×10^{-8}	8.685×10^{-6}	2.250×10^{14}	4.599×10^{4}	1.112	4.136×10^{4}	2.502	1.838×10^{4}	3.435×10^{4}
94.489	58.712	949.55	27.38	281.3	8.989	7.166×10^{-3}	7.071×10^{-6}	8.395×10^{-9}	7.124×10^{-6}	1.860×10^{14}	4.662×10^{4}	1.346	3.464×10^{4}	3.029	1.539×10^{4}	3.484×10^{4}
96.013	59.659	949.10	27.18	286.8	9.235	6.067×10^{-3}	5.986×10^{-6}	6.920×10^{-9}	5.872×10^{-6}	1.544×10^{14}	4.725×10^{4}	1.621	2.915×10^{4}	3.647	1.296×10^{4}	3.534×10^{4}
97.537	60.606	948.65	26.97	292.3	9.488	5.158×10^{-3}	5.089×10^{-6}	5.730×10^{-9}	4.862×10^{-6}	1.288×10^{14}	4.788×10^{4}	1.943	2.464×10^{4}	4.372	1.095×10^{4}	3.583×10^{4}
99.061	61.553	948.20	26.77	297.7	9.744	4.404×10^{-3}	4.346×10^{-6}	4.767×10^{-9}	4.045×10^{-6}	1.079×10^{14}	4.850×10^{4}	2.318	2.092×10^{4}	5.215	9.300×10^{3}	3.633×10^{4}
100.58	62.500	947.75	26.57	303.2	1.000×10	3.777×10^{-3}	3.727×10^{-6}	3.983×10^{-9}	3.380×10^{-6}	9.089×10^{13}	4.913×10^{4}	2.753	1.785×10^{4}	6.194	7.932×10^{3}	3.683×10^{4}
102.11	63.447	947.30	26.37	308.7	1.027×10	3.251×10^{-3}	3.208×10^{-6}	3.343×10^{-9}	2.837×10^{-6}	7.686×10^{13}	4.977×10^{4}	3.256	1.528×10^{4}	7.325	6.794×10^{3}	3.734×10^{4}
103.63	64.394	946.86	26.17	314.2	1.053×10	2.810×10^{-3}	2.773×10^{-6}	2.817×10^{-9}	2.390×10^{-6}	6.526×10^{13}	5.040×10^{4}	3.834	1.314×10^{4}	8.626	5.842×10^{3}	3.784×10^{4}
105.16	65.341	946.41	25.97	319.6	1.081×10	2.437×10^{-3}	2.405×10^{-6}	2.383×10^{-9}	2.022×10^{-6}	5.563×10^{13}	5.103×10^{4}	4.497	1.135×10^{4}	1.012×10	5.043×10^{3}	3.835×10^{4}
106.68	66.288	945.97	25.76	325.1	1.108×10	2.122×10^{-3}	2.093×10^{-6}	2.023×10^{-9}	1.717×10^{-6}	4.761×10^{13}	5.167×10^{4}	5.255	9.832×10^{3}	1.182×10	4.370×10^{3}	3.886×10^{4}
108.20	67.235	945.51	25.56	330.6	1.136×10	1.853×10^{-3}	1.829×10^{-6}	1.725×10^{-9}	1.464×10^{-6}	4.090×10^{13}	5.231×10^{4}	6.118	8.550×10^{3}	1.376×10	3.800×10^{3}	3.937×10^{4}
109.73	68.182	945.07	25.36	336.1	1.165×10	1.624×10^{-3}	1.603×10^{-6}	1.475×10^{-9}	1.252×10^{-6}	3.526×10^{13}	5.294×10^{4}	7.096	7.460×10^{3}	1.596×10	3.316×10^{3}	3.988×10^{4}
111.25	69.129	944.62	25.16	341.6	1.194×10	1.428×10^{-3}	1.409×10^{-6}	1.266×10^{-9}	1.074×10^{-6}	3.051×10^{13}	5.359×10^{4}	8.201	6.535×10^{3}	1.845×10	2.904×10^{3}	4.040×10^{4}
112.78	70.076	944.18	24.96	347.0	1.223×10	1.260×10^{-3}	1.243×10^{-6}	1.090×10^{-9}	9.252×10^{-7}	2.649×10^{13}	5.424×10^{4}	9.447	5.741×10^{3}	2.126×10	2.552×10^{3}	4.092×10^{4}
114.30	71.023	943.73	24.75	352.5	1.254×10	1.114×10^{-3}	1.100×10^{-6}	9.419×10^{-10}	7.994×10^{-7}	2.307×10^{13}	5.489×10^{4}	1.085×10	5.060×10^{3}	2.440×10	2.249×10^{3}	4.144×10^{4}
115.82	71.970	943.29	24.55	358.0	1.284×10	9.889×10^{-4}	9.758×10^{-7}	8.163×10^{-10}	6.927×10^{-7}	2.016×10^{13}	5.554×10^{4}	1.241×10	4.474×10^{3}	2.793×10	1.988×10^{3}	4.196×10^{4}
117.35	72.917	942.84	24.35	363.5	1.315×10	8.799×10^{-4}	8.687×10^{-7}	7.095×10^{-10}	6.021×10^{-7}	1.767×10^{13}	5.619×10^{4}	1.416×10	3.967×10^{3}	3.187×10	1.763×10^{3}	4.249×10^{4}
118.87	73.864	942.40	24.15	369.0	1.347×10	7.851×10^{-4}	7.751×10^{-7}	6.185×10^{-10}	5.249×10^{-7}	1.553×10^{13}	5.685×10^{4}	1.611×10	3.528×10^{3}	3.626×10	1.568×10^{3}	4.302×10^{4}
120.00	74.564	942.07	24.00	373.0	1.370×10	7.034×10^{-4}	6.944×10^{-7}	5.447×10^{-10}	4.622×10^{-7}	1.376×10^{13}	5.734×10^{4}	1.818×10	3.153×10^{3}	4.092×10	1.401×10^{3}	4.342×10^{4}
120.40	74.811	941.95	24.00	375.0	1.378×10	6.833×10^{-4}	6.746×10^{-7}	5.263×10^{-10}	4.466×10^{-7}	1.330×10^{13}	5.749×10^{4}	1.882×10	3.055×10^{3}	4.235×10	1.358×10^{3}	4.354×10^{4}
121.92	75.758	941.50	24.00	382.8	1.407×10	6.125×10^{-4}	6.047×10^{-7}	4.622×10^{-10}	3.923×10^{-7}	1.168×10^{13}	5.809×10^{4}	2.143×10	2.711×10^{3}	4.821×10	1.205×10^{3}	4.398×10^{4}

Table 12 *(Cont'd)*

Latitude, 0°. Metric Units. p_a = 1013 mb, ρ_a = 1.178×10^{-3} gm/cm³

Height h km	Height h mi	Apparent Gravity g' cm/sec²	Mean Mol Wt M	Temp T °K	Scale Height H km	Pressure p millibars	Pressure Ratio p/p_a	Density ρ gm/cm³	Density Ratio σ ρ/ρ_a	Number Density n particles/cm³	Mean Particle Speed v cm/sec	$d = 3 \times 10^{-8}$ cm: Mean Free Path L cm	$d = 3 \times 10^{-8}$ cm: Mean Collision Freq ν 1/sec	$d = 2 \times 10^{-8}$ cm: Mean Free Path L cm	$d = 2 \times 10^{-8}$ cm: Mean Collision Freq ν 1/sec	Speed of Sound c cm/sec
137.2	85.23	937.08	24.00	460.5	1.701×10	2.30×10^{-4}	2.27×10^{-7}	1.44×10^{-10}	1.22×10^{-7}	3.64×10^{12}	6.37×10^{4}	6.86×10	9.28×10^{2}	1.54×10^{2}	4.13×10^{2}	4.82×10^{4}
154.2	94.70	932.69	24.00	538.1	1.997×10	1.02×10^{-4}	1.00×10^{-7}	5.46×10^{-11}	4.64×10^{-8}	1.38×10^{12}	6.89×10^{4}	1.81×10^{2}	3.80×10^{2}	4.08×10^{2}	1.69×10^{2}	5.21×10^{4}
160.9	100.0	930.25	24.00	581.6	2.164×10	6.71×10^{-5}	6.62×10^{-8}	3.32×10^{-11}	2.82×10^{-8}	8.40×10^{11}	7.16×10^{4}	2.98×10^{2}	2.40×10^{2}	6.70×10^{2}	1.07×10^{2}	5.42×10^{4}
167.6	104.2	928.33	24.00	615.8	2.296×10	4.98×10^{-5}	4.92×10^{-8}	2.33×10^{-11}	1.98×10^{-8}	5.90×10^{11}	7.37×10^{4}	4.24×10^{2}	1.74×10^{2}	9.55×10^{2}	7.72×10	
182.9	113.6	924.00	24.00	693.5	2.598×10	2.67×10^{-5}	2.63×10^{-8}	1.11×10^{-11}	9.41×10^{-9}	2.80×10^{11}	7.82×10^{4}	8.94×10^{2}	8.75×10	2.01×10^{3}	3.89×10	
198.1	123.1	919.67	24.00	771.1	2.902×10	1.53×10^{-5}	1.51×10^{-8}	5.72×10^{-12}	4.86×10^{-9}	1.44×10^{11}	8.24×10^{4}	1.73×10^{3}	4.76×10	3.90×10^{3}	2.12×10	
213.4	132.6	915.41	24.00	848.8	3.210×10	9.29×10^{-6}	9.17×10^{-9}	3.16×10^{-12}	2.68×10^{-9}	7.98×10^{10}	8.65×10^{4}	3.13×10^{3}	2.76×10	7.05×10^{3}	1.23×10	
228.6	142.0	911.17	24.00	926.5	3.520×10	5.94×10^{-6}	5.86×10^{-9}	1.85×10^{-12}	1.57×10^{-9}	4.66×10^{10}	9.04×10^{4}	5.35×10^{3}	1.69×10	1.20×10^{4}	7.50	
243.8	151.5	906.93	24.00	1004	3.832×10	3.91×10^{-6}	3.86×10^{-9}	1.12×10^{-12}	9.54×10^{-10}	2.84×10^{10}	9.41×10^{4}	8.82×10^{3}	1.07×10	1.98×10^{4}	4.74	
259.1	161.0	902.76	24.00	1082	4.148×10	2.67×10^{-6}	2.63×10^{-9}	7.11×10^{-13}	6.04×10^{-10}	1.80×10^{10}	9.76×10^{4}	1.39×10^{4}	7.01	3.13×10^{4}	3.12	
274.3	170.4	898.61	24.00	1160	4.466×10	1.87×10^{-6}	1.85×10^{-9}	4.66×10^{-13}	3.96×10^{-10}	1.18×10^{10}	1.01×10^{5}	2.12×10^{4}	4.76	4.78×10^{4}	2.12	
289.6	179.9	894.50	24.00	1237	4.787×10	1.35×10^{-6}	1.33×10^{-9}	3.14×10^{-13}	2.66×10^{-10}	7.95×10^{9}	1.04×10^{5}	3.16×10^{4}	3.31	7.10×10^{4}	1.47	
304.8	189.4	890.38	24.00	1315	5.111×10	9.91×10^{-7}	9.79×10^{-10}	2.18×10^{-13}	1.85×10^{-10}	5.51×10^{9}	1.08×10^{5}	4.54×10^{4}	2.37	1.02×10^{5}	1.05	
320.0	198.9	886.33	24.00	1393	5.438×10	7.42×10^{-7}	7.33×10^{-10}	1.54×10^{-13}	1.31×10^{-10}	3.88×10^{9}	1.11×10^{5}	6.43×10^{4}	1.72	1.45×10^{5}	7.66×10^{-1}	
321.9	200.0	885.84	24.00	1402	5.478×10	7.18×10^{-7}	7.09×10^{-10}	1.48×10^{-13}	1.26×10^{-10}	3.74×10^{9}	1.11×10^{5}	6.70×10^{4}	1.66	1.51×10^{5}	7.38×10^{-1}	
335.3	208.3	882.27	24.00	1470	5.768×10	5.65×10^{-7}	5.58×10^{-10}	1.11×10^{-13}	9.41×10^{-11}	2.80×10^{9}	1.14×10^{5}	8.94×10^{4}	1.27	2.01×10^{5}	5.66×10^{-1}	
350.5	217.8	878.28	24.00	1548	6.100×10	4.37×10^{-7}	4.31×10^{-10}	8.14×10^{-14}	6.91×10^{-11}	2.06×10^{9}	1.17×10^{5}	1.22×10^{5}	9.60×10^{-1}	2.74×10^{5}	4.27×10^{-1}	
365.8	227.3	874.26	24.00	1626	6.436×10	3.42×10^{-7}	3.38×10^{-10}	6.08×10^{-14}	5.16×10^{-11}	1.54×10^{9}	1.20×10^{5}	1.63×10^{5}	7.35×10^{-1}	3.66×10^{5}	3.27×10^{-1}	
381.0	236.7	870.30	24.00	1703	6.774×10	2.72×10^{-7}	2.69×10^{-10}	4.61×10^{-14}	3.92×10^{-11}	1.17×10^{9}	1.23×10^{5}	2.15×10^{5}	5.71×10^{-1}	4.83×10^{5}	2.54×10^{-1}	
396.2	246.2	866.39	24.00	1781	7.115×10	2.18×10^{-7}	2.16×10^{-10}	3.54×10^{-14}	3.01×10^{-11}	8.93×10^{8}	1.25×10^{5}	2.80×10^{5}	4.48×10^{-1}	6.29×10^{5}	1.99×10^{-1}	
400.0	248.6	865.42	24.00	1800	7.199×10	2.07×10^{-7}	2.05×10^{-10}	3.32×10^{-14}	2.82×10^{-11}	8.40×10^{8}	1.26×10^{5}	2.98×10^{5}	4.23×10^{-1}	6.70×10^{5}	1.88×10^{-1}	

1 millibar (mb) = 10^3 dynes/cm² = 0.750 mm of Hg

Table 13

VALUES OF TEMPERATURE, PRESSURE, AND DENSITY UP TO THE F_2 LAYER

Latitude, 45°. Engineering Units. p_a = 2116 lb/ft², ρ_a = 2.375 × 10⁻³ slug/ft³.

Height h ft	Height h mi	Apparent Gravity g' ft/sec²	Mean Mol Wt M	Temp T °R	Scale Height H ft	Pressure P lb/ft²	Pressure Ratio P/P_a	Density ρ slug/ft³	Density Ratio σ ρ/ρ_a	Number Density n particles/ft³	Mean Particle Speed v ft/sec	$d = 3 \times 10^{-8}$cm Mean Free Path L ft	$d = 3 \times 10^{-8}$cm Mean Collision Freq ν 1/sec	$d = 2 \times 10^{-8}$cm Mean Free Path L ft	$d = 2 \times 10^{-8}$cm Mean Collision Freq ν 1/sec	Speed of Sound c ft/sec
0	0	32.174	28.90	518.4	2.770×10^4	2116	1.0000	2.375×10^{-3}	1.0000	7.272×10^{23}	1.506×10^3	3.197×10^{-7}	4.712×10^9	7.193×10^{-7}	2.094×10^9	1.119×10^3
5,000	.947	32.159	28.90	500.6	2.676×10^4	1761	.8322	2.047×10^{-3}	.8619	6.268×10^{23}	1.480×10^3	3.709×10^{-7}	3.991×10^9	8.345×10^{-7}	1.774×10^9	1.100×10^3
10,000	1.894	32.144	28.90	482.7	2.582×10^4	1456	.6882	1.755×10^{-3}	.7390	5.374×10^{23}	1.454×10^3	4.325×10^{-7}	3.362×10^9	9.732×10^{-7}	1.494×10^9	1.080×10^3
15,000	2.841	32.128	28.90	464.9	2.487×10^4	1196	.5650	1.496×10^{-3}	.6301	4.582×10^{23}	1.427×10^3	5.074×10^{-7}	2.813×10^9	1.142×10^{-6}	1.250×10^9	1.060×10^3
20,000	3.788	32.113	28.90	447.1	2.393×10^4	974.6	.4605	1.268×10^{-3}	.5340	3.883×10^{23}	1.399×10^3	5.986×10^{-7}	2.337×10^9	1.347×10^{-6}	1.039×10^9	1.039×10^3
25,000	4.735	32.097	28.90	429.2	2.299×10^4	787.8	.3723	1.068×10^{-3}	.4496	3.269×10^{23}	1.371×10^3	7.111×10^{-7}	1.928×10^9	1.600×10^{-6}	8.569×10^8	1.018×10^3
30,000	5.682	32.082	28.90	411.4	2.204×10^4	631.2	.2983	8.926×10^{-4}	.3758	2.733×10^{23}	1.342×10^3	8.505×10^{-7}	1.578×10^9	1.914×10^{-6}	7.013×10^8	9.968×10^2
35,000	6.629	32.066	28.90	393.6	2.110×10^4	500.9	.2367	7.404×10^{-4}	.3118	2.267×10^{23}	1.313×10^3	1.025×10^{-6}	1.280×10^9	2.307×10^{-6}	5.689×10^8	9.750×10^2
35,332	6.692	32.065	28.90	392.4	2.104×10^4	493.1	.2330	7.311×10^{-4}	.3078	2.239×10^{23}	1.311×10^3	1.038×10^{-6}	1.262×10^9	2.337×10^{-6}	5.609×10^8	9.735×10^2
40,000	7.576	32.051	28.90	392.4	2.104×10^4	395.0	.1867	5.856×10^{-4}	.2466	1.793×10^{23}	1.311×10^3	1.296×10^{-6}	1.011×10^9	2.917×10^{-6}	4.493×10^8	9.735×10^2
45,000	8.523	32.036	28.90	392.4	2.105×10^4	311.6	.1472	4.619×10^{-4}	.1945	1.414×10^{23}	1.311×10^3	1.644×10^{-6}	7.976×10^8	3.698×10^{-6}	3.545×10^8	9.735×10^2
50,000	9.470	32.020	28.90	392.4	2.106×10^4	245.8	.1161	3.644×10^{-4}	.1534	1.116×10^{23}	1.311×10^3	2.084×10^{-6}	6.292×10^8	4.688×10^{-6}	2.796×10^8	9.735×10^2
55,000	10.417	32.005	28.90	392.4	2.107×10^4	193.9	9.164×10^{-2}	2.875×10^{-4}	.1211	8.804×10^{22}	1.311×10^3	2.640×10^{-6}	4.965×10^8	5.941×10^{-6}	2.207×10^8	9.735×10^2
60,000	11.364	31.990	28.90	392.4	2.108×10^4	153.1	7.232×10^{-2}	2.269×10^{-4}	9.554×10^{-2}	6.948×10^{22}	1.311×10^3	3.346×10^{-6}	3.918×10^8	7.528×10^{-6}	1.741×10^8	9.735×10^2
65,000	12.311	31.974	28.90	392.4	2.110×10^4	120.8	5.709×10^{-2}	1.791×10^{-4}	7.542×10^{-2}	5.484×10^{22}	1.311×10^3	4.238×10^{-6}	3.093×10^8	9.536×10^{-6}	1.375×10^8	9.735×10^2
70,000	13.258	31.959	28.89	392.4	2.111×10^4	95.46	4.511×10^{-2}	1.415×10^{-4}	5.957×10^{-2}	4.333×10^{22}	1.311×10^3	5.364×10^{-6}	2.444×10^8	1.207×10^{-5}	1.086×10^8	9.737×10^2
75,000	14.205	31.944	28.88	392.4	2.113×10^4	75.46	3.566×10^{-2}	1.118×10^{-4}	4.706×10^{-2}	3.425×10^{22}	1.311×10^3	6.787×10^{-6}	1.931×10^8	1.527×10^{-5}	8.582×10^7	9.739×10^2
80,000	15.152	31.929	28.86	392.4	2.115×10^4	59.67	2.820×10^{-2}	8.836×10^{-5}	3.720×10^{-2}	2.709×10^{22}	1.311×10^3	8.582×10^{-6}	1.528×10^8	1.931×10^{-5}	6.791×10^7	9.741×10^2
85,000	16.098	31.913	28.85	392.4	2.117×10^4	47.21	2.231×10^{-2}	6.988×10^{-5}	2.942×10^{-2}	2.143×10^{22}	1.312×10^3	1.085×10^{-5}	1.210×10^8	2.441×10^{-5}	5.378×10^7	9.743×10^2
90,000	17.045	31.898	28.84	392.4	2.119×10^4	37.36	1.765×10^{-2}	5.528×10^{-5}	2.327×10^{-2}	1.696×10^{22}	1.312×10^3	1.371×10^{-5}	9.572×10^7	3.084×10^{-5}	4.254×10^7	9.745×10^2
95,000	17.992	31.883	28.83	392.4	2.121×10^4	29.59	1.398×10^{-2}	4.376×10^{-5}	1.842×10^{-2}	1.343×10^{22}	1.312×10^3	1.731×10^{-5}	7.580×10^7	3.894×10^{-5}	3.369×10^7	9.747×10^2
100,000	18.939	31.868	28.82	392.4	2.123×10^4	23.44	1.107×10^{-2}	3.462×10^{-5}	1.459×10^{-2}	1.063×10^{22}	1.312×10^3	2.187×10^{-5}	6.002×10^7	4.920×10^{-5}	2.668×10^7	9.749×10^2
104,986	19.884	31.852	28.80	392.4	2.125×10^4	18.58	8.781×10^{-3}	2.746×10^{-5}	1.156×10^{-2}	8.437×10^{21}	1.313×10^3	2.755×10^{-5}	4.765×10^7	6.200×10^{-5}	2.118×10^7	9.751×10^2
105,000	19.886	31.852	28.80	392.5	2.125×10^4	18.57	8.775×10^{-3}	2.744×10^{-5}	1.155×10^{-2}	8.429×10^{21}	1.313×10^3	2.758×10^{-5}	4.761×10^7	6.205×10^{-5}	2.116×10^7	9.752×10^2
110,000	20.833	31.837	28.79	413.3	2.240×10^4	14.77	6.979×10^{-3}	2.071×10^{-5}	8.720×10^{-3}	6.365×10^{21}	1.348×10^3	3.652×10^{-5}	3.691×10^7	8.218×10^{-5}	1.640×10^7	1.001×10^3
115,000	21.780	31.822	28.78	434.2	2.355×10^4	11.88	5.615×10^{-3}	1.586×10^{-5}	6.676×10^{-3}	4.875×10^{21}	1.381×10^3	4.768×10^{-5}	2.896×10^7	1.073×10^{-4}	1.287×10^7	1.026×10^3
120,000	22.727	31.807	28.77	455.1	2.471×10^4	9.665	4.567×10^{-3}	1.230×10^{-5}	5.178×10^{-3}	3.783×10^{21}	1.415×10^3	6.145×10^{-5}	2.303×10^7	1.383×10^{-4}	1.024×10^7	1.051×10^3
125,000	23.674	31.792	28.76	476.0	2.586×10^4	7.936	3.750×10^{-3}	9.651×10^{-6}	4.063×10^{-3}	2.970×10^{21}	1.447×10^3	7.827×10^{-5}	1.849×10^7	1.761×10^{-4}	8.218×10^6	1.075×10^3
130,000	24.621	31.776	28.74	496.9	2.702×10^4	6.574	3.106×10^{-3}	7.655×10^{-6}	3.223×10^{-3}	2.357×10^{21}	1.479×10^3	9.863×10^{-5}	1.499×10^7	2.219×10^{-4}	6.662×10^6	1.098×10^3
135,000	25.568	31.761	28.73	517.7	2.818×10^4	5.490	2.594×10^{-3}	6.133×10^{-6}	2.582×10^{-3}	1.889×10^{21}	1.510×10^3	1.231×10^{-4}	1.227×10^7	2.769×10^{-4}	5.453×10^6	1.122×10^3
140,000	26.515	31.746	28.72	538.6	2.935×10^4	4.620	2.183×10^{-3}	4.958×10^{-6}	2.088×10^{-3}	1.528×10^{21}	1.540×10^3	1.522×10^{-4}	1.012×10^7	3.423×10^{-4}	4.498×10^6	1.144×10^3
145,000	27.462	31.731	28.71	559.5	3.051×10^4	3.914	1.850×10^{-3}	4.043×10^{-6}	1.702×10^{-3}	1.246×10^{21}	1.570×10^3	1.865×10^{-4}	8.417×10^6	4.197×10^{-4}	3.741×10^6	1.166×10^3
150,000	28.409	31.716	28.69	580.4	3.168×10^4	3.338	1.577×10^{-3}	3.322×10^{-6}	1.399×10^{-3}	1.024×10^{21}	1.600×10^3	2.269×10^{-4}	7.051×10^6	5.106×10^{-4}	3.134×10^6	1.188×10^3
155,000	29.356	31.701	28.68	601.2	3.285×10^4	2.863	1.353×10^{-3}	2.449×10^{-6}	1.158×10^{-3}	8.482×10^{20}	1.628×10^3	2.740×10^{-4}	5.941×10^6	6.166×10^{-4}	2.640×10^6	1.210×10^3
160,000	30.303	31.686	28.67	622.1	3.402×10^4	2.470	1.167×10^{-3}	2.291×10^{-6}	9.647×10^{-4}	7.071×10^{20}	1.657×10^3	3.287×10^{-4}	5.041×10^6	7.396×10^{-4}	2.240×10^6	1.231×10^3
164,040	31.068	31.673	28.66	639.0	3.497×10^4	2.200	1.040×10^{-3}	1.986×10^{-6}	8.364×10^{-4}	6.133×10^{20}	1.679×10^3	3.790×10^{-4}	4.430×10^6	8.528×10^{-4}	1.969×10^6	1.248×10^3
165,000	31.250	31.670	28.66	639.0	3.497×10^4	2.140	1.011×10^{-3}	1.933×10^{-6}	8.138×10^{-4}	5.967×10^{20}	1.679×10^3	3.896×10^{-4}	4.310×10^6	8.765×10^{-4}	1.916×10^6	1.248×10^3
170,000	32.197	31.655	28.66	639.0	3.499×10^4	1.856	8.768×10^{-4}	1.675×10^{-6}	7.054×10^{-4}	5.177×10^{20}	1.679×10^3	4.494×10^{-4}	3.736×10^6	1.011×10^{-3}	1.660×10^6	1.248×10^3
175,000	33.144	31.640	28.66	639.0	3.501×10^4	1.609	7.601×10^{-4}	1.452×10^{-6}	6.115×10^{-4}	4.484×10^{20}	1.679×10^3	5.183×10^{-4}	3.239×10^6	1.166×10^{-3}	1.440×10^6	1.248×10^3
180,000	34.091	31.625	28.66	639.0	3.502×10^4	1.395	6.591×10^{-4}	1.259×10^{-6}	5.303×10^{-4}	3.888×10^{20}	1.679×10^3	5.978×10^{-4}	2.809×10^6	1.345×10^{-3}	1.248×10^6	1.248×10^3
185,000	35.038	31.610	28.66	639.0	3.504×10^4	1.210	5.716×10^{-4}	1.092×10^{-6}	4.599×10^{-4}	3.372×10^{20}	1.679×10^3	6.893×10^{-4}	2.436×10^6	1.551×10^{-3}	1.083×10^6	1.248×10^3
190,000	35.985	31.595	28.66	639.0	3.506×10^4	1.049	4.958×10^{-4}	9.473×10^{-7}	3.988×10^{-4}	2.925×10^{20}	1.679×10^3	7.948×10^{-4}	2.113×10^6	1.788×10^{-3}	9.391×10^5	1.248×10^3
195,000	36.932	31.580	28.66	639.0	3.507×10^4	.9101	4.300×10^{-4}	8.217×10^{-7}	3.460×10^{-4}	2.537×10^{20}	1.679×10^3	9.163×10^{-4}	1.832×10^6	2.062×10^{-3}	8.142×10^5	1.248×10^3
196,848	37.282	31.574	28.66	639.0	3.508×10^4	.8635	4.080×10^{-4}	7.797×10^{-7}	3.283×10^{-4}	2.407×10^{20}	1.679×10^3	9.657×10^{-4}	1.739×10^6	2.173×10^{-3}	7.729×10^5	1.248×10^3
200,000	37.879	31.565	28.66	628.0	3.448×10^4	.7887	3.727×10^{-4}	7.246×10^{-7}	3.051×10^{-4}	2.237×10^{20}	1.668×10^3	1.039×10^{-3}	1.605×10^6	2.338×10^{-3}	7.133×10^5	1.237×10^3

Table 13 *(Cont'd)*

Latitude, 45°. Engineering Units. p_a = 2116 lb/ft², ρ_a = 2.375 × 10⁻³ slug/ft³.

Height h ft	Height h mi	Apparent Gravity g' ft/sec²	Mean Mol Wt M	Temp T °R	Scale Height H ft	Pressure p lb/ft²	Pressure Ratio p/p_a	Density ρ slug/ft³	Density Ratio σ ρ/ρ_a	Number Density n particles/ft³	Mean Particle Speed v ft/sec	$d = 3 \times 10^{-8}$ cm Mean Free Path L ft	$d = 3 \times 10^{-8}$ cm Mean Collision Freq ν 1/sec	$d = 2 \times 10^{-8}$ cm Mean Free Path L ft	$d = 2 \times 10^{-8}$ cm Mean Collision Freq ν 1/sec	Speed of Sound c ft/sec
205,000	38.826	31.550	28.66	610.4	3.354×10^4	.6809	3.218×10^{-4}	6.436×10^{-7}	2.710×10^{-4}	1.987×10^{20}	1.641×10^3	1.170×10^{-3}	1.403×10^5	2.632×10^{-3}	6.236×10^5	1.219×10^3
210,000	39.773	31.535	28.66	592.9	3.259×10^4	.5854	2.766×10^{-4}	5.697×10^{-7}	2.399×10^{-4}	1.759×10^{20}	1.618×10^3	1.322×10^{-3}	1.224×10^5	2.974×10^{-3}	5.440×10^5	1.202×10^3
215,000	40.720	31.520	28.66	575.4	3.164×10^4	.5011	2.368×10^{-4}	5.025×10^{-7}	2.116×10^{-4}	1.552×10^{20}	1.594×10^3	1.498×10^{-3}	1.064×10^5	3.371×10^{-3}	4.729×10^5	1.184×10^3
220,000	41.667	31.505	28.66	557.8	3.069×10^4	.4270	2.018×10^{-4}	4.416×10^{-7}	1.859×10^{-4}	1.363×10^{20}	1.569×10^3	1.705×10^{-3}	9.202×10^5	3.836×10^{-3}	4.090×10^5	1.166×10^3
225,000	42.614	31.490	28.66	540.3	2.974×10^4	.3633	1.717×10^{-4}	3.880×10^{-7}	1.634×10^{-4}	1.198×10^{20}	1.544×10^3	1.941×10^{-3}	7.956×10^5	4.367×10^{-3}	3.536×10^5	1.147×10^3
230,000	43.561	31.475	28.66	522.8	2.879×10^4	.3053	1.443×10^{-4}	3.369×10^{-7}	1.418×10^{-4}	1.040×10^{20}	1.519×10^3	2.235×10^{-3}	6.797×10^5	5.028×10^{-3}	3.021×10^5	1.128×10^3
235,000	44.508	31.460	28.66	505.3	2.784×10^4	.2560	1.210×10^{-4}	2.923×10^{-7}	1.231×10^{-4}	9.025×10^{19}	1.493×10^3	2.576×10^{-3}	5.796×10^5	5.795×10^{-3}	2.576×10^5	1.109×10^3
240,000	45.455	31.445	28.66	487.7	2.689×10^4	.2134	1.008×10^{-4}	2.524×10^{-7}	1.063×10^{-4}	7.792×10^{19}	1.467×10^3	2.983×10^{-3}	4.918×10^5	6.712×10^{-3}	2.186×10^5	1.090×10^3
245,000	46.402	31.430	28.66	470.2	2.593×10^4	.1767	8.349×10^{-5}	2.168×10^{-7}	9.128×10^{-5}	6.693×10^{19}	1.441×10^3	3.473×10^{-3}	4.149×10^5	7.814×10^{-3}	1.844×10^5	1.070×10^3
250,000	47.348	31.415	28.66	452.7	2.497×10^4	.1453	6.865×10^{-5}	1.852×10^{-7}	7.797×10^{-5}	5.717×10^{19}	1.414×10^3	4.066×10^{-3}	3.478×10^5	9.148×10^{-3}	1.546×10^5	1.050×10^3
255,000	48.295	31.400	28.66	435.2	2.402×10^4	.1186	5.603×10^{-5}	1.572×10^{-7}	6.619×10^{-5}	4.854×10^{19}	1.386×10^3	4.789×10^{-3}	2.894×10^5	1.078×10^{-2}	1.286×10^5	1.029×10^3
255,902	48.466	31.398	28.66	432.0	2.385×10^4	.1142	5.396×10^{-5}	1.525×10^{-7}	6.422×10^{-5}	4.709×10^{19}	1.381×10^3	4.937×10^{-3}	2.797×10^5	1.111×10^{-2}	1.243×10^5	1.026×10^3
260,000	49.242	31.385	28.66	432.0	2.386×10^4	9.618×10^{-2}	4.545×10^{-5}	1.284×10^{-7}	5.408×10^{-5}	3.966×10^{19}	1.381×10^3	5.862×10^{-3}	2.356×10^5	1.319×10^{-2}	1.047×10^5	1.026×10^3
265,000	50.189	31.371	28.66	432.0	2.387×10^4	7.801×10^{-2}	3.686×10^{-5}	1.042×10^{-7}	4.386×10^{-5}	3.217×10^{19}	1.381×10^3	7.227×10^{-3}	1.911×10^5	1.626×10^{-2}	8.493×10^4	1.026×10^3
270,000	51.136	31.356	28.66	432.0	2.388×10^4	6.328×10^{-2}	2.990×10^{-5}	8.451×10^{-8}	3.558×10^{-5}	2.609×10^{19}	1.381×10^3	8.908×10^{-3}	1.550×10^5	2.004×10^{-2}	6.889×10^4	1.026×10^3
272,306	51.573	31.349	28.66	432.0	2.389×10^4	5.746×10^{-2}	2.715×10^{-5}	7.674×10^{-8}	3.231×10^{-5}	2.369×10^{19}	1.381×10^3	9.811×10^{-3}	1.408×10^5	2.207×10^{-2}	6.258×10^4	1.026×10^3
275,000	52.083	31.341	28.56	437.4	2.427×10^4	5.139×10^{-2}	2.428×10^{-5}	6.756×10^{-8}	2.845×10^{-5}	2.093×10^{19}	1.392×10^3	1.110×10^{-2}	1.253×10^5	2.499×10^{-2}	5.570×10^4	1.034×10^3
280,000	53.030	31.326	28.39	447.4	2.499×10^4	4.197×10^{-2}	1.983×10^{-5}	5.361×10^{-8}	2.257×10^{-5}	1.671×10^{19}	1.412×10^3	1.391×10^{-2}	1.015×10^5	3.130×10^{-2}	4.512×10^4	1.050×10^3
285,000	53.977	31.311	28.21	457.4	2.573×10^4	3.449×10^{-2}	1.630×10^{-5}	4.282×10^{-8}	1.803×10^{-5}	1.343×10^{19}	1.432×10^3	1.731×10^{-2}	8.274×10^4	3.894×10^{-2}	3.677×10^4	1.066×10^3
290,000	54.924	31.296	28.03	467.4	2.647×10^4	2.849×10^{-2}	1.364×10^{-5}	3.440×10^{-8}	1.448×10^{-5}	1.086×10^{19}	1.452×10^3	2.141×10^{-2}	6.782×10^4	4.817×10^{-2}	3.014×10^4	1.082×10^3
295,000	55.871	31.281	27.85	477.4	2.722×10^4	2.367×10^{-2}	1.118×10^{-5}	2.779×10^{-8}	1.170×10^{-5}	8.830×10^{18}	1.472×10^3	2.633×10^{-2}	5.593×10^4	5.924×10^{-2}	2.486×10^4	1.098×10^3
300,000	56.818	31.266	27.68	487.4	2.798×10^4	1.976×10^{-2}	9.336×10^{-6}	2.258×10^{-8}	9.508×10^{-6}	7.220×10^{18}	1.493×10^3	3.220×10^{-2}	4.636×10^4	7.244×10^{-2}	2.060×10^4	1.114×10^3
305,000	57.765	31.252	27.50	497.4	2.875×10^4	1.657×10^{-2}	7.832×10^{-6}	1.844×10^{-8}	7.766×10^{-6}	5.935×10^{18}	1.513×10^3	3.917×10^{-2}	3.862×10^4	8.813×10^{-2}	1.716×10^4	1.130×10^3
310,000	58.712	31.237	27.32	507.5	2.954×10^4	1.397×10^{-2}	6.610×10^{-6}	1.514×10^{-8}	6.375×10^{-6}	4.904×10^{18}	1.533×10^3	4.741×10^{-2}	3.234×10^4	1.067×10^{-1}	1.437×10^4	1.146×10^3
315,000	59.659	31.222	27.14	517.5	3.033×10^4	1.183×10^{-2}	5.588×10^{-6}	1.249×10^{-8}	5.258×10^{-6}	4.071×10^{18}	1.553×10^3	5.710×10^{-2}	2.720×10^4	1.285×10^{-1}	1.209×10^4	1.161×10^3
320,000	60.606	31.207	26.97	527.5	3.114×10^4	1.006×10^{-2}	4.752×10^{-6}	1.035×10^{-8}	4.358×10^{-6}	3.396×10^{18}	1.573×10^3	6.844×10^{-2}	2.298×10^4	1.540×10^{-1}	1.021×10^4	1.177×10^3
325,000	61.553	31.193	26.79	537.5	3.195×10^4	8.588×10^{-3}	4.058×10^{-6}	8.616×10^{-9}	3.628×10^{-6}	2.846×10^{18}	1.593×10^3	8.168×10^{-2}	1.950×10^4	1.838×10^{-1}	8.668×10^3	1.193×10^3
330,000	62.500	31.178	26.61	547.5	3.278×10^4	7.362×10^{-3}	3.479×10^{-6}	7.204×10^{-9}	3.033×10^{-6}	2.395×10^{18}	1.613×10^3	9.704×10^{-2}	1.662×10^4	2.184×10^{-1}	7.387×10^3	1.209×10^3
335,000	63.447	31.163	26.43	557.5	3.362×10^4	6.336×10^{-3}	2.994×10^{-6}	6.048×10^{-9}	2.546×10^{-6}	2.024×10^{18}	1.633×10^3	1.148×10^{-1}	1.422×10^4	2.584×10^{-1}	6.320×10^3	1.226×10^3
340,000	64.394	31.148	26.26	567.5	3.447×10^4	5.474×10^{-3}	2.586×10^{-6}	5.098×10^{-9}	2.146×10^{-6}	1.718×10^{18}	1.654×10^3	1.353×10^{-1}	1.222×10^4	3.044×10^{-1}	5.431×10^3	1.242×10^3
345,000	65.341	31.134	26.08	577.5	3.533×10^4	4.746×10^{-3}	2.242×10^{-6}	4.314×10^{-9}	1.816×10^{-6}	1.464×10^{18}	1.674×10^3	1.588×10^{-1}	1.054×10^4	3.573×10^{-1}	4.684×10^3	1.258×10^3
350,000	66.288	31.119	25.90	587.5	3.621×10^4	4.129×10^{-3}	1.951×10^{-6}	3.664×10^{-9}	1.543×10^{-6}	1.252×10^{18}	1.694×10^3	1.857×10^{-1}	9.122×10^3	4.178×10^{-1}	4.054×10^3	1.274×10^3
355,000	67.235	31.104	25.72	597.5	3.710×10^4	3.604×10^{-3}	1.703×10^{-6}	3.123×10^{-9}	1.315×10^{-6}	1.074×10^{18}	1.714×10^3	2.164×10^{-1}	7.921×10^3	4.869×10^{-1}	3.520×10^3	1.290×10^3
360,000	68.182	31.090	25.55	607.5	3.800×10^4	3.156×10^{-3}	1.491×10^{-6}	2.672×10^{-9}	1.125×10^{-6}	9.253×10^{17}	1.734×10^3	2.512×10^{-1}	6.902×10^3	5.652×10^{-1}	3.068×10^3	1.306×10^3
365,000	69.129	31.075	25.37	617.6	3.892×10^4	2.773×10^{-3}	1.310×10^{-6}	2.293×10^{-9}	9.654×10^{-7}	7.998×10^{17}	1.755×10^3	2.906×10^{-1}	6.038×10^3	6.540×10^{-1}	2.684×10^3	1.323×10^3
370,000	70.076	31.060	25.19	627.6	3.984×10^4	2.443×10^{-3}	1.154×10^{-6}	1.974×10^{-9}	8.312×10^{-7}	6.935×10^{17}	1.775×10^3	3.352×10^{-1}	5.295×10^3	7.542×10^{-1}	2.353×10^3	1.339×10^3
375,000	71.023	31.046	25.01	637.6	4.078×10^4	2.159×10^{-3}	1.020×10^{-6}	1.705×10^{-9}	7.180×10^{-7}	6.033×10^{17}	1.796×10^3	3.853×10^{-1}	4.661×10^3	8.670×10^{-1}	2.072×10^3	1.356×10^3
380,000	71.970	31.031	24.84	647.6	4.174×10^4	1.914×10^{-3}	9.043×10^{-7}	1.478×10^{-9}	6.221×10^{-7}	5.264×10^{17}	1.816×10^3	4.416×10^{-1}	4.112×10^3	9.936×10^{-1}	1.828×10^3	1.372×10^3
385,000	72.917	31.016	24.66	657.6	4.271×10^4	1.701×10^{-3}	8.037×10^{-7}	1.284×10^{-9}	5.406×10^{-7}	4.607×10^{17}	1.837×10^3	5.045×10^{-1}	3.641×10^3	1.135	1.618×10^3	1.389×10^3
390,000	73.864	31.002	24.48	667.6	4.370×10^4	1.516×10^{-3}	7.162×10^{-7}	1.119×10^{-9}	4.711×10^{-7}	4.044×10^{17}	1.857×10^3	5.748×10^{-1}	3.231×10^3	1.293	1.436×10^3	1.406×10^3
393,696	74.564	31.991	24.35	675.0	4.444×10^4	1.394×10^{-3}	6.587×10^{-7}	1.012×10^{-9}	4.263×10^{-7}	3.679×10^{17}	1.873×10^3	6.318×10^{-1}	2.964×10^3	1.422	1.317×10^3	1.418×10^3
395,000	74.811	30.987	24.35	677.9	4.463×10^4	1.354×10^{-3}	6.397×10^{-7}	9.790×10^{-10}	4.122×10^{-7}	3.558×10^{17}	1.890×10^3	6.534×10^{-1}	2.893×10^3	1.470	1.286×10^3	1.421×10^3
400,000	75.758	30.972	24.35	688.9	4.538×10^4	1.212×10^{-3}	5.725×10^{-7}	8.620×10^{-10}	3.629×10^{-7}	3.132×10^{17}	1.898×10^3	7.421×10^{-1}	2.558×10^3	1.670	1.137×10^3	1.432×10^3

Table 13 *(Cont'd)*

Latitude, 45°. Engineering Units. p_a = 2116 lb/ft², ρ_a = 2.375 × 10⁻³ slug/ft³.

Height h ft	Height h mi	Apparent Gravity g' ft/sec²	Mean Mol Wt M	Temp T °R	Scale Height H ft	Pressure p lb/ft²	Pressure Ratio p/p_a	Density ρ slug/ft³	Density Ratio σ ρ/ρ_a	Number Density n particles/ft³	Mean Particle Speed v ft/sec	$d = 3 \times 10^{-8}$cm Mean Free Path L ft	$d = 3 \times 10^{-8}$cm Mean Collision Freq ν 1/sec	$d = 2 \times 10^{-8}$cm Mean Free Path L ft	$d = 2 \times 10^{-8}$cm Mean Collision Freq ν 1/sec	Speed of Sound c ft/sec
4.500×10^5	85.227	30.827	24.35	799.4	5.291×10^4	4.37×10^{-4}	2.06×10^{-7}	2.68×10^{-10}	1.13×10^{-7}	9.75×10^{16}	2.04×10^3	2.38	8.55×10^2	5.36	3.80×10^2	1.54×10^3
5.000×10^5	94.697	30.682	24.35	909.9	6.050×10^4	1.81×10^{-4}	8.55×10^{-8}	9.75×10^{-11}	4.11×10^{-8}	3.55×10^{16}	2.17×10^3	6.55	3.32×10^2	1.47×10	1.48×10^2	1.64×10^3
5.280×10^5	100.00	30.602	24.35	971.8	6.478×10^4	1.16×10^{-4}	5.48×10^{-8}	5.82×10^{-11}	2.45×10^{-8}	2.12×10^{16}	2.25×10^3	1.10×10	2.05×10^2	2.47×10	9.11×10	1.70×10^3
5.500×10^5	104.17	30.539	24.35	1020	6.817×10^4	8.30×10^{-5}	3.92×10^{-8}	3.99×10^{-11}	1.68×10^{-8}	1.45×10^{16}	2.30×10^3	1.60×10	1.44×10^2	3.61×10	6.38×10	
6.000×10^5	113.64	30.396	24.35	1131	7.590×10^4	4.14×10^{-5}	1.96×10^{-8}	1.79×10^{-11}	7.54×10^{-8}	6.51×10^{15}	2.42×10^3	3.57×10	6.79×10	8.03×10	3.02×10	
6.500×10^5	123.11	30.255	24.35	1241	8.371×10^4	2.21×10^{-5}	1.04×10^{-8}	8.73×10^{-12}	3.68×10^{-9}	3.17×10^{16}	2.54×10^3	7.33×10	3.46×10	1.65×10^2	1.54×10	
7.000×10^5	132.58	30.114	24.35	1352	9.158×10^4	1.25×10^{-5}	5.91×10^{-9}	4.53×10^{-12}	1.91×10^{-9}	1.65×10^{15}	2.65×10^3	1.41×10^2	1.88×10	3.17×10^2	8.35	
7.500×10^5	142.05	29.975	24.35	1462	9.953×10^4	7.40×10^{-6}	3.50×10^{-9}	2.48×10^{-12}	1.04×10^{-9}	9.02×10^{14}	2.76×10^3	2.58×10^2	1.07×10	5.80×10^2	4.75	
8.000×10^5	151.57	29.836	24.35	1573	1.075×10^5	4.57×10^{-6}	2.16×10^{-9}	1.42×10^{-12}	5.98×10^{-10}	5.16×10^{14}	2.86×10^3	4.50×10^2	6.35	1.01×10^3	2.82	
8.500×10^5	160.98	29.699	24.35	1683	1.156×10^5	2.92×10^{-6}	1.38×10^{-9}	8.50×10^{-13}	3.58×10^{-10}	3.09×10^{14}	2.96×10^3	7.52×10^2	3.93	1.69×10^3	1.75	
9.000×10^5	170.45	29.562	24.35	1794	1.238×10^5	1.92×10^{-6}	9.07×10^{-10}	5.25×10^{-13}	2.21×10^{-10}	1.91×10^{14}	3.05×10^3	1.22×10^3	2.51	2.74×10^3	1.11	
9.500×10^5	179.92	29.426	24.35	1904	1.320×10^5	1.30×10^{-6}	6.14×10^{-10}	3.35×10^{-13}	1.41×10^{-10}	1.22×10^{14}	3.15×10^3	1.91×10^3	1.65	4.29×10^3	7.34×10^{-1}	
9.842×10^5	186.41	29.334	24.35	1980	1.377×10^5	1.01×10^{-6}	4.77×10^{-10}	2.50×10^{-13}	1.05×10^{-10}	9.09×10^{13}	3.21×10^3	2.56×10^3	1.25	5.75×10^3	5.57×10^{-1}	

1 lb/ft² = 0.3591 mm of Hg

Table 14

VALUES OF TEMPERATURE, PRESSURE, AND DENSITY UP TO THE F_2 LAYER

Latitude, 45°. Metric Units. p_a = 1014 mb, $\rho_a = 1.223 \times 10^{-3}$ gm/cm³

Height h km	Height h mi	Apparent Gravity g' cm/sec²	Mean Mol Wt M	Temp T °K	Scale Height H km	Pressure p millibars	Pressure Ratio p/p_a	Density ρ gm/cm³	Density Ratio σ ρ/ρ_a	Number Density n particles/cm³	Mean Particle Speed v cm/sec	$d = 3 \times 10^{-8}$ cm: Mean Free Path L cm	$d = 3 \times 10^{-8}$ cm: Mean Collision Freq ν 1/sec	$d = 2 \times 10^{-8}$ cm: Mean Free Path L cm	$d = 2 \times 10^{-8}$ cm: Mean Collision Freq ν 1/sec	Speed of Sound c cm/sec
0	0	980.69	28.90	288.0	8.443	1014	1.0000	1.223×10^{-3}	1.0000	2.568×10^{19}	4.590×10^{4}	9.744×10^{-6}	4.712×10^{9}	2.192×10^{-5}	2.094×10^{8}	3.410×10^{4}
1.524	.947	980.22	28.90	278.1	8.157	843.5	.8322	1.055×10^{-3}	.8619	2.213×10^{19}	4.511×10^{4}	1.130×10^{-5}	3.991×10^{8}	2.544×10^{-5}	1.774×10^{8}	3.351×10^{4}
3.048	1.894	979.74	28.90	268.2	7.870	697.5	.6882	9.047×10^{-4}	.7390	1.898×10^{19}	4.432×10^{4}	1.318×10^{-5}	3.362×10^{8}	2.966×10^{-5}	1.494×10^{8}	3.291×10^{4}
4.572	2.841	979.27	28.90	258.3	7.580	572.7	.5650	7.713×10^{-4}	.6301	1.618×10^{19}	4.350×10^{4}	1.546×10^{-5}	2.813×10^{8}	3.479×10^{-5}	1.250×10^{8}	3.230×10^{4}
6.096	3.788	978.80	28.90	248.4	7.294	466.8	.4605	6.537×10^{-4}	.5340	1.371×10^{19}	4.264×10^{4}	1.825×10^{-5}	2.337×10^{8}	4.106×10^{-5}	1.039×10^{8}	3.167×10^{4}
7.620	4.735	978.34	28.90	238.5	7.007	377.3	.3723	5.503×10^{-4}	.4496	1.155×10^{19}	4.179×10^{4}	2.167×10^{-5}	1.928×10^{8}	4.876×10^{-5}	8.569×10^{8}	3.104×10^{4}
9.144	5.682	977.87	28.90	228.6	6.718	302.3	.2983	4.601×10^{-4}	.3758	9.652×10^{18}	4.090×10^{4}	2.592×10^{-5}	1.578×10^{8}	5.833×10^{-5}	7.013×10^{8}	3.038×10^{4}
10.668	6.629	977.40	28.90	218.7	6.431	239.9	.2367	3.816×10^{-4}	.3118	8.006×10^{18}	4.002×10^{4}	3.125×10^{-5}	1.280×10^{8}	7.032×10^{-5}	5.689×10^{8}	2.972×10^{4}
10.769	6.692	977.37	28.90	218.0	6.413	236.2	.2330	3.768×10^{-4}	.3078	7.905×10^{18}	3.996×10^{4}	3.165×10^{-5}	1.262×10^{8}	7.122×10^{-5}	5.609×10^{8}	2.967×10^{4}
12.192	7.576	976.93	28.90	218.0	6.413	189.2	.1867	3.019×10^{-4}	.2466	6.333×10^{18}	3.996×10^{4}	3.951×10^{-5}	1.011×10^{8}	8.890×10^{-5}	4.493×10^{8}	2.967×10^{4}
13.716	8.523	976.46	28.90	218.0	6.416	149.2	.1472	2.381×10^{-4}	.1945	4.995×10^{18}	3.996×10^{4}	5.010×10^{-5}	7.976×10^{7}	1.127×10^{-4}	3.545×10^{8}	2.967×10^{4}
15.240	9.470	975.99	28.90	218.0	6.419	117.7	.1161	1.878×10^{-4}	.1534	3.940×10^{18}	3.996×10^{4}	6.351×10^{-5}	6.292×10^{7}	1.429×10^{-4}	2.796×10^{8}	2.967×10^{4}
16.764	10.417	975.52	28.90	218.0	6.422	92.88	9.164×10^{-2}	1.482×10^{-4}	.1211	3.109×10^{18}	3.996×10^{4}	8.048×10^{-5}	4.965×10^{7}	1.811×10^{-4}	2.207×10^{8}	2.967×10^{4}
18.288	11.364	975.06	28.90	218.0	6.425	73.30	7.232×10^{-2}	1.170×10^{-4}	9.554×10^{-2}	2.454×10^{18}	3.996×10^{4}	1.020×10^{-4}	3.918×10^{7}	2.295×10^{-4}	1.741×10^{8}	2.967×10^{4}
19.812	12.311	974.59	28.90	218.0	6.431	57.86	5.709×10^{-2}	9.232×10^{-5}	7.542×10^{-2}	1.937×10^{18}	3.996×10^{4}	1.292×10^{-4}	3.093×10^{7}	2.907×10^{-4}	1.375×10^{8}	2.967×10^{4}
21.336	13.258	974.12	28.89	218.0	6.434	45.72	4.511×10^{-2}	7.292×10^{-5}	5.957×10^{-2}	1.530×10^{18}	3.996×10^{4}	1.635×10^{-4}	2.444×10^{7}	3.679×10^{-4}	1.086×10^{8}	2.968×10^{4}
22.860	14.205	973.66	28.88	218.0	6.440	36.14	3.566×10^{-2}	5.761×10^{-5}	4.706×10^{-2}	1.210×10^{18}	3.996×10^{4}	2.069×10^{-4}	1.931×10^{7}	4.654×10^{-4}	8.582×10^{7}	2.968×10^{4}
24.384	15.152	973.19	28.86	218.0	6.447	28.58	2.820×10^{-2}	4.554×10^{-5}	3.720×10^{-2}	9.566×10^{17}	3.996×10^{4}	2.616×10^{-4}	1.528×10^{7}	5.886×10^{-4}	6.791×10^{7}	2.969×10^{4}
25.908	16.098	972.72	28.85	218.0	6.453	22.61	2.231×10^{-2}	3.602×10^{-5}	2.942×10^{-2}	7.568×10^{17}	3.999×10^{4}	3.306×10^{-4}	1.210×10^{7}	7.439×10^{-4}	5.378×10^{7}	2.970×10^{4}
27.432	17.045	972.26	28.84	218.0	6.459	17.89	1.765×10^{-2}	2.849×10^{-5}	2.327×10^{-2}	5.989×10^{17}	3.999×10^{4}	4.178×10^{-4}	9.572×10^{7}	9.400×10^{-4}	4.254×10^{7}	2.970×10^{4}
28.956	17.992	971.80	28.83	218.0	6.465	14.17	1.398×10^{-2}	2.255×10^{-5}	1.842×10^{-2}	4.743×10^{17}	3.999×10^{4}	5.276×10^{-4}	7.580×10^{7}	1.187×10^{-3}	3.369×10^{7}	2.971×10^{4}
30.480	18.939	971.33	28.82	218.0	6.471	11.23	1.107×10^{-2}	1.784×10^{-5}	1.459×10^{-2}	3.754×10^{17}	4.001×10^{4}	6.665×10^{-4}	6.002×10^{7}	1.500×10^{-3}	2.668×10^{7}	2.972×10^{4}
32.000	19.884	970.87	28.80	218.0	6.477	8.901	8.781×10^{-3}	1.415×10^{-5}	1.156×10^{-2}	2.979×10^{17}	4.002×10^{4}	8.399×10^{-4}	4.765×10^{7}	1.890×10^{-3}	2.118×10^{7}	2.972×10^{4}
32.004	19.886	970.40	28.80	218.0	6.477	8.894	8.775×10^{-3}	1.414×10^{-5}	1.155×10^{-2}	2.977×10^{17}	4.002×10^{4}	8.406×10^{-4}	4.761×10^{7}	1.891×10^{-3}	2.116×10^{7}	2.972×10^{4}
33.528	20.833	970.40	28.79	229.6	6.828	7.073	6.979×10^{-3}	1.067×10^{-5}	8.720×10^{-3}	2.248×10^{17}	4.109×10^{4}	1.113×10^{-3}	3.691×10^{7}	2.505×10^{-3}	1.640×10^{7}	3.051×10^{4}
35.052	21.780	969.94	28.78	241.2	7.178	5.692	5.615×10^{-3}	8.173×10^{-6}	6.676×10^{-3}	1.722×10^{17}	4.209×10^{4}	1.453×10^{-3}	2.896×10^{7}	3.270×10^{-3}	1.287×10^{7}	3.128×10^{4}
36.576	22.727	969.47	28.77	252.8	7.532	4.629	4.567×10^{-3}	6.339×10^{-6}	5.178×10^{-3}	1.336×10^{17}	4.313×10^{4}	1.873×10^{-3}	2.303×10^{7}	4.214×10^{-3}	1.021×10^{7}	3.203×10^{4}
38.100	23.674	969.00	28.76	264.4	7.882	3.801	3.750×10^{-3}	4.974×10^{-6}	4.063×10^{-3}	1.049×10^{17}	4.410×10^{4}	2.386×10^{-3}	1.849×10^{7}	5.368×10^{-3}	8.218×10^{6}	3.276×10^{4}
39.624	24.621	968.54	28.74	276.0	8.236	3.148	3.106×10^{-3}	3.946×10^{-6}	3.223×10^{-3}	8.323×10^{16}	4.508×10^{4}	3.006×10^{-3}	1.499×10^{7}	6.764×10^{-3}	6.662×10^{6}	3.348×10^{4}
41.148	25.568	968.08	28.73	287.6	8.589	2.630	2.594×10^{-3}	3.161×10^{-6}	2.582×10^{-3}	6.671×10^{16}	4.602×10^{4}	3.751×10^{-3}	1.227×10^{7}	8.440×10^{-3}	5.453×10^{6}	3.418×10^{4}
42.673	26.515	967.62	28.72	299.2	8.946	2.212	2.183×10^{-3}	2.556×10^{-6}	2.088×10^{-3}	5.395×10^{16}	4.694×10^{4}	4.638×10^{-3}	1.012×10^{7}	1.043×10^{-2}	4.498×10^{6}	3.487×10^{4}
44.197	27.462	967.15	28.71	310.8	9.299	1.875	1.850×10^{-3}	2.084×10^{-6}	1.702×10^{-3}	4.401×10^{16}	4.785×10^{4}	5.685×10^{-3}	8.417×10^{6}	1.279×10^{-2}	3.741×10^{6}	3.555×10^{4}
45.721	28.409	966.69	28.69	322.4	9.656	1.599	1.577×10^{-3}	1.712×10^{-6}	1.399×10^{-3}	3.618×10^{16}	4.877×10^{4}	6.917×10^{-3}	7.051×10^{6}	1.556×10^{-2}	3.134×10^{6}	3.621×10^{4}
47.245	29.356	966.23	28.68	334.0	1.001×10	1.371	1.353×10^{-3}	1.417×10^{-6}	1.158×10^{-3}	2.995×10^{16}	4.962×10^{4}	8.353×10^{-3}	5.941×10^{6}	1.879×10^{-2}	2.640×10^{6}	3.687×10^{4}
48.769	30.303	965.77	28.67	345.6	1.037×10	1.183	1.167×10^{-3}	1.181×10^{-6}	9.647×10^{-4}	2.497×10^{16}	5.051×10^{4}	1.002×10^{-2}	5.041×10^{6}	2.254×10^{-2}	2.240×10^{6}	3.751×10^{4}
50.000	31.068	965.40	28.66	355.0	1.066×10	1.054	1.040×10^{-3}	1.024×10^{-6}	8.364×10^{-4}	2.166×10^{16}	5.118×10^{4}	1.155×10^{-2}	4.430×10^{6}	2.599×10^{-2}	1.969×10^{6}	3.802×10^{4}
50.293	31.250	965.31	28.66	355.0	1.066×10	1.025	1.011×10^{-3}	9.962×10^{-7}	8.138×10^{-4}	2.107×10^{16}	5.118×10^{4}	1.180×10^{-2}	4.310×10^{6}	2.672×10^{-2}	1.916×10^{6}	3.802×10^{4}
51.817	32.197	964.85	28.66	355.0	1.066×10	8.887×10^{-1}	8.768×10^{-4}	8.635×10^{-7}	7.054×10^{-4}	1.827×10^{16}	5.118×10^{4}	1.370×10^{-2}	3.736×10^{6}	3.082×10^{-2}	1.660×10^{6}	3.802×10^{4}
53.341	33.144	964.39	28.66	355.0	1.067×10	7.705×10^{-1}	7.601×10^{-4}	7.486×10^{-7}	6.115×10^{-4}	1.584×10^{16}	5.118×10^{4}	1.580×10^{-2}	3.239×10^{6}	3.555×10^{-2}	1.440×10^{6}	3.802×10^{4}
54.865	34.091	963.93	28.66	355.0	1.067×10	6.681×10^{-1}	6.591×10^{-4}	6.491×10^{-7}	5.303×10^{-4}	1.373×10^{16}	5.118×10^{4}	1.822×10^{-2}	2.809×10^{6}	4.100×10^{-2}	1.248×10^{6}	3.802×10^{4}
56.389	35.038	963.48	28.66	355.0	1.068×10	5.794×10^{-1}	5.716×10^{-4}	5.630×10^{-7}	4.599×10^{-4}	1.191×10^{16}	5.118×10^{4}	2.101×10^{-2}	2.436×10^{6}	4.728×10^{-2}	1.083×10^{6}	3.802×10^{4}
57.913	35.985	963.01	28.66	355.0	1.069×10	5.025×10^{-1}	4.958×10^{-4}	4.883×10^{-7}	3.988×10^{-4}	1.033×10^{16}	5.118×10^{4}	2.423×10^{-2}	2.113×10^{6}	5.451×10^{-2}	9.391×10^{5}	3.802×10^{4}
59.437	36.932	962.56	28.66	355.0	1.069×10	4.359×10^{-1}	4.300×10^{-4}	4.235×10^{-7}	3.460×10^{-4}	8.959×10^{15}	5.118×10^{4}	2.793×10^{-2}	1.832×10^{6}	6.284×10^{-2}	8.142×10^{5}	3.802×10^{4}
60.000	37.282	962.39	28.66	355.0	1.069×10	4.136×10^{-1}	4.080×10^{-4}	4.019×10^{-7}	3.283×10^{-4}	8.501×10^{15}	5.118×10^{4}	2.943×10^{-2}	1.739×10^{6}	6.623×10^{-2}	7.729×10^{5}	3.802×10^{4}
60.961	37.879	962.10	28.66	348.9	1.051×10	3.777×10^{-1}	3.727×10^{-4}	3.735×10^{-7}	3.051×10^{-4}	7.901×10^{15}	5.084×10^{4}	3.167×10^{-2}	1.605×10^{6}	7.126×10^{-2}	7.133×10^{5}	3.769×10^{4}

Table 14 *(Cont'd)*

Latitude, 45°. Metric Units. p_a = 1014 mb, ρ_a = 1.223 × 10^{-3} gm/cm³

Height h km	Height h mi	Apparent Gravity g' cm/sec²	Mean Mol Wt M	Temp T °K	Scale Height H km	Pressure p millibars	Pressure Ratio p/p_a	Density ρ gm/cm³	Density Ratio σ ρ/ρ_a	Number Density n particles/cm³	Mean Particle Speed v cm/sec	$d = 3 \times 10^{-8}$ cm: Mean Free Path L cm	$d = 3 \times 10^{-8}$ cm: Mean Collision Freq ν 1/sec	$d = 2 \times 10^{-8}$ cm: Mean Free Path L cm	$d = 2 \times 10^{-8}$ cm: Mean Collision Freq ν 1/sec	Speed of Sound c cm/sec
62.485	38.826	961.64	28.66	339.1	1.022 × 10	3.261 × 10^{-1}	3.218 × 10^{-4}	3.317 × 10^{-7}	2.710 × 10^{-4}	7.017 × 10^{15}	5.002 × 10^{4}	3.566 × 10^{-8}	1.403 × 10^{8}	8.023 × 10^{-8}	6.236 × 10^{8}	3.716 × 10^{4}
64.009	39.773	961.18	28.66	329.4	9.933	2.804 × 10^{-1}	2.766 × 10^{-4}	2.936 × 10^{-7}	2.399 × 10^{-4}	6.212 × 10^{15}	4.932 × 10^{4}	4.028 × 10^{-8}	1.224 × 10^{8}	9.064 × 10^{-8}	5.440 × 10^{8}	3.662 × 10^{4}
65.553	40.720	960.72	28.66	319.7	9.644	2.400 × 10^{-1}	2.368 × 10^{-4}	2.590 × 10^{-7}	2.116 × 10^{-4}	5.479 × 10^{15}	4.859 × 10^{4}	4.567 × 10^{-8}	1.064 × 10^{8}	1.028 × 10^{-1}	4.729 × 10^{8}	3.608 × 10^{4}
67.057	41.667	960.27	28.66	309.9	9.354	2.045 × 10^{-1}	2.018 × 10^{-4}	2.276 × 10^{-7}	1.859 × 10^{-4}	4.815 × 10^{15}	4.782 × 10^{4}	5.197 × 10^{-8}	9.202 × 10^{8}	1.169 × 10^{-1}	4.090 × 10^{8}	3.553 × 10^{4}
68.581	42.614	959.81	28.66	300.2	9.065	1.740 × 10^{-1}	1.717 × 10^{-4}	2.000 × 10^{-7}	1.634 × 10^{-4}	4.230 × 10^{15}	4.706 × 10^{4}	5.915 × 10^{-8}	7.956 × 10^{8}	1.331 × 10^{-1}	3.536 × 10^{8}	3.496 × 10^{4}
70.105	43.561	959.36	28.66	290.4	8.775	1.462 × 10^{-1}	1.443 × 10^{-4}	1.736 × 10^{-7}	1.418 × 10^{-4}	3.673 × 10^{15}	4.630 × 10^{4}	6.811 × 10^{-8}	6.797 × 10^{8}	1.533 × 10^{-1}	3.021 × 10^{8}	3.439 × 10^{4}
71.629	44.508	958.90	28.66	280.7	8.486	1.226 × 10^{-1}	1.210 × 10^{-4}	1.507 × 10^{-7}	1.231 × 10^{-4}	3.187 × 10^{15}	4.551 × 10^{4}	7.851 × 10^{-8}	5.796 × 10^{8}	1.766 × 10^{-1}	2.576 × 10^{8}	3.381 × 10^{4}
73.153	45.455	958.45	28.66	271.0	8.196	1.022 × 10^{-1}	1.008 × 10^{-4}	1.301 × 10^{-7}	1.063 × 10^{-4}	2.752 × 10^{15}	4.471 × 10^{4}	9.093 × 10^{-8}	4.918 × 10^{8}	2.046 × 10^{-1}	2.186 × 10^{8}	3.322 × 10^{4}
74.677	46.402	957.99	28.66	261.2	7.903	8.462 × 10^{-2}	8.349 × 10^{-5}	1.117 × 10^{-7}	9.128 × 10^{-5}	2.364 × 10^{15}	4.392 × 10^{4}	1.059 × 10^{-1}	4.149 × 10^{8}	2.382 × 10^{-1}	1.844 × 10^{8}	3.262 × 10^{4}
76.201	47.348	957.54	28.66	251.5	7.611	6.958 × 10^{-2}	6.865 × 10^{-5}	9.544 × 10^{-8}	7.797 × 10^{-5}	2.019 × 10^{15}	4.310 × 10^{4}	1.239 × 10^{-1}	3.478 × 10^{8}	2.788 × 10^{-1}	1.546 × 10^{8}	3.200 × 10^{4}
77.725	48.295	957.08	28.66	241.8	7.321	5.679 × 10^{-2}	5.603 × 10^{-5}	8.103 × 10^{-8}	6.619 × 10^{-5}	1.714 × 10^{15}	4.225 × 10^{4}	1.460 × 10^{-1}	2.894 × 10^{8}	3.285 × 10^{-1}	1.286 × 10^{8}	3.138 × 10^{4}
78.000	48.466	957.00	28.66	240.0	7.269	5.469 × 10^{-2}	5.396 × 10^{-5}	7.860 × 10^{-8}	6.422 × 10^{-5}	1.663 × 10^{15}	4.209 × 10^{4}	1.505 × 10^{-1}	2.797 × 10^{8}	3.386 × 10^{-1}	1.243 × 10^{8}	3.126 × 10^{4}
79.249	49.242	956.63	28.66	240.0	7.273	4.606 × 10^{-2}	4.545 × 10^{-5}	6.620 × 10^{-8}	5.408 × 10^{-5}	1.400 × 10^{15}	4.209 × 10^{4}	1.787 × 10^{-1}	2.356 × 10^{8}	4.020 × 10^{-1}	1.047 × 10^{8}	3.126 × 10^{4}
80.773	50.189	956.18	28.66	240.0	7.276	3.736 × 10^{-2}	3.686 × 10^{-5}	5.370 × 10^{-8}	4.386 × 10^{-5}	1.136 × 10^{15}	4.209 × 10^{4}	2.203 × 10^{-1}	1.911 × 10^{8}	4.956 × 10^{-1}	8.493 × 10^{4}	3.126 × 10^{4}
82.297	51.136	955.72	28.66	240.0	7.279	3.031 × 10^{-2}	2.990 × 10^{-5}	4.356 × 10^{-8}	3.558 × 10^{-5}	9.215 × 10^{14}	4.209 × 10^{4}	2.715 × 10^{-1}	1.550 × 10^{8}	6.110 × 10^{-1}	6.889 × 10^{4}	3.126 × 10^{4}
83.000	51.573	955.51	28.66	240.0	7.281	2.752 × 10^{-2}	2.715 × 10^{-5}	3.956 × 10^{-8}	3.231 × 10^{-5}	8.367 × 10^{14}	4.209 × 10^{4}	2.990 × 10^{-1}	1.408 × 10^{8}	6.728 × 10^{-1}	6.256 × 10^{4}	3.126 × 10^{4}
83.821	52.083	955.26	28.56	243.0	7.398	2.461 × 10^{-2}	2.428 × 10^{-5}	3.482 × 10^{-8}	2.845 × 10^{-5}	7.391 × 10^{14}	4.243 × 10^{4}	3.385 × 10^{-1}	1.253 × 10^{8}	7.617 × 10^{-1}	5.570 × 10^{4}	3.152 × 10^{4}
85.345	53.030	954.81	28.39	248.6	7.618	2.010 × 10^{-2}	1.983 × 10^{-5}	2.763 × 10^{-8}	2.257 × 10^{-5}	5.901 × 10^{14}	4.304 × 10^{4}	4.240 × 10^{-1}	1.015 × 10^{8}	9.540 × 10^{-1}	4.512 × 10^{4}	3.201 × 10^{4}
86.869	53.977	954.36	28.21	254.1	7.841	1.652 × 10^{-2}	1.630 × 10^{-5}	2.207 × 10^{-8}	1.803 × 10^{-5}	4.743 × 10^{14}	4.365 × 10^{4}	5.276 × 10^{-1}	8.274 × 10^{4}	1.187	3.677 × 10^{4}	3.249 × 10^{4}
88.393	54.924	953.91	28.03	259.7	8.067	1.365 × 10^{-2}	1.364 × 10^{-5}	1.773 × 10^{-8}	1.448 × 10^{-5}	3.834 × 10^{14}	4.426 × 10^{4}	6.526 × 10^{-1}	6.782 × 10^{4}	1.468	3.014 × 10^{4}	3.298 × 10^{4}
89.917	55.871	953.45	27.85	265.2	8.297	1.133 × 10^{-2}	1.118 × 10^{-5}	1.432 × 10^{-8}	1.170 × 10^{-5}	3.118 × 10^{14}	4.488 × 10^{4}	8.025 × 10^{-1}	5.593 × 10^{4}	1.806	2.486 × 10^{4}	3.346 × 10^{4}
91.441	56.818	953.00	27.68	270.8	8.529	9.462 × 10^{-3}	9.336 × 10^{-6}	1.164 × 10^{-8}	9.508 × 10^{-6}	2.550 × 10^{14}	4.549 × 10^{4}	9.813 × 10^{-1}	4.636 × 10^{4}	2.208	2.060 × 10^{4}	3.394 × 10^{4}
92.965	57.765	952.55	27.50	276.4	8.764	7.938 × 10^{-3}	7.832 × 10^{-6}	9.507 × 10^{-9}	7.766 × 10^{-6}	2.096 × 10^{14}	4.612 × 10^{4}	1.194	3.862 × 10^{4}	2.686	1.716 × 10^{4}	3.443 × 10^{4}
94.489	58.712	952.10	27.32	281.9	9.003	6.690 × 10^{-3}	6.610 × 10^{-6}	7.804 × 10^{-9}	6.375 × 10^{-6}	1.732 × 10^{14}	4.673 × 10^{4}	1.445	3.234 × 10^{4}	3.251	1.437 × 10^{4}	3.492 × 10^{4}
96.013	59.659	951.65	27.14	287.5	9.245	5.664 × 10^{-3}	5.588 × 10^{-6}	6.437 × 10^{-9}	5.258 × 10^{-6}	1.438 × 10^{14}	4.734 × 10^{4}	1.740	2.720 × 10^{4}	3.916	1.209 × 10^{4}	3.540 × 10^{4}
97.537	60.606	951.20	26.97	293.0	9.491	4.817 × 10^{-3}	4.752 × 10^{-6}	5.335 × 10^{-9}	4.358 × 10^{-6}	1.199 × 10^{14}	4.795 × 10^{4}	2.086	2.298 × 10^{4}	4.694	1.021 × 10^{4}	3.589 × 10^{4}
99.061	61.553	950.75	26.79	298.6	9.739	4.113 × 10^{-3}	4.058 × 10^{-6}	4.441 × 10^{-9}	3.628 × 10^{-6}	1.005 × 10^{14}	4.856 × 10^{4}	2.490	1.950 × 10^{4}	5.602	8.668 × 10^{3}	3.638 × 10^{4}
100.58	62.500	950.30	26.61	304.2	9.991	3.526 × 10^{-3}	3.479 × 10^{-6}	3.713 × 10^{-9}	3.033 × 10^{-6}	8.459 × 10^{13}	4.916 × 10^{4}	2.958	1.662 × 10^{4}	6.655	7.387 × 10^{3}	3.686 × 10^{4}
102.11	63.447	949.85	26.43	309.7	1.025 × 10	3.034 × 10^{-3}	2.994 × 10^{-6}	3.117 × 10^{-9}	2.546 × 10^{-6}	7.149 × 10^{13}	4.977 × 10^{4}	3.500	1.422 × 10^{4}	7.875	6.320 × 10^{3}	3.735 × 10^{4}
103.63	64.394	949.40	26.26	315.3	1.051 × 10	2.621 × 10^{-3}	2.586 × 10^{-6}	2.628 × 10^{-9}	2.146 × 10^{-6}	6.067 × 10^{13}	5.040 × 10^{4}	4.124	1.222 × 10^{4}	9.280	5.431 × 10^{3}	3.784 × 10^{4}
105.16	65.341	948.96	26.08	320.8	1.077 × 10	2.273 × 10^{-3}	2.242 × 10^{-6}	2.223 × 10^{-9}	1.816 × 10^{-6}	5.169 × 10^{13}	5.102 × 10^{4}	4.841	1.054 × 10^{4}	1.089 × 10	4.684 × 10^{3}	3.834 × 10^{4}
106.68	66.288	948.50	25.90	326.4	1.104 × 10	1.977 × 10^{-3}	1.951 × 10^{-6}	1.889 × 10^{-9}	1.543 × 10^{-6}	4.421 × 10^{13}	5.163 × 10^{4}	5.660	9.122 × 10^{3}	1.274 × 10	4.054 × 10^{3}	3.883 × 10^{4}
108.20	67.235	948.06	25.72	332.0	1.131 × 10	1.726 × 10^{-3}	1.703 × 10^{-6}	1.610 × 10^{-9}	1.315 × 10^{-6}	3.794 × 10^{13}	5.224 × 10^{4}	6.595	7.921 × 10^{3}	1.484 × 10	3.520 × 10^{3}	3.933 × 10^{4}
109.73	68.182	947.61	25.55	337.5	1.158 × 10	1.512 × 10^{-3}	1.491 × 10^{-6}	1.377 × 10^{-9}	1.125 × 10^{-6}	3.268 × 10^{13}	5.285 × 10^{4}	7.657	6.902 × 10^{3}	1.723 × 10	3.068 × 10^{3}	3.982 × 10^{4}
111.25	69.129	947.16	25.37	343.1	1.186 × 10	1.328 × 10^{-3}	1.310 × 10^{-6}	1.182 × 10^{-9}	9.654 × 10^{-7}	2.824 × 10^{13}	5.349 × 10^{4}	8.859	6.038 × 10^{3}	1.993 × 10	2.684 × 10^{3}	4.032 × 10^{4}
112.78	70.076	946.72	25.19	348.6	1.214 × 10	1.170 × 10^{-3}	1.154 × 10^{-6}	1.018 × 10^{-9}	8.312 × 10^{-7}	2.449 × 10^{13}	5.410 × 10^{4}	1.022 × 10	5.295 × 10^{3}	2.299 × 10	2.353 × 10^{3}	4.082 × 10^{4}
114.30	71.023	946.27	25.01	354.2	1.243 × 10	1.034 × 10^{-3}	1.020 × 10^{-6}	8.790 × 10^{-10}	7.180 × 10^{-7}	2.130 × 10^{13}	5.474 × 10^{4}	1.175 × 10	4.661 × 10^{3}	2.643 × 10	2.072 × 10^{3}	4.132 × 10^{4}
115.82	71.970	945.82	24.84	359.8	1.272 × 10	9.166 × 10^{-4}	9.043 × 10^{-7}	7.615 × 10^{-10}	6.221 × 10^{-7}	1.859 × 10^{13}	5.535 × 10^{4}	1.346 × 10	4.112 × 10^{3}	3.028 × 10	1.828 × 10^{3}	4.182 × 10^{4}
117.35	72.917	945.38	24.66	365.3	1.302 × 10	8.146 × 10^{-4}	8.037 × 10^{-7}	6.618 × 10^{-10}	5.406 × 10^{-7}	1.627 × 10^{13}	5.599 × 10^{4}	1.538 × 10	3.641 × 10^{3}	3.460 × 10	1.618 × 10^{3}	4.233 × 10^{4}
118.87	73.864	944.93	24.48	370.9	1.332 × 10	7.259 × 10^{-4}	7.162 × 10^{-7}	5.767 × 10^{-10}	4.711 × 10^{-7}	1.428 × 10^{13}	5.660 × 10^{4}	1.752 × 10	3.231 × 10^{3}	3.942 × 10	1.436 × 10^{3}	4.284 × 10^{4}
120.00	74.564	944.60	24.35	375.0	1.354 × 10	6.677 × 10^{-4}	6.587 × 10^{-7}	5.218 × 10^{-10}	4.263 × 10^{-7}	1.299 × 10^{13}	5.708 × 10^{4}	1.926 × 10	2.964 × 10^{3}	4.333 × 10	1.317 × 10^{3}	4.322 × 10^{4}
120.40	74.811	944.49	24.35	376.6	1.360 × 10	6.484 × 10^{-4}	6.397 × 10^{-7}	5.046 × 10^{-10}	4.122 × 10^{-7}	1.256 × 10^{13}	5.761 × 10^{4}	1.992 × 10	2.893 × 10^{3}	4.481 × 10	1.286 × 10^{3}	4.331 × 10^{4}
121.92	75.758	944.04	24.35	382.7	1.383 × 10	5.802 × 10^{-4}	5.725 × 10^{-7}	4.443 × 10^{-10}	3.629 × 10^{-7}	1.106 × 10^{13}	5.785 × 10^{4}	2.262 × 10	2.558 × 10^{3}	5.089 × 10	1.137 × 10^{3}	4.365 × 10^{4}
137.16	85.227	939.60	24.35	444.1	1.613 × 10	2.09 × 10^{-4}	2.06 × 10^{-7}	1.38 × 10^{-10}	1.13 × 10^{-7}	3.44 × 10^{12}	6.21 × 10^{4}	7.27 × 10	8.55 × 10^{2}	1.64 × 10^{3}	3.80 × 10^{2}	4.70 × 10^{4}
152.40	94.697	935.20	24.35	505.5	1.844 × 10	8.67 × 10^{-5}	8.55 × 10^{-8}	5.02 × 10^{-11}	4.11 × 10^{-8}	1.25 × 10^{12}	6.63 × 10^{4}	2.00 × 10^{2}	3.32 × 10^{2}	4.49 × 10^{2}	1.48 × 10^{2}	5.02 × 10^{4}

Table 14 *(Cont'd)*

Latitude, 45°. Metric Units. p_a = 1014 mb, $\rho_a = 1.223 \times 10^{-3}$ gm/cm³

Height h km	Height h mi	Apparent Gravity g' cm/sec²	Mean Mol Wt M	Temp T °K	Scale Height H km	Pressure p millibars	Pressure Ratio p/p_a	Density ρ gm/cm³	Density Ratio σ ρ/ρ_a	Number Density n particles/cm³	Mean Particle Speed v cm/sec	$d = 3 \times 10^{-8}$ cm: Mean Free Path L cm	$d = 3 \times 10^{-8}$ cm: Mean Collision Freq ν 1/sec	$d = 2 \times 10^{-8}$ cm: Mean Free Path L cm	$d = 2 \times 10^{-8}$ cm: Mean Collision Freq ν 1/sec	Speed of Sound c cm/sec
160.94	100.00	932.75	24.35	539.9	1.975×10	5.53×10^{-5}	5.48×10^{-8}	3.00×10^{-11}	2.45×10^{-8}	7.49×10^{11}	6.85×10^{4}	3.34×10^{2}	2.05×10^{2}	7.52×10^{2}	9.11×10	5.19×10^{4}
167.64	104.17	930.83	24.35	566.9	2.078×10	3.98×10^{-5}	3.92×10^{-8}	2.05×10^{-11}	1.68×10^{-8}	5.12×10^{11}	7.02×10^{4}	4.89×10^{2}	1.44×10^{2}	1.10×10^{3}	6.38×10	
182.88	113.64	926.48	24.35	628.3	2.313×10	1.98×10^{-5}	1.96×10^{-8}	9.22×10^{-12}	7.54×10^{-9}	2.30×10^{11}	7.39×10^{4}	1.09×10^{3}	6.79×10	2.45×10^{3}	3.02×10	
198.12	123.11	922.17	24.35	689.7	2.551×10	1.06×10^{-5}	1.04×10^{-8}	4.50×10^{-12}	3.68×10^{-9}	1.12×10^{11}	7.74×10^{4}	2.24×10^{3}	3.46×10	5.03×10^{3}	1.54×10	
213.36	132.58	917.88	24.35	751.0	2.791×10	5.99×10^{-6}	5.91×10^{-9}	2.33×10^{-12}	1.91×10^{-9}	5.83×10^{10}	8.07×10^{4}	4.29×10^{3}	1.88×10	9.66×10^{3}	8.35	
228.60	142.05	913.63	24.35	812.4	3.034×10	3.54×10^{-6}	3.50×10^{-9}	1.28×10^{-12}	1.04×10^{-9}	3.19×10^{10}	8.40×10^{4}	7.86×10^{3}	1.07×10	1.77×10^{4}	4.75	
243.84	151.57	909.41	24.35	873.8	3.278×10	2.19×10^{-6}	2.16×10^{-9}	7.31×10^{-13}	5.98×10^{-10}	1.82×10^{10}	8.71×10^{4}	1.37×10^{4}	6.35×10	3.09×10^{4}	2.82	
259.08	160.98	905.21	24.35	935.2	3.525×10	1.40×10^{-6}	1.38×10^{-9}	4.38×10^{-13}	3.58×10^{-10}	1.09×10^{10}	9.01×10^{4}	2.29×10^{4}	3.93×10	5.16×10^{4}	1.75	
274.32	170.45	901.05	24.35	996.6	3.773×10	9.20×10^{-7}	9.07×10^{-10}	2.70×10^{-13}	2.21×10^{-10}	6.75×10^{9}	9.30×10^{4}	3.71×10^{4}	2.51×10	8.35×10^{4}	1.11	
289.56	179.92	896.91	24.35	1058	4.024×10	6.23×10^{-7}	6.14×10^{-10}	1.73×10^{-13}	1.41×10^{-10}	4.31×10^{9}	9.59×10^{4}	5.81×10^{4}	1.65×10	1.31×10^{5}	7.34×10^{-1}	
300.00	186.41	894.09	24.35	1100	4.197×10	4.84×10^{-7}	4.77×10^{-10}	1.29×10^{-13}	1.05×10^{-10}	3.21×10^{9}	9.78×10^{4}	7.79×10^{4}	1.25×10	1.75×10^{5}	5.57×10^{-1}	

1 millibar (mb) = 10^3 dynes/cm² = 0.750 mm of Hg

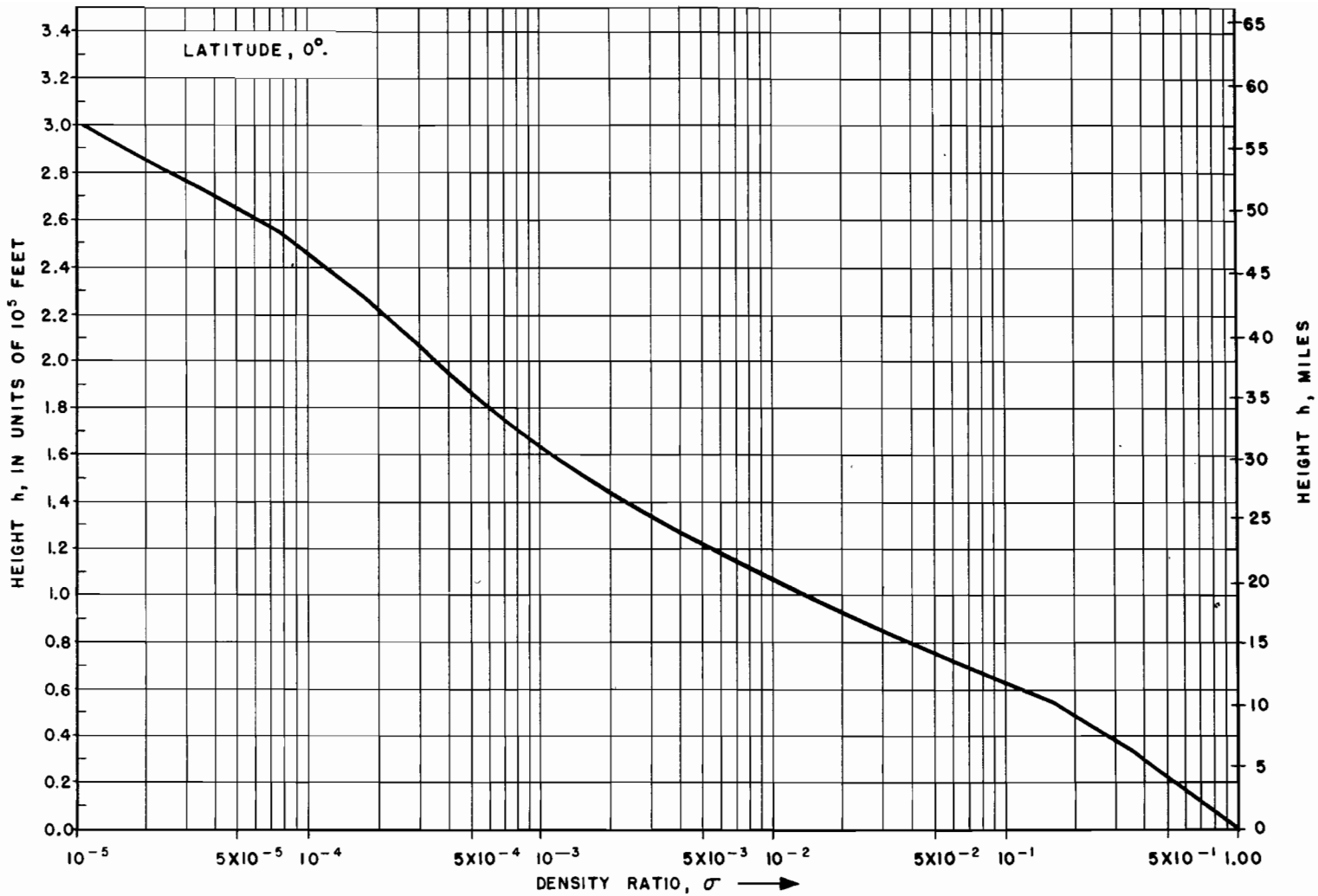

VERTICAL DISTRIBUTION OF THE DENSITY RATIO σ FROM SEA LEVEL UP TO THE F_2 LAYER.
LATITUDE 0°. ENGINEERING UNITS.

FIG. 10 (a)

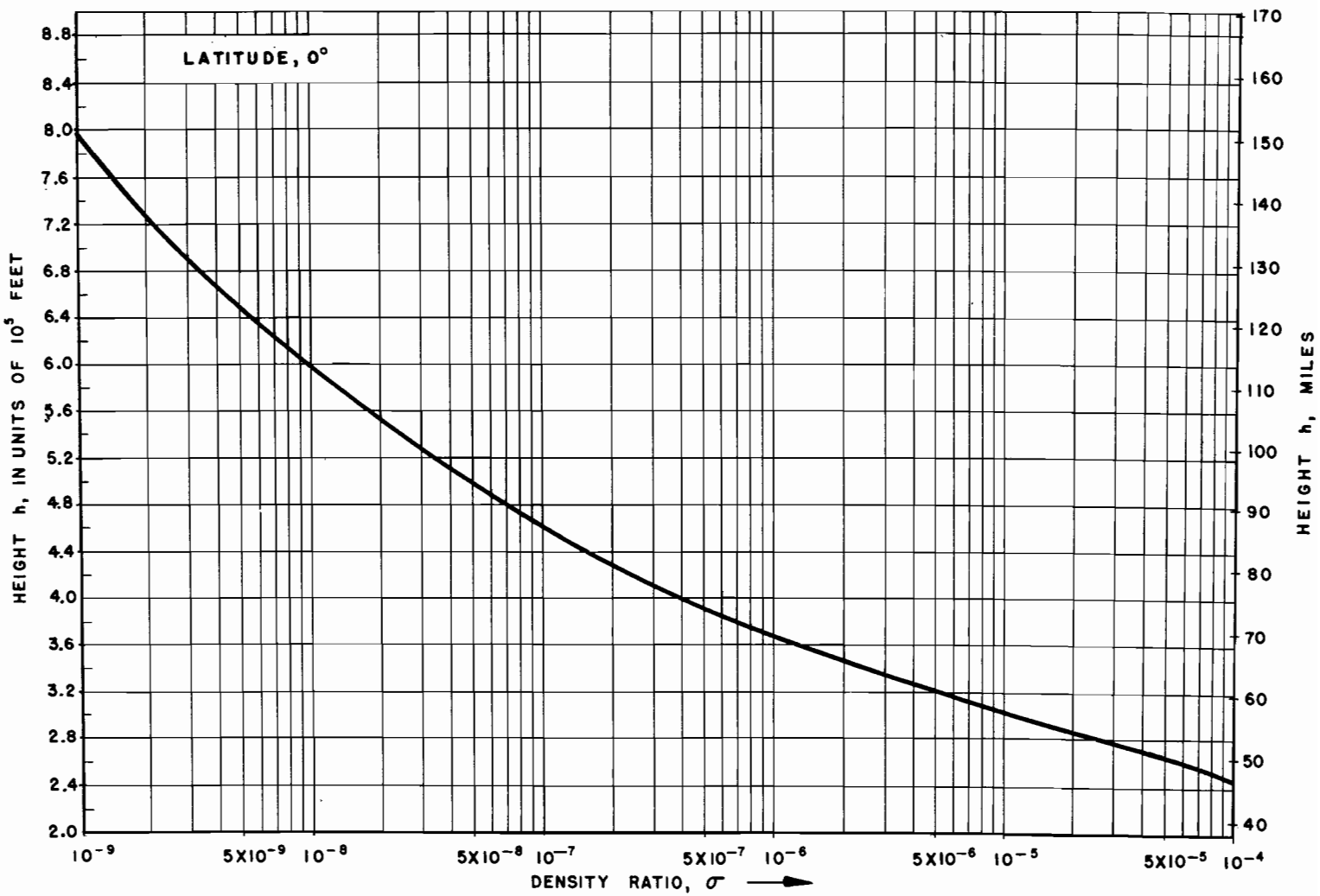

VERTICAL DISTRIBUTION OF THE DENSITY RATIO σ FROM SEA LEVEL UP TO THE F_2 LAYER.
LATITUDE 0°. ENGINEERING UNITS.

FIG. 10 (b)

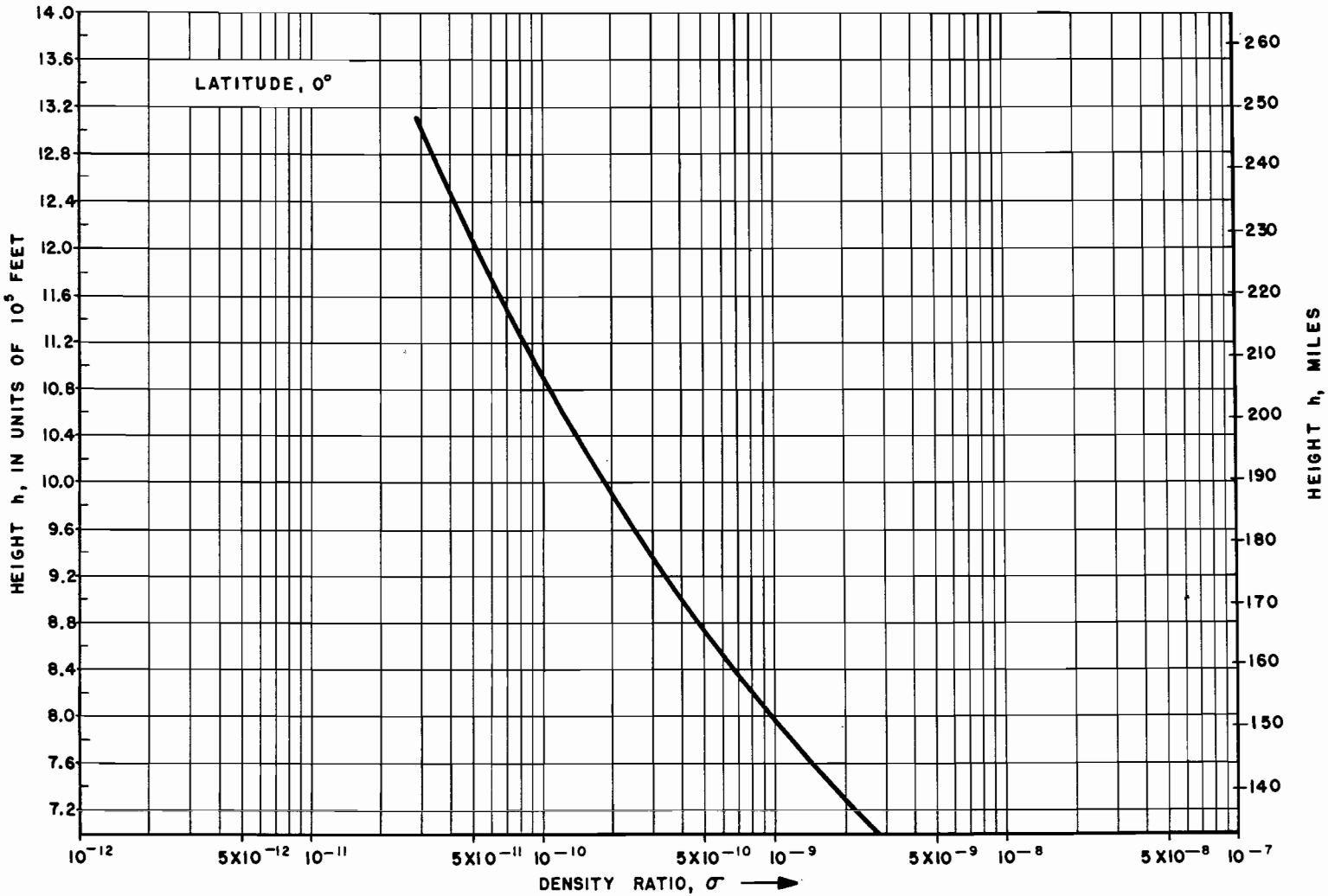

VERTICAL DISTRIBUTION OF THE DENSITY RATIO σ FROM SEA LEVEL UP TO THE F_2 LAYER.
LATITUDE 0° ENGINEERING UNITS.

FIG. 10 (c)

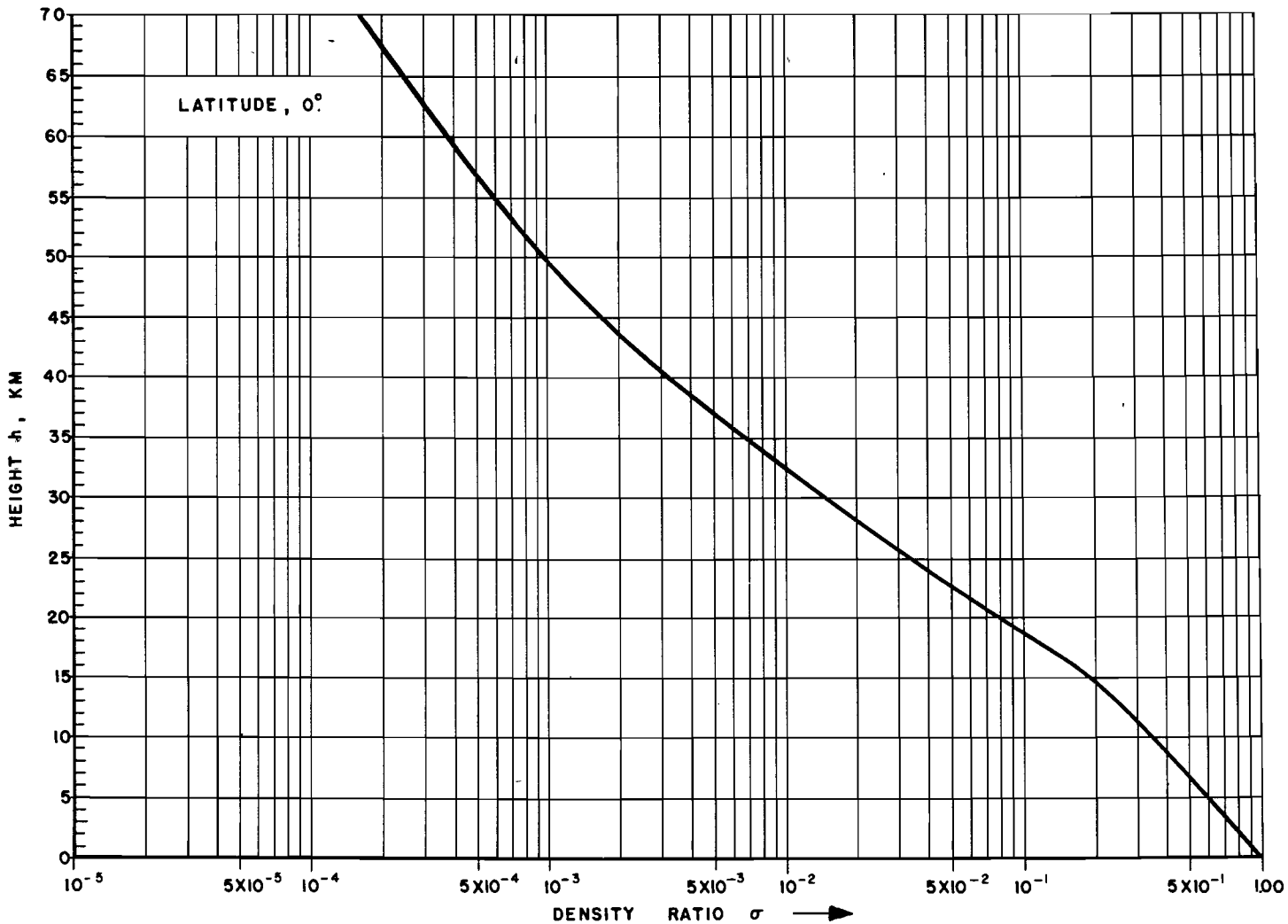

VERTICAL DISTRIBUTION OF THE DENSITY RATIO σ FROM SEA LEVEL UP TO THE F_2 LAYER.
LATITUDE 0° METRIC UNITS.

FIG. 11 (a)

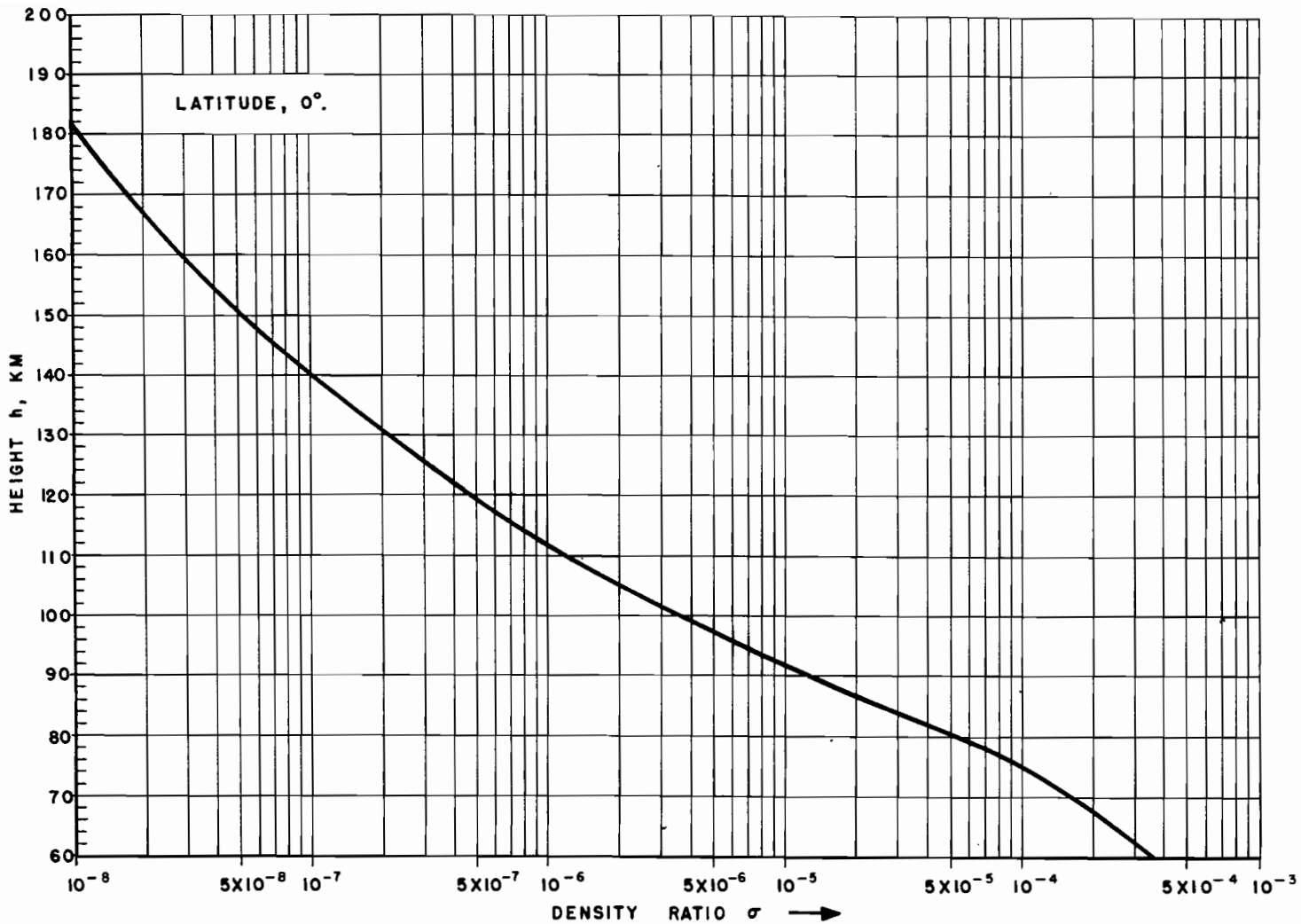

VERTICAL DISTRIBUTION OF THE DENSITY RATIO σ FROM SEA LEVEL UP TO THE F_2 LAYER.
LATITUDE 0°. METRIC UNITS.

FIG. 11 (b)

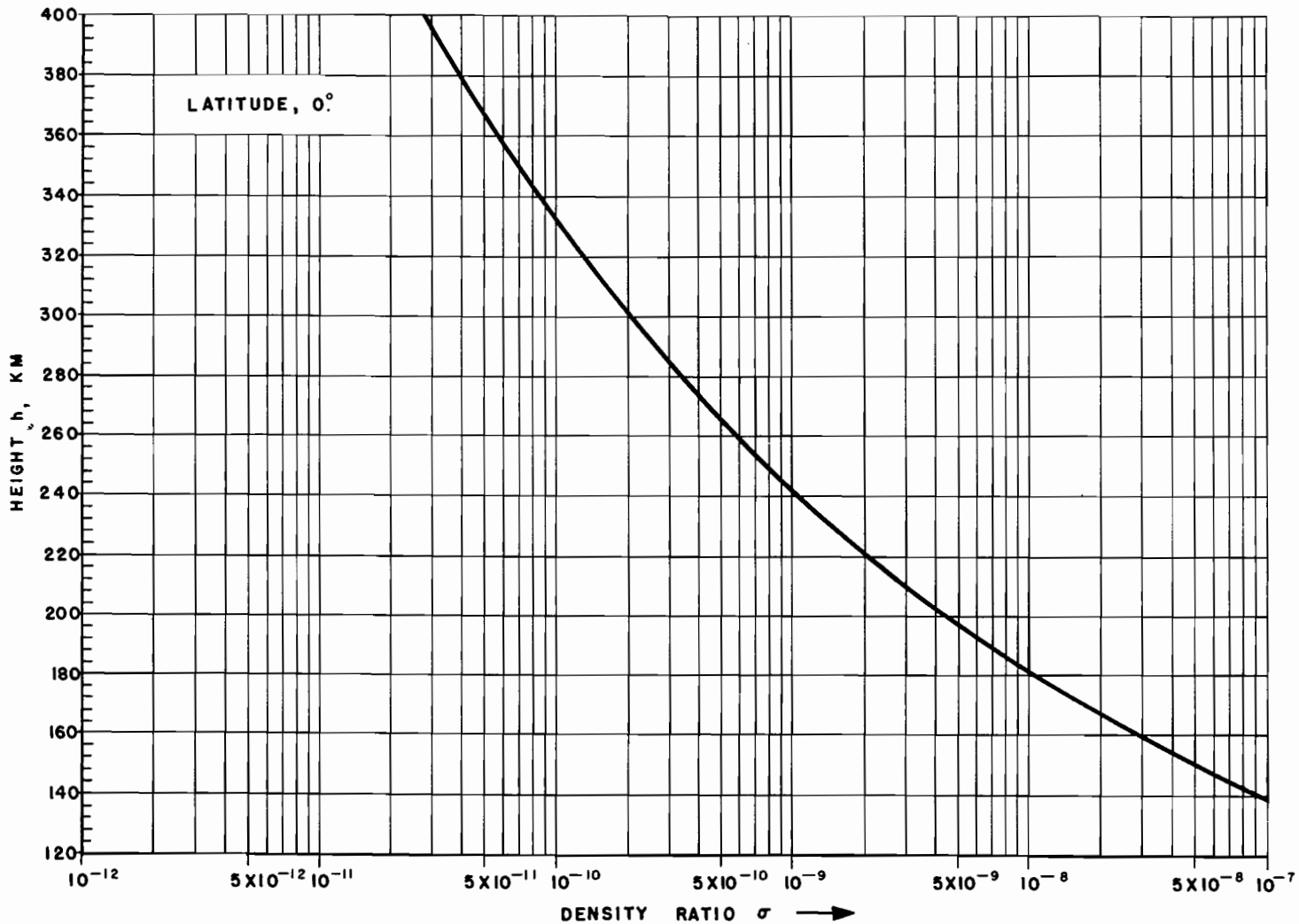

VERTICAL DISTRIBUTION OF THE DENSITY RATIO σ FROM SEA LEVEL UP TO THE F_2 LAYER.
LATITUDE 0°. METRIC UNITS.

FIG. 11 (c)

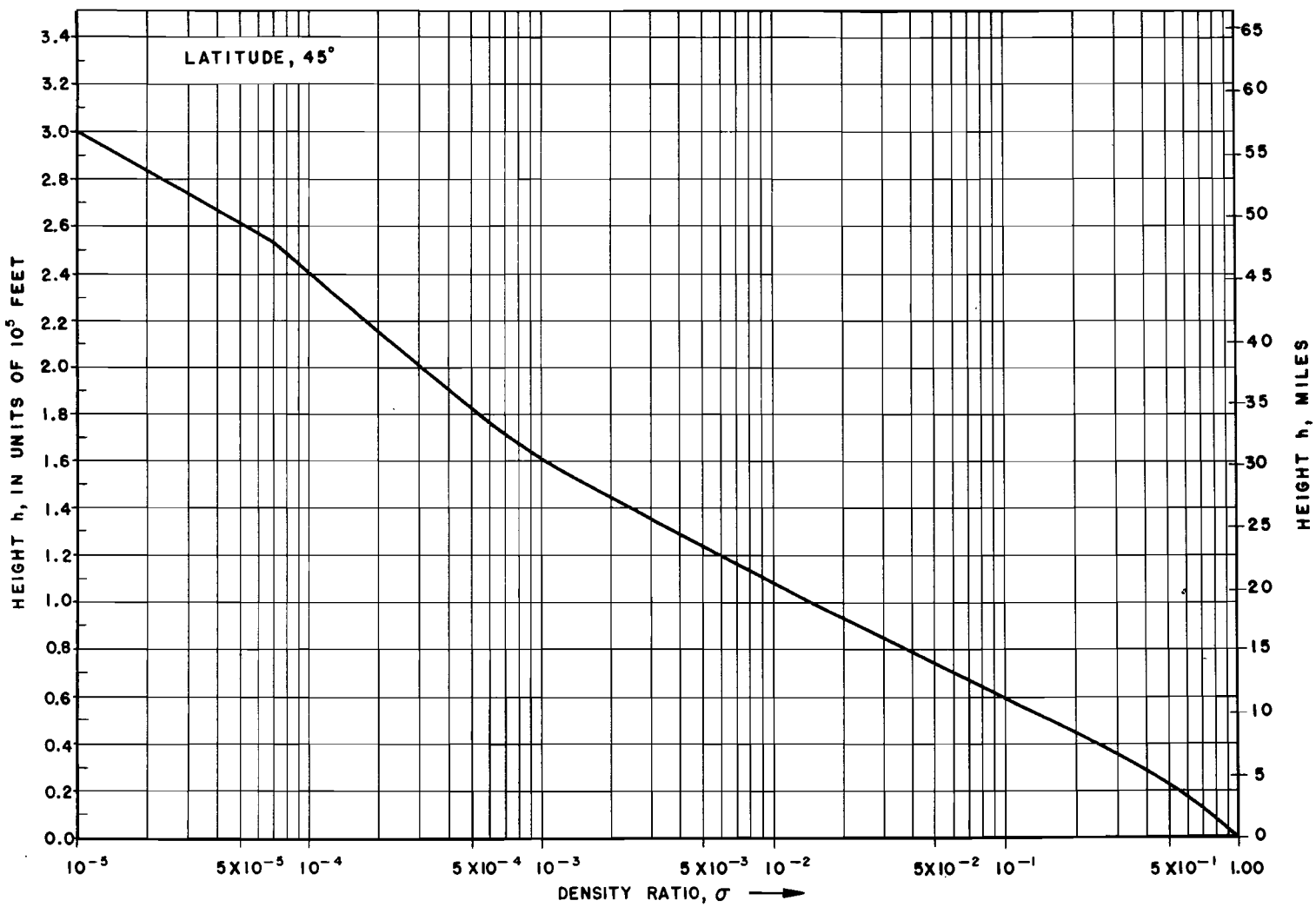

VERTICAL DISTRIBUTION OF THE DENSITY RATIO σ FROM SEA LEVEL UP TO THE F_2 LAYER.
LATITUDE 45°. ENGINEERING UNITS.

FIG. 12 (a)

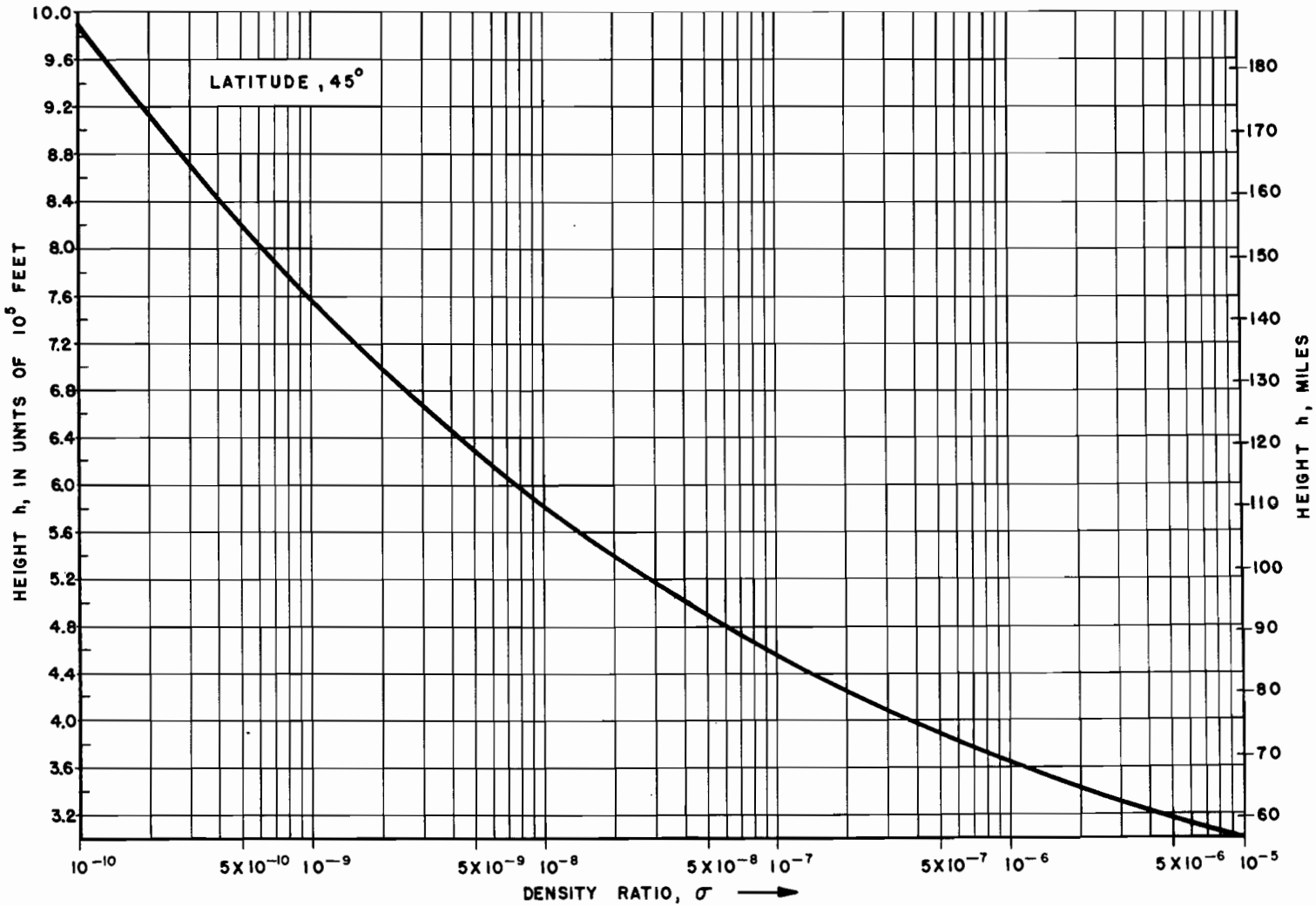

VERTICAL DISTRIBUTION OF THE DENSITY RATIO σ FROM SEA LEVEL UP TO THE F_2 LAYER.
LATITUDE 45° ENGINEERING UNITS.

FIG. 12 (b)

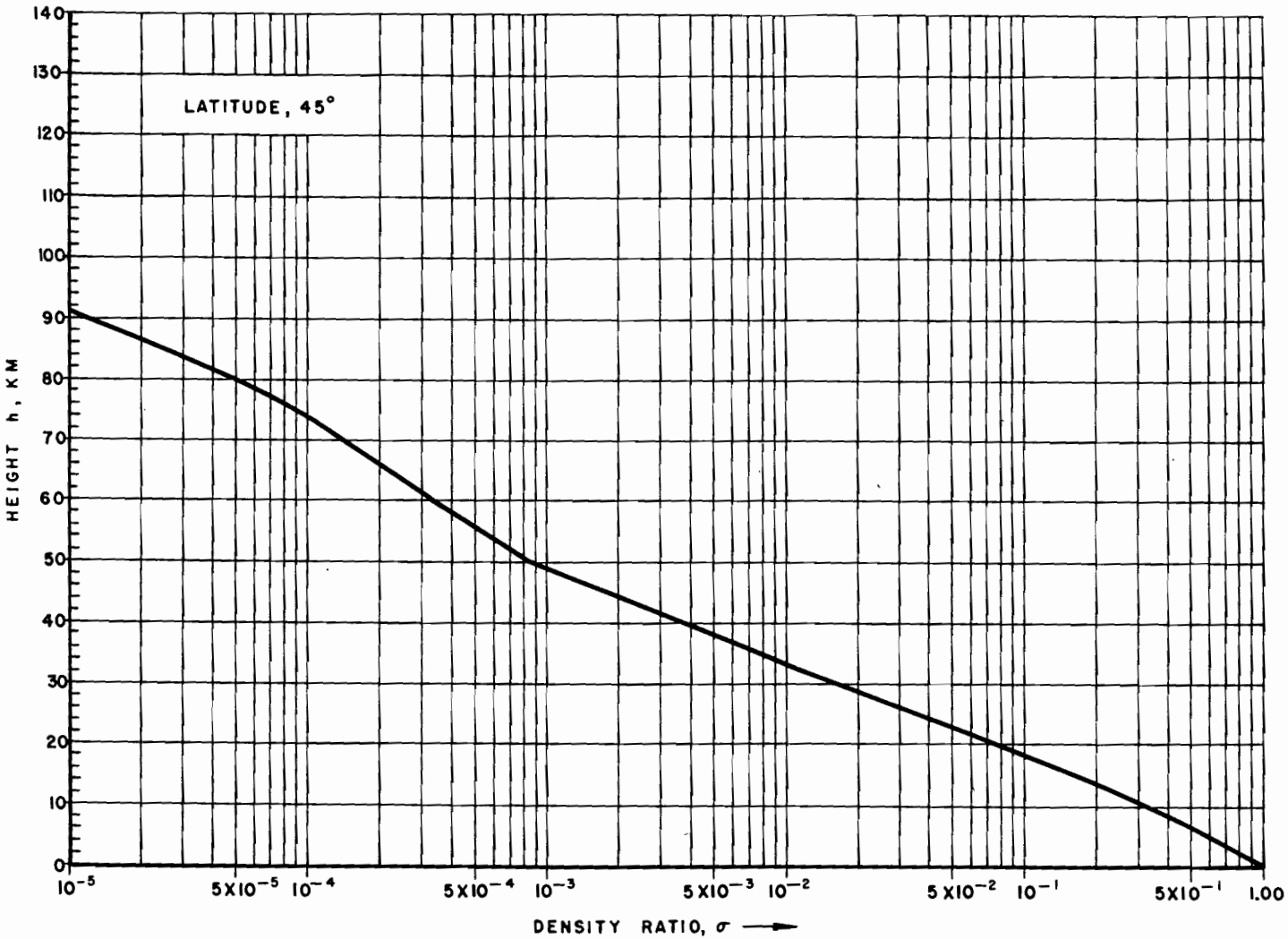

VERTICAL DISTRIBUTION OF THE DENSITY RATIO σ FROM SEA LEVEL UP TO THE F_2 LAYER. LATITUDE 45° METRIC UNITS.

FIG. 13 (a)

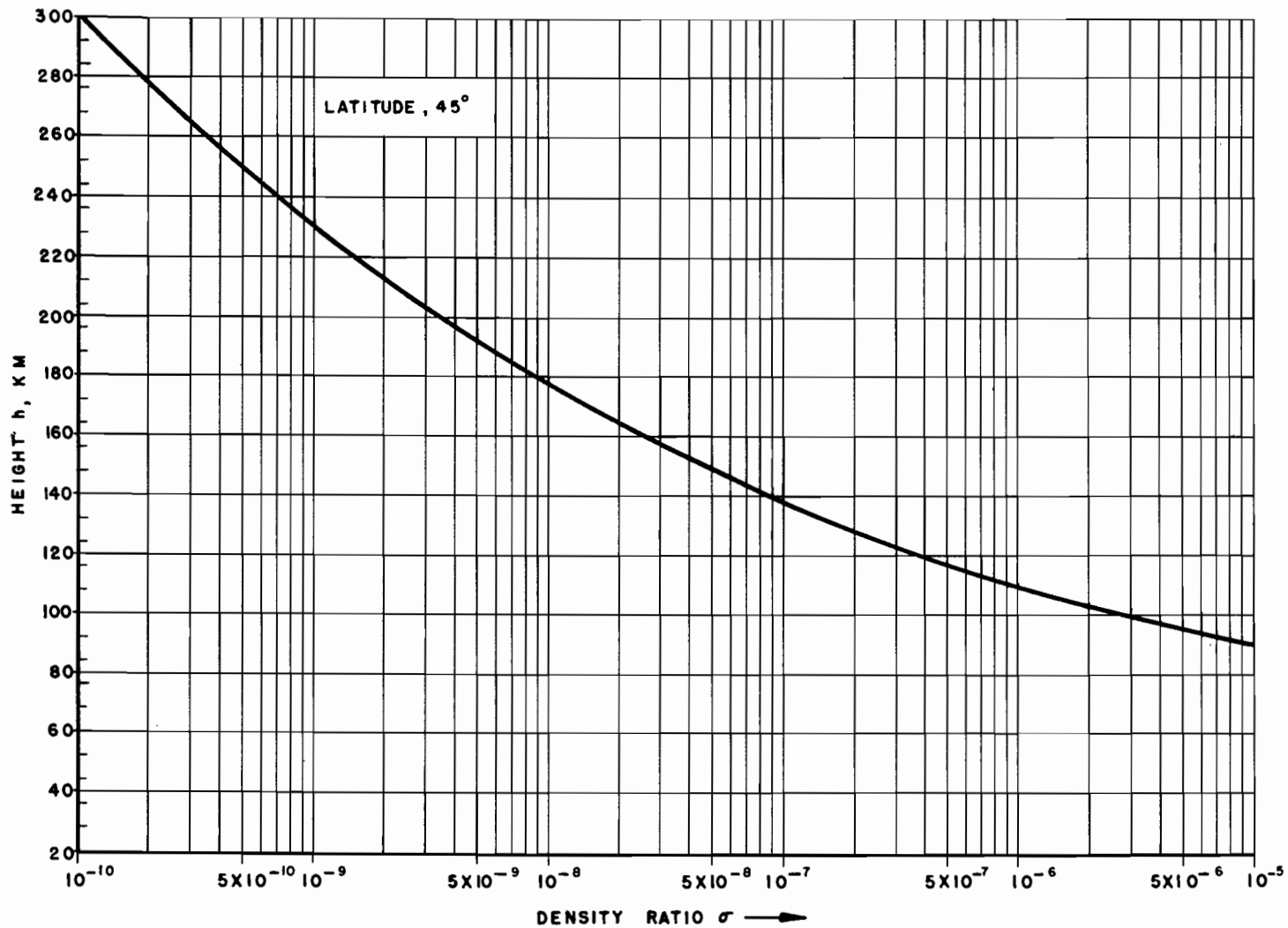

VERTICAL DISTRIBUTION OF THE DENSITY RATIO σ FROM SEA LEVEL UP TO THE F_2 LAYER.
LATITUDE 45° METRIC UNITS.

FIG. 13 (b)

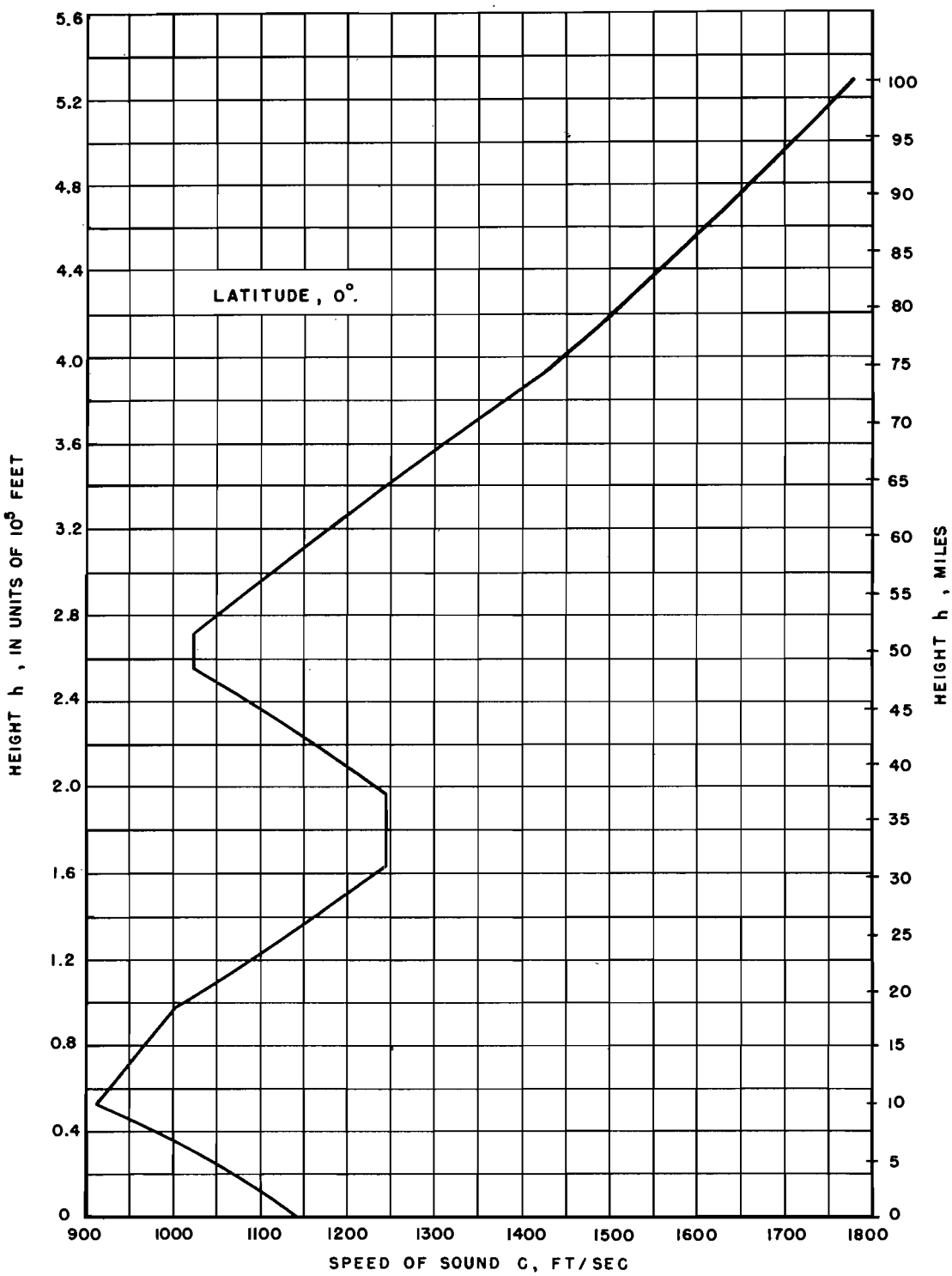

VERTICAL DISTRIBUTION OF THE SONIC VELOCITY FROM SEA LEVEL UP TO 100 MILES. LATITUDE 0°. ENGINEERING UNITS.

FIG. 14

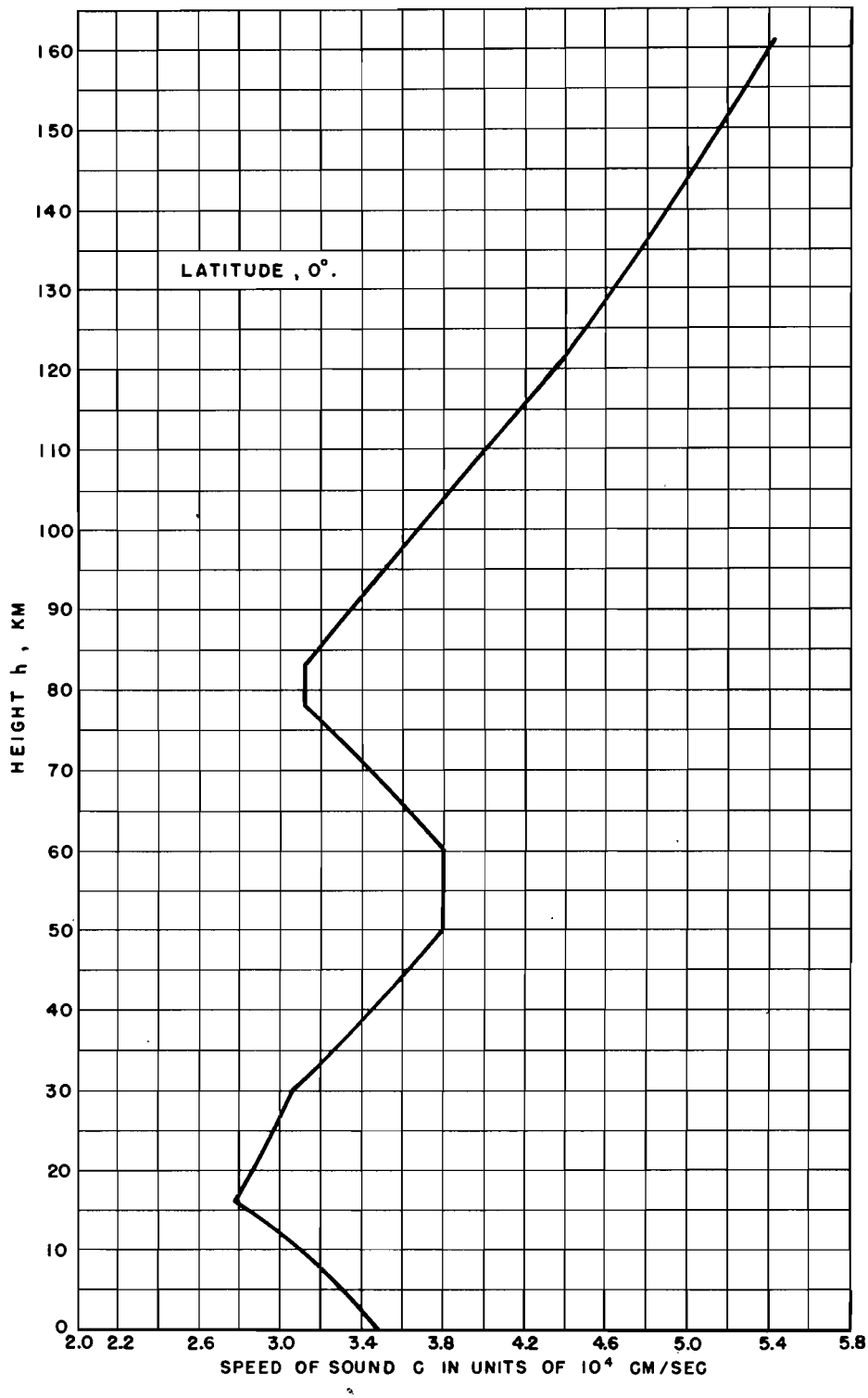

VERTICAL DISTRIBUTION OF THE SONIC VELOCITY FROM SEA LEVEL UP TO 160 KM. LATITUDE 0°. METRIC UNITS.

FIG. 15

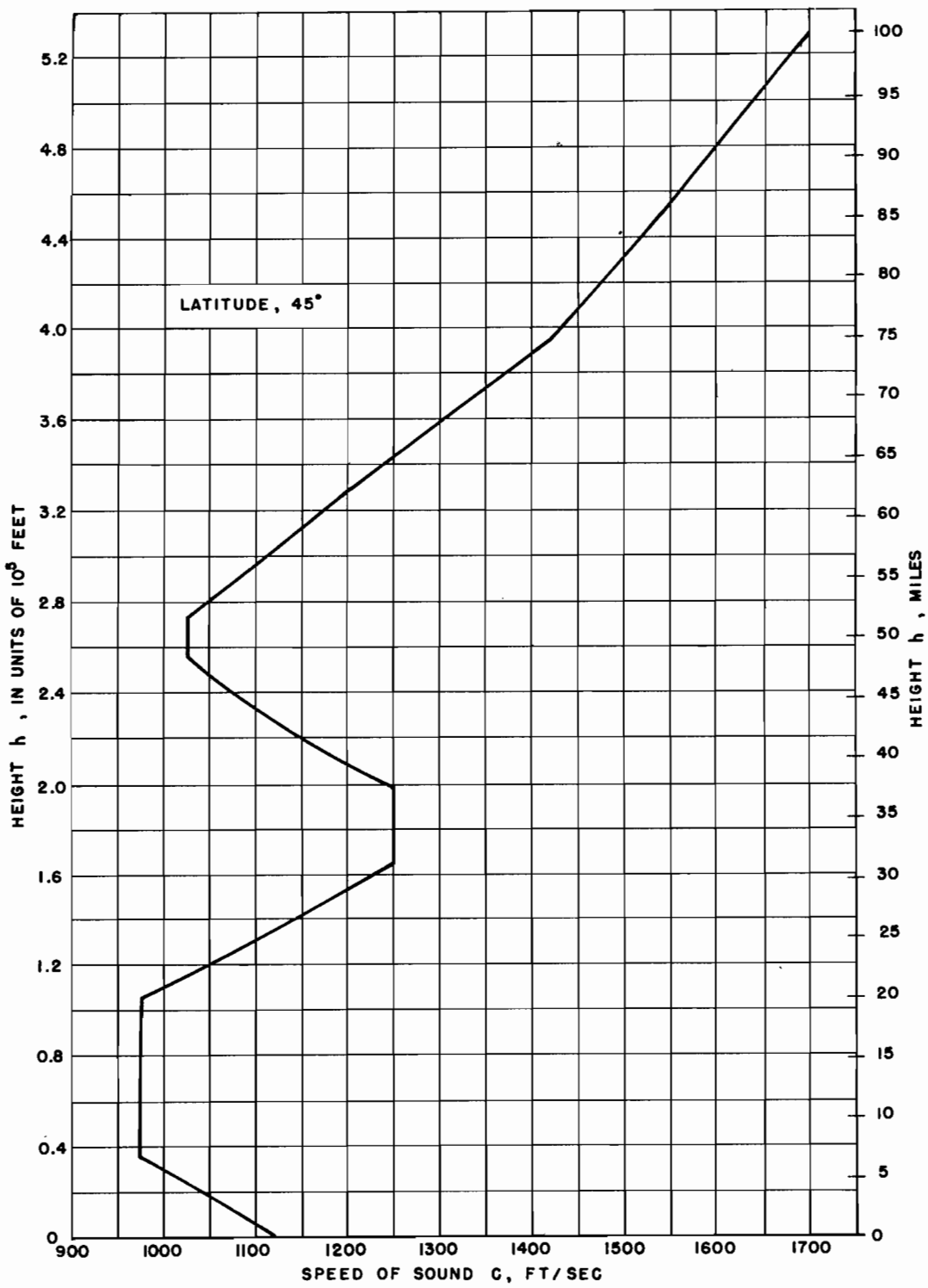

VERTICAL DISTRIBUTION OF THE SONIC VELOCITY FROM SEA LEVEL UP TO 100 MILES. LATITUDE 45°. ENGINEERING UNITS.

FIG. 16

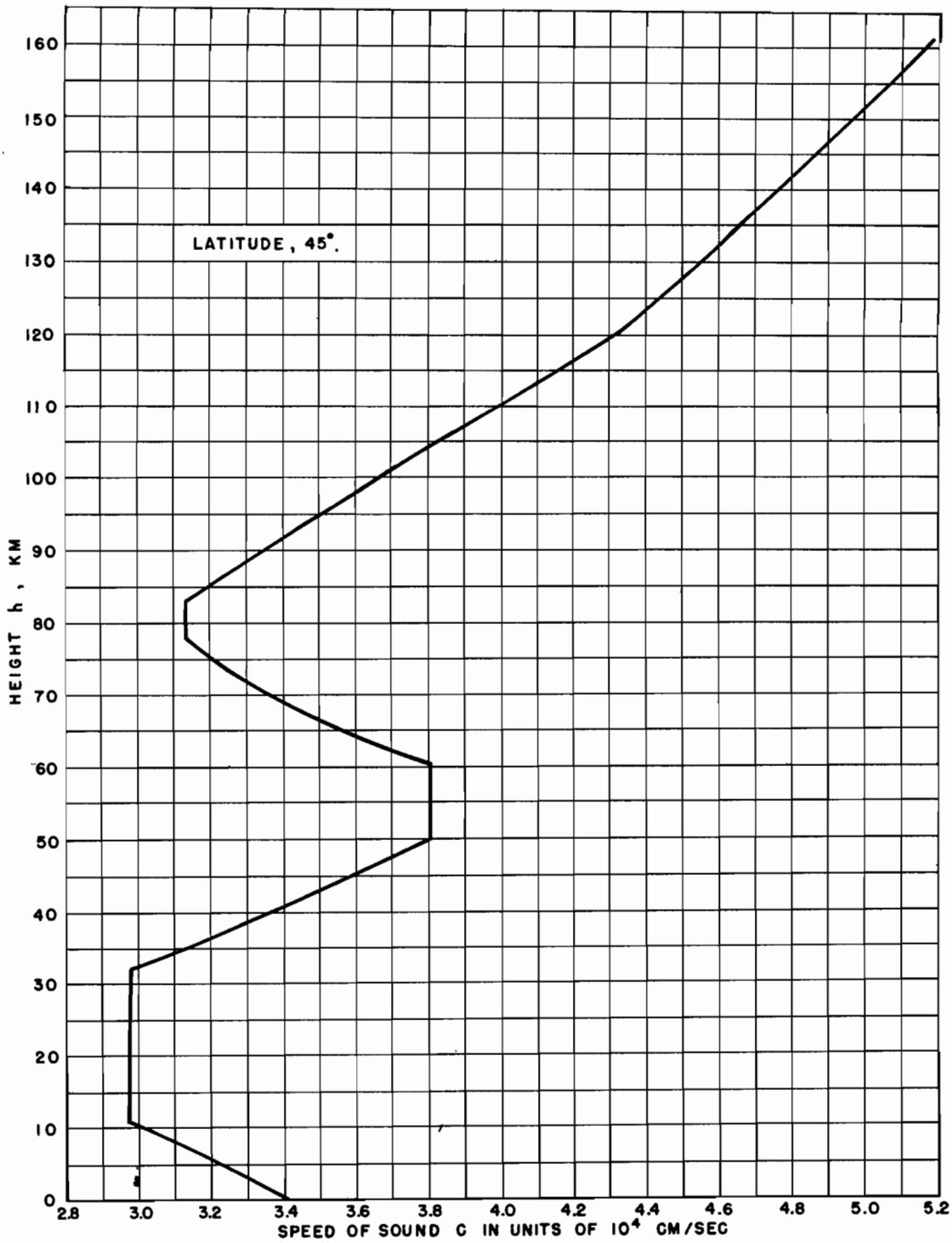

VERTICAL DISTRIBUTION OF THE SONIC VELOCITY FROM SEA LEVEL UP TO 160 KM. LATITUDE 45°. METRIC UNITS.

FIG. 17

II - THE ATMOSPHERE ABOVE THE F_2 LAYER - MODELS I AND II

Above the F_2 layer there is little if any direct information available concerning the atmosphere. Although the mass of atmosphere in this region is extremely small compared with the total atmospheric mass, yet the vertical extent of this region of the atmosphere is relatively large compared with the height of the F_2 layer. In fact as far as the knowledge of the atmosphere is concerned, it might well be divided into two major regions, the region below the F_2 layer and that above.

In view of the uncertainties and lack of information concerning the properties of the atmosphere above the F_2 layer, it becomes necessary to analyze this region on the basis of whatever concepts or hypotheses appear reasonable or possible; and it is hardly likely, owing to the present lack of knowledge, that any single concept would prove entirely satisfactory at the present time. The manner in which this region of the atmosphere is analyzed here is based on three different atmospheric models or concepts which are intended to serve as a preliminary approach to the problem. The first atmospheric model is based on the concept that there is a limiting region far beyond the F_2 layer where the atmosphere is in thermal equilibrium with the interstellar gas. The second model is based on the concept that at a sufficient height above the F_2 layer the particles begin to move as free bodies in a gravitational field, rising and falling over large distances without colliding with another particle, and that this region is isothermal. The third model is discussed in Part III.

II-A. THE TEMPERATURE DISTRIBUTION AND THE INTERSTELLAR† GAS

Perhaps the first question which arises concerning this region of the upper atmosphere is that of temperature. The temperature rises rapidly from the E layer to the F_2 layer; and one may ask whether, above the F_2 layer, the temperature continues to rise, remains more or less constant, or decreases. The answer is certainly not clear, and a consideration of conditions existing in this region is necessarily somewhat hypothetical and speculative. Thus when it is desired to consider the atmosphere above the F_2 layer, it becomes necessary, in view of the lack of any direct information, to find some means of extrapolation. For example, there are certain conditions which exist in interstellar space, and an attempt may be made to use these as a possible basis for extrapolation. Thus it is known that gas particles exist in interstellar space[39],[40], and it is tempting to make the hypothesis that the outer limit of the atmosphere is defined by the condition that equilibrium exist between the atmospheric gas and the interstellar gas. It is generally recognized[41],[42],[43],[44] that the interstellar gas has a high kinetic temperature of the order of 10,000 to 15,000°K, and according to the equilibrium hypothesis, it will therefore be assumed in Model I that the outer limit of the atmosphere is in thermal equilibrium with the interplanetary gas particles at this temperature.

† As used in the present connection it would probably be more appropriate to use the term interplanetary gas, since it is the gas in the vicinity of the planet Earth which is being considered.

Thus it will be assumed as a first approach that at the outer limit of the atmosphere the atmospheric gas particles have a kinetic temperature of 10,000°K. In view of the rather hypothetical nature of this approach, a second and perhaps more acceptable atmospheric model will be used in which the limit of the atmosphere is defined by the existence of an outer region where the mean free path becomes so large that the the gas particles begin to establish dynamical orbits. With the first atmospheric model in which it is assumed that the atmosphere at its outer limit is in thermal equilibrium with the interstellar gas at a temperature of 10,000°K, it is reasonable to suppose that the temperature increases monotonically from the F_2 layer out to the atmospheric limit; and it will be assumed that this is the case.

The exact form of the vertical temperature distribution must next be decided upon. This of course is somewhat arbitrary; and if we wished, the vertical temperature distribution could be taken as a linear one. However it seems more satisfactory physically to have a temperature distribution such that dT/dr (where r is distance measured from the center of the earth) is smaller at large distances, since this gives more uniform continuity with the limiting conditions. In fact if the analogy is made here with the transfer of heat between two concentric spheres, we are led to the conclusion that dT/dr is proportional to $1/r^2$. Since this relation seems satisfactory as far as conditions at the limits are concerned, it will be adopted to represent the approximate manner in which the temperature changes with the vertical distance r. Thus the approximate relation will be $dT/dr = A/r^2$. The reason that this relation will be satisfied only approximately in the calculations will become clear from the following discussion.

As will be discussed in Section II-B, in this upper region of the atmosphere it will no longer be assumed that the atmosphere rotates with the earth as a solid; and the constant angular velocity Ω in Eq. (11) must be replaced by a variable angular velocity $\omega = \omega(r)$. The apparent gravity relation then becomes

$$g' = g_a \left(\frac{a}{r}\right)^2 - r\,\omega^2 \cos^2\theta \quad , \tag{25}$$

where the first term is the absolute gravity force and the second term is the centrifugal force. It will be found convenient to use, instead of g', the apparent gravity potential function ϕ defined by

$$\frac{d\phi}{dr} = g' = g_a \left(\frac{a}{r}\right)^2 - r\,\omega^2 \cos^2\theta. \tag{26}$$

It will be shown in Section II-B that the centrifugal force term, which in itself is small, goes to zero as r increases so that $d\phi/dr$ is approximately proportional to $1/r^2$, the approximation becoming more exact with increasing r. Thus $d\phi/dr$ will be very nearly directly proportional to dT/dr, that is, to $1/r^2$.

From Eq. (18) we have

$$\phi = \int g'\,dr + \text{const.} \tag{27}$$

It will be convenient to choose the constant of integration so that $\phi = 0$ at the distance r_0 corresponding to the height of the F_2 layer. The expression for ϕ then becomes

$$\phi = g_a a^2 \left(\frac{1}{r_0} - \frac{1}{r}\right) - \cos^2\theta \int_{r_0}^{r} r\left[\omega(r)\right]^2 dr \ , \tag{28}$$

where $\cos\theta$ is a constant depending upon the latitude θ. It will be seen later on that the integration of the hydrostatic equation becomes especially easy if the temperature distribution, starting from the value T_0 in the F_2 layer, is linear in ϕ and therefore of the form

$$T = T_0 + \alpha\phi \ . \tag{29}$$

In addition it is seen that, since $dT/dr = \alpha\, d\phi/dr \approx 1/r^2$, this form for the temperature distribution is a satisfactory representation of the inverse square relation for the temperature. It will therefore be assumed that the temperature distribution is of the form given by (29). The constant α is evaluated from the relation

$$\alpha = \frac{T_L - T_0}{\phi_L} \ , \tag{30}$$

where ϕ_L and T_L denote the values at the limit of the atmosphere where it is assumed that $T_L = 10{,}000°K$.

II-B. THE DISTRIBUTION OF ANGULAR VELOCITY

In the treatment of the atmosphere from sea level up to the F_2 layer it was assumed that the atmosphere rotated with the earth as a solid body with angular velocity Ω. This is the usual assumption in the meteorology of the lower atmosphere, and since there seems to be no evidence to the contrary at higher levels, say up to 100 km, the assumption of constant angular velocity was more or less arbitrarily extended to include the F_2 layer. However it does not seem acceptable physically to assume the constant angular velocity Ω at all heights, since at the limit of the atmosphere where by hypothesis we have equilibrium with the non-rotating interplanetary gas one should certainly expect the linear velocity and therefore the angular velocity to approach zero. This, of course, does not include the thermal molecular velocities but only the mean motion of the gas as a whole.

Thus it seems reasonable to assume that starting with the value $\omega = \Omega$ at the F_2 layer, the angular velocity begins to decrease and becomes zero at the limit of the atmosphere. As in the case of the temperature, here again there is little to serve

as a guide to show how ω should vary with r. However, Jeans[45] has found that in the outermost gaseous layers of a star the angular velocity ω must vary as $1/r^2$; and since this also seems acceptable as far as the atmosphere is concerned, it is the law of variation which will be adopted. Above the F_2 layer it is therefore assumed that $d\omega/dr = C/r^2$ which gives

$$\omega = \Omega - C\left(\frac{1}{r_0} - \frac{1}{r}\right) . \tag{31}$$

The constant C is evaluated from the relation

$$C = \frac{\Omega}{\frac{1}{r_0} - \frac{1}{r_L}} , \tag{32}$$

where r_L is the distance from the center of the earth to the limit of the atmosphere. The expression for ω may then be written

$$\omega = \Omega \left[1 - \frac{\frac{1}{r_0} - \frac{1}{r}}{\frac{1}{r_0} - \frac{1}{r_L}}\right] . \tag{33}$$

Using this expression for ω, the formula for ϕ, Eq. (28), becomes

$$\phi = g_a a^2 \left(\frac{1}{r_0} - \frac{1}{r}\right) - \cos^2\theta \int_{r_0}^{r} r\,\Omega^2 \left[1 - \frac{\frac{1}{r_0} - \frac{1}{r}}{\frac{1}{r_0} - \frac{1}{r_L}}\right]^2 dr , \tag{34}$$

which, when integrated, results in the expression

$$\phi = g_a \frac{a^2}{r_0} \frac{1}{\frac{r}{r_0}}\left(\frac{r}{r_0} - 1\right) - r_0^2\,\Omega^2 \cos^2\theta \left[\frac{1}{2}\left(\frac{r^2}{r_0^2} - 1\right) - \frac{r_L}{r_0} \frac{\left(\frac{r}{r_0} - 1\right)^2}{\left(\frac{r_L}{r_0} - 1\right)}\right.$$

$$\left. + \frac{1}{2}\left(\frac{r_L}{r_0}\right)^2 \frac{\left(\frac{r^2}{r_0^2} - 1\right)}{\left(\frac{r_L}{r_0} - 1\right)^2} - 2\left(\frac{r_L}{r_0}\right)^2 \frac{\frac{r}{r_0} - 1}{\left(\frac{r_L}{r_0} - 1\right)^2} + \frac{\left(\frac{r_L}{r_0}\right)^2}{\left(\frac{r_L}{r_0} - 1\right)^2} \log \frac{r}{r_0}\right] . \tag{35}$$

II-C. THE COMPOSITION

As mentioned before in the discussion of the composition up to the F_2 layer, the evidence from the aurora and the light of the night sky indicates that the upper atmosphere is composed mainly of nitrogen and oxygen. This is certainly true up to 1200 km since the aurora has been observed to this height. However we are concerned here with heights which, as will be seen later, are much greater than this. Although there is no evidence of the presence of hydrogen or helium, the presence of these gases has not been absolutely disproved. Lindemann[46] is of the opinion that helium may form the major part of the gas in the limit regions of the atmosphere. The argument here is, that since helium is being continually supplied at the surface of the earth and since the total amount in the atmosphere remains constant, it must be continually escaping from the top of the atmosphere and may therefore constitute the major portion of the gas in this limit region. This of course presupposes that somewhere above the F_2 layer the gases reach a state of diffusion equilibrium in which the constituent gases are distributed in the vertical according to their molecular weights with the lightest gases predominating at the top of the atmosphere. As mentioned previously, Mitra and Rakshit[35] have shown that diffusion equilibrium of neutral gas particles should be practically complete above 350 km if there are no forces in operation which would produce mixing of the gases or prevent their settling out once they are mixed.

However, it seems a possibility that in the outer limit region of the atmosphere practically all of the gas particles may be ionized, and in this case it would be necessary to consider the effect on diffusion of the earth's magnetic field. The effect of the earth's magnetic field on the motion of a charged particle in the upper atmosphere is discussed by Chapman[15], and a study of the effect on diffusion in the F_2 layer has been made by Ferraro[47] and Cowling[34].

In any event, if neutral hydrogen and helium are present in the outer portions of the ionosphere, it follows as a necessary consequence of the high temperature which has been assumed to exist there that they must be continually escaping into space, since their mean molecular velocities will much exceed the critical escape velocity. According to Jones[48], it would require a temperature as low as 400°K at the top of the atmosphere in order that the rate of loss for neutral particles should be small for hydrogen and therefore negligible for the other gases. However, it seems quite possible that the gases in the outer limit region of the atmosphere may be ionized, so that the presence of the earth's magnetic field may be expected to alter considerably the mechanism of the escape process. In particular, the effect of the magnetic field is to cause a spiral motion which, in effect, limits the size of the mean free path and which should therefore make the escape of a particle much more difficult. However, in view of the high temperatures assumed here (10,000°K), if the molecular velocity distribution is Maxwellian, it appears likely that there will be some escape of gas, although perhaps small, regardless of what the gas is. To preserve continuity the mass of escaped gas would have to be made good by equal replenishment at the bottom of the atmosphere. From this point of view one could refer to the outer limits of the ionosphere as the dissipationsphere, since the processes there would be quite analogous to those which occur in the evaporation of a liquid.

Aside from the question of what are the constituent gases in the outer ionosphere, there are also the questions of dissociation and ionization. It has already been pointed out that dissociation of oxygen takes place in the E layer and that there is increasing ionization up to the F_2 layer. The question of the dissociation of nitrogen, on the other hand, is a very controversial one. Although Chapman and others favor the view, based on auroral observations, that there is no appreciable dissociation of nitrogen, it seems quite possible that at sufficiently great heights the dissociation of nitrogen could take place due to solar radiation and that eventually, at sufficient distances, all nitrogen would be in the atomic form. This is supported to some extent perhaps by the work of Wulf and Deming (Ref. 33, p. 291) who point out that the short wave-length radiation available for the nitrogen absorptions, although much less intense than that in the oxygen absorption region, will be absorbed at greater heights where the gas pressure is much lower than for the oxygen absorptions, and where, therefore, the dissociating and ionizing effects on nitrogen may be as important as those produced at lower levels on oxygen by much more intense radiation. These authors state further (Ref. 33, pp. 287 and 295) that at least the positive nitrogen-molecule ion N_2^+ must certainly exist in the high atmosphere and that it seems quite possible that (even) in the F region the nitrogen absorptions may lead to the production of N_2^+, N^+, and N, that is, to some dissociation as well as ionization of nitrogen.

As far as ionization is concerned, it is seen in Fig. 9 that the degree of ionization is increasing in the F_2 layer even though the ion density goes through a maximum in this layer. The maximum in the ion density is a peculiar circumstance resulting from degree of ionization plus the variation of density with height, and it is not to be inferred that the degree of ionization itself goes through a maximum in the F_2 layer. On the contrary, all evidence points toward increasing degree of ionization with height; and it will be assumed for model I that complete ionization exists at the limit of the atmosphere so that the atmospheric gas there consists of positive ions and free electrons in equal number.

In fact if the formulas for thermal dissociation[36] and ionization[50] be applied to the limiting region of the atmosphere assumed here, it will be found that at such low pressures and high kinetic temperatures complete dissociation and ionization would be indicated. Thus in order to be consistent with the high kinetic temperature assumed to exist at the limit of our hypothetical atmosphere, it appears necessary to assume also that complete dissociation and ionization exist in this region. It is not intended to imply here that the dissociation and ionization are due to the direct addition of heat, as would be the case for example, in a high-temperature flame, since the initial process responsible for producing the high kinetic temperatures must be something quite different. However, once the high kinetic temperature (high kinetic energy of particles) is attained, regardless of the mechanism responsible, it would seem that the formulas for thermal dissociation and ionization must apply, since they are based upon the impact effects of the mutual collisions of high-speed particles and electrons.

From the remarks which have been made so far concerning the composition, Table 15 has been prepared to show the range of possibilities regarding the state of the atmosphere at its limit. The molecular weight at the limit r_L is denoted by M_L and free electrons in the gas by e.

Table 15

ATMOSPHERIC MODEL I

Possible Composition States of the Atmosphere at Its Outer Limit

1.	$H^+ + e.$ $M_L = \frac{1}{2}$.	Diffusion equilibrium with hydrogen present. Hydrogen dissociated and ionized.
2.	$H_2^+ + e.$ $M_L = 1$.	The same as case 1, except hydrogen ionized but not dissociated.
3.	$He^+ + e.$ $M_L = 2$.	Diffusion equilibrium. Helium present but no hydrogen. Helium ionized.
4.	He. $M_L = 4$.	The same as case 3, except helium not ionized.
5.	$N^+ + e.$ $M_L = 7$.	Diffusion equilibrium. Hydrogen and helium absent. Nitrogen dissociated and ionized.
6.	$20\%O^+ + e + 80\%N^+ + e.$ $M_L = 7.2$.	Complete mixing. Same percentage composition as at 83 km, but oxygen and nitrogen dissociated and ionized. Hydrogen and helium can be present if the amounts are small.
7.	$O^+ + e.$ $M_L = 8$.	Diffusion equilibrium. Hydrogen and helium absent. Nitrogen not dissociated but can be ionized. Oxygen dissociated and ionized.
8.	$33\%O^+ + e + 67\%N_2^+ + e.$ $M_L = 12.02$.	Complete mixing. Same percentage composition as in F_2 layer, but oxygen and nitrogen ionized. Hydrogen and helium can be present if the amounts are small.
9.	N + N. $M_L = 14$.	Diffusion equilibrium. Hydrogen and helium absent. Nitrogen dissociated but not ionized. Oxygen can be dissociated and ionized.

It will be readily appreciated that it is not easy to specify just which one of these possibilities is to be chosen as the most likely, although it would seem that some may be more likely than others. The tabulation does show, however, the limits within which the value of M_L must lie, and it is to be concluded that M_L must certainly lie between ½ and 14. Although this leaves a large range in the possible choice for M_L, it will be found that for heights of the order of 500 to 1000 miles, which is probably the limiting height of interest at present in connection with rocket applications, it makes very little difference what value is used for M_L, since any of the possible values for M_L will give about the same values for the density at these heights. In view of the remarks concerning helium this would seem to be the most tempting possibility to consider for the composition at the outer limit. Owing to the relatively large ionization potential for helium, this might very well remain in the neutral state, and in this case the value $M_L = 4$ would be appropriate. However in choosing any single value to be used for M_L, it would be necessary, in view of the high kinetic temperature, to investigate the escape mechanism to make sure that the composition assumed would not lead to extravagant losses of the earth's atmosphere. Although some loss is required for helium, this is not especially permissible for the other gases, except possibly in the case of hydrogen, for, since the interstellar gas is composed mainly of hydrogen, it would be permissible to have hydrogen escaping from the atmosphere provided an equal amount were returned from the interstellar gas.

If the composition consists of charged particles (positive ions and free electrons), the effects of magnetic and electric fields would play a large role in the escape process. For example it might be supposed that at a temperature as high as 10,000°K the free electrons, which have a much higher velocity than the ions, would easily escape from the atmosphere in large numbers. However, it is found that there can be very little separation of positive and negative charges and that positive ions and the associated free electrons must remain together to give a field which is neutral as a whole. It is readily shown that the loss of only relatively few electrons would immediately set up an electrostatic field sufficient to hold all the remaining electrons in the atmosphere.

As discussed by Chapman[15], a free electric charge moving in the presence of a magnetic field will execute a spiral motion around the lines of magnetic force so that a balance is established between the centrifugal force and the deflecting force due to the magnetic field. For a kinetic temperature which would give a transverse component of velocity of 10^7 cm/sec for an electron or $10^7/200 = 5\times10^4$ cm/sec for an ion (based on $M = 20$ for ions), the radius of the spiral in the F_2 layer at the equator is found to be 2 cm for electrons and 400 cm for ions. Thus, in the F_2 layer, when the mean free path is greater than 4 meters, the paths of the charged particles would be determined in large part by the spiral motion; and it would appear that this effect would reduce considerably the probability of escape of a particle as far as heights of the order of that of the F_2 layer are concerned. It is seen that the magnetic field has the effect, essentially, of limiting the size of the mean free path. It can be shown, incidentally (Ref. 57, p. 95), that a Maxwellian velocity distribution is unaffected by the presence of a magnetic field. However, the limiting effect of the magnetic field on the mean free path decreases fairly rapidly with distance from the center of the earth at a rate approximately as the inverse cube of the distance, Hewson[51], and at distances of the order of 5000 to 10,000 miles the magnetic effects would be considerably reduced.

Rather than attempt to deduce the variation of $M = M(r)$ as a function of r on some basis of diffusion equilibrium, etc., it is considered sufficient here simply to assume a reasonable function for $M(r)$. Here again a variation with dM/dr proportional to $1/r^2$ is considered satisfactory; and, as in the case of the temperature, this is closely approximated by the linear relation,

$$M = M_0 - \beta\phi \quad , \tag{36}$$

where M_0 is the molecular weight at the F_2 layer, and β is given by

$$\beta = \frac{M_0 - M_L}{\phi_L} \, . \tag{37}$$

The relation (36) is supposed to represent adequately the effects of whatever degree of diffusion equilibrium is present. Thus M first decreases rapidly above the F_2 layer and then decreases very slowly at great distances near the outer limit, which agrees qualitatively at least with the concept of diffusion equilibrium.

It will be assumed that the composition of the interstellar gas is that given by Langer[52], Table 16.

Table 16

ASSUMED COMPOSITION OF THE INTERSTELLAR GAS IN THE VICINITY OF THE PLANET EARTH

Ionic Species	e	H^+	H	Na
No. per cm^3	1	1	10^{-2}	2×10^{-9}
Density, gram/cm^3	10^{-27}	1.7×10^{-24}	1.6×10^{-26}	10^{-31}
Ionic Species	Na^+	Ca	Ca^+	Ca^{++}
No. per cm^3	3×10^{-5}	2×10^{-14}	10^{-9}	3×10^{-7}
Density, gram/cm^3	10^{-27}	1.3×10^{-35}	6×10^{-32}	2×10^{-29}

It is usually considered, (Ref. 39), that about half the mass of the interstellar gas is due to dust particles. These have been omitted in the tabulation above, since at the earth's distance from the sun the solar radiation pressure would probably be sufficient to "blow" the dust particles out of the solar system. The radiation pressure on ionized gas particles is considerably less, and it is assumed that they would remain in the solar system.

It is at once evident from Table 16 that the main constituents of the interstellar gas are the positive hydrogen atom ion and the free electron, and, as far as the density and molecular weight of this gas is concerned, all of the other constituents may be neglected. It should be pointed out here that the equilibrium condition as-

sumed between the atmospheric and interstellar gases does not necessarily imply equality of composition. It is seen however that if the atmospheric composition at the outer limit is taken to be $H^+ + e$, then the two gases are of practically the same composition (the other constituents of the interstellar gas being negligible in comparison to the proportion of $H^+ + e$ present), and in this case equilibrium would also be accompanied by equality of composition.

II-D. THE LIMIT OF THE ATMOSPHERE

A limit for the height of a planetary atmosphere may be defined in a number of different ways, each according to the concept used, and each leading to a different result. In fact, if one can imagine an isothermal atmosphere on a non-rotating planet for which there is no variation of gravity with distance, it is found, Jeans(53), mathematically at least, that the atmosphere would extend to infinity. If, on the other hand, an atmosphere be maintained with an adiabatic temperature distribution, it is found(53) that the gas must have a definite upper limit. If an isothermal atmosphere rotates as a solid with a rotating planet in which gravity obeys the inverse square law, it is found, Bjerknes(54), Jeans(53), that there is a limiting distance where the gravity and centrifugal forces exactly balance producing a minimum in the density distribution. For the equatorial plane this distance is found to be $r = 6.607a$ or $h = r - a = 21{,}826$ miles above sea level, and this value might be regarded as an indication of the order of magnitude of the limiting height of the atmosphere. In this type of analysis no account is taken of the ultimate molecular structure of the gas, nor is it necessary to specify the isothermal temperature of the gas.

As conceived by Bryan(55), Milne(56), and Jeans(53), at sufficiently great heights where the mean free path becomes very large and the collision frequency very small, the gas particles, in the time interval between collisions, will begin to behave as free bodies in a gravitational field and will therefore begin to move in elliptic, parabolic, and hyperbolic orbits depending upon the velocity possessed by the particle. In this region of the atmosphere the particles will move outward over large distances and fall back again into the denser atmosphere under the influence of gravity. Those which are moving fast enough will establish parabolic or hyperbolic orbits; and, if there are no further collisions, will escape from the earth entirely, since they will have attained the escape velocity.†

This type of atmospheric configuration has been considered in detail by Milne(56), who considers the limit of the atmosphere, which he calls the "surface region", to be situated at the height where the particles begin to move approximately in free flight as described above. In his analysis, which was made before the high ionosphere temperatures were known, Milne assumed a temperature distribution which started with the value 219°K in the stratosphere and decreased continually with height at a rate proportional to $1/r^{2/3}$ where r is the distance from the center of the earth. For molecular hydrogen he finds the height of the "limit" of the atmosphere to be 1400 km

† Also see Jones, J.E., "Free Paths in a Non-Uniform Rarefied Gas With an Application to the Escape of Molecules from Isothermal Atmospheres", *Transactions of the Cambridge Philosophical Society*, Cambridge University Press, Vol.22, No.28, pp.535-556, 1923.

and for helium, 630 km. In view of the high temperatures now known to exist in the ionosphere, it would be interesting to apply Milne's analysis anew, assuming a temperature distribution above the F_2 layer comparable with the results derived here.

The concept of a limit of the atmosphere may be considered in still another way. From this point of view one may gain an approximate indication of the *greatest* value which the height of the limit of the atmosphere might have by assuming, for example, a constant speed gas at temperature T_L at its limit, and considering the critical distance r_L at which the escape velocity will exist. The escape velocity v_L at this distance is specified by the condition that the kinetic energy of the particle be equal to the work done against gravity in transporting the particle from the position r_L to infinity. This condition is imposed through the relation

$$\frac{1}{2} m v_L^2 = \frac{3}{2} k T_L = m \int_{r_L}^{\infty} g_a \left(\frac{a}{r}\right)^2 dr = \frac{g_a a^2 m}{r_L} , \tag{38}$$

which gives

$$r_L = \frac{2}{3} \frac{g_a a^2 m}{k T_L} \equiv \frac{2}{3} \frac{g_a a^2 M}{R_u T_L} . \tag{39}$$

Introducing the values of the constants gives

$$r_L = 1.973 \times 10^5 \frac{M}{T} \text{ miles}, \tag{40}$$

where T is in °K. This is tabulated in Table 17 for different values of M with T = 10,000°K.

Table 17

MAXIMUM POSSIBLE HEIGHT OF LIMIT OF ATMOSPHERE
BASED ON ESCAPE VELOCITY FOR A CONSTANT SPEED GAS

Gas	M	T °K	r_L miles	$h_L^* = r_L - a$ miles
H	1	10,000	1973	-1990
H_2	2	10,000	3947	-17
He	4	10,000	7893	3930
N	14	10,000	27,627	23,663
O	16	10,000	31,573	27,610
N_2	28	10,000	55,253	51,290
O_2	32	10,000	63,146	59,183

*h_L = height above sea level.

The calculations, through Eq. (38), are based essentially on the assumption that the gas particles do not undergo any collisions so that all of the kinetic energy is available to overcome gravity. On this basis it is seen that H and H_2 could not remain within the earth's gravitational field even at sea level, although the other gases can remain to relatively great heights. For a Maxwellian gas these heights would be somewhat lower, since there would always be a certain percentage of the particles with velocities greater than the mean velocity.

Consider again the concept of the atmosphere in which an "outer" region is reached where the mean free path becomes so large that the gas particles, between collisions, move over dynamical orbits under the influence of the earth's gravitational field. In the denser region at the lower boundary of this region the gas particles will have a Maxwellian velocity distribution. It can be shown, Kennard (see pp. 74-78, 90, of Ref. 57), that when the particles move upward in a force field for which a scalar potential exists, such as the field of apparent gravity, the Maxwellian distribution is automatically preserved at all levels above the lower boundary provided the temperature is the same at all levels in this outer region[3c]. Thus if the dynamical orbit region is isothermal, the velocities there will be Maxwellian; and therefore the density distribution will be given by the Boltzmann law,

$$\rho = \rho_* e^{\frac{-m_*}{kT_*}(\phi - \phi_*)} , \tag{41}$$

for an isothermal Maxwellian gas in a potential force field, where ϕ is the apparent gravity potential, see Eq. (28), and the star subscript denotes conditions at the lower boundary of the dynamic orbit region where $r = r_*$, $h = h_*$. Since the hydrostatic equation in terms of the potential function is $dp = -\rho\, d\phi$, where $\rho = mn$ and $p = nkT$, the use of this equation gives the same result as (41). Therefore even in the case where there is a dynamic orbit region, the hydrostatic equation may still be applied provided the atmosphere in this region is in thermal equilibrium, i.e., isothermal temperature distribution. This would not be especially evident *a priori*. When the interval of height is small enough that the variation of gravity may be neglected, the density distribution may be written

$$\rho = \rho_* e^{\frac{-m_* g'_*}{kT_*}(r - r_*)} \equiv \rho_* e^{\frac{-M_* g'_*}{R_u T_*}(r - r_*)} , \tag{42}$$

where, in terms of height above sea level, $r - r_*$ may be replaced by $h - h_*$. It will be observed that since this equation is based on constant temperature, increases in energy resulting from radiation absorption are not allowed; and since the composition (M_*) must be treated as constant, dissociation and ionization are also not allowed.

[3c] In models II and III the dynamical orbit region is considered to be isothermal, since the average time of flight of a particle in this region is negligibly small compared with the time necessary for radiation to affect the particle.

Since the motion of the particles in the dynamical orbit region is conservative if the temperature distribution is isothermal, the total energy of each particle (kinetic plus potential) must remain constant as expressed by

$$\frac{1}{2} m_* (v^2 - v_*^2) + m_*(\phi - \phi_*) = 0. \tag{43}$$

Introducing the kinetic temperature from Eq. (5a) and neglecting variations in gravity, this may be written

$$k (T - T_*) + m_* g'_* (h - h_*) = 0 , \tag{44}$$

which shows how the temperature of each individual particle must vary over the dynamical orbit. However, owing to the existence of the Maxwellian distribution, the mean temperature at any level, considering the integrated effect of all the particles at that level, will be such that the vertical temperature distribution is isothermal throughout the dynamic orbit region.

Realizing that a limit of the atmosphere may be defined in several different ways, we proceed first with the analysis based on the atmospheric model I, which is defined or specified by the assumed condition that it be in equilibrium at its outer limit with the interstellar gas. Thus this condition of equilibrium automatically defines the outer limit of the atmosphere. Although this atmosphere will not be isothermal in the dynamic orbit regions, it will be assumed nevertheless that the hydrostatic equation may be used to calculate the pressure. Before proceeding to the calculations it is necessary to obtain the values ϕ_L and the corresponding limiting distances r_L of the top of the atmosphere. These values are needed in order to determine the values of the constants α [Eq. (30)], C [Eq. (32)], and β [Eq. (37)]. Using the potential function ϕ, the hydrostatic equation becomes simply

$$dp = -\rho \, d\phi , \tag{45}$$

which, when combined with the equation of state, gives

$$\frac{dp}{p} = -\frac{1}{R_u} \frac{M}{T} d\phi . \tag{46}$$

Introducing the expressions (29) and (36) for T and M, this becomes

$$\frac{dp}{p} = -\frac{1}{R_u} \frac{M_o - \beta \phi}{T_o + \alpha \phi} d\phi \tag{47}$$

which is easily integrated giving

$$\frac{p}{p_o} = \frac{e^{\frac{\beta}{R_u \alpha}\phi}}{\left[1 + \frac{\alpha}{T_o}\phi\right]^{\frac{M_o\alpha + \beta T_o}{R_u \alpha^2}}} , \tag{48}$$

the subscript zero referring to the F_2 layer where ϕ is zero.

Replacing α and β from Eqs. (30) and (37), the pressure ratio may be written

$$\frac{p}{p_o} = \frac{\exp\left[\frac{1}{R_u}\frac{M_o}{T_o}\frac{(1 - M_L/M_o)}{(T_L/T_o - 1)}\phi\right]}{\left[1 + \left(\frac{T_L}{T_o} - 1\right)\frac{\phi}{\phi_L}\right]^{\frac{1}{R_u}\frac{M_o}{T_o}\frac{(T_L/T_o - M_L/M_o)}{(T_L/T_o - 1)^2}\phi_L}} . \tag{49}$$

At the limit of the atmosphere where $p = p_L$, $\phi = \phi_L$, this becomes

$$\frac{p_L}{p_o} = \frac{\exp\left[\frac{1}{R_u}\frac{M_o}{T_o}\frac{(1 - M_L/M_o)}{(T_L/T_o - 1)}\phi_L\right]}{\left[T_L/T_o\right]^{\frac{1}{R_u}\frac{M_o}{T_o}\frac{(T_L/T_o - M_L/M_o)}{(T_L/T_o - 1)^2}\phi_L}} . \tag{50}$$

Having values for M_o, T_o, M_L, T_L, and p_L, the corresponding value of ϕ_L may then be determined from Eq. (50).

Now, introducing the limit conditions, $\phi = \phi_L$ when $r = r_L$, in Eq. (35) we have

$$\phi_L = g_a \frac{a^2}{r_o} \frac{1}{\frac{r_L}{r_o}} \left(\frac{r_L}{r_o} - 1\right) - r_o^2 \Omega^2 \cos^2\theta \left[\frac{1}{2}\left(\frac{r_L^2}{r_o^2} - 1\right) - \frac{r_L}{r_o}\left(\frac{r_L}{r_o} - 1\right) \right.$$

$$\left. + \frac{1}{2}\left(\frac{r_L}{r_o}\right)^2 \frac{\left(\frac{r_L}{r_o} + 1\right)}{\left(\frac{r_L}{r_o} - 1\right)} - 2\,\frac{\left(\frac{r_L}{r_o}\right)^2}{\left(\frac{r_L}{r_o} - 1\right)} + \frac{\frac{r_L}{r_o}}{\left(\frac{r_L}{r_o} - 1\right)^2} \log \frac{r_L}{r_o} \right] . \qquad (51)$$

Then by using the value of ϕ_L found from Eq. (50) the corresponding value of r_L is evaluated from Eq. (51).

To evaluate ϕ_L from the relation (50) the value of p_L must be known. By analogy with the condition for equilibrium of two fluids in contact it will be assumed that at the distance r_L the pressure is the same in the atmospheric gas as in the interstellar gas. It is possible of course to impose an equilibrium condition which would require continuity of density with the interstellar gas, but this in general would not allow continuity of pressure. For, since it has been assumed that thermal equilibrium must exist, it follows from the equation of state $p = \rho T R_u/M$ that continuity of pressure and density can exist simultaneously only when the composition M is the same for both gases. In the cases treated here it will be assumed that the condition of continuity in pressure must be satisfied regardless of the density.

Since the composition of the interstellar gas is mainly $H^+ + e$, the density for one hydrogen atom per cm^3 is 1.67×10^{-24} gram/cm^3, the molecular weight is 1/2, and if the value $T = 18{,}000°R$ (10,000°K) is used in the equation of state [4], it will be found that $p_L = 5.78 \times 10^{-15}$ lb/ft^2. This is the value which will be used for the pressure at the limit of the atmosphere. For the equatorial atmosphere we had $h_o = 400$ km, $M_o = 24.0$, $p_o = 2.08 \times 10^{-7}$ millibars, and $T_o = 1800°K$. Using these values plus the value for p_L derived above, the values of ϕ_L and r_L for various values of M_L are found as shown in Table 18. In determining the values of ϕ_L it is convenient to use the plot shown in Fig. 18 (p. 68), which represents solutions of Eq. (50). This is also convenient to use if it is desired to investigate other values for p_L. The values

[4] This may also be computed from the formula $p = nkT$, where n is the number of particles per unit volume (in this case 2 particles per cm^3), and k = Boltzmann's constant = 1.381×10^{-16} erg/deg.

in Table 18 show that the lowest value of h_L to be expected is 6600 miles and that the greatest value is about 2.5 times this large. Similar results may be obtained for the atmosphere in middle latitudes.

Table 18

ATMOSPHERIC MODEL I. LIMIT OF THE ATMOSPHERE AT LATITUDE 0°, BASED ON CONTINUITY OF PRESSURE WITH THE INTERSTELLAR GAS

Values of ϕ_L and r_L for the equatorial atmosphere[1].

Gas	M_L	ϕ_L, ft-lb	r_L, miles	$h_L = r_L - a$, miles
$H + e$	1/2	5.018×10^8	20,490	16,530
$H_2^+ + e$ or H	1	4.960×10^8	19,580	15,620
$He^+ + e$	2	4.851×10^8	18,110	14,150
He	4	4.640×10^8	15,880	11,920
$N^+ + e$	7	4.351×10^8	13,520	9,560
$O^+ + e$	8	4.249×10^8	12,820	8,860
$33\% O^+ + e + 67\% N_2^+ + e$	12	3.950×10^8	11,210	7,250
$N + N$	14	3.808×10^8	10,590	6,630

[1] Based on $p_L = 5.78 \times 10^{-15}$ lb/ft^2. h_L = height of limit of atmosphere.

If the condition for continuity of density had been specified at the distance r_L rather than continuity of pressure, the values of h_L contained in Table 19 would be obtained.

Table 19

ATMOSPHERIC MODEL I. LIMIT OF THE ATMOSPHERE AT LATITUDE 0°, BASED ON CONTINUITY OF DENSITY WITH INTERSTELLAR GAS[1].

Gas	M_L	ϕ_L, ft-lb	r_L, miles	$h_L = r_L - a$, miles
$H + e$	1/2	5.018×10^8	20,490	16,530
$H_2^+ + e$ or H	1	5.149×10^8	23,810	19,850
$He^+ + e$	2	5.212×10^8	24,060	20,100
He	4	5.169×10^8	23,200	19,240
$H^+ + e$	7	4.985×10^8	19,970	16,010
$O^+ + e$	8	4.926×10^8	19,090	15,130
$33\% O^+ + e + 67\% N_2^+ + e$	12	4.644×10^8	15,910	11,950
$N + N$	14	4.509×10^8	14,710	10,750

[1] Based on $\rho_L = 3.24 \times 10^{-24} \frac{\text{slug}}{\text{ft}^3} = 1.67 \times 10^{-24} \frac{\text{gram}}{\text{cm}^3}$

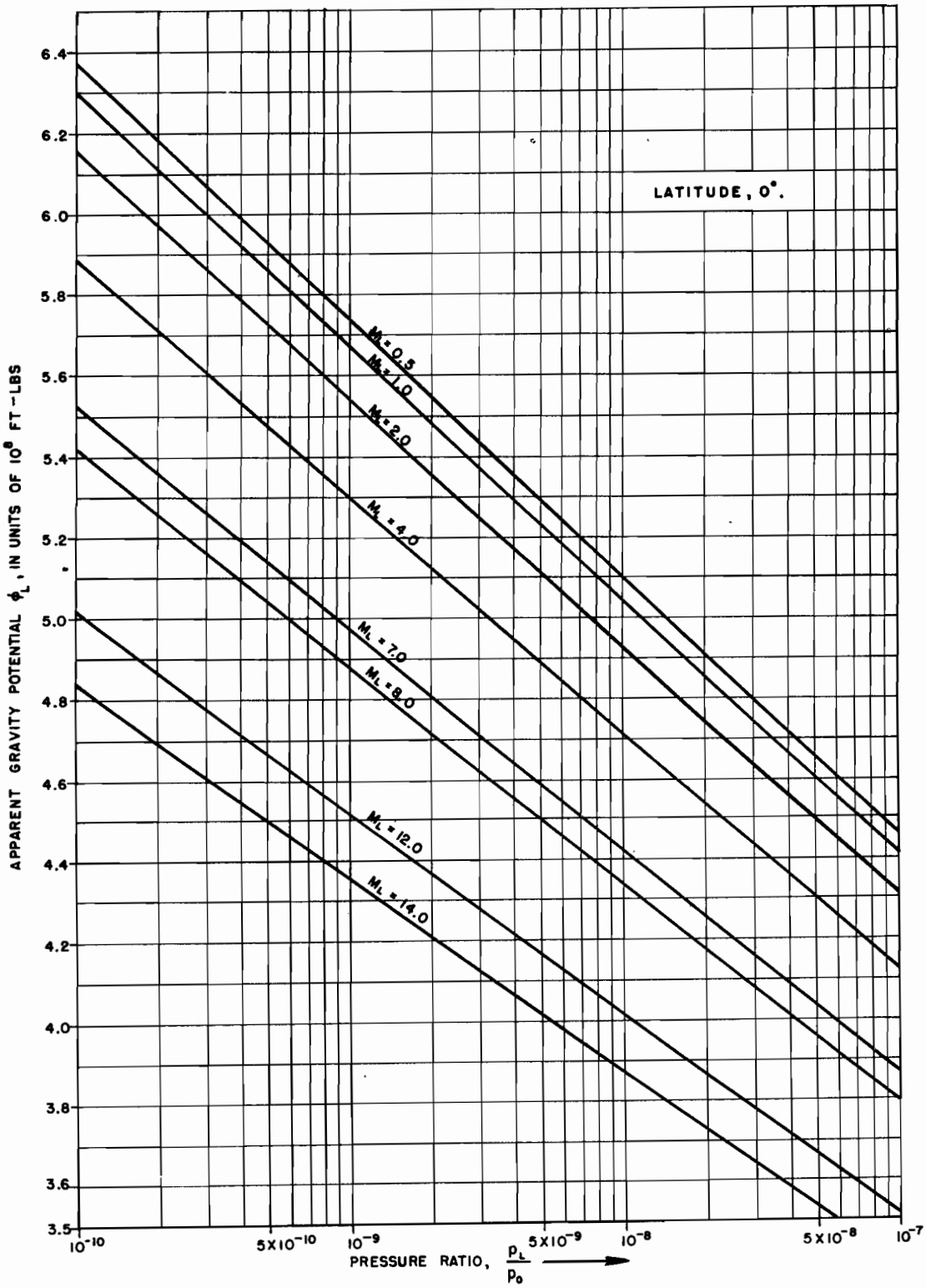

SOLUTIONS OF EQUATION (50) CORRESPONDING TO CONDITIONS AT LATITUDE 0°.

FIG. 18

II-E. THE CALCULATIONS FOR ATMOSPHERIC MODEL I

Having obtained the values of ϕ_L and r_L, the calculations for the temperature, pressure, and density may now be carried out. The pressure is computed from Eq. (49) using values of ϕ computed from Eq. (35) for various assumed values of r. Knowing ϕ_L the values of α and β are determined, and the temperature and molecular weight are calculated from Eqs. (29) and (36). The density is computed from the equation of state (16) using the calculated values of T, M, and p.

The final results depend, of course, upon the value used for M_L, that is, upon the composition assumed for the atmosphere at its outer limit. It was seen from Table 15 that the appropriate value of M_L must certainly lie between ½ and 14. In view of the difficulty of specifying any single, most representative value for M_L, the calculations are carried out for M_L = ½, 7, and 14, which appear to cover the entire range of possibility. The results of the calculations for the equatorial atmosphere are tabulated in Tables 20 to 22 in engineering units, and in Tables 23 to 25 in the metric system.

Comparing the density values in Tables 20, 21, and 22, for example, it is somewhat surprising perhaps to find that the vertical distribution of density is of the same order of magnitude, clear up to the limit h_L, regardless of the value of M_L. In view of this result it is considered quite adequate to use the results for the average value $M_L = 7$, Tables 21 and 24, as representative of the conditions in this region of the atmosphere; and these results may be considered as the adopted values for the atmospheric model I. These adopted values based on $M_L = 7$ are plotted in Figs. 19 and 20 up to a height of 1000 miles (1609 km), and the corresponding variation of the density ratio σ is shown in Figs. 21 and 22. In view of the results found above concerning the small effect of M_L, the atmospheric values at latitude 45° were computed for the single case $M_L = 7$. These results are given in Tables 26 and 27. The temperature distribution up to a height of 1000 miles is plotted in Figs. 23 and 24 while the corresponding variation of the density ratio σ is shown in Figs. 25 and 26.

It is seen from Eqs. (19) and (23) that the estimate of the mean free path L and collision frequency ν is rather strongly affected by the value used for the diameter d. According to Chapman[15], when a gas contains free electrons and gas particles, d is usually interpreted as the weighted mean (weighted according to the relative number of electrons and gas particles) of the electron and gas particle diameters. Since the electron diameter is negligibly small as far as physical size is concerned, when electrons and gas particles are present in *equal* numbers (complete ionization) the mean value used for d is about half that of the gas particle diameter. On this basis the value $d = 1 \times 10^{-8}$ cm would be associated with completely ionized atoms and $d = 1.5 \times 10^{-8}$ cm with completely ionized molecules, corresponding to the value $d = 2 \times 10^{-8}$ cm for neutral atoms and $d = 3 \times 10^{-8}$ cm for neutral molecules. It should be mentioned that the effective gas particle diameter is somewhat temperature dependent [58], [59] in such a way that at high temperatures (high particle velocities) the effective diameter decreases. On the other hand when a gas is highly ionized, the effect of the electrostatic fields of the particles is to give a considerably greater effective collision cross section. However, except at extreme heights, the degree of ionization in atmospheric model I remains quite small and most of this atmosphere can probably be represented with sufficient accuracy by a value of d lying within the limits 2×10^{-8} cm $\leqq d \leqq 3 \times 10^{-8}$ cm.

Table 20

ATMOSPHERIC MODEL I - VALUES OF TEMPERATURE, PRESSURE, AND DENSITY ABOVE THE F_2 LAYER, BASED ON M_L = 0.5

Latitude, 0°. Engineering Units. p_a = 2115 lb/ft², ρ_a = 2.286 × 10⁻³ slug/ft³

Height h		Potential φ	Apparent Gravity g'	Mean Mol Wt M	Temp T	Scale Height H	Pressure p	Pressure Ratio p/p_a	Density ρ	Density Ratio σ	Number Density n	Mean Particle Speed v	$d = 3 \times 10^{-8}$ cm		$d = 2 \times 10^{-8}$ cm	
													Mean Free Path L	Mean Collision Freq ν	Mean Free Path L	Mean Collision Freq ν
mi	ft	ft-lb	ft/sec²		°R	ft	lb/ft²		slug/ft³		particles/ft³	ft/sec	ft	1/sec	ft	1/sec
248.6	1.312×10^6	0.000	28.393	24.00	3,240	2.362×10^5	4.33×10^{-7}	2.05×10^{-10}	6.45×10^{-14}	2.82×10^{-11}	2.38×10^{12}	4.13×10^3	9.77×10^3	4.23×10^{-1}	2.20×10^4	1.88×10^{-1}
300	1.584×10^6	7.612×10^6	27.726	23.64	3,464	2.625×10^5	1.46×10^{-7}	6.90×10^{-11}	2.00×10^{-14}	8.75×10^{-12}	7.49×10^{12}	4.30×10^3	3.10×10^4	1.39×10^{-1}	6.98×10^4	6.16×10^{-2}
350	1.848×10^6	1.484×10^7	27.087	23.30	3,677	2.894×10^5	5.60×10^{-8}	2.65×10^{-11}	7.14×10^{-15}	3.12×10^{-12}	2.71×10^{12}	4.47×10^3	8.58×10^4	5.21×10^{-2}	1.93×10^5	2.32×10^{-2}
400	2.112×10^6	2.191×10^7	26.498	22.97	3,885	3.171×10^5	2.34×10^{-8}	1.11×10^{-11}	2.79×10^{-15}	1.22×10^{-12}	1.07×10^{12}	4.62×10^3	2.17×10^5	2.13×10^{-2}	4.89×10^5	9.45×10^{-3}
450	2.376×10^6	2.881×10^7	25.872	22.65	4,987	3.465×10^5	1.06×10^{-8}	5.01×10^{-12}	1.18×10^{-15}	5.16×10^{-13}	4.61×10^{11}	4.78×10^3	5.04×10^5	9.48×10^{-3}	1.13×10^6	4.21×10^{-3}
500	2.640×10^6	3.556×10^7	25.295	22.33	4,286	3.769×10^5	5.09×10^{-9}	2.41×10^{-12}	5.34×10^{-16}	2.34×10^{-13}	2.12×10^{11}	4.93×10^3	1.10×10^6	4.50×10^{-3}	2.47×10^6	2.00×10^{-3}
600	3.168×10^6	4.862×10^7	24.197	21.72	4,670	4.414×10^5	1.40×10^{-9}	6.62×10^{-13}	1.31×10^{-16}	5.73×10^{-14}	5.34×10^{10}	5.21×10^3	4.35×10^6	1.20×10^{-3}	9.79×10^6	5.32×10^{-4}
700	3.696×10^6	6.111×10^7	23.170	21.14	5,038	5.110×10^5	4.60×10^{-10}	2.17×10^{-13}	3.88×10^{-17}	1.70×10^{-14}	1.62×10^{10}	5.49×10^3	1.44×10^7	3.83×10^{-4}	3.23×10^7	1.70×10^{-4}
800	4.224×10^6	7.308×10^7	22.206	20.58	5,390	5.859×10^5	1.75×10^{-10}	8.27×10^{-14}	1.35×10^{-17}	5.91×10^{-15}	5.80×10^9	5.76×10^3	4.01×10^7	1.44×10^{-4}	9.02×10^7	6.39×10^{-5}
900	4.752×10^6	8.456×10^7	21.301	20.04	5,727	6.665×10^5	7.53×10^{-11}	3.56×10^{-14}	5.30×10^{-18}	2.32×10^{-15}	2.34×10^9	6.01×10^3	9.93×10^7	6.05×10^{-5}	2.24×10^8	2.69×10^{-5}
1,000	5.280×10^6	9.557×10^7	20.451	19.52	6,051	7.530×10^5	3.58×10^{-11}	1.69×10^{-14}	2.32×10^{-18}	1.01×10^{-15}	1.05×10^9	6.26×10^3	2.21×10^8	2.83×10^{-5}	4.98×10^8	1.26×10^{-5}
1,200	6.336×10^6	1.163×10^8	18.897	18.55	6,661	9.440×10^5	1.02×10^{-11}	4.82×10^{-15}	5.73×10^{-19}	2.51×10^{-16}	2.73×10^8	6.74×10^3	8.52×10^8	7.92×10^{-6}	1.92×10^9	3.52×10^{-6}
1,400	7.392×10^6	1.355×10^8	17.512	17.65	7,226	1.161×10^6	3.73×10^{-12}	1.76×10^{-15}	1.83×10^{-19}	8.01×10^{-17}	9.17×10^7	7.20×10^3	2.54×10^9	2.84×10^{-6}	5.70×10^9	1.26×10^{-6}
1,500	7.920×10^6	1.446×10^8	16.876	17.23	7,494	1.280×10^6	2.42×10^{-12}	1.14×10^{-15}	1.12×10^{-19}	4.90×10^{-17}	5.75×10^7	7.42×10^3	4.04×10^9	1.84×10^{-6}	9.10×10^9	8.16×10^{-7}
1,750	9.240×10^6	1.659×10^8	15.430	16.23	8,120	1.611×10^6	9.64×10^{-13}	4.56×10^{-16}	3.88×10^{-20}	1.70×10^{-17}	2.12×10^7	7.96×10^3	1.10×10^{10}	7.26×10^{-7}	2.47×10^{10}	3.23×10^{-7}
2,000	1.056×10^7	1.854×10^8	14.162	15.32	8,694	1.991×10^6	4.61×10^{-13}	2.18×10^{-16}	1.64×10^{-20}	7.17×10^{-18}	9.47×10^6	8.47×10^3	2.45×10^{10}	3.45×10^{-7}	5.52×10^{10}	1.53×10^{-7}
2,500	1.320×10^7	2.199×10^8	12.709	13.70	9,709	2.770×10^6	1.54×10^{-13}	7.28×10^{-17}	4.37×10^{-21}	1.91×10^{-18}	2.82×10^6	9.47×10^3	8.24×10^{10}	1.15×10^{-7}	1.85×10^{11}	5.11×10^{-8}
3,000	1.584×10^7	2.494×10^8	10.385	12.32	10,577	4.107×10^6	7.18×10^{-14}	3.39×10^{-17}	1.68×10^{-21}	7.35×10^{-19}	1.21×10^6	1.04×10^4	1.92×10^{11}	5.41×10^{-8}	4.32×10^{11}	2.41×10^{-8}
4,000	2.112×10^7	2.973×10^8	7.940	10.08	11,986	7.440×10^6	2.75×10^{-14}	1.30×10^{-17}	4.65×10^{-22}	2.03×10^{-19}	4.08×10^5	1.23×10^4	5.70×10^{11}	2.16×10^{-8}	1.28×10^{12}	9.59×10^{-9}
5,000	2.640×10^7	3.346×10^8	6.267	8.33	13,083	1.245×10^7	1.58×10^{-14}	7.47×10^{-18}	2.03×10^{-22}	8.88×10^{-20}	2.16×10^5	1.41×10^4	1.08×10^{12}	1.31×10^{-8}	2.42×10^{12}	5.82×10^{-9}
6,000	3.168×10^7	3.644×10^8	5.073	6.93	13,959	1.973×10^7	1.13×10^{-14}	5.34×10^{-18}	1.13×10^{-22}	4.94×10^{-20}	1.44×10^5	1.60×10^4	1.61×10^{12}	9.91×10^{-9}	3.63×10^{12}	4.41×10^{-9}
7,000	3.696×10^7	3.887×10^8	4.190	5.79	14,674	3.005×10^7	9.07×10^{-15}	4.29×10^{-18}	7.20×10^{-22}	3.15×10^{-20}	1.10×10^5	1.79×10^4	2.11×10^{12}	8.47×10^{-9}	4.75×10^{12}	3.76×10^{-9}
8,000	4.224×10^7	4.090×10^8	3.520	4.84	15,271	4.453×10^7	7.84×10^{-15}	3.71×10^{-18}	5.00×10^{-22}	2.19×10^{-20}	9.14×10^4	2.00×10^4	2.54×10^{12}	7.86×10^{-9}	5.72×10^{12}	3.50×10^{-9}
9,000	4.752×10^7	4.262×10^8	2.999	4.04	15,777	6.469×10^7	7.10×10^{-15}	3.36×10^{-18}	3.66×10^{-22}	1.60×10^{-20}	8.02×10^4	2.22×10^4	2.89×10^{12}	7.68×10^{-9}	6.51×10^{12}	3.41×10^{-9}
10,000	5.280×10^7	4.409×10^8	2.586	3.35	16,210	9.295×10^7	6.63×10^{-15}	3.13×10^{-18}	2.76×10^{-22}	1.21×10^{-20}	7.29×10^4	2.47×10^4	3.19×10^{12}	7.75×10^{-9}	7.17×10^{12}	3.44×10^{-9}
11,000	5.808×10^7	4.536×10^8	2.252	2.76	16,583	1.325×10^8	6.32×10^{-15}	2.99×10^{-18}	2.12×10^{-22}	9.27×10^{-21}	6.80×10^4	2.76×10^4	3.42×10^{12}	8.07×10^{-9}	7.69×10^{12}	3.59×10^{-9}
12,000	6.336×10^7	4.648×10^8	1.980	2.23	16,913	1.903×10^8	6.11×10^{-15}	2.89×10^{-18}	1.62×10^{-22}	7.09×10^{-21}	6.43×10^4	3.10×10^4	3.62×10^{12}	8.57×10^{-9}	8.13×10^{12}	3.81×10^{-9}
13,000	6.846×10^7	4.746×10^8	1.754	1.77	17,201	2.752×10^8	5.97×10^{-15}	2.82×10^{-18}	1.24×10^{-22}	5.42×10^{-21}	6.20×10^4	3.51×10^4	3.75×10^{12}	9.36×10^{-9}	8.44×10^{12}	4.16×10^{-9}
14,000	7.392×10^7	4.834×10^8	1.565	1.36	17,460	4.076×10^8	5.88×10^{-15}	2.78×10^{-18}	9.22×10^{-24}	4.03×10^{-21}	6.00×10^4	4.03×10^4	3.87×10^{12}	1.04×10^{-8}	8.72×10^{12}	4.62×10^{-9}
15,000	7.920×10^7	4.913×10^8	1.405	.99	17,692	6.318×10^8	5.82×10^{-15}	2.75×10^{-18}	6.55×10^{-24}	2.87×10^{-21}	5.85×10^4	4.76×10^4	3.97×10^{12}	1.20×10^{-8}	8.94×10^{12}	5.32×10^{-9}
16,000	8.448×10^7	4.983×10^8	1.268	.66	17,898	1.062×10^9	5.79×10^{-15}	2.74×10^{-18}	4.29×10^{-24}	1.88×10^{-21}	5.75×10^4	5.86×10^4	4.04×10^{12}	1.45×10^{-8}	9.10×10^{12}	6.44×10^{-9}
16,523	8.724×10^7	5.017×10^8	1.206	.50	18,000	1.483×10^9	5.78×10^{-15}	2.73×10^{-18}	3.24×10^{-24}	1.42×10^{-21}	5.66×10^4	6.75×10^4	4.11×10^{12}	1.64×10^{-8}	9.24×10^{12}	7.30×10^{-9}

1 lb/ft² = 0.3591 mm of Hg

Table 21

ATMOSPHERIC MODEL I - VALUES OF TEMPERATURE, PRESSURE, AND DENSITY ABOVE THE F_2 LAYER, BASED ON $M_L = 7$

Latitude, 0°. Engineering Units. $p_a = 2115$ lb/ft², $\rho_a = 2.286 \times 10^{-3}$ slug/ft³

Height h		Potential ϕ	Apparent Gravity g'	Mean Mol Wt M	Temp T	Scale Height H	Pressure p	Pressure Ratio p/p_a	Density ρ	Density Ratio σ	Number Density n	Mean Particle Speed v	$d = 3 \times 10^{-8}$ cm		$d = 2 \times 10^{-8}$ cm	
													Mean Free Path L	Mean Collision Freq ν	Mean Free Path L	Mean Collision Freq ν
mi	ft	ft-lb	ft/sec²		°R	ft	lb/ft²		slug/ft³	ρ/ρ_a	particles/ft³	ft/sec	ft	1/sec	ft	1/sec
248.6	1.312×10^6	0.000	28.393	24.00	3,240	2.362×10^5	4.33×10^{-7}	2.05×10^{-10}	6.46×10^{-14}	2.83×10^{-11}	2.38×10^{13}	4.13×10^3	9.77×10^6	4.23×10^{-1}	2.20×10^4	1.88×10^{-1}
300	1.584×10^6	7.613×10^6	27.719	23.70	3,498	2.645×10^5	1.46×10^{-7}	6.90×10^{-11}	1.99×10^{-14}	8.71×10^{-12}	7.43×10^{12}	4.32×10^3	3.13×10^4	1.38×10^{-1}	7.04×10^4	6.14×10^{-2}
350	1.848×10^6	1.484×10^7	27.078	23.42	3,743	2.932×10^5	5.67×10^{-8}	2.68×10^{-11}	7.14×10^{-15}	3.12×10^{-12}	2.70×10^{12}	4.50×10^3	8.61×10^4	5.23×10^{-2}	1.94×10^5	2.32×10^{-2}
400	2.112×10^6	2.191×10^7	26.459	23.14	3,983	3.232×10^5	2.41×10^{-8}	1.14×10^{-11}	2.82×10^{-15}	1.23×10^{-12}	1.08×10^{12}	4.67×10^3	2.15×10^5	2.17×10^{-2}	4.84×10^5	9.64×10^{-3}
450	2.376×10^6	2.881×10^7	25.861	22.87	4,217	3.542×10^5	1.10×10^{-8}	5.20×10^{-12}	1.20×10^{-15}	5.25×10^{-13}	4.64×10^{11}	4.83×10^3	5.01×10^5	9.64×10^{-3}	1.13×10^6	4.28×10^{-3}
500	2.640×10^6	3.557×10^7	25.284	22.61	4,447	3.864×10^5	5.40×10^{-9}	2.55×10^{-12}	5.53×10^{-16}	2.42×10^{-13}	2.16×10^{11}	4.99×10^3	1.08×10^6	4.64×10^{-3}	2.42×10^6	2.06×10^{-3}
600	3.168×10^6	4.862×10^7	24.184	22.10	4,889	4.544×10^5	1.53×10^{-9}	7.23×10^{-13}	1.39×10^{-16}	6.08×10^{-14}	5.57×10^{10}	5.29×10^3	4.17×10^6	1.27×10^{-3}	9.39×10^6	5.63×10^{-4}
700	3.696×10^6	6.112×10^7	23.155	21.61	5,313	5.275×10^5	5.21×10^{-10}	2.46×10^{-13}	4.27×10^{-17}	1.87×10^{-14}	1.75×10^{10}	5.58×10^3	1.33×10^7	4.20×10^{-4}	2.99×10^7	1.87×10^{-4}
800	4.224×10^6	7.309×10^7	22.190	21.14	5,719	6.056×10^5	2.05×10^{-10}	9.69×10^{-14}	1.53×10^{-17}	6.69×10^{-15}	6.40×10^9	5.85×10^3	3.63×10^7	1.61×10^{-4}	8.17×10^7	7.16×10^{-5}
900	4.752×10^6	8.457×10^7	21.284	20.70	6,109	6.888×10^5	9.03×10^{-11}	4.27×10^{-14}	6.16×10^{-18}	2.69×10^{-15}	2.63×10^9	6.11×10^3	8.84×10^7	6.91×10^{-5}	1.99×10^8	3.07×10^{-5}
1,000	5.280×10^6	9.559×10^7	20.432	20.27	6,482	7.775×10^5	4.39×10^{-11}	2.08×10^{-14}	2.76×10^{-18}	1.21×10^{-15}	1.20×10^9	6.36×10^3	1.92×10^8	3.31×10^{-5}	4.32×10^8	1.47×10^{-5}
1,200	6.336×10^6	1.163×10^8	18.904	19.46	7,185	9.702×10^5	1.30×10^{-11}	6.15×10^{-16}	7.09×10^{-19}	3.10×10^{-16}	3.22×10^8	6.83×10^3	7.22×10^8	9.46×10^{-6}	1.62×10^9	4.20×10^{-6}
1,400	7.392×10^6	1.356×10^8	17.520	18.70	7,840	1.189×10^6	4.87×10^{-12}	2.30×10^{-15}	2.34×10^{-19}	1.02×10^{-16}	1.11×10^8	7.28×10^3	2.09×10^9	3.48×10^{-6}	4.71×10^9	1.55×10^{-6}
1,500	7.920×10^6	1.446×10^8	16.885	18.35	8,145	1.306×10^6	3.19×10^{-12}	1.51×10^{-15}	1.45×10^{-19}	6.34×10^{-17}	6.99×10^7	7.49×10^3	3.33×10^9	2.25×10^{-6}	7.48×10^9	1.00×10^{-6}
1,750	9.240×10^6	1.659×10^8	15.440	17.52	8,867	1.628×10^6	1.29×10^{-12}	6.10×10^{-16}	5.13×10^{-20}	2.24×10^{-17}	2.59×10^7	8.00×10^3	8.98×10^9	8.91×10^{-7}	2.02×10^{10}	3.96×10^{-7}
2,000	1.056×10^7	1.854×10^8	14.173	16.76	9,529	1.993×10^6	6.20×10^{-13}	2.93×10^{-16}	2.20×10^{-20}	9.62×10^{-18}	1.16×10^7	8.48×10^3	2.00×10^{10}	4.23×10^{-7}	4.51×10^{10}	1.88×10^{-7}
2,500	1.320×10^7	2.200×10^8	12.720	15.40	10,703	2.714×10^6	2.05×10^{-13}	9.69×10^{-17}	5.94×10^{-21}	2.60×10^{-18}	3.41×10^6	9.38×10^3	6.82×10^{10}	1.38×10^{-7}	1.53×10^{11}	6.12×10^{-8}
3,000	1.584×10^7	2.495×10^8	10.398	14.25	11,703	3.924×10^6	9.32×10^{-14}	4.41×10^{-17}	2.28×10^{-21}	9.97×10^{-19}	1.42×10^6	1.02×10^4	1.64×10^{11}	6.23×10^{-8}	3.68×10^{11}	2.77×10^{-8}
4,000	2.112×10^7	2.975×10^8	7.953	12.38	13,331	6.721×10^6	3.32×10^{-14}	1.57×10^{-17}	6.21×10^{-22}	2.72×10^{-19}	4.44×10^5	1.17×10^4	5.24×10^{11}	2.23×10^{-8}	1.18×10^{12}	9.93×10^{-9}
5,000	2.640×10^7	3.349×10^8	6.281	10.92	14,600	1.057×10^7	1.78×10^{-14}	8.42×10^{-18}	2.68×10^{-22}	1.17×10^{-19}	2.17×10^5	1.30×10^4	1.07×10^{12}	1.21×10^{-8}	2.41×10^{12}	5.39×10^{-9}
6,000	3.168×10^7	3.647×10^8	5.086	9.75	15,611	1.564×10^7	1.18×10^{-14}	5.58×10^{-18}	1.48×10^{-22}	6.47×10^{-20}	1.34×10^5	1.42×10^4	1.73×10^{12}	8.19×10^{-9}	3.90×10^{12}	3.64×10^{-9}
7,000	3.696×10^7	3.891×10^8	4.203	8.80	16,439	2.208×10^7	8.85×10^{-15}	4.18×10^{-18}	9.54×10^{-23}	4.17×10^{-20}	9.59×10^4	1.54×10^4	2.42×10^{12}	6.35×10^{-9}	5.45×10^{12}	2.82×10^{-9}
8,000	4.224×10^7	4.095×10^8	3.531	8.00	17,131	3.013×10^7	7.21×10^{-15}	3.41×10^{-18}	6.78×10^{-23}	2.97×10^{-20}	7.50×10^4	1.65×10^4	3.10×10^{12}	5.32×10^{-9}	6.97×10^{12}	2.37×10^{-9}
9,000	4.752×10^7	4.267×10^8	3.009	7.33	17,714	3.990×10^7	6.19×10^{-15}	2.93×10^{-18}	5.16×10^{-23}	2.26×10^{-20}	6.23×10^4	1.75×10^4	3.73×10^{12}	4.69×10^{-9}	8.40×10^{12}	2.08×10^{-9}
9,553	5.044×10^7	4.351×10^8	2.768	7.00	18,000	4.615×10^7	5.78×10^{-15}	2.73×10^{-18}	4.43×10^{-23}	1.94×10^{-20}	5.66×10^4	1.80×10^4	4.11×10^{12}	4.38×10^{-9}	9.24×10^{12}	1.95×10^{-9}

1 lb/ft² = 0.3591 mm of Hg

Table 22

ATMOSPHERIC MODEL I - VALUES OF TEMPERATURE, PRESSURE, AND DENSITY ABOVE THE F_2 LAYER, BASED ON M_L = 14

Latitude 0°. Engineering Units. p_a = 2115 lb/ft², ρ_a = 2.286 × 10⁻³ slug/ft³

Height h		Potential ϕ	Apparent Gravity g'	Mean Mol Wt M	Temp T	Scale Height H	Pressure p	Pressure Ratio p/p_a	Density ρ	Density Ratio σ ρ/ρ_a	Number Density n	Mean Particle Speed v	$d = 3 \times 10^{-8}$ cm		$d = 2 \times 10^{-8}$ cm	
mi	ft	ft-lb	ft/sec²		°R	ft	lb/ft²		slug/ft³		particles/ft³	ft/sec	Mean Free Path L ft	Mean Collision Freq ν 1/sec	Mean Free Path L ft	Mean Collision Freq ν 1/sec
248.6	1.312×10^6	0.000	28.393	24.00	3240	2.3620×10^5	4.33×10^{-7}	2.05×10^{-10}	6.46×10^{-14}	2.83×10^{-11}	2.38×10^{13}	4.13×10^3	9.775×10^8	4.228×10^{-1}	2.1994×10^4	1.88×10^{-1}
300	1.584×10^6	7.613×10^6	27.732	23.80	3535	2.6606×10^5	1.47×10^{-7}	6.95×10^{-11}	1.99×10^{-14}	8.71×10^{-12}	7.40×10^{12}	4.33×10^3	3.141×10^4	1.3785×10^{-1}	7.067×10^4	6.13×10^{-2}
350	1.848×10^6	1.484×10^7	27.093	23.61	3815	2.9627×10^5	5.74×10^{-8}	2.71×10^{-11}	7.15×10^{-15}	3.13×10^{-12}	2.68×10^{12}	4.52×10^3	8.674×10^4	5.211×10^{-2}	1.952×10^5	2.32×10^{-2}
400	2.112×10^6	2.191×10^7	26.505	23.42	4089	3.2723×10^5	2.46×10^{-8}	1.16×10^{-11}	2.84×10^{-15}	1.24×10^{-12}	1.07×10^{12}	4.70×10^3	2.173×10^5	2.163×10^{-2}	4.888×10^5	9.61×10^{-3}
450	2.376×10^6	2.881×10^7	25.879	23.24	4357	3.5988×10^5	1.14×10^{-8}	5.39×10^{-12}	1.22×10^{-15}	5.34×10^{-13}	4.65×10^{11}	4.87×10^3	4.999×10^5	9.742×10^{-3}	1.125×10^6	4.33×10^{-3}
500	2.640×10^6	3.557×10^7	25.303	23.07	4619	3.9308×10^5	5.66×10^{-9}	2.68×10^{-13}	5.69×10^{-16}	2.49×10^{-13}	2.18×10^{11}	5.03×10^3	1.066×10^6	4.7186×10^{-3}	2.398×10^6	2.10×10^{-3}
600	3.168×10^6	4.862×10^7	24.207	22.72	5125	4.6291×10^5	1.64×10^{-9}	7.75×10^{-13}	1.46×10^{-16}	6.39×10^{-14}	5.69×10^{10}	5.34×10^3	4.085×10^6	1.307×10^{-3}	9.191×10^6	5.81×10^{-4}
700	3.696×10^6	6.112×10^7	23.180	22.39	5609	5.3687×10^5	5.70×10^{-10}	2.70×10^{-13}	4.58×10^{-17}	2.00×10^{-14}	1.81×10^{10}	5.63×10^3	1.284×10^7	4.385×10^{-4}	2.889×10^7	1.95×10^{-4}
800	4.224×10^6	7.310×10^7	22.218	22.08	6074	6.1507×10^5	2.28×10^{-10}	1.08×10^{-13}	1.67×10^{-17}	7.31×10^{-15}	6.69×10^9	5.90×10^3	3.475×10^7	1.698×10^{-4}	7.819×10^7	7.55×10^{-5}
900	4.752×10^6	8.458×10^7	21.314	21.78	6519	6.9761×10^5	1.02×10^{-10}	4.82×10^{-14}	6.86×10^{-18}	3.00×10^{-15}	2.79×10^9	6.15×10^3	8.332×10^7	7.381×10^{-5}	1.875×10^8	3.28×10^{-5}
1000	5.280×10^6	9.560×10^7	20.465	21.49	6946	7.8459×10^5	4.99×10^{-11}	2.36×10^{-14}	3.11×10^{-18}	1.36×10^{-15}	1.28×10^9	6.39×10^3	1.816×10^8	3.519×10^{-5}	4.086×10^8	1.56×10^{-5}
1200	6.336×10^6	1.164×10^8	18.912	20.94	7752	9.7241×10^5	1.49×10^{-11}	7.04×10^{-15}	8.10×10^{-19}	3.54×10^{-16}	3.42×10^8	6.84×10^3	6.797×10^8	1.006×10^{-5}	1.529×10^9	4.47×10^{-6}
1400	7.392×10^6	1.356×10^8	17.529	20.44	8496	1.1780×10^6	5.55×10^{-12}	2.62×10^{-15}	2.69×10^{-19}	1.18×10^{-16}	1.16×10^8	7.25×10^3	2.004×10^9	3.618×10^{-6}	4.509×10^9	1.61×10^{-6}
1500	7.920×10^6	1.447×10^8	16.894	20.20	8849	1.2881×10^6	3.61×10^{-12}	1.71×10^{-15}	1.66×10^{-19}	7.26×10^{-17}	7.27×10^7	7.44×10^3	3.1975×10^9	2.327×10^{-6}	7.194×10^9	1.03×10^{-6}
1750	9.240×10^6	1.660×10^8	15.450	19.64	9675	1.5839×10^6	1.44×10^{-12}	6.81×10^{-16}	5.88×10^{-20}	2.57×10^{-17}	2.65×10^7	7.89×10^3	8.772×10^9	8.995×10^{-7}	1.974×10^{10}	4.00×10^{-7}
2000	1.056×10^7	1.855×10^8	14.183	19.13	10,430	1.9097×10^6	6.73×10^{-13}	3.18×10^{-16}	2.48×10^{-20}	1.08×10^{-17}	1.15×10^7	8.30×10^3	2.021×10^{10}	4.107×10^{-7}	4.547×10^{10}	1.83×10^{-7}
2500	1.320×10^7	2.201×10^8	12.732	18.22	11,772	2.5209×10^6	2.08×10^{-13}	9.83×10^{-17}	6.48×10^{-21}	2.83×10^{-18}	3.15×10^6	9.04×10^3	7.380×10^{10}	1.225×10^{-7}	1.660×10^{11}	5.44×10^{-8}
3000	1.584×10^7	2.497×10^8	10.409	17.42	12,919	3.5354×10^6	8.79×10^{-14}	4.16×10^{-17}	2.39×10^{-21}	1.05×10^{-18}	1.21×10^6	9.68×10^3	1.921×10^{11}	5.039×10^{-8}	4.322×10^{11}	2.24×10^{-8}
4000	2.112×10^7	2.977×10^8	7.964	16.18	14,779	5.6974×10^6	2.71×10^{-14}	1.28×10^{-17}	5.97×10^{-22}	2.61×10^{-19}	3.27×10^5	1.07×10^4	7.109×10^{11}	1.505×10^{-8}	1.600×10^{12}	6.69×10^{-9}
5000	2.640×10^7	3.351×10^8	6.290	15.20	16,229	8.4324×10^6	1.27×10^{-14}	6.00×10^{-18}	2.39×10^{-22}	1.05×10^{-19}	1.39×10^5	1.16×10^4	1.672×10^{12}	6.938×10^{-9}	3.762×10^{12}	3.08×10^{-9}
6000	3.168×10^7	3.650×10^8	5.094	14.41	17,388	1.1767×10^7	7.44×10^{-15}	3.52×10^{-18}	1.24×10^{-22}	5.42×10^{-20}	7.61×10^4	1.24×10^4	3.055×10^{12}	4.059×10^{-9}	6.874×10^{12}	1.80×10^{-9}
6622	3.496×10^7	3.808×10^8	4.514	14.00	18,000	1.4149×10^7	5.78×10^{-15}	2.73×10^{-18}	9.26×10^{-23}	4.05×10^{-20}	5.66×10^4	1.28×10^4	4.107×10^{12}	3.117×10^{-9}	9.241×10^{12}	1.39×10^{-9}

1 lb/ft² = 0.3591 mm of Hg

Table 23

ATMOSPHERIC MODEL I - VALUES OF TEMPERATURE, PRESSURE, AND DENSITY ABOVE THE F_2 LAYER, BASED ON $M_L = 0.5$

Latitude 0°. Metric Units. $p_a = 1013$ mb, $\rho_a = 1.178 \times 10^{-3}$ gm/cm³

Height h km	Height h mi	Potential ϕ ergs	Apparent Gravity g' cm/sec²	Mean Mol Wt M	Temp T °K	Scale Height H km	Pressure p millibars	Pressure Ratio p/p_a	Density ρ gm/cm³	Density Ratio σ ρ/ρ_a	Number Density n particles/cm³	Mean Particle Speed v cm/sec	$d = 3 \times 10^{-8}$cm Mean Free Path L cm	$d = 3 \times 10^{-8}$cm Mean Collision Freq ν 1/sec	$d = 2 \times 10^{-8}$cm Mean Free Path L cm	$d = 2 \times 10^{-8}$cm Mean Collision Freq ν 1/sec
400.0	248.6	0.000	865.42	24.00	1800	7.199×10	2.08×10^{-7}	2.05×10^{-10}	3.32×10^{-14}	2.82×10^{-11}	8.40×10^{8}	1.26×10^{5}	2.98×10^{5}	4.23×10^{-1}	6.70×10^{5}	1.88×10^{-1}
482.8	300	1.032×10^{14}	845.10	23.64	1924	8.002×10	6.98×10^{-8}	6.90×10^{-11}	1.03×10^{-14}	8.75×10^{-12}	2.65×10^{8}	1.31×10^{5}	9.46×10^{5}	1.39×10^{-1}	2.13×10^{6}	6.16×10^{-2}
563.3	350	2.012×10^{14}	825.60	23.30	2043	8.822×10	2.68×10^{-8}	2.65×10^{-11}	3.68×10^{-15}	3.12×10^{-12}	9.57×10^{7}	1.36×10^{5}	2.61×10^{6}	5.21×10^{-2}	5.88×10^{6}	2.32×10^{-2}
643.8	400	2.971×10^{14}	807.66	22.97	2158	9.665×10	1.12×10^{-8}	1.11×10^{-11}	1.44×10^{-15}	1.22×10^{-12}	3.78×10^{7}	1.41×10^{5}	6.62×10^{6}	2.13×10^{-2}	1.49×10^{7}	9.45×10^{-3}
724.2	450	3.907×10^{14}	788.57	22.65	2271	1.056×10^{3}	5.07×10^{-9}	5.01×10^{-12}	6.08×10^{-16}	5.16×10^{-13}	1.63×10^{7}	1.46×10^{5}	1.54×10^{7}	9.48×10^{-3}	3.46×10^{7}	4.21×10^{-3}
804.7	500	4.822×10^{14}	770.99	22.33	2381	1.149×10^{3}	2.44×10^{-9}	2.41×10^{-12}	2.75×10^{-16}	2.34×10^{-13}	7.49×10^{6}	1.50×10^{5}	3.34×10^{7}	4.50×10^{-3}	7.52×10^{7}	2.00×10^{-3}
965.6	600	6.593×10^{14}	737.53	21.72	2594	1.345×10^{3}	6.68×10^{-10}	6.62×10^{-13}	6.75×10^{-17}	5.73×10^{-14}	1.89×10^{6}	1.59×10^{5}	1.33×10^{8}	1.20×10^{-3}	2.99×10^{8}	5.32×10^{-4}
1127	700	8.287×10^{14}	706.21	21.14	2799	1.557×10^{3}	2.20×10^{-10}	2.17×10^{-13}	2.00×10^{-17}	1.70×10^{-14}	5.72×10^{5}	1.67×10^{5}	4.37×10^{8}	3.83×10^{-4}	9.84×10^{8}	1.70×10^{-4}
1287	800	9.910×10^{14}	676.84	20.58	2994	1.786×10^{3}	8.39×10^{-11}	8.27×10^{-14}	6.95×10^{-18}	5.91×10^{-15}	2.05×10^{5}	1.76×10^{5}	1.22×10^{9}	1.44×10^{-4}	2.75×10^{9}	6.39×10^{-5}
1448	900	1.147×10^{15}	649.26	20.04	3182	2.031×10^{3}	3.60×10^{-11}	3.56×10^{-14}	2.73×10^{-18}	2.32×10^{-15}	8.26×10^{4}	1.83×10^{5}	3.03×10^{9}	6.05×10^{-5}	6.81×10^{9}	2.69×10^{-5}
1609	1000	1.296×10^{15}	623.34	19.52	3362	2.295×10^{3}	1.71×10^{-11}	1.69×10^{-14}	1.19×10^{-18}	1.01×10^{-15}	3.71×10^{4}	1.91×10^{5}	6.75×10^{9}	2.83×10^{-5}	1.52×10^{10}	1.26×10^{-5}
1931	1200	1.577×10^{15}	575.94	18.55	3701	2.877×10^{3}	4.90×10^{-12}	4.82×10^{-15}	2.95×10^{-19}	2.51×10^{-16}	9.64×10^{3}	2.05×10^{5}	2.60×10^{10}	7.92×10^{-6}	5.84×10^{10}	3.52×10^{-6}
2253	1400	1.837×10^{15}	533.75	17.65	4014	3.540×10^{3}	1.79×10^{-12}	1.76×10^{-15}	9.42×10^{-20}	8.01×10^{-17}	3.24×10^{3}	2.19×10^{5}	7.73×10^{10}	2.84×10^{-6}	1.74×10^{11}	1.26×10^{-6}
2414	1500	1.961×10^{15}	514.37	17.23	4163	3.902×10^{3}	1.16×10^{-12}	1.14×10^{-15}	5.77×10^{-20}	4.90×10^{-17}	2.03×10^{3}	2.26×10^{5}	1.23×10^{11}	1.84×10^{-6}	2.77×10^{11}	8.16×10^{-7}
2816	1750	2.250×10^{15}	470.31	16.23	4511	4.909×10^{3}	4.61×10^{-13}	4.56×10^{-16}	2.00×10^{-20}	1.70×10^{-17}	7.49×10^{2}	2.43×10^{5}	3.34×10^{11}	7.26×10^{-7}	7.52×10^{11}	3.23×10^{-7}
3219	2000	2.514×10^{15}	431.67	15.32	4830	6.067×10^{3}	2.21×10^{-13}	2.17×10^{-16}	8.45×10^{-21}	7.17×10^{-18}	3.34×10^{2}	2.58×10^{5}	7.48×10^{11}	3.45×10^{-7}	1.68×10^{12}	1.53×10^{-7}
4023	2500	2.982×10^{15}	387.36	13.70	5394	8.444×10^{3}	7.38×10^{-14}	7.28×10^{-17}	2.25×10^{-21}	1.91×10^{-18}	9.96×10	2.89×10^{5}	2.51×10^{12}	1.15×10^{-7}	5.65×10^{12}	5.11×10^{-8}
4828	3000	3.382×10^{15}	316.52	12.32	5876	1.252×10^{4}	3.44×10^{-14}	3.39×10^{-17}	8.65×10^{-22}	7.35×10^{-19}	4.27×10	3.17×10^{5}	5.86×10^{12}	5.41×10^{-8}	1.32×10^{13}	2.41×10^{-8}
6437	4000	4.031×10^{15}	242.00	10.08	6659	2.268×10^{4}	1.32×10^{-14}	1.30×10^{-17}	2.39×10^{-22}	2.03×10^{-19}	1.44×10	3.75×10^{5}	1.74×10^{13}	2.16×10^{-8}	3.91×10^{13}	9.59×10^{-9}
8047	5000	4.537×10^{15}	191.02	8.33	7268	3.795×10^{4}	7.58×10^{-15}	7.47×10^{-18}	1.05×10^{-22}	8.88×10^{-20}	7.63	4.30×10^{5}	3.28×10^{13}	1.31×10^{-8}	7.38×10^{13}	5.82×10^{-9}
9656	6000	4.941×10^{15}	154.62	6.93	7755	6.012×10^{4}	5.40×10^{-15}	5.34×10^{-18}	5.82×10^{-23}	4.94×10^{-20}	5.09	4.88×10^{5}	4.92×10^{13}	9.91×10^{-9}	1.11×10^{14}	4.41×10^{-9}
11,266	7000	5.271×10^{15}	127.72	5.79	8152	9.159×10^{4}	4.35×10^{-15}	4.29×10^{-18}	3.71×10^{-23}	3.15×10^{-20}	3.88	5.46×10^{5}	6.44×10^{13}	8.47×10^{-9}	1.45×10^{14}	3.76×10^{-9}
12,875	8000	5.546×10^{15}	107.92	4.84	8484	1.357×10^{5}	3.76×10^{-15}	3.71×10^{-18}	2.58×10^{-23}	2.19×10^{-20}	3.23	6.10×10^{5}	7.75×10^{13}	7.86×10^{-9}	1.74×10^{14}	3.50×10^{-9}
14,484	9000	5.779×10^{15}	91.40	4.04	8765	1.972×10^{5}	3.40×10^{-15}	3.36×10^{-18}	1.88×10^{-23}	1.60×10^{-20}	2.83	6.77×10^{5}	8.81×10^{13}	7.68×10^{-9}	1.98×10^{14}	3.41×10^{-9}
16,094	10,000	5.979×10^{15}	78.81	3.35	9006	2.833×10^{5}	3.17×10^{-15}	3.13×10^{-18}	1.42×10^{-23}	1.21×10^{-20}	2.57	7.53×10^{5}	9.72×10^{13}	7.75×10^{-9}	2.19×10^{14}	3.44×10^{-9}
17,703	11,000	6.151×10^{15}	68.65	2.76	9213	4.040×10^{5}	3.03×10^{-15}	2.99×10^{-18}	1.09×10^{-23}	9.27×10^{-21}	2.40	8.41×10^{5}	1.04×10^{14}	8.07×10^{-9}	2.34×10^{14}	3.59×10^{-9}
19,312	12,000	6.303×10^{15}	60.35	2.23	9396	5.800×10^{5}	2.93×10^{-15}	2.89×10^{-18}	8.34×10^{-24}	7.09×10^{-21}	2.27	9.45×10^{5}	1.10×10^{14}	8.57×10^{-9}	2.48×10^{14}	3.81×10^{-9}
20,922	13,000	6.436×10^{15}	53.46	1.77	9556	8.389×10^{5}	2.87×10^{-15}	2.82×10^{-18}	6.39×10^{-24}	5.42×10^{-21}	2.19	1.07×10^{6}	1.14×10^{14}	9.36×10^{-9}	2.57×10^{14}	4.16×10^{-9}
22,531	14,000	6.555×10^{15}	47.70	1.36	9700	1.242×10^{6}	2.81×10^{-15}	2.78×10^{-18}	4.75×10^{-24}	4.03×10^{-21}	2.12	1.23×10^{6}	1.18×10^{14}	1.04×10^{-8}	2.66×10^{14}	4.62×10^{-9}
24,140	15,000	6.662×10^{15}	42.81	.99	9829	1.926×10^{6}	2.79×10^{-15}	2.75×10^{-18}	3.37×10^{-24}	2.87×10^{-21}	2.07	1.45×10^{6}	1.21×10^{14}	1.20×10^{-8}	2.73×10^{14}	5.32×10^{-9}
25,750	16,000	6.757×10^{15}	38.65	.66	9943	3.238×10^{6}	2.77×10^{-15}	2.74×10^{-18}	2.21×10^{-24}	1.88×10^{-21}	2.03	1.79×10^{6}	1.23×10^{14}	1.45×10^{-8}	2.77×10^{14}	6.44×10^{-9}
26,591	16,523	6.803×10^{15}	36.76	.50	10,000	4.520×10^{6}	2.78×10^{-15}	2.73×10^{-18}	1.67×10^{-24}	1.42×10^{-21}	2.00	2.06×10^{6}	1.25×10^{14}	1.64×10^{-8}	2.82×10^{14}	7.30×10^{-9}

1 millibar (mb) = 10^3 dynes/cm² = 0.750 mm of Hg

Table 24

ATMOSPHERIC MODEL I - VALUES OF TEMPERATURE, PRESSURE, AND DENSITY ABOVE THE F_2 LAYER, BASED ON $M_L = 7$

Latitude 0°. Metric Units. $p_a = 1013$ mb, $\rho_a = 1.178 \times 10^{-3}$ gm/cm³

Height h km	Height h mi	Potential ϕ ergs	Apparent Gravity g' cm/sec²	Mean Mol Wt M	Temp T °K	Scale Height H km	Pressure p millibars	Pressure Ratio p/p_a	Density ρ gm/cm³	Density Ratio σ ρ/ρ_a	Number Density n particles/cm³	Mean Particle Speed v cm/sec	$d = 3 \times 10^{-8}$ cm: Mean Free Path L cm	$d = 3 \times 10^{-8}$ cm: Mean Collision Freq ν 1/sec	$d = 2 \times 10^{-8}$ cm: Mean Free Path L cm	$d = 2 \times 10^{-8}$ cm: Mean Collision Freq ν 1/sec
400.0	248.6	0	865.42	24.00	1800	7.199×10	2.07×10^{-7}	2.05×10^{-10}	3.33×10^{-14}	2.83×10^{-11}	8.40×10^{8}	1.26×10^{5}	2.98×10^{5}	4.23×10^{-1}	6.70×10^{5}	1.88×10^{-1}
482.8	300	1.032×10^{14}	845.18	23.70	1943	8.062×10	6.99×10^{-8}	6.90×10^{-11}	1.02×10^{-14}	8.71×10^{-12}	2.62×10^{8}	1.32×10^{5}	9.54×10^{5}	1.38×10^{-1}	2.15×10^{6}	6.14×10^{-2}
563.3	350	2.012×10^{14}	825.69	23.42	2079	8.937×10	2.72×10^{-8}	2.68×10^{-11}	3.68×10^{-15}	3.12×10^{-12}	9.54×10^{7}	1.37×10^{5}	2.62×10^{6}	5.23×10^{-2}	5.90×10^{6}	2.32×10^{-2}
643.8	400	2.971×10^{14}	807.76	23.14	2213	9.850×10	1.15×10^{-8}	1.14×10^{-11}	1.45×10^{-15}	1.23×10^{-12}	3.81×10^{7}	1.42×10^{5}	6.56×10^{6}	2.17×10^{-2}	1.48×10^{7}	9.64×10^{-3}
724.2	450	3.907×10^{14}	788.69	22.87	2343	1.080×10^{2}	5.27×10^{-9}	5.20×10^{-12}	6.18×10^{-16}	5.25×10^{-13}	1.64×10^{7}	1.47×10^{5}	1.53×10^{7}	9.64×10^{-3}	3.44×10^{7}	4.28×10^{-3}
804.7	500	4.823×10^{14}	771.11	22.61	2471	1.178×10^{2}	2.59×10^{-9}	2.55×10^{-12}	2.85×10^{-16}	2.42×10^{-13}	7.63×10^{6}	1.52×10^{5}	3.28×10^{7}	4.64×10^{-3}	7.38×10^{7}	2.06×10^{-3}
965.6	600	6.593×10^{14}	737.68	22.10	2716	1.385×10^{2}	7.33×10^{-10}	7.23×10^{-13}	7.16×10^{-17}	6.08×10^{-14}	1.97×10^{6}	1.61×10^{5}	1.27×10^{8}	1.27×10^{-3}	2.86×10^{8}	5.63×10^{-4}
1127	700	8.288×10^{14}	706.37	21.61	2952	1.608×10^{2}	2.50×10^{-10}	2.46×10^{-13}	2.20×10^{-17}	1.87×10^{-14}	6.18×10^{5}	1.70×10^{5}	4.05×10^{8}	4.20×10^{-4}	9.11×10^{8}	1.87×10^{-4}
1287	800	9.911×10^{14}	677.02	21.14	3177	1.846×10^{2}	9.82×10^{-11}	9.69×10^{-14}	7.88×10^{-18}	6.69×10^{-15}	2.26×10^{5}	1.78×10^{5}	1.11×10^{9}	1.61×10^{-4}	2.49×10^{9}	7.16×10^{-5}
1448	900	1.147×10^{15}	649.46	20.70	3394	2.100×10^{2}	4.32×10^{-11}	4.27×10^{-14}	3.17×10^{-18}	2.69×10^{-15}	9.29×10^{4}	1.86×10^{5}	2.69×10^{9}	6.91×10^{-5}	6.06×10^{9}	3.07×10^{-5}
1609	1000	1.296×10^{15}	623.56	20.27	3601	2.370×10^{2}	2.10×10^{-11}	2.08×10^{-14}	1.42×10^{-18}	1.21×10^{-15}	4.24×10^{4}	1.94×10^{5}	5.86×10^{9}	3.31×10^{-5}	1.32×10^{10}	1.47×10^{-5}
1931	1200	1.577×10^{15}	576.19	19.46	3992	2.957×10^{2}	6.23×10^{-12}	6.15×10^{-15}	3.65×10^{-19}	3.10×10^{-16}	1.14×10^{4}	2.08×10^{5}	2.20×10^{10}	9.46×10^{-6}	4.95×10^{10}	4.20×10^{-6}
2253	1400	1.839×10^{15}	534.02	18.70	4356	3.623×10^{2}	2.33×10^{-12}	2.30×10^{-15}	1.21×10^{-19}	1.02×10^{-16}	3.92×10^{3}	2.22×10^{5}	6.38×10^{10}	3.48×10^{-6}	1.44×10^{11}	1.55×10^{-6}
2414	1500	1.961×10^{15}	514.65	18.35	4525	3.980×10^{2}	1.53×10^{-12}	1.51×10^{-15}	7.47×10^{-20}	6.34×10^{-17}	2.47×10^{3}	2.28×10^{5}	1.01×10^{11}	2.25×10^{-6}	2.28×10^{11}	1.00×10^{-6}
2816	1750	2.250×10^{15}	470.61	17.52	4926	4.963×10^{2}	6.18×10^{-13}	6.10×10^{-16}	2.64×10^{-20}	2.24×10^{-17}	9.15×10^{2}	2.44×10^{5}	2.74×10^{11}	8.91×10^{-7}	6.15×10^{11}	3.96×10^{-7}
3219	2000	2.514×10^{15}	432.00	16.76	5294	6.074×10^{2}	2.97×10^{-13}	2.93×10^{-16}	1.13×10^{-20}	9.62×10^{-18}	4.10×10^{2}	2.58×10^{5}	6.11×10^{11}	4.23×10^{-7}	1.37×10^{12}	1.88×10^{-7}
4023	2500	2.983×10^{15}	387.73	15.40	5946	8.273×10^{2}	9.82×10^{-14}	9.69×10^{-17}	3.06×10^{-21}	2.60×10^{-18}	1.20×10^{2}	2.86×10^{5}	2.08×10^{12}	1.38×10^{-7}	4.68×10^{12}	6.12×10^{-8}
4828	3000	3.383×10^{15}	316.92	14.25	6502	1.196×10^{3}	4.46×10^{-14}	4.41×10^{-17}	1.17×10^{-21}	9.97×10^{-19}	5.01×10	3.11×10^{5}	4.99×10^{12}	6.23×10^{-8}	1.12×10^{13}	2.77×10^{-8}
6437	4000	4.034×10^{15}	242.42	12.38	7406	2.048×10^{3}	1.59×10^{-14}	1.57×10^{-17}	3.20×10^{-22}	2.72×10^{-19}	1.57×10	3.57×10^{5}	1.60×10^{13}	2.23×10^{-8}	3.59×10^{13}	9.93×10^{-9}
8047	5000	4.541×10^{15}	191.44	10.92	8111	3.223×10^{3}	8.52×10^{-15}	8.42×10^{-18}	1.38×10^{-22}	1.17×10^{-19}	7.66	3.96×10^{5}	3.26×10^{13}	1.21×10^{-8}	7.35×10^{13}	5.39×10^{-9}
9656	6000	4.945×10^{15}	155.02	9.75	8673	4.767×10^{3}	5.65×10^{-15}	5.58×10^{-18}	7.62×10^{-23}	6.47×10^{-20}	4.73	4.33×10^{5}	5.29×10^{13}	8.19×10^{-9}	1.19×10^{14}	3.64×10^{-9}
11,266	7000	5.276×10^{15}	128.10	8.80	9133	6.730×10^{3}	4.24×10^{-15}	4.18×10^{-18}	4.91×10^{-23}	4.17×10^{-20}	3.39	4.69×10^{5}	7.39×10^{13}	6.35×10^{-9}	1.66×10^{14}	2.82×10^{-9}
12,875	8000	5.553×10^{15}	107.63	8.00	9517	9.182×10^{3}	3.45×10^{-15}	3.41×10^{-18}	3.49×10^{-23}	2.97×10^{-20}	2.65	5.03×10^{5}	9.45×10^{13}	5.32×10^{-9}	2.13×10^{14}	2.37×10^{-9}
14,484	9000	5.786×10^{15}	91.70	7.33	9841	1.216×10^{4}	2.96×10^{-15}	2.93×10^{-18}	2.66×10^{-23}	2.26×10^{-20}	2.20	5.33×10^{5}	1.14×10^{14}	4.69×10^{-9}	2.56×10^{14}	2.08×10^{-9}
15,374	9553	5.903×10^{15}	84.38	7.00	10,000	1.407×10^{4}	2.71×10^{-15}	2.73×10^{-18}	2.28×10^{-23}	1.94×10^{-20}	2.00	5.50×10^{5}	1.25×10^{14}	4.38×10^{-9}	2.82×10^{14}	1.95×10^{-9}

1 millibar (mb) = 10^3 dynes/cm² = 0.750 mm of Hg

Table 25

ATMOSPHERIC MODEL I - VALUES OF TEMPERATURE, PRESSURE, AND DENSITY ABOVE THE F_2 LAYER, BASED ON M_L = 14

Latitude 0°. Metric Units. p_a = 1013 mb, ρ_a = 1.178 × 10^{-3} gm/cm³

Height h km	Height h mi	Potential ϕ ergs	Apparent Gravity g' cm/sec²	Mean Mol Wt M	Temp T °K	Scale Height H km	Pressure p millibars	Pressure Ratio p/p_a	Density ρ gm/cm³	Density Ratio σ ρ/ρ_a	Number Density n particles/cm³	Mean Particle Speed v cm/sec	$d = 3\times10^{-8}$ cm: Mean Free Path L cm	$d = 3\times10^{-8}$ cm: Mean Collision Freq ν 1/sec	$d = 2\times10^{-8}$ cm: Mean Free Path L cm	$d = 2\times10^{-8}$ cm: Mean Collision Freq ν 1/sec
400.0	248.6	0	865.42	24.00	1800	7.199 × 10	2.07 × 10^{-7}	2.05 × 10^{-10}	3.33 × 10^{-14}	2.83 × 10^{-11}	8.40 × 10^{8}	1.26 × 10^{5}	2.98 × 10^{5}	4.23 × 10^{-1}	6.70 × 10^{5}	1.88 × 10^{-1}
482.8	300	1.032 × 10^{14}	845.26	23.80	1964	8.110 × 10	7.04 × 10^{-8}	6.95 × 10^{-11}	1.02 × 10^{-14}	8.71 × 10^{-12}	2.61 × 10^{8}	1.32 × 10^{5}	9.57 × 10^{5}	1.38 × 10^{-1}	2.15 × 10^{6}	6.13 × 10^{-2}
563.3	350	2.012 × 10^{14}	825.79	23.61	2119	9.030 × 10	2.75 × 10^{-8}	2.71 × 10^{-11}	3.68 × 10^{-15}	3.13 × 10^{-12}	9.46 × 10^{7}	1.38 × 10^{5}	2.64 × 10^{6}	5.21 × 10^{-2}	5.95 × 10^{6}	2.32 × 10^{-2}
643.8	400	2.971 × 10^{14}	807.87	23.42	2272	9.974 × 10	1.18 × 10^{-8}	1.16 × 10^{-11}	1.46 × 10^{-15}	1.24 × 10^{-12}	3.78 × 10^{7}	1.43 × 10^{5}	6.62 × 10^{6}	2.16 × 10^{-2}	1.49 × 10^{7}	9.61 × 10^{-3}
724.2	450	3.907 × 10^{14}	788.80	23.24	2421	1.097 × 10^{2}	5.46 × 10^{-9}	5.39 × 10^{-12}	6.28 × 10^{-16}	5.34 × 10^{-13}	1.64 × 10^{7}	1.48 × 10^{5}	1.52 × 10^{7}	9.74 × 10^{-3}	3.43 × 10^{7}	4.33 × 10^{-3}
804.7	500	4.823 × 10^{14}	771.24	23.07	2566	1.198 × 10^{2}	2.71 × 10^{-9}	2.68 × 10^{-12}	2.93 × 10^{-16}	2.49 × 10^{-13}	7.70 × 10^{6}	1.53 × 10^{5}	3.25 × 10^{7}	4.72 × 10^{-3}	7.31 × 10^{7}	2.10 × 10^{-3}
965.6	600	6.593 × 10^{14}	737.83	22.72	2847	1.411 × 10^{2}	7.85 × 10^{-10}	7.75 × 10^{-13}	7.52 × 10^{-17}	6.39 × 10^{-14}	2.01 × 10^{6}	1.63 × 10^{5}	1.25 × 10^{8}	1.31 × 10^{-3}	2.80 × 10^{8}	5.81 × 10^{-4}
1127	700	8.288 × 10^{14}	706.54	22.39	3116	1.636 × 10^{2}	2.73 × 10^{-10}	2.70 × 10^{-13}	2.36 × 10^{-17}	2.00 × 10^{-14}	6.39 × 10^{5}	1.72 × 10^{5}	3.91 × 10^{8}	4.38 × 10^{-4}	8.81 × 10^{8}	1.95 × 10^{-4}
1287	800	9.912 × 10^{14}	677.20	22.08	3374	1.875 × 10^{2}	1.09 × 10^{-10}	1.08 × 10^{-13}	8.60 × 10^{-18}	7.31 × 10^{-15}	2.36 × 10^{5}	1.80 × 10^{5}	1.06 × 10^{9}	1.70 × 10^{-4}	2.38 × 10^{9}	7.55 × 10^{-5}
1448	900	1.147 × 10^{15}	649.66	21.78	3622	2.126 × 10^{2}	4.89 × 10^{-11}	4.82 × 10^{-14}	3.53 × 10^{-18}	3.00 × 10^{-15}	9.85 × 10^{4}	1.87 × 10^{5}	2.54 × 10^{9}	7.38 × 10^{-5}	5.72 × 10^{9}	3.28 × 10^{-5}
1609	1000	1.296 × 10^{15}	623.77	21.49	3859	2.391 × 10^{2}	2.39 × 10^{-11}	2.36 × 10^{-14}	1.60 × 10^{-18}	1.36 × 10^{-15}	4.52 × 10^{4}	1.95 × 10^{5}	5.54 × 10^{9}	3.52 × 10^{-5}	1.25 × 10^{10}	1.56 × 10^{-5}
1931	1200	1.578 × 10^{15}	576.43	20.94	4307	2.964 × 10^{2}	7.14 × 10^{-12}	7.04 × 10^{-15}	4.17 × 10^{-19}	3.54 × 10^{-16}	1.21 × 10^{4}	2.08 × 10^{5}	2.07 × 10^{10}	1.01 × 10^{-5}	4.66 × 10^{10}	4.47 × 10^{-6}
2253	1400	1.839 × 10^{15}	534.29	20.44	4720	3.591 × 10^{2}	2.66 × 10^{-12}	2.62 × 10^{-15}	1.39 × 10^{-19}	1.18 × 10^{-16}	4.10 × 10^{3}	2.21 × 10^{5}	6.11 × 10^{10}	3.62 × 10^{-5}	1.37 × 10^{11}	1.61 × 10^{-5}
2414	1500	1.962 × 10^{15}	514.93	20.20	4916	3.926 × 10^{2}	1.73 × 10^{-12}	1.71 × 10^{-15}	8.55 × 10^{-20}	7.26 × 10^{-17}	2.57 × 10^{3}	2.27 × 10^{5}	9.75 × 10^{10}	2.33 × 10^{-6}	2.19 × 10^{11}	1.03 × 10^{-6}
2816	1750	2.251 × 10^{15}	470.91	19.64	5375	4.828 × 10^{2}	6.90 × 10^{-13}	6.81 × 10^{-16}	3.03 × 10^{-20}	2.57 × 10^{-17}	9.36 × 10^{2}	2.40 × 10^{5}	2.67 × 10^{11}	9.00 × 10^{-7}	6.02 × 10^{11}	4.00 × 10^{-7}
3219	2000	2.515 × 10^{15}	432.30	19.13	5794	5.821 × 10^{2}	3.22 × 10^{-13}	3.18 × 10^{-16}	1.28 × 10^{-20}	1.08 × 10^{-17}	4.06 × 10^{2}	2.53 × 10^{5}	6.16 × 10^{11}	4.11 × 10^{-7}	1.39 × 10^{12}	1.83 × 10^{-7}
4023	2500	2.985 × 10^{15}	388.07	18.22	6540	7.684 × 10^{2}	9.96 × 10^{-14}	9.83 × 10^{-17}	3.34 × 10^{-21}	2.83 × 10^{-18}	1.11 × 10^{2}	2.76 × 10^{5}	2.25 × 10^{12}	1.22 × 10^{-7}	5.06 × 10^{12}	5.44 × 10^{-8}
4828	3000	3.386 × 10^{15}	317.26	17.42	7177	1.078 × 10^{3}	4.21 × 10^{-14}	4.16 × 10^{-17}	1.23 × 10^{-21}	1.05 × 10^{-18}	4.27 × 10	2.95 × 10^{5}	5.86 × 10^{12}	5.04 × 10^{-8}	1.32 × 10^{13}	2.24 × 10^{-8}
6437	4000	4.037 × 10^{15}	242.75	16.18	8211	1.737 × 10^{3}	1.30 × 10^{-14}	1.28 × 10^{-17}	3.07 × 10^{-22}	2.61 × 10^{-19}	1.15 × 10	3.26 × 10^{5}	2.17 × 10^{13}	1.51 × 10^{-8}	4.88 × 10^{13}	6.69 × 10^{-9}
8047	5000	4.544 × 10^{15}	191.73	15.20	9016	2.570 × 10^{3}	6.08 × 10^{-15}	6.00 × 10^{-18}	1.23 × 10^{-22}	1.05 × 10^{-19}	4.91	3.54 × 10^{5}	5.10 × 10^{13}	6.94 × 10^{-9}	1.15 × 10^{14}	3.08 × 10^{-9}
9656	6000	4.949 × 10^{15}	155.25	14.41	9660	3.587 × 10^{5}	3.56 × 10^{-15}	3.52 × 10^{-18}	6.39 × 10^{-23}	5.42 × 10^{-20}	2.69	3.78 × 10^{5}	9.31 × 10^{13}	4.06 × 10^{-9}	2.10 × 10^{14}	1.80 × 10^{-9}
10,657	6622	5.163 × 10^{15}	137.58	14.00	10,000	4.313 × 10^{3}	2.83 × 10^{-15}	2.73 × 10^{-18}	4.77 × 10^{-23}	4.05 × 10^{-20}	2.00	3.89 × 10^{5}	1.25 × 10^{14}	3.12 × 10^{-9}	2.82 × 10^{14}	1.39 × 10^{-9}

1 millibar (mb) = 10^{3} dynes/cm² = 0.750 mm of Hg

Table 26

ATMOSPHERIC MODEL I - VALUES OF TEMPERATURE, PRESSURE, AND DENSITY ABOVE THE F_2 LAYER, BASED ON $M_L = 7$

Latitude 45°. Engineering Units. $p_a = 2116$ lb/ft², $\rho_a = 2.375 \times 10^{-3}$ slug/ft³

Height h mi	Height h ft	Potential ϕ ft-lb	Apparent Gravity g' ft/sec²	Mean Mol Wt M	Temp T °R	Scale Height H ft	Pressure p lb/ft²	Pressure Ratio p/p_a	Density ρ slug/ft³	Density Ratio σ ρ/ρ_a	Number Density n particles/ft³	Mean Particle Speed v ft/sec	$d = 3 \times 10^{-8}$ cm Mean Free Path L ft	$d = 3 \times 10^{-8}$ cm Mean Collision Freq ν 1/sec	$d = 2 \times 10^{-8}$ cm Mean Free Path L ft	$d = 2 \times 10^{-8}$ cm Mean Collision Freq ν 1/sec
186.41	9.842×10^5	0	29.308	24.35	1980	1.378×10^6	1.01×10^{-6}	4.77×10^{-10}	2.50×10^{-13}	1.05×10^{-10}	9.09×10^{12}	3.21×10^3	2.56×10^3	1.26	5.75×10^3	5.58×10^{-1}
200	1.056×10^6	2.098×10^6	29.117	24.25	2072	1.458×10^6	6.07×10^{-7}	2.87×10^{-10}	1.43×10^{-13}	6.02×10^{-11}	5.22×10^{12}	3.29×10^3	4.45×10^3	7.39×10^{-1}	1.00×10^4	3.28×10^{-1}
225	1.188×10^6	5.922×10^6	28.769	24.07	2239	1.606×10^6	2.56×10^{-7}	1.21×10^{-10}	5.54×10^{-14}	2.33×10^{-11}	2.04×10^{12}	3.43×10^3	1.14×10^4	3.01×10^{-1}	2.56×10^4	1.34×10^{-1}
250	1.320×10^6	9.700×10^6	28.427	23.89	2404	1.758×10^6	1.17×10^{-7}	5.53×10^{-11}	2.34×10^{-14}	9.85×10^{-12}	8.67×10^{12}	3.57×10^3	2.68×10^4	1.33×10^{-1}	6.03×10^4	5.92×10^{-2}
275	1.452×10^6	1.343×10^7	28.091	23.71	2567	1.915×10^6	5.68×10^{-8}	2.68×10^{-11}	1.06×10^{-14}	4.46×10^{-12}	3.96×10^{12}	3.70×10^3	5.87×10^4	6.30×10^{-2}	1.32×10^5	2.80×10^{-2}
300	1.584×10^6	1.712×10^7	27.762	23.54	2728	2.074×10^6	2.93×10^{-8}	1.38×10^{-11}	5.09×10^{-15}	2.14×10^{-12}	1.91×10^{12}	3.83×10^3	1.22×10^5	3.15×10^{-2}	2.74×10^5	1.40×10^{-2}
350	1.848×10^6	2.438×10^7	27.119	23.20	3045	2.404×10^6	8.96×10^{-9}	4.23×10^{-12}	1.37×10^{-15}	5.77×10^{-13}	5.23×10^{11}	4.07×10^3	4.44×10^5	9.16×10^{-2}	1.00×10^6	4.07×10^{-2}
400	2.112×10^6	3.146×10^7	26.499	22.86	3354	2.750×10^6	3.21×10^{-9}	1.52×10^{-12}	4.40×10^{-16}	1.85×10^{-13}	1.70×10^{11}	4.31×10^3	1.37×10^6	3.15×10^{-2}	3.08×10^6	1.40×10^{-2}
450	2.376×10^6	3.838×10^7	25.900	22.53	3656	3.112×10^6	1.30×10^{-9}	6.14×10^{-13}	1.61×10^{-16}	6.78×10^{-14}	6.32×10^{10}	4.53×10^3	1.68×10^6	1.23×10^{-2}	8.28×10^6	5.47×10^{-4}
500	2.640×10^6	4.515×10^7	25.320	22.21	3952	3.491×10^6	5.83×10^{-10}	2.75×10^{-13}	6.60×10^{-17}	2.78×10^{-14}	2.63×10^{10}	4.74×10^3	8.84×10^6	5.36×10^{-4}	1.99×10^7	2.38×10^{-4}
600	3.168×10^6	5.825×10^7	24.219	21.59	4524	4.298×10^6	1.49×10^{-10}	7.04×10^{-14}	1.43×10^{-17}	6.02×10^{-16}	5.86×10^9	5.15×10^3	3.97×10^7	1.30×10^{-4}	8.93×10^7	5.77×10^{-5}
700	3.696×10^6	7.078×10^7	23.187	21.00	5072	5.174×10^6	4.85×10^{-11}	2.29×10^{-14}	4.04×10^{-18}	1.70×10^{-15}	1.70×10^9	5.53×10^3	1.37×10^8	4.04×10^{-5}	3.08×10^8	1.80×10^{-5}
800	4.224×10^6	8.278×10^7	22.221	20.43	5596	6.123×10^6	1.90×10^{-11}	8.98×10^{-15}	1.40×10^{-18}	5.89×10^{-16}	6.06×10^8	5.89×10^3	3.84×10^8	1.54×10^{-5}	8.63×10^8	6.82×10^{-6}
900	4.752×10^6	9.430×10^7	21.313	19.89	6099	7.147×10^6	8.52×10^{-12}	4.03×10^{-15}	5.59×10^{-19}	2.35×10^{-16}	2.49×10^8	6.23×10^3	9.30×10^8	6.70×10^{-6}	2.09×10^9	2.98×10^{-6}
1000	5.280×10^6	1.053×10^8	20.460	19.37	6580	8.248×10^6	4.29×10^{-12}	2.03×10^{-15}	2.54×10^{-19}	1.07×10^{-16}	1.16×10^8	6.56×10^3	2.00×10^9	3.24×10^{-6}	4.51×10^9	1.44×10^{-6}
1200	6.336×10^6	1.262×10^8	18.901	18.38	7493	1.068×10^6	1.38×10^{-12}	6.52×10^{-16}	6.81×10^{-20}	2.87×10^{-17}	3.27×10^7	7.18×10^3	7.11×10^9	1.01×10^{-6}	1.60×10^{10}	4.49×10^{-7}
1400	7.392×10^6	1.454×10^8	17.513	17.47	8331	1.353×10^6	5.76×10^{-13}	2.72×10^{-16}	2.43×10^{-20}	1.02×10^{-17}	1.23×10^7	7.77×10^3	1.89×10^{10}	4.11×10^{-7}	4.25×10^{10}	1.83×10^{-7}
1500	7.920×10^6	1.545×10^8	16.876	17.04	8729	1.508×10^6	3.98×10^{-13}	1.88×10^{-16}	1.56×10^{-20}	6.57×10^{-18}	8.10×10^6	8.05×10^3	2.87×10^{10}	2.80×10^{-7}	6.46×10^{10}	1.25×10^{-7}
1750	9.240×10^6	1.759×10^8	15.428	16.03	9663	1.941×10^6	1.83×10^{-13}	8.65×10^{-17}	6.11×10^{-21}	2.57×10^{-18}	3.37×10^6	8.73×10^3	6.90×10^{10}	1.27×10^{-7}	1.55×10^{11}	5.62×10^{-8}
2000	1.056×10^7	1.954×10^8	14.158	15.11	10,515	2.442×10^6	9.99×10^{-14}	4.72×10^{-17}	2.89×10^{-21}	1.22×10^{-18}	1.69×10^6	9.38×10^3	1.38×10^{11}	6.82×10^{-8}	3.09×10^{11}	3.03×10^{-8}
2500	1.320×10^7	2.300×10^8	12.049	13.47	12,027	3.681×10^6	4.12×10^{-14}	1.95×10^{-17}	9.29×10^{-22}	3.91×10^{-19}	6.10×10^5	1.06×10^4	3.81×10^{11}	2.78×10^{-8}	8.57×10^{11}	1.24×10^{-8}
3000	1.584×10^7	2.597×10^8	10.381	12.06	13,324	5.287×10^6	2.25×10^{-14}	1.06×10^{-17}	4.10×10^{-22}	1.73×10^{-19}	3.01×10^5	1.18×10^4	7.72×10^{11}	1.53×10^{-8}	1.74×10^{12}	6.79×10^{-9}
3500	1.848×10^7	2.854×10^8	9.038	10.85	14,446	7.318×10^6	1.47×10^{-14}	6.95×10^{-18}	2.22×10^{-22}	9.35×10^{-20}	1.81×10^5	1.30×10^4	1.28×10^{12}	1.01×10^{-8}	2.89×10^{12}	4.50×10^{-9}
4000	2.112×10^7	3.078×10^8	7.942	9.79	15,425	9.855×10^6	1.08×10^{-14}	5.10×10^{-18}	1.38×10^{-22}	5.81×10^{-20}	1.25×10^5	1.41×10^4	1.86×10^{12}	7.58×10^{-9}	4.18×10^{12}	3.37×10^{-9}
4500	2.376×10^7	3.276×10^8	7.037	8.85	16,290	1.340×10^7	8.52×10^{-15}	4.03×10^{-18}	9.32×10^{-23}	3.92×10^{-20}	9.32×10^4	1.53×10^4	2.49×10^{12}	6.13×10^{-9}	5.61×10^{12}	2.73×10^{-9}
5000	2.640×10^7	3.452×10^8	6.280	8.02	17,059	1.683×10^7	7.12×10^{-15}	3.36×10^{-18}	6.74×10^{-23}	2.84×10^{-20}	7.44×10^4	1.64×10^4	3.12×10^{12}	5.25×10^{-9}	7.03×10^{12}	2.33×10^{-9}
5500	2.904×10^7	3.609×10^8	5.642	7.28	17,744	2.146×10^7	6.19×10^{-15}	2.92×10^{-18}	5.11×10^{-23}	2.15×10^{-20}	6.21×10^4	1.76×10^4	3.74×10^{12}	4.70×10^{-9}	8.42×10^{12}	2.09×10^{-9}
5526	2.917×10^7	3.668×10^8	5.402	7.00	18,000	2.365×10^7	5.78×10^{-15}	2.73×10^{-18}	4.52×10^{-23}	1.91×10^{-20}	5.66×10^4	1.80×10^4	4.11×10^{12}	4.38×10^{-9}	9.24×10^{12}	1.95×10^{-9}

1 lb/ft² = 0.3591 mm of Hg

Table 27

ATMOSPHERIC MODEL I - VALUES OF TEMPERATURE, PRESSURE, AND DENSITY ABOVE THE F_2 LAYER, BASED ON $M_L = 7$

Latitude 45°. Metric Units. p_a = 1014 mb, $\rho_a = 1.223 \times 10^{-3}$ gm/cm³

Height h		Potential ϕ	Apparent Gravity g'	Mean Mol Wt M	Temp T	Scale Height H	Pressure p	Pressure Ratio	Density ρ	Density Ratio σ	Number Density n	Mean Particle Speed v	$d = 3 \times 10^{-8}$ cm		$d = 2 \times 10^{-8}$ cm	
													Mean Free Path L	Mean Collision Freq ν	Mean Free Path L	Mean Collision Freq ν
km	mi	ergs	cm/sec²		°K	km	millibars	p/p_a	gm/cm³	ρ/ρ_a	particles/cm³	cm/sec	cm	1/sec	cm	1/sec
300.0	186.41	0	893.31	24.35	1100	4.201×10	4.84×10^{-7}	4.77×10^{-10}	1.29×10^{-13}	1.05×10^{-10}	3.21×10^{9}	9.78×10^{4}	7.79×10^{4}	1.26	1.754×10^{5}	5.58×10^{-1}
321.9	200	2.845×10^{15}	887.49	24.25	1151	4.443×10	2.91×10^{-7}	2.87×10^{-10}	7.36×10^{-14}	6.02×10^{-10}	1.84×10^{9}	1.00×10^{5}	1.36×10^{5}	7.39×10^{-1}	3.05×10^{5}	3.28×10^{-1}
362.1	225	8.030×10^{15}	876.88	24.07	1244	4.896×10	1.23×10^{-7}	1.21×10^{-10}	2.85×10^{-14}	2.33×10^{-11}	7.20×10^{8}	1.05×10^{5}	3.47×10^{5}	3.01×10^{-1}	7.82×10^{5}	1.34×10^{-1}
402.3	250	1.315×10^{14}	866.45	23.89	1336	5.360×10	5.60×10^{-8}	5.53×10^{-11}	1.21×10^{-14}	9.85×10^{-12}	3.06×10^{8}	1.09×10^{5}	8.17×10^{5}	1.33×10^{-1}	1.84×10^{6}	5.92×10^{-2}
442.6	275	1.821×10^{14}	856.21	23.71	1426	5.836×10	2.72×10^{-8}	2.68×10^{-11}	5.46×10^{-15}	4.46×10^{-12}	1.40×10^{8}	1.13×10^{5}	1.79×10^{6}	6.30×10^{-2}	4.03×10^{6}	2.80×10^{-2}
482.8	300	2.321×10^{14}	846.19	23.54	1516	6.321×10	1.40×10^{-8}	1.38×10^{-11}	2.62×10^{-15}	2.14×10^{-12}	6.75×10^{7}	1.17×10^{5}	3.71×10^{6}	3.15×10^{-2}	8.35×10^{6}	1.40×10^{-2}
563.3	350	3.306×10^{14}	826.59	23.20	1692	7.328×10	4.29×10^{-9}	4.23×10^{-12}	7.06×10^{-16}	5.77×10^{-13}	1.85×10^{7}	1.24×10^{5}	1.35×10^{7}	9.16×10^{-3}	3.05×10^{7}	4.07×10^{-3}
643.8	400	4.266×10^{14}	807.69	22.86	1863	8.384×10	1.54×10^{-9}	1.52×10^{-12}	2.27×10^{-16}	1.85×10^{-13}	6.00×10^{6}	1.31×10^{5}	4.17×10^{7}	3.15×10^{-3}	9.38×10^{7}	1.40×10^{-3}
724.2	450	5.204×10^{14}	789.43	22.53	2031	9.487×10	6.23×10^{-10}	6.14×10^{-13}	8.29×10^{-17}	6.78×10^{-14}	2.23×10^{6}	1.38×10^{5}	1.12×10^{8}	1.23×10^{-3}	2.52×10^{8}	5.47×10^{-4}
804.7	500	6.122×10^{14}	771.75	22.21	2196	1.064×10^{2}	2.79×10^{-10}	2.75×10^{-13}	3.40×10^{-17}	2.78×10^{-14}	9.29×10^{5}	1.44×10^{5}	2.69×10^{8}	5.36×10^{-4}	6.06×10^{8}	2.38×10^{-4}
965.6	600	7.899×10^{14}	738.20	21.59	2513	1.310×10^{2}	7.14×10^{-11}	7.04×10^{-14}	7.36×10^{-18}	6.02×10^{-15}	2.07×10^{5}	1.57×10^{5}	1.21×10^{9}	1.30×10^{-4}	2.72×10^{9}	5.77×10^{-5}
1127	700	9.598×10^{14}	706.74	21.00	2818	1.577×10^{2}	2.32×10^{-11}	2.29×10^{-14}	2.08×10^{-18}	1.70×10^{-15}	6.00×10^{4}	1.69×10^{5}	4.17×10^{9}	4.04×10^{-5}	9.38×10^{9}	1.80×10^{-5}
1288	800	1.122×10^{15}	677.30	20.43	3109	1.866×10^{2}	9.10×10^{-12}	8.98×10^{-15}	7.21×10^{-19}	5.89×10^{-16}	2.14×10^{4}	1.80×10^{5}	1.17×10^{10}	1.54×10^{-5}	2.63×10^{10}	6.82×10^{-6}
1448	900	1.279×10^{15}	649.62	19.89	3388	2.178×10^{2}	4.08×10^{-12}	4.03×10^{-15}	2.88×10^{-19}	2.35×10^{-16}	8.79×10^{3}	1.90×10^{5}	2.83×10^{10}	6.70×10^{-6}	6.38×10^{10}	2.98×10^{-6}
1609	1000	1.428×10^{15}	623.62	19.37	3656	2.514×10^{2}	2.05×10^{-12}	2.03×10^{-15}	1.31×10^{-19}	1.07×10^{-16}	4.10×10^{3}	2.00×10^{5}	6.11×10^{10}	3.24×10^{-6}	1.37×10^{11}	1.44×10^{-6}
1931	1200	1.711×10^{15}	576.10	18.38	4163	3.254×10^{2}	6.61×10^{-13}	6.52×10^{-16}	3.51×10^{-20}	2.87×10^{-17}	1.15×10^{3}	2.19×10^{5}	2.17×10^{11}	1.01×10^{-6}	4.87×10^{11}	4.49×10^{-7}
2253	1400	1.972×10^{15}	533.80	17.47	4628	4.123×10^{2}	2.76×10^{-13}	2.72×10^{-16}	1.25×10^{-20}	1.02×10^{-17}	4.34×10^{2}	2.37×10^{5}	5.76×10^{11}	4.11×10^{-7}	1.30×10^{12}	1.83×10^{-7}
2414	1500	2.095×10^{15}	514.38	17.04	4849	4.596×10^{2}	1.91×10^{-13}	1.88×10^{-16}	8.03×10^{-21}	6.57×10^{-18}	2.86×10^{2}	2.45×10^{5}	8.75×10^{11}	2.80×10^{-7}	1.97×10^{12}	1.25×10^{-7}
2816	1750	2.385×10^{15}	470.25	16.03	5368	5.916×10^{2}	8.76×10^{-14}	8.65×10^{-17}	3.15×10^{-21}	2.57×10^{-18}	1.19×10^{2}	2.66×10^{5}	2.10×10^{12}	1.27×10^{-7}	4.73×10^{12}	5.62×10^{-8}
3219	2000	2.650×10^{15}	431.54	15.11	5842	7.442×10^{2}	4.78×10^{-14}	4.72×10^{-17}	1.49×10^{-21}	1.22×10^{-18}	5.97×10	2.86×10^{5}	4.19×10^{12}	6.82×10^{-8}	9.43×10^{12}	3.03×10^{-8}
4023	2500	3.119×10^{15}	367.25	13.47	6682	1.122×10^{3}	1.97×10^{-14}	1.95×10^{-17}	4.78×10^{-22}	3.91×10^{-19}	2.15×10	3.23×10^{5}	1.16×10^{13}	2.78×10^{-8}	2.61×10^{13}	1.24×10^{-8}
4828	3000	3.522×10^{15}	316.41	12.06	7402	1.612×10^{3}	1.08×10^{-14}	1.06×10^{-17}	2.11×10^{-22}	1.73×10^{-19}	1.06×10	3.60×10^{5}	2.35×10^{13}	1.53×10^{-8}	5.30×10^{13}	6.79×10^{-9}
5633	3500	3.870×10^{15}	275.48	10.85	8026	2.231×10^{3}	7.04×10^{-15}	6.95×10^{-18}	1.14×10^{-22}	9.35×10^{-20}	6.39	3.96×10^{5}	3.91×10^{13}	1.01×10^{-8}	8.81×10^{13}	4.50×10^{-9}
6437	4000	4.174×10^{15}	242.07	9.79	8569	3.004×10^{3}	5.17×10^{-15}	5.10×10^{-18}	7.11×10^{-23}	5.81×10^{-20}	4.41	4.30×10^{5}	5.67×10^{13}	7.58×10^{-9}	1.28×10^{14}	3.37×10^{-9}
7242	4500	4.442×10^{15}	214.49	8.85	9050	4.085×10^{3}	4.08×10^{-15}	4.03×10^{-18}	4.80×10^{-23}	3.92×10^{-20}	3.29	4.66×10^{5}	7.60×10^{13}	6.13×10^{-9}	1.71×10^{14}	2.73×10^{-9}
8047	5000	4.681×10^{15}	191.41	8.02	9477	5.129×10^{3}	3.41×10^{-15}	3.36×10^{-18}	3.47×10^{-23}	2.84×10^{-20}	2.63	5.00×10^{5}	9.52×10^{13}	5.25×10^{-9}	2.14×10^{14}	2.33×10^{-9}
8852	5500	4.894×10^{15}	171.97	7.28	9858	6.541×10^{3}	2.96×10^{-15}	2.92×10^{-18}	2.63×10^{-23}	2.15×10^{-20}	2.19	5.36×10^{5}	1.14×10^{14}	4.70×10^{-9}	2.57×10^{14}	2.09×10^{-9}
8890	5526	4.973×10^{15}	164.65	7.00	10,000	7.208×10^{3}	2.78×10^{-15}	2.73×10^{-18}	2.34×10^{-23}	1.91×10^{-20}	2.00	5.50×10^{5}	1.25×10^{14}	4.38×10^{-9}	2.82×10^{14}	1.95×10^{-9}

1 millibar (mb) = 10^{3} dynes/cm² = 0.750 mm of Hg

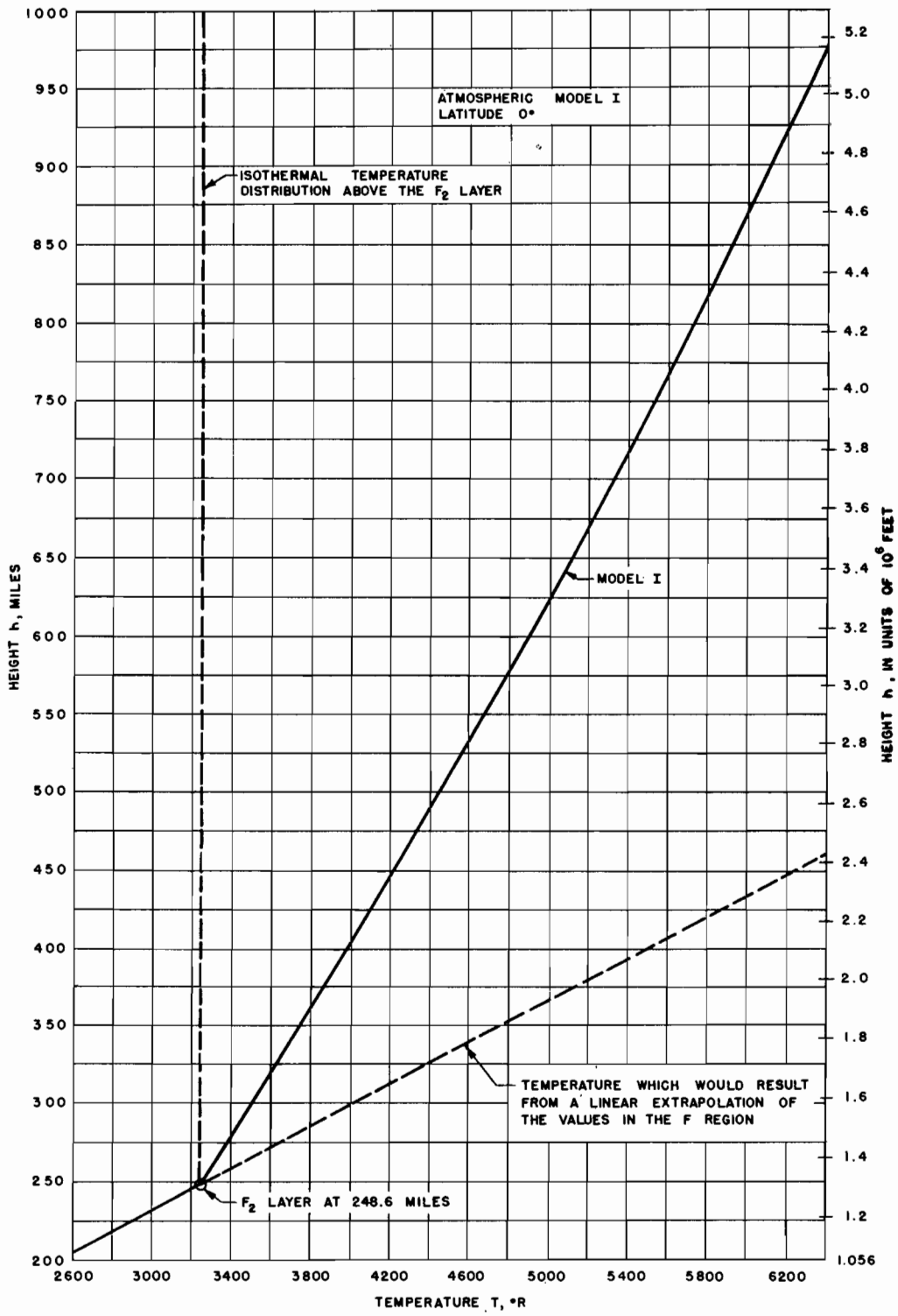

ADOPTED VALUES OF TEMPERATURE FOR ATMOSPHERIC MODEL I FROM THE F_2 LAYER UP TO 1000 MILES. LATITUDE 0°. ENGINEERING UNITS

FIG. 19

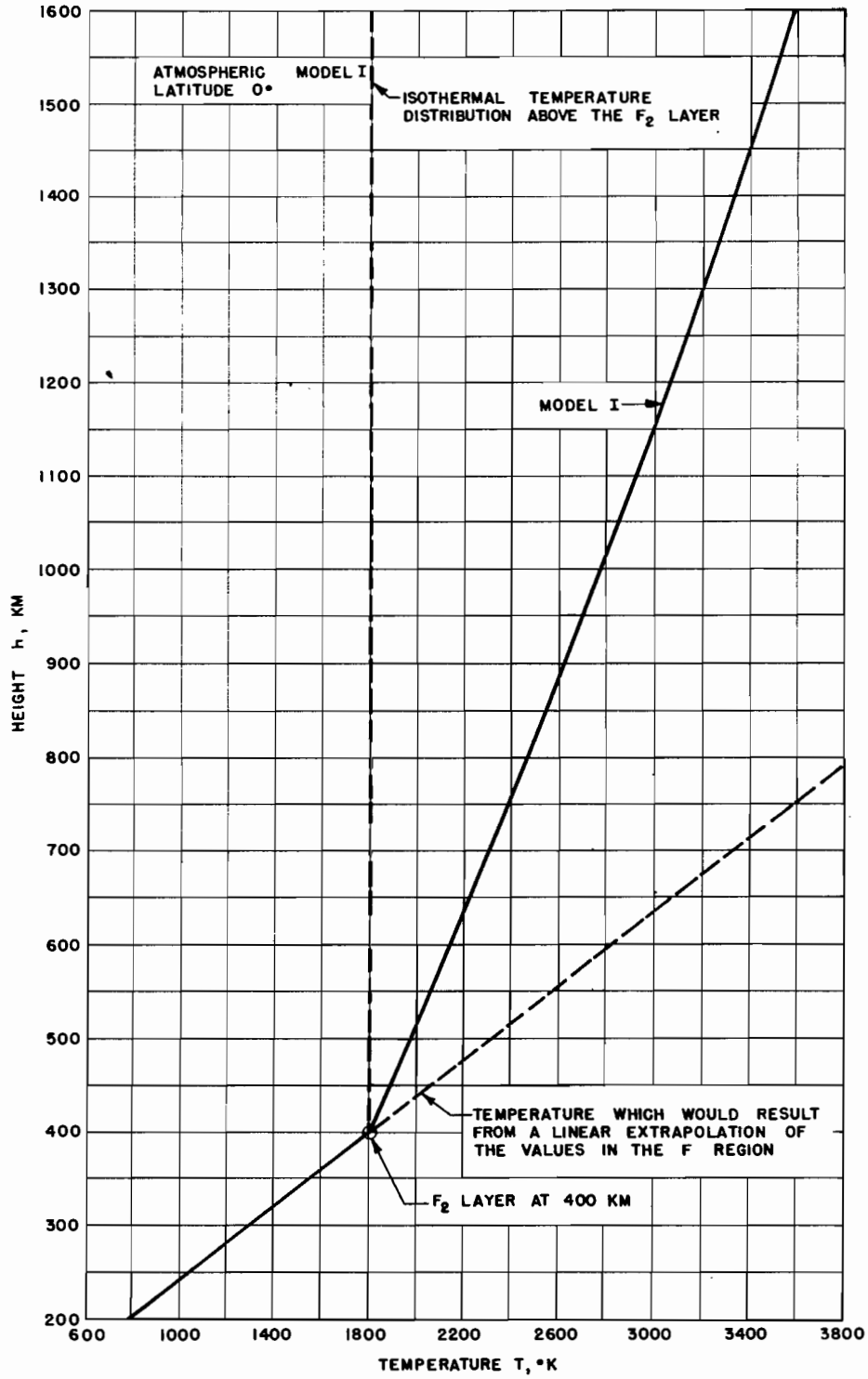

ADOPTED VALUES OF TEMPERATURE FOR ATMOSPHERIC MODEL I FROM THE F_2 LAYER UP TO 1600 KM. LATITUDE 0°. METRIC UNITS.

FIG. 20

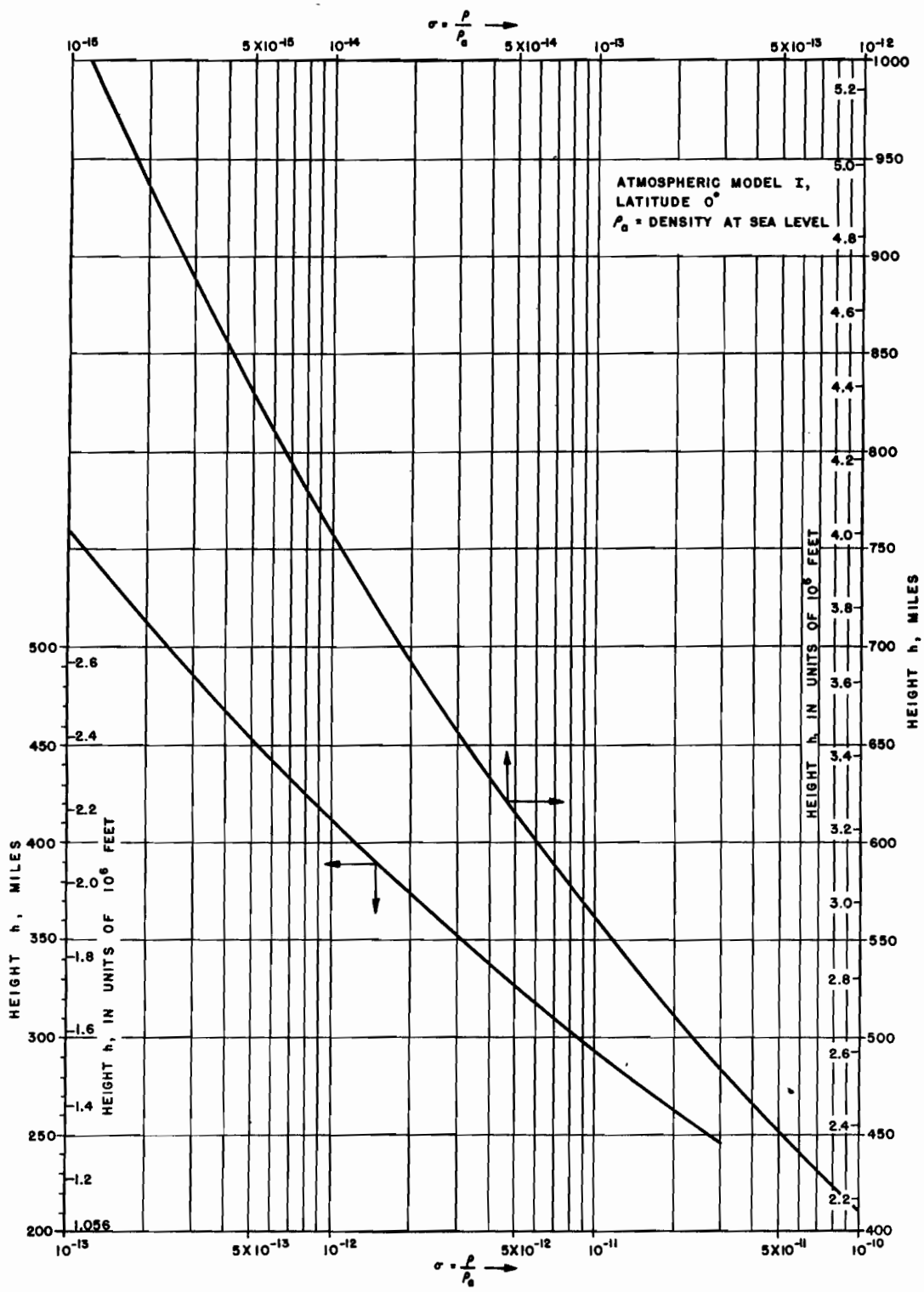

ADOPTED VALUES OF THE DENSITY RATIO σ FOR ATMOSPHERIC MODEL I FROM THE F_2 LAYER UP TO 1000 MILES. LATITUDE 0°. ENGINEERING UNITS.

FIG. 21

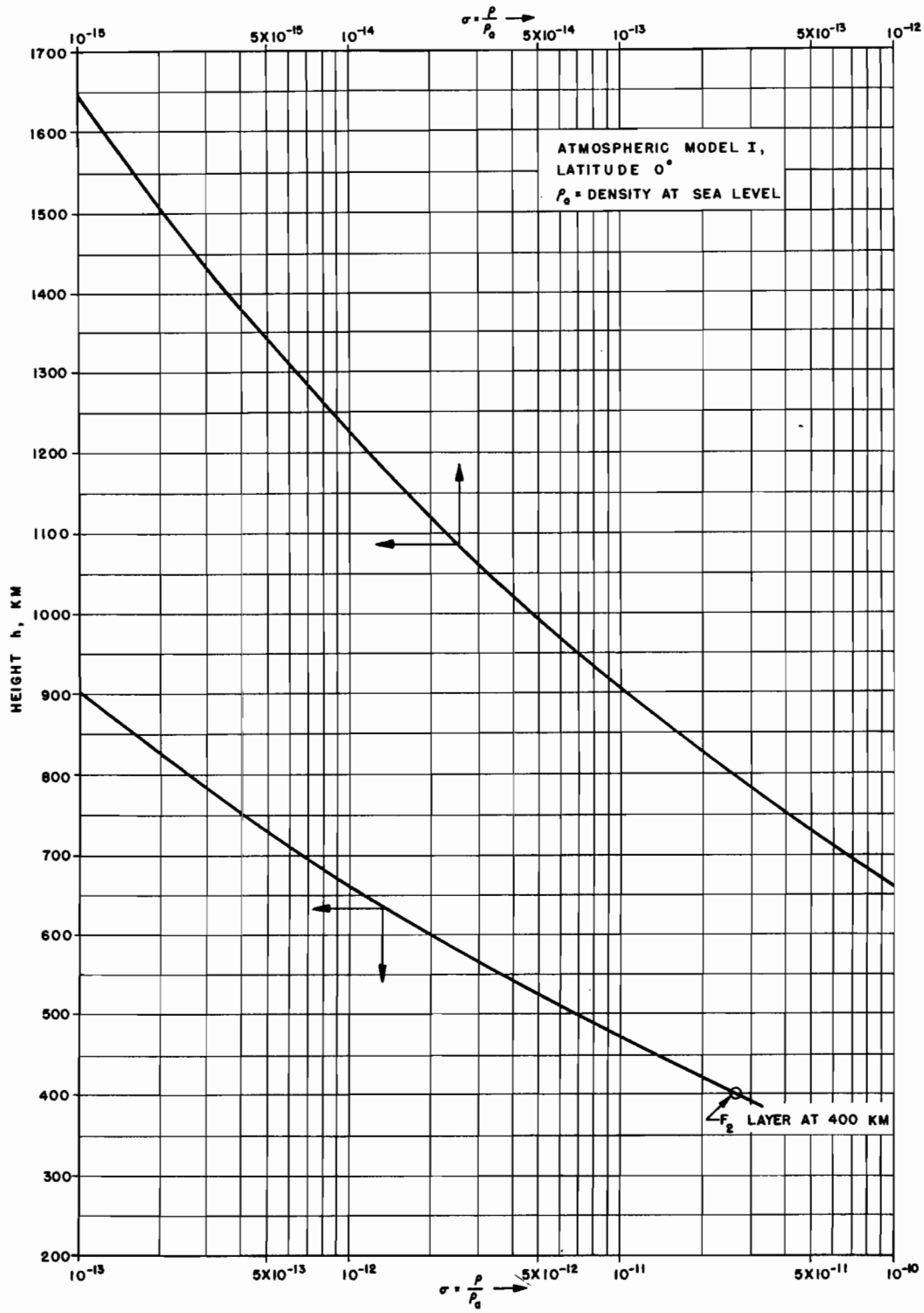

ADOPTED VALUES OF THE DENSITY RATIO σ FOR ATMOSPHERIC MODEL I FROM THE F_2 LAYER UP TO 1600 KM. LATITUDE 0°. METRIC UNITS.

FIG. 22

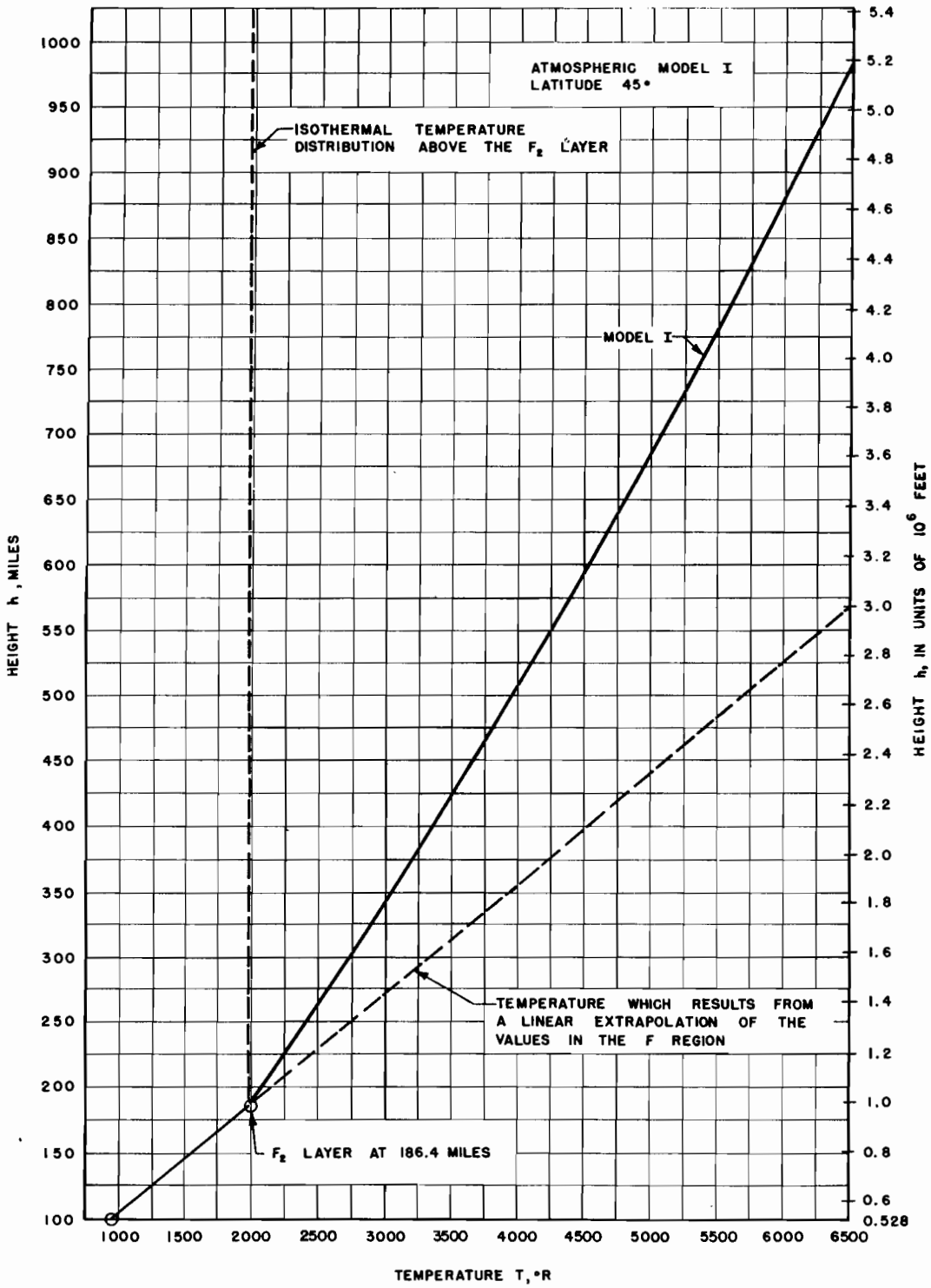

ADOPTED VALUES OF TEMPERATURE FOR ATMOSPHERIC MODEL I FROM THE F_2 LAYER UP TO 1000 MILES. LATITUDE 45°. ENGINEERING UNITS.

FIG. 23

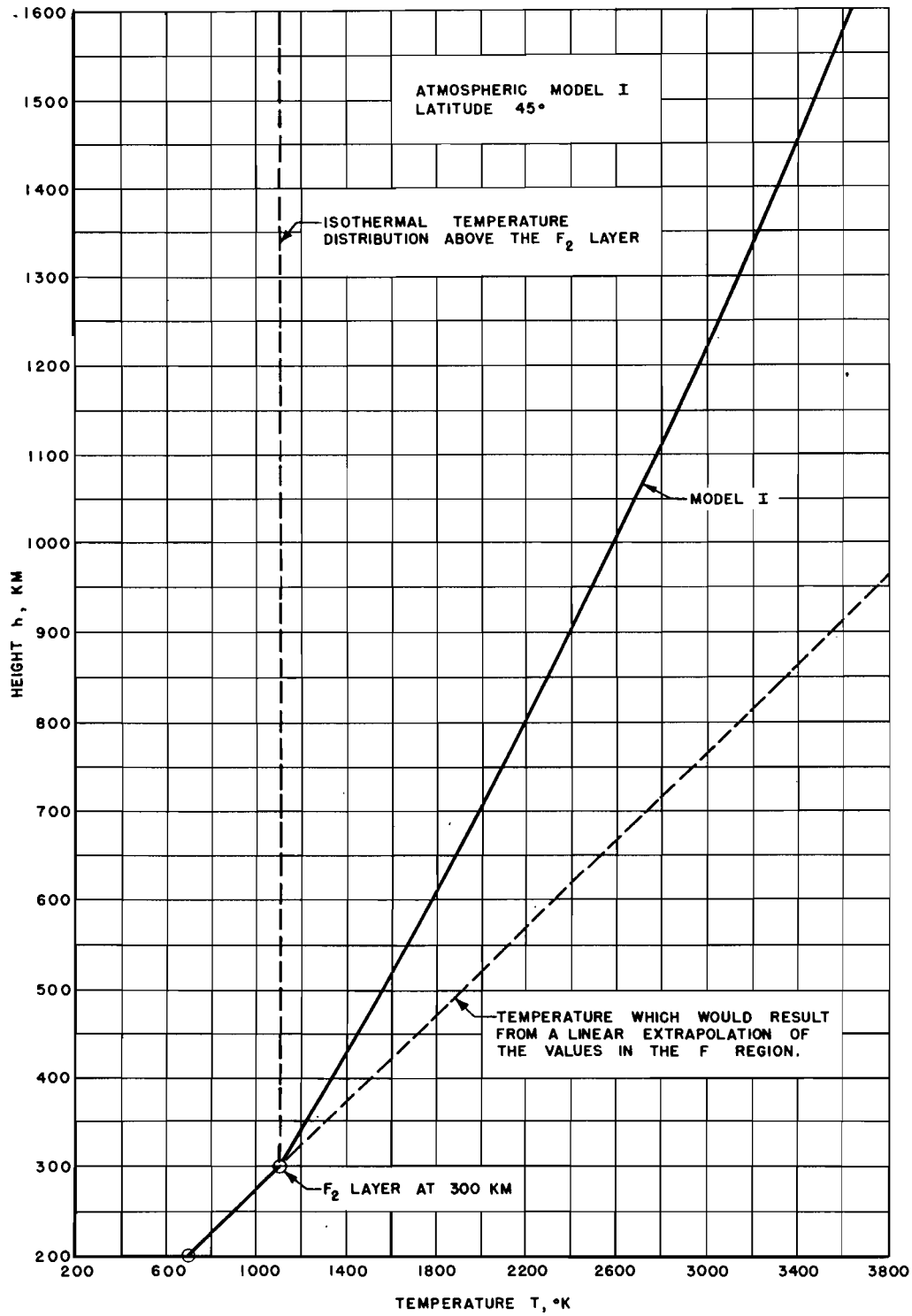

ADOPTED VALUES OF TEMPERATURE FOR ATMOSPHERIC MODEL I FROM THE F_2 LAYER UP TO 1600 KM. LATITUDE 45°. METRIC UNITS.

FIG. 24

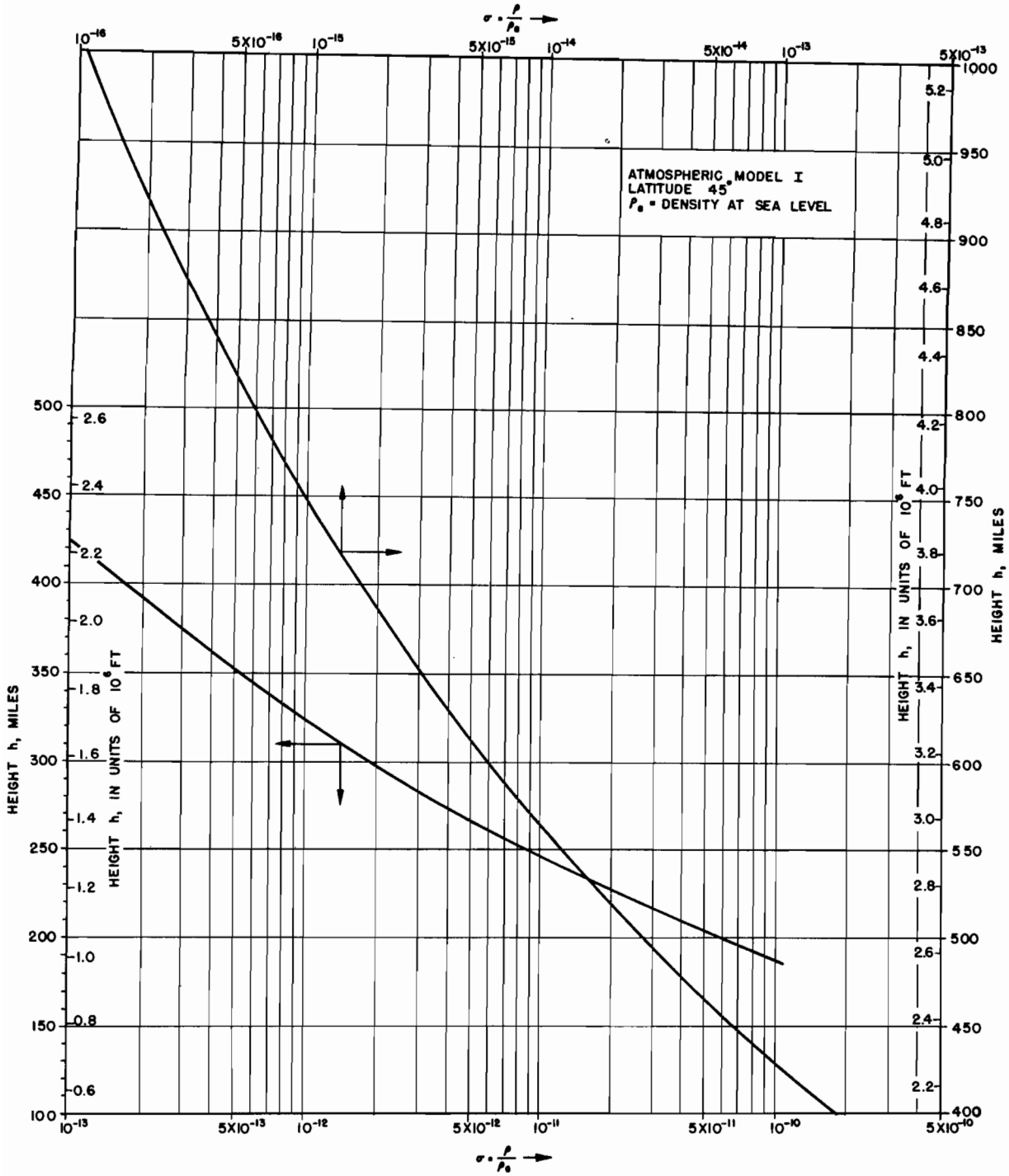

ADOPTED VALUES OF THE DENSITY RATIO σ FOR ATMOSPHERIC MODEL I FROM THE F_2 - LAYER UP TO 1000 MILES. LATITUDE 45 ENGINEERING UNITS.

FIG. 25

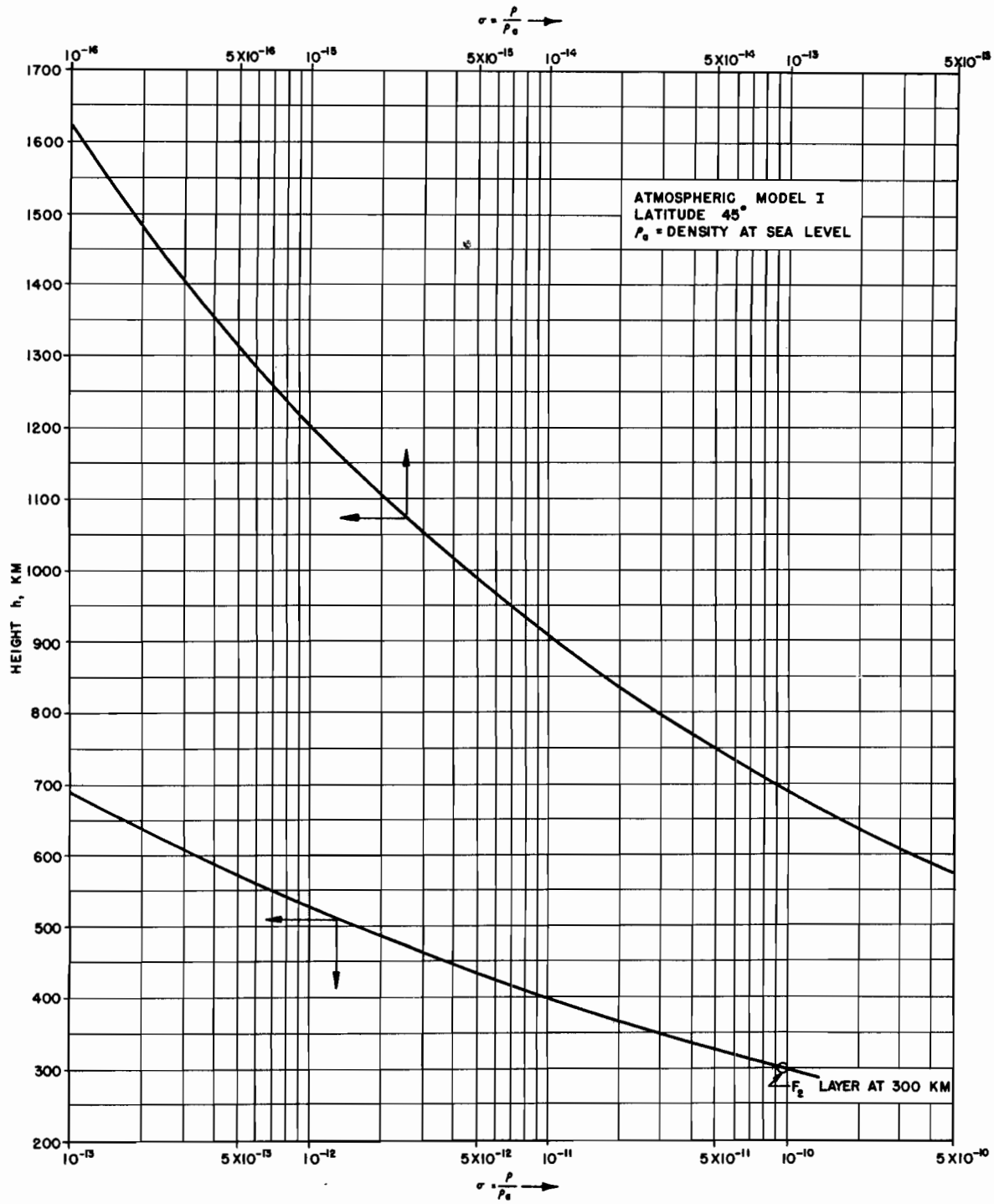

ADOPTED VALUES OF THE DENSITY RATIO σ FOR ATMOSPHERIC MODEL I FROM THE F_2 LAYER UP TO 1600 KM. LATITUDE 45° METRIC UNITS.

FIG. 26

II-F. THE CALCULATIONS FOR ATMOSPHERIC MODEL II

There is no doubt that many objections may be raised concerning the use of atmospheric model I as a representation of conditions existing in the atmosphere, and it was originally conceived only as a means for extrapolating beyond the F_2 layer up to heights of the order of 500 to 1000 miles. It may be more acceptable from many points of view to treat the atmosphere beginning somewhere above the F_2 layer on the basis of the existence of a dynamical orbit region composed of particles moving essentially in free flight in a gravity field, as conceived by Bryan[55] and Milne[56]. This concept, which was discussed to some extent in Section II-D, will be made the basis for atmospheric model II. Thus, according to this alternate concept designated as atmospheric model II, there will exist a certain height h_* situated somewhere above the F_2 layer, where the mean free path becomes so large and the collision frequency so small that the gas particles may be considered to behave more or less as free bodies in a gravity field. A particle moving upward from h_* would find so few particles above it that if it had sufficient velocity [the escape velocity, Eq. (38)], it could escape from the earth entirely with but little chance of having a collision with another particle. The height h_* will therefore be defined by the condition that there is but small probability of collision for a particle moving upward from this height with the escape velocity, that is, for a particle moving through the remainder of the atmosphere above h_*.

In model II it is assumed that the interstellar gas has no effect upon the atmosphere, and that the dynamical orbit region is isothermal. Reasons for assuming the isothermal property are given by Spitzer[61], where it is pointed out that the kinetic energy (kinetic temperature) of a particle is increased whenever a molecule is dissociated by the absorption of radiation or whenever an atom is photo-ionized. Kinetic energy is lost by the reverse processes and also by inelastic collisions between electrons, atoms, and molecules. Since, by definition, there is little probability of collision in the dynamical orbit region, it is concluded that there can be no temperature change resulting from collisions. Also, by comparing the small time of flight of a particle in the dynamical orbit region with the large time interval required for radiation to affect the temperature, Spitzer concludes that radiation effects are unimportant, and that this region of the atmosphere must be isothermal. The main problem in the analysis of atmospheric model II is the determination of the height h_* at which the dynamical orbit, or free-flight region, may be supposed to begin[†], and the temperature T_* of this isothermal region.

In order to determine the height h_*, it is first necessary to specify the probability that an upward-moving atmospheric gas particle will have a collision in the course of its flight with some other such particle. The only criterion that we have here is that the collision probability must be small (compared to 1), but otherwise the choice is quite arbitrary. Let this probability be denoted by P. In a Maxwellian gas the collision rate or frequency ν, as determined by the relation

$$\nu = \sqrt{2}\,\pi\, n\, v\, d^2 ,$$

[†] The writer is indebted to Dr. Lyman Spitzer, Jr., for valuable discussions concerning this region of the atmosphere.

may also be thought of as the probability per second that a particular particle will undergo a collision, and from this point of view could be called the collision probability per unit time (Ref. 57, pp. 99, 100, 113). Letting t be the time required for a particle moving upward from h_* to reach the top of its trajectory, which is assumed to be at a great distance (i.e., infinity), the probability P that the particle will undergo a collision in its upward travel may be expressed by

$$P = \int_0^t \nu \, dt = \sqrt{2}\,\pi\, d^2 \int_0^t n\, v\, dt = \sqrt{2}\,\pi\, d^2 \int_{h_*}^{\infty} n\, dh \,, \tag{52}$$

since $v = dh/dt$. Since n is the number of particles per cm^3, the integral is simply the total number of particles above the level h_* contained in a column of 1 cm^2 cross section. Indicating this number by N_*, it follows that

$$N_* = \frac{P}{\sqrt{2}\,\pi\, d^2} \,. \tag{53}$$

Using in this region a mean value $d = 2 \times 10^{-8}$ cm, which corresponds to a collision cross section $S = \pi\, d^2 = 12.6 \times 10^{-16}$ cm^2, the values obtained for N_* are tabulated below, Table 28, for several assumed values of the probability P.

Table 28

ATMOSPHERIC MODEL II. TOTAL NUMBER OF PARTICLES N_* TO GIVE THE COLLISION PROBABILITY P[1].

P	1/5	1/10	1/20	1/100	1/1000
N_*	1.13×10^{14}	5.64×10^{13}	2.08×10^{13}	5.64×10^{12}	5.64×10^{11}

[1] Based on $d = 2 \times 10^{-8}$ cm.

Before proceeding further it is necessary to introduce the concept of the scale-height H which was mentioned previously in connection with Eq. (1). This may be done by use of the Boltzmann distribution of particles in a gravitational field, see Eq. (42), or more directly by use of the hydrostatic equation $dp = -\rho\, g'\, dh$. Using $\rho = nm$ and $p = nkT$, it follows from the hydrostatic equation that

$$\frac{dp}{p} = -\frac{mg'}{kT}\, dh = -\frac{1}{H}\, dh \,, \tag{53a}$$

where m is the mean particle mass and $H = \frac{kT}{mg'}$. When m, T, and g' may be considered to remain constant in a given interval of h and have, for example, the values m_1, T_1, and g_1' appropriate to the initial height h_1, the equation may be integrated to give

$$p = p_1 e^{-\frac{(h-h_1)}{H_1}}, \tag{54}$$

where $H_1 = \frac{kT_1}{m_1 g_1'} \equiv \frac{R_u T_1}{M_1 g_1'}$. Since m_1 and T_1 are assumed to remain constant above the height h_1, it follows from (54) that

$$n = n_1 e^{-\frac{(h-h_1)}{H_1}}, \quad \text{and} \quad \rho = \rho_1 e^{-\frac{(h-h_1)}{H_1}}. \tag{55}$$

To interpret the meaning of H_1 it is pointed out that when $h - h_1 = H_1$, it follows that

$$p = \frac{p_1}{e}, \quad \rho = \frac{\rho_1}{e}, \quad \text{and} \quad n = \frac{n_1}{e},$$

showing that in the distance H_1 the atmospheric values decrease to $1/e$ of their values at the height h_1. The total number of particles N_1 above h_1 contained in a column of unit cross section may be obtained from Eq. (55) by the integration

$$N_1 = n_1 \int_{h_1}^{\infty} e^{-\frac{(h-h_1)}{H_1}} dh, \quad \text{or} \tag{56}$$

$$N_1 = n_1 H_1 . \tag{57}$$

The relation $N_1 = n_1 H_1$ points out a further interpretation of H_1 as the distance to which the atmosphere would extend above the height h_1 if the atmosphere in this region were homogeneous (i.e., constant temperature, density, and composition corresponding to the values at h_1).

Eqs. (55) and (56) were obtained by assuming a constant value of gravity ($g' = g_1'$ = const.) even though in Eq. (56) the upper limit of integration extended to infinity. The question may be asked, how serious is the assumption of constant gravity as far as the determination of the value for h_* is concerned. Actually it would not be necessary to integrate to infinity in Eq. (56) or in Eq. (52), but only to an upper limit h_u such that most of the particles contained in a unit column would be included in the integration. Since the number density decreases approximately in a logarithmic fashion, this upper limit does not have to be so very large. This may be seen from the following considerations.

Since the kinetic temperature of the equatorial atmosphere at the height h_* will be of the order of 2000°K, the mean speed of the particles at this height, Eq. (21), will be of the order of $v_* = 1.5 \times 10^5$ cm/sec (based on $M_* = 20$). Accordingly, as far as the particles having the mean speed are concerned, it follows from the relation $\Delta v = \sqrt{2g\Delta h} = 1.5 \times 10^5$ that these particles would be able to rise only about 130 km above h_* before they are pulled back again by the action of gravity. Taking a speed of $3 \times 1.5 \times 10^5$ cm/sec, which is certainly large enough to include practically all of the particles of a Maxwellian distribution at 2000°K, it is found that particles having this speed at h_* are able to rise about 1200 km above h_*. Hence, for all practical purposes, instead of infinity, the value $h_u = h_1 + 1200$ km could be used for the upper limit in (52) and (56). Over this range in height the variation in gravity is about 25 per cent, which is considered negligible in view of the approximate method used for the determination of h_*. Although it is possible to take the variation of gravity into account, by using the potential function as is done below in calculating the pressure, this refinement is hardly justified as far as the determination of h_* is concerned.

The relation (57) when used in conjunction with relation (53) makes it possible to determine the value of h_*. To do this it is necessary to have values for H and n for heights immediately above the F_2 layer. These could be obtained, for example, by assuming constant temperature above the F_2 layer, or by extrapolating the linear distribution of temperature existing in the F region. This represents two possible extremes. However, it is considered more satisfactory to use the results obtained for atmospheric model I in this region, since these values are intermediate between the two extreme possibilities mentioned. Using values for h_1, M_1, T_1, g_1', and n_1 from Table 24 for the equatorial atmosphere, the values obtained for H_1 and N_1 are shown in Table 29; a plot of N_1 as a function of h_1 is given in Fig.27 (p.92). Corresponding values for H_1, and N_1, at Latitude 45° are found in Table 31a (p.94).

The determination of h_* is based upon the fact that when the value of $N_1 = f(h_1)$, Fig. 27, is equal to the value of N_* given by Eq. (53), see Table 28, the condition is such that $h_* = h_1$, and h_* is thus determined from Fig. 27. Using Fig. 27 in this way ($h_* = h_1$ when $N_1 = N_*$), the heights h_* corresponding to the different probabilities P have the values given in Table 30. Depending upon the value of P, it is seen that h_* may have values ranging from 800 to 1800 km. To specify h_* more definitely, it will be assumed that $P = 1/10$ is a sufficiently small collision probability[5] to satisfy the conditions for h_*, and the value $h_* = 865$ km (537 miles) is therefore adopted. Making use of Table 24, the conditions found at this height in the equatorial atmosphere are as given in Table 31. The value of g_*' is derived on the basis that the atmosphere rotates with the earth as a solid up to the height h_*. It differs only slightly from the value g' contained in Table 24 .

It is worth noting that since the effective diameter d of the gas particles occurs to the second power in Eq. (53), the value derived for the height h_* will depend rather strongly upon the value used for d. If $d = 3 \times 10^{-8}$ cm were used, for example, the resulting value for h_* would be 980 for $P = 1/10$. Thus an increase in d from 2×10^{-8} to 3×10^{-8} cm causes an increase in h_* of about 100 km. It is apparent from Eq. (53) that as far as the determination of h_* is concerned, an increase in d (or the collision cross section S) has the same effect as a decrease in the collision

[5] See Section III-B, where the collision probability is specified with less ambiguity.

probability P. Accordingly, the value $h_* = 865$ km will remain unchanged for variations in P and d provided these variations are such as to give the constant value $1/10 / \pi \times 4 \times 10^{-16} = 7.97 \times 10^{13}$ for the ratio $P/\pi d^2$ or P/S, where S is the collision cross section.

Following the same procedure used for the equatorial atmosphere, the values for the atmosphere at latitude 45° are obtained as shown in Fig. 28 and Table 32. Corresponding to $P = 1/10$, the value $h_* = 630$ km (391 miles) is adopted. Making use of Table 27, the atmospheric conditions given in Table 33 are found for the height h_* at latitude 45°.

Having decided upon an appropriate value for h_*, the calculation then proceeds on the basis of an isothermal atmosphere in static equilibrium. As pointed out in Section II-D, even in this outer (dynamic orbit) region of the atmosphere, if conditions are isothermal the density will be distributed according to the Boltzmann law, which gives a result identical with that of static equilibrium. Since variations in the acceleration of gravity and the centrifugal force will be taken into account in the calculation of the pressure, it will not be permissible to use the approximate formula (54) but rather the hydrostatic equation will be used in the form, Eq. (46),

$$d \log p = -\frac{M_*}{R_u T_*} d\phi \equiv -\frac{1}{H_* g_*'} d\phi , \tag{58}$$

where $H_* = R_u T_* / M_* g_*'$ and where it is assumed that the composition and temperature remain constant above h_* with the values M_* and T_* respectively. Defining the potential function so that $\phi = 0$ when $r = r_*$ the integration gives

$$p = p_* e^{-\frac{M_*}{R_u T_*} \phi} \equiv p_* e^{-\frac{\phi}{H_* g_*'}} . \tag{59}$$

From Eq. (28) with $\phi = 0$ when $r = r_*$, it follows that

$$\phi = g_a a^2 \left(\frac{1}{r_*} - \frac{1}{r} \right) - \cos^2 \theta \int_{r_*}^{r} r \omega^2 (r) \, dr . \tag{60}$$

It will be assumed that the atmosphere out to the distance r_* rotates with the earth as a solid with angular velocity Ω. In the dynamic orbit region where the particles are considered to be more or less in free flight, they will move under the condition of constant angular momentum such that $r^2 \omega (r) =$ constant. Since $r^2 \omega = r_*^2 \Omega$ at the distance r_*, the angular velocity ω must satisfy the relation

$$\omega = \left(\frac{r_*}{r} \right)^2 \Omega , \tag{61}$$

which, when introduced into (60), results in the expression

$$\phi = g_a a^2 \left(\frac{1}{r_*} - \frac{1}{r}\right) - \frac{1}{2} r_*^4 \Omega^2 \left(\frac{1}{r_*^2} - \frac{1}{r^2}\right) \cos^2\theta \ . \tag{62}$$

For computing, it is more convenient to write this in the form

$$\phi = g_a \frac{a^2}{r_*} \frac{1}{\frac{r}{r_*}} \left(\frac{r}{r_*} - 1\right) - \frac{1}{2} r_*^2 \Omega^2 \left[1 - \left(\frac{r_*}{r}\right)^2\right] \cos^2\theta \ . \tag{63}$$

Thus, the pressure is computed from Eq. (59), using ϕ as given by (63). The density is then computed as usual from the equation of state, (16). Using $h_* = 865$ km (537 miles) and the values of Table 31 for the equatorial atmosphere, and $h_* = 630$ km (391 miles) and the values of Table 33 for the atmosphere at latitude 45°, the computations give the results shown in Tables 34 to 37.

It will be recalled that in determining the value for h_*, it was assumed that the conditions existing in the region between the F_2 layer and the height h_* were those corresponding to atmospheric model I with $M_L = 7$, Tables 24 and 27. For completeness, the values in this range are repeated in Tables 34 to 37. The variation of the density ratio σ from the height h_* up to 1000 miles is shown in Figs. 29 to 32.

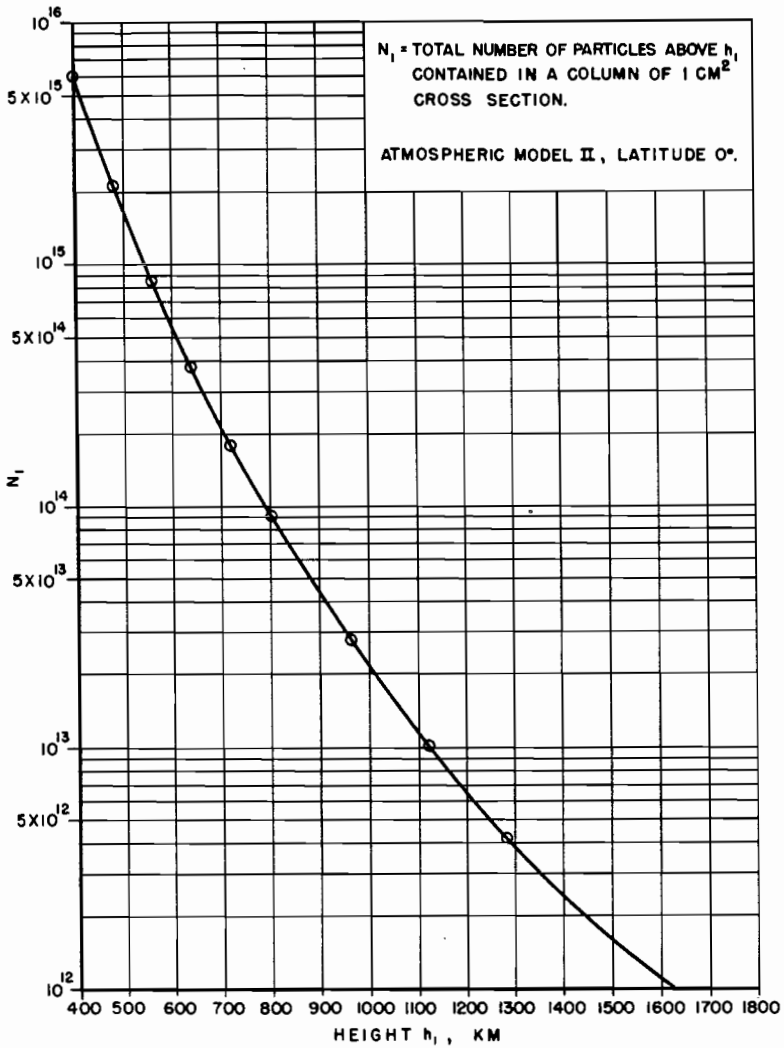

TOTAL NUMBER OF PARTICLES ABOVE THE HEIGHT h_1 CONTAINED IN A COLUMN OF UNIT CROSS SECTION. LATITUDE 0°. ATMOSPHERIC MODEL II.

FIG. 27

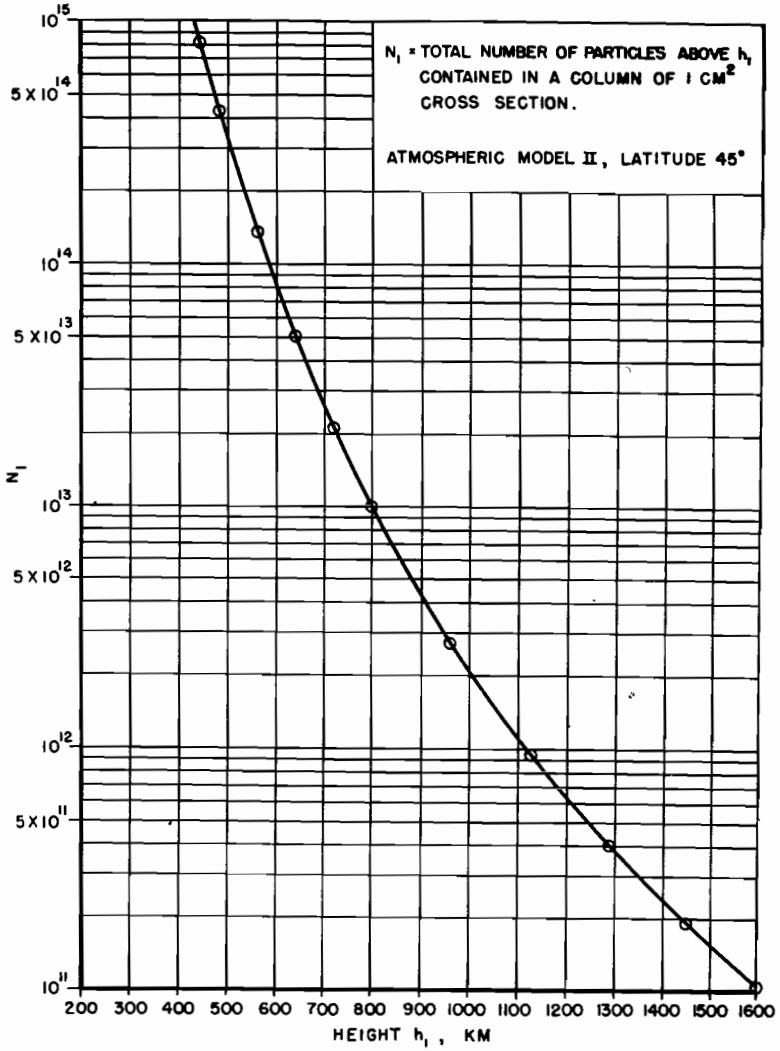

TOTAL NUMBER OF PARTICLES ABOVE THE HEIGHT h_1 CONTAINED IN A COLUMN OF UNIT CROSS SECTION. LATITUDE 45°. ATMOSPHERIC MODEL II.

FIG. 28

Table 29

ATMOSPHERIC MODEL II. LATITUDE 0°.

TOTAL NUMBER OF PARTICLES N_1 ABOVE THE HEIGHT h_1

CONTAINED IN A COLUMN OF 1 CM^2 CROSS SECTION.

h_1, km	400	483	563	644	724	805	966	1287
H_1, km	72.1	80.7	89.4	98.5	108.0	117.9	138.6	184.6
n_1, $1/cm^3$	8.40×10^8	2.62×10^8	9.53×10^7	3.81×10^7	1.64×10^7	7.63×10^6	1.97×10^6	2.26×10^5
N_1	6.05×10^{15}	2.11×10^{15}	8.52×10^{14}	3.75×10^{14}	1.77×10^{14}	8.99×10^{13}	2.72×10^{13}	4.17×10^{12}

Table 30

ATMOSPHERIC MODEL II. LATITUDE 0°.

Values of the height h_* as a function of the probability P[1].

P	1/5	1/10	1/20	1/100
N_*	1.13×10^{14}	5.64×10^{13}	2.82×10^{13}	5.64×10^{12}
h_*, km	780	865	960	1225

[1] Based on Eq. (53), Fig. 27, and $d = 2 \times 10^{-8}$ cm.

Table 31

ATMOSPHERIC MODEL II. LATITUDE 0°.

Conditions at the height $h_* = 865$ km (537 miles).

g'_*	M_*	T_*	p_*	ρ_*	n_*	L_*	v_*	ν_*
757.2 cm/sec^2	22.42	2563°K	1.18×10^{-9} mm of Hg	1.66×10^{-16} gram/cm^3	4.48×10^{6} 1/cm^3	2.23×10^{8} cm	1.55×10^{5} cm/sec	6.97×10^{-4} 1/sec
24.84 ft/sec^2	22.42	4613°R	3.30×10^{-9} lb/ft^2	3.23×10^{-16} slug/ft^3	1.27×10^{11} 1/ft^3	7.32×10^{6} ft	5.10×10^{3} ft/sec	6.97×10^{-4} 1/sec

Table 31a

ATMOSPHERIC MODEL II. LATITUDE 45°.

TOTAL NUMBER OF PARTICLES N_1 ABOVE THE HEIGHT h_1 CONTAINED IN A COLUMN OF 1 cm^2 CROSS SECTION.

h_1, km	300	322	402	483	563	644	724	805	966	1127
H_1 km	42.0	44.3	53.3	62.6	72.4	82.6	93.3	104.4	128.2	153.9
n_1, 1/cm^2	5.38×10^{9}	3.10×10^{9}	5.14×10^{8}	1.13×10^{8}	3.07×10^{7}	9.87×10^{6}	3.63×10^{6}	1.49×10^{6}	3.24×10^{5}	9.22×10^{4}
N_1	2.26×10^{16}	1.38×10^{16}	2.74×10^{15}	7.07×10^{14}	2.22×10^{14}	8.15×10^{13}	3.38×10^{13}	1.55×10^{13}	4.16×10^{12}	1.42×10^{12}

Table 32

ATMOSPHERIC MODEL II. LATITUDE 45°.

Values of height h_* as a function of the probability $P^{(1)}$.

P	1/5	1/10	1/20	1/100	1/1000
N_*	1.13×10^{14}	5.64×10^{13}	2.82×10^{13}	5.64×10^{12}	5.64×10^{11}
h_*, km	575	630	695	870	1220

(1) Based on Eq. (53), Fig. 28, and $d = 2 \times 10^{-8}$ cm.

Table 33

ATMOSPHERIC MODEL II. LATITUDE 45°.

Conditions at the height $h_* = 630$ km (391 miles).

g'_*	M_*	T_*	p_*	ρ_*	n_*	L_*	v_*	ν_*
810.28 cm/sec^2	22.92	1833°K	1.37×10^{-9} mm of Hg	2.75×10^{-16} gram/cm^3	7.27×10^{6} 1/cm^3	1.37×10^{8} cm	1.30×10^{5} cm/sec	9.46×10^{-4} 1/sec
26.584 ft/sec^2	22.92	3299°R	3.82×10^{-9} lb/ft^2	5.34×10^{-16} slug/ft^3	2.06×10^{11} 1/ft^3	4.51×10^{6} ft	4.27×10^{3} ft/sec	9.46×10^{-4} 1/sec

Table 34

ATMOSPHERIC MODEL II - VALUES OF TEMPERATURE, PRESSURE, AND DENSITY ABOVE THE F_2 LAYER

Latitude 0°. Engineering Units. p_a = 2115 lb/ft², ρ_a = 2.286 × 10⁻³ slug/ft³

Height h		Potential ϕ	Apparent Gravity g'	Mean Mol Wt M	Temp T	Scale Height H	Pressure p	Pressure Ratio p/p_a	Density ρ	Density Ratio σ ρ/ρ_a	Number Density n	Mean Particle Speed $\bar{v}$	$d = 3 \times 10^{-8}$ cm		$d = 2 \times 10^{-8}$ cm	
													Mean Free Path L	Mean Collision Freq ν	Mean Free Path L	Mean Collision Freq ν
mi	ft	ft-lb	ft/sec²		°R	ft	lb/ft²		slug/ft³		particles/ft³	ft/sec	ft	1/sec	ft	1/sec
248.6	1.312×10^6		28.393	24.00	3240	2.362×10^5	4.33×10^{-7}	2.05×10^{-10}	6.46×10^{-18}	2.83×10^{-11}	2.38×10^{12}	4.13×10^3	9.77×10^3	4.23×10^{-1}	2.20×10^4	1.88×10^{-1}
300	1.584×10^6		27.707	23.70	3498	2.646×10^5	1.46×10^{-7}	6.90×10^{-11}	1.99×10^{-14}	8.71×10^{-12}	7.43×10^{12}	4.32×10^3	3.13×10^4	1.38×10^{-1}	7.04×10^4	6.14×10^{-2}
350	1.848×10^6		27.064	23.42	3743	2.934×10^5	5.67×10^{-8}	2.68×10^{-11}	7.14×10^{-15}	3.12×10^{-12}	2.70×10^{12}	4.50×10^3	8.61×10^4	5.03×10^{-2}	1.94×10^5	2.23×10^{-2}
400	2.112×10^6		26.444	23.14	3983	3.234×10^5	2.41×10^{-8}	1.14×10^{-11}	2.82×10^{-15}	1.23×10^{-12}	1.08×10^{12}	4.67×10^3	2.15×10^5	2.17×10^{-2}	4.84×10^5	9.64×10^{-3}
450	2.376×10^6		25.844	22.87	4217	3.544×10^5	1.10×10^{-8}	5.20×10^{-12}	1.20×10^{-15}	5.25×10^{-13}	4.64×10^{11}	4.83×10^3	5.01×10^5	9.64×10^{-3}	1.13×10^6	4.28×10^{-3}
500	2.640×10^6		25.264	22.61	4447	3.867×10^5	5.40×10^{-9}	2.55×10^{-12}	5.53×10^{-16}	2.42×10^{-13}	2.16×10^{11}	4.99×10^3	1.08×10^6	4.64×10^{-3}	2.42×10^6	2.06×10^{-3}
537	2.835×10^6	0.000	24.847	22.42	4613	4.114×10^5	3.30×10^{-9}	1.56×10^{-12}	3.23×10^{-16}	1.41×10^{-13}	1.27×10^{11}	5.10×10^3	1.83×10^6	2.79×10^{-3}	4.12×10^6	1.24×10^{-3}
550	2.904×10^6	1.61×10^6	24.704	22.42	4613	4.137×10^5	2.82×10^{-9}	1.33×10^{-12}	2.76×10^{-16}	1.21×10^{-13}	1.09×10^{11}	5.10×10^3	2.13×10^6	2.39×10^{-3}	4.80×10^6	1.06×10^{-3}
600	3.168×10^6	8.06×10^6	24.167	22.42	4613	4.229×10^5	1.50×10^{-9}	7.09×10^{-13}	1.47×10^{-16}	6.43×10^{-14}	5.80×10^{10}	5.10×10^3	4.01×10^6	1.27×10^{-3}	9.02×10^6	5.66×10^{-4}
650	3.432×10^6	1.44×10^7	23.648	22.42	4613	4.322×10^5	8.07×10^{-10}	3.82×10^{-13}	7.90×10^{-17}	3.46×10^{-14}	3.12×10^{10}	5.10×10^3	7.45×10^6	6.85×10^{-4}	1.68×10^7	3.04×10^{-4}
700	3.696×10^6	2.06×10^7	23.144	22.42	4613	4.416×10^5	4.40×10^{-10}	2.08×10^{-13}	4.30×10^{-17}	1.88×10^{-14}	1.70×10^{10}	5.10×10^3	1.37×10^7	3.73×10^{-4}	3.08×10^7	1.66×10^{-4}
750	3.960×10^6	2.66×10^7	22.657	22.42	4613	4.511×10^5	2.45×10^{-10}	1.16×10^{-13}	2.40×10^{-17}	1.05×10^{-14}	9.47×10^9	5.10×10^3	2.45×10^7	2.08×10^{-4}	5.52×10^7	9.23×10^{-5}
800	4.224×10^6	3.25×10^7	22.185	22.42	4613	4.607×10^5	1.37×10^{-10}	6.48×10^{-14}	1.34×10^{-17}	5.86×10^{-15}	5.29×10^9	5.10×10^3	4.39×10^7	1.16×10^{-4}	9.89×10^7	5.16×10^{-5}
900	4.752×10^6	4.40×10^7	21.284	22.42	4613	4.802×10^5	4.46×10^{-11}	2.11×10^{-14}	4.36×10^{-18}	1.91×10^{-15}	1.72×10^9	5.10×10^3	1.35×10^8	3.77×10^{-5}	3.04×10^8	1.68×10^{-5}
1000	5.280×10^6	5.50×10^7	20.437	22.42	4613	5.001×10^5	1.52×10^{-11}	7.19×10^{-15}	1.49×10^{-18}	6.52×10^{-16}	5.88×10^8	5.10×10^3	3.95×10^8	1.29×10^{-5}	8.90×10^8	5.73×10^{-6}
1200	6.339×10^6	7.58×10^7	18.888	22.42	4613	5.411×10^5	1.99×10^{-12}	9.41×10^{-16}	1.95×10^{-19}	8.53×10^{-17}	7.70×10^7	5.10×10^3	3.02×10^9	1.69×10^{-6}	6.79×10^9	7.51×10^{-7}
1400	7.392×10^6	9.50×10^7	17.509	22.42	4613	5.838×10^5	3.03×10^{-13}	1.43×10^{-16}	2.96×10^{-20}	1.29×10^{-17}	1.17×10^7	5.10×10^3	1.99×10^{10}	2.57×10^{-7}	4.47×10^{10}	1.14×10^{-7}
1500	7.920×10^6	1.04×10^8	17.151	22.42	4613	5.959×10^5	1.26×10^{-13}	5.96×10^{-17}	1.23×10^{-20}	5.38×10^{-18}	4.85×10^6	5.10×10^3	4.79×10^{10}	1.06×10^{-7}	1.08×10^{11}	4.73×10^{-8}
1750	9.240×10^6	1.25×10^8	15.433	22.42	4613	6.623×10^5	1.61×10^{-14}	7.61×10^{-18}	1.58×10^{-21}	6.91×10^{-19}	6.24×10^5	5.10×10^3	3.73×10^{11}	1.37×10^{-8}	8.38×10^{11}	6.08×10^{-9}
2000	1.056×10^7	1.45×10^8	14.169	22.42	4613	7.214×10^5	2.28×10^{-15}	1.08×10^{-18}	2.23×10^{-22}	9.75×10^{-20}	8.80×10^4	5.10×10^3	2.64×10^{12}	1.93×10^{-9}	5.94×10^{12}	8.58×10^{-10}
2500	1.320×10^7	1.79×10^8	12.065	22.42	4613	8.472×10^5	8.18×10^{-17}	3.87×10^{-20}	8.00×10^{-24}	3.50×10^{-21}	3.16×10^3	5.10×10^3	7.36×10^{12}	6.93×10^{-11}	1.66×10^{14}	3.08×10^{-11}
3000	1.584×10^7	2.09×10^8	10.397	22.42	4613	9.831×10^5	4.35×10^{-18}	2.06×10^{-21}	4.26×10^{-25}	1.86×10^{-22}	1.68×10^2	5.10×10^3	1.38×10^{15}	3.69×10^{-12}	3.11×10^{15}	1.64×10^{-12}
4000	2.112×10^7	2.569×10^8	7.953	22.42	4613	1.285×10^6	4.01×10^{-20}	1.90×10^{-23}	3.92×10^{-27}	1.71×10^{-24}	1.55	5.10×10^3	1.50×10^{17}	3.40×10^{-14}	3.37×10^{17}	1.51×10^{-14}
5000	2.640×10^7	2.943×10^8	6.279	22.42	4613	1.628×10^6	1.03×10^{-21}	4.87×10^{-25}	1.01×10^{-28}	4.46×10^{-26}	3.99×10^{-2}	5.10×10^3	5.83×10^{18}	8.75×10^{-16}	1.31×10^{19}	3.89×10^{-16}
6000	3.168×10^7	3.241×10^8	5.084	22.42	4613	2.011×10^6	5.59×10^{-22}	2.63×10^{-26}	5.47×10^{-30}	2.39×10^{-27}	2.16×10^{-3}	5.10×10^3	1.08×10^{20}	4.74×10^{-17}	2.42×10^{20}	2.11×10^{-17}
7000	3.696×10^7	3.485×10^8	4.199	22.42	4613	2.435×10^6	5.14×10^{-24}	2.43×10^{-27}	5.03×10^{-31}	2.20×10^{-28}	1.99×10^{-4}	5.10×10^3	1.17×10^{21}	4.37×10^{-18}	2.63×10^{21}	1.94×10^{-18}
8000	4.224×10^7	3.688×10^8	3.527	22.42	4613	2.898×10^6	7.05×10^{-25}	3.33×10^{-28}	6.90×10^{-32}	3.02×10^{-29}	2.72×10^{-5}	5.10×10^3	8.55×10^{21}	5.97×10^{-19}	1.92×10^{22}	2.65×10^{-19}
9000	4.752×10^7	3.860×10^8	3.004	22.42	4613	3.402×10^6	1.31×10^{-26}	6.19×10^{-29}	1.28×10^{-32}	5.60×10^{-30}	5.05×10^{-6}	5.10×10^3	4.60×10^{22}	1.11×10^{-19}	1.04×10^{23}	4.92×10^{-20}

1 lb/ft² = 0.3591 mm of Hg

Table 35

ATMOSPHERIC MODEL II - VALUES OF TEMPERATURE, PRESSURE, AND DENSITY ABOVE THE F_2 LAYER

Latitude 0°. Metric Units. p_a = 1013 mb, $\rho_a = 1.178 \times 10^{-3}$ gm/cm³

Height h km	Height h mi	Potential ϕ ergs	Apparent Gravity g' cm/sec	Mol Wt M	Temp T °K	Scale Height H km	Pressure p millibars	Pressure Ratio p/p_a	Density ρ gm/cm³	Density Ratio σ ρ/ρ_a	Number Density n particles/cm³	Mean Particle Speed v cm/sec	$d = 3 \times 10^{-8}$cm Mean Free Path L cm	$d = 3 \times 10^{-8}$cm Mean Collision Freq ν 1/sec	$d = 2 \times 10^{-8}$cm Mean Free Path L cm	$d = 2 \times 10^{-8}$cm Mean Collision Freq ν 1/sec
	248.6		865.41	24.00	1800	7.199×10	2.07×10^{-7}	2.05×10^{-10}	3.33×10^{-14}	2.83×10^{-11}	8.40×10^{6}	1.26×10^{5}	2.98×10^{5}	4.23×10^{-1}	6.70×10^{5}	1.88×10^{-1}
483	300		844.52	23.70	1943	8.066×10	6.99×10^{-8}	6.90×10^{-11}	1.02×10^{-14}	8.71×10^{-12}	2.62×10^{6}	1.32×10^{5}	9.54×10^{5}	1.38×10^{-1}	2.15×10^{6}	6.14×10^{-2}
563	350		824.92	23.42	2079	8.941×10	2.72×10^{-8}	2.68×10^{-11}	3.68×10^{-15}	3.12×10^{-12}	9.54×10^{7}	1.37×10^{5}	2.62×10^{6}	5.03×10^{-2}	5.90×10^{6}	2.23×10^{-2}
644	400		806.00	23.14	2213	9.856×10	1.15×10^{-8}	1.14×10^{-11}	1.45×10^{-15}	1.23×10^{-12}	3.81×10^{7}	1.42×10^{5}	6.56×10^{6}	2.17×10^{-2}	1.48×10^{7}	9.64×10^{-3}
724	450		787.71	22.87	2343	1.080×10^{2}	5.27×10^{-9}	5.20×10^{-12}	6.18×10^{-16}	5.25×10^{-13}	1.64×10^{7}	1.47×10^{5}	1.53×10^{7}	9.64×10^{-3}	3.44×10^{7}	4.28×10^{-3}
805	500		770.03	22.61	2471	1.179×10^{2}	2.59×10^{-9}	2.55×10^{-12}	2.85×10^{-16}	2.42×10^{-13}	7.63×10^{6}	1.52×10^{5}	3.28×10^{7}	4.64×10^{-3}	7.38×10^{7}	2.06×10^{-3}
865	537	0.000	757.34	22.42	2563	1.254×10^{2}	1.58×10^{-9}	1.56×10^{-12}	1.66×10^{-16}	1.41×10^{-13}	4.48×10^{6}	1.55×10^{5}	5.58×10^{7}	2.79×10^{-3}	1.26×10^{8}	1.24×10^{-3}
885	550	2.18×10^{13}	752.98	22.42	2563	1.261×10^{2}	1.35×10^{-9}	1.33×10^{-12}	1.42×10^{-16}	1.21×10^{-13}	3.85×10^{6}	1.55×10^{5}	6.50×10^{7}	2.39×10^{-3}	1.46×10^{8}	1.06×10^{-3}
966	600	1.09×10^{14}	736.62	22.42	2563	1.289×10^{2}	7.18×10^{-10}	7.09×10^{-13}	7.57×10^{-17}	6.43×10^{-14}	2.05×10^{6}	1.55×10^{5}	1.22×10^{8}	1.27×10^{-3}	2.75×10^{8}	5.66×10^{-4}
1046	650	1.95×10^{14}	720.78	22.42	2563	1.317×10^{2}	3.86×10^{-10}	3.82×10^{-13}	4.07×10^{-17}	3.46×10^{-14}	1.10×10^{6}	1.55×10^{5}	2.27×10^{8}	6.85×10^{-4}	5.11×10^{8}	3.04×10^{-4}
1127	700	2.79×10^{14}	705.44	22.42	2563	1.346×10^{2}	2.11×10^{-10}	2.08×10^{-13}	2.21×10^{-17}	1.88×10^{-14}	6.00×10^{5}	1.55×10^{5}	4.17×10^{8}	3.73×10^{-4}	9.38×10^{8}	1.66×10^{-4}
1207	750	3.61×10^{14}	690.59	22.42	2563	1.375×10^{2}	1.17×10^{-10}	1.16×10^{-13}	1.24×10^{-17}	1.05×10^{-14}	3.34×10^{5}	1.55×10^{5}	7.48×10^{8}	2.08×10^{-4}	1.68×10^{9}	9.23×10^{-5}
1288	800	4.41×10^{14}	676.20	22.42	2563	1.404×10^{2}	6.56×10^{-11}	6.48×10^{-14}	6.90×10^{-18}	5.86×10^{-15}	1.87×10^{5}	1.55×10^{5}	1.34×10^{9}	1.16×10^{-4}	3.01×10^{9}	5.16×10^{-5}
1448	900	5.97×10^{14}	648.74	22.42	2563	1.464×10^{2}	2.14×10^{-11}	2.11×10^{-14}	2.25×10^{-18}	1.91×10^{-15}	6.07×10^{4}	1.55×10^{5}	4.12×10^{9}	3.77×10^{-5}	9.27×10^{9}	1.68×10^{-5}
1609	1000	7.46×10^{14}	622.92	22.42	2563	1.524×10^{2}	7.28×10^{-12}	7.19×10^{-15}	7.67×10^{-19}	6.52×10^{-16}	2.08×10^{4}	1.55×10^{5}	1.21×10^{10}	1.29×10^{-5}	2.71×10^{10}	5.73×10^{-6}
1931	1200	1.03×10^{15}	575.70	22.42	2563	1.649×10^{2}	9.53×10^{-13}	9.41×10^{-16}	1.00×10^{-19}	8.53×10^{-17}	2.72×10^{3}	1.55×10^{5}	9.20×10^{10}	1.69×10^{-6}	2.07×10^{11}	7.51×10^{-7}
2253	1400	1.29×10^{15}	533.66	22.42	2563	1.779×10^{2}	1.45×10^{-13}	1.43×10^{-16}	1.52×10^{-20}	1.29×10^{-17}	4.13×10^{2}	1.55×10^{5}	6.06×10^{11}	2.57×10^{-7}	1.36×10^{12}	1.14×10^{-7}
2414	1500	1.41×10^{15}	522.77	22.42	2563	1.816×10^{2}	6.03×10^{-14}	5.96×10^{-17}	6.33×10^{-21}	5.38×10^{-18}	1.71×10^{2}	1.55×10^{5}	1.46×10^{12}	1.06×10^{-7}	3.29×10^{12}	4.73×10^{-8}
2816	1750	1.70×10^{15}	470.39	22.42	2563	2.019×10^{2}	7.71×10^{-15}	7.61×10^{-18}	8.14×10^{-22}	6.91×10^{-19}	2.20×10	1.55×10^{5}	1.14×10^{13}	1.37×10^{-8}	2.55×10^{13}	6.08×10^{-9}
3219	2000	1.97×10^{15}	431.86	22.42	2563	2.198×10^{2}	1.09×10^{-15}	1.08×10^{-18}	1.15×10^{-22}	9.75×10^{-20}	3.11	1.55×10^{5}	8.05×10^{13}	1.93×10^{-9}	1.81×10^{14}	8.58×10^{-10}
4023	2500	2.43×10^{15}	367.73	22.42	2563	2.582×10^{2}	3.92×10^{-17}	3.87×10^{-20}	4.12×10^{-24}	3.50×10^{-21}	1.12×10^{-1}	1.55×10^{5}	2.24×10^{15}	6.93×10^{-11}	5.05×10^{15}	3.08×10^{-11}
4828	3000	2.83×10^{15}	316.90	22.42	2563	2.996×10^{2}	2.08×10^{-18}	2.06×10^{-21}	2.19×10^{-25}	1.86×10^{-22}	5.93×10^{-3}	1.55×10^{5}	4.22×10^{16}	3.69×10^{-12}	9.49×10^{16}	1.64×10^{-12}
6438	4000	3.48×10^{15}	242.41	22.42	2563	3.917×10^{2}	1.92×10^{-20}	1.90×10^{-23}	2.02×10^{-27}	1.71×10^{-24}	5.47×10^{-5}	1.55×10^{5}	4.57×10^{18}	3.40×10^{-14}	1.03×10^{19}	1.51×10^{-14}
8047	5000	3.99×10^{15}	191.40	22.42	2563	4.961×10^{2}	4.93×10^{-22}	4.87×10^{-25}	5.20×10^{-29}	4.46×10^{-26}	1.41×10^{-6}	1.55×10^{5}	1.78×10^{20}	8.75×10^{-16}	4.00×10^{20}	3.89×10^{-16}
9656	6000	4.39×10^{15}	154.95	22.42	2563	6.129×10^{2}	2.68×10^{-23}	2.63×10^{-26}	2.82×10^{-30}	2.39×10^{-27}	7.63×10^{-8}	1.55×10^{5}	3.28×10^{21}	4.74×10^{-17}	7.38×10^{21}	2.11×10^{-17}
11,266	7000	4.72×10^{15}	127.99	22.42	2563	7.422×10^{2}	2.46×10^{-24}	2.43×10^{-27}	2.59×10^{-31}	2.20×10^{-28}	7.03×10^{-9}	1.55×10^{5}	3.56×10^{22}	4.37×10^{-18}	8.01×10^{22}	1.94×10^{-18}
12,875	8000	5.00×10^{15}	107.51	22.42	2563	8.833×10^{2}	3.38×10^{-25}	3.33×10^{-28}	3.55×10^{-32}	3.02×10^{-29}	9.61×10^{-10}	1.55×10^{5}	2.60×10^{23}	5.97×10^{-19}	5.86×10^{23}	2.65×10^{-19}
14,484	9000	5.23×10^{15}	91.57	22.42	2563	1.037×10^{3}	6.27×10^{-26}	6.19×10^{-29}	6.59×10^{-33}	5.60×10^{-30}	1.78×10^{-10}	1.55×10^{5}	1.40×10^{24}	1.11×10^{-18}	3.16×10^{24}	4.92×10^{-20}

1 millibar (mb) = 10^3 dynes/cm² = 0.750 mm of Hg

Table 36

ATMOSPHERIC MODEL II - VALUES OF TEMPERATURE, PRESSURE, AND DENSITY ABOVE THE F_2 LAYER

Latitude 45°. Engineering Units. p_a = 2116 lb/ft², ρ_a = 2.375 × 10⁻³ slug/ft³

Height h mi	Height h ft	Potential ϕ ft-lb	Apparent Gravity g' ft/sec²	Mean Mol Wt M	Temp T °R	Scale Height H ft	Pressure p lb/ft²	Pressure Ratio p/p_a	Density ρ slug/ft³	Density Ratio σ ρ/ρ_a	Number Density n particles/ft³	Mean Particle Speed v ft/sec	$d = 3 \times 10^{-8}$ cm Mean Free Path L ft	$d = 3 \times 10^{-8}$ cm Mean Collision Freq ν 1/sec	$d = 2 \times 10^{-8}$ cm Mean Free Path L ft	$d = 2 \times 10^{-8}$ cm Mean Collision Freq ν 1/sec
186.41	9.842×10^5		29.334	24.35	1980	1.377×10^5	1.01×10^{-6}	4.77×10^{-10}	2.50×10^{-13}	1.05×10^{-10}	9.09×10^{12}	3.21×10^3	2.56×10^3	1.26	5.75×10^3	5.58×10^{-1}
200	1.056×10^6		29.141	24.25	2072	1.457×10^5	6.07×10^{-7}	2.87×10^{-10}	1.43×10^{-13}	6.02×10^{-11}	5.22×10^{12}	3.29×10^3	4.45×10^3	7.39×10^{-1}	1.00×10^4	3.28×10^{-1}
225	1.188×10^6		28.793	24.08	2239	1.604×10^5	2.56×10^{-7}	1.21×10^{-10}	5.54×10^{-14}	2.33×10^{-11}	2.04×10^{12}	3.43×10^3	1.14×10^4	3.01×10^{-1}	2.56×10^4	1.34×10^{-1}
250	1.320×10^6		28.450	23.90	2404	1.756×10^5	1.17×10^{-7}	5.53×10^{-11}	2.34×10^{-14}	9.85×10^{-12}	8.67×10^{12}	3.56×10^3	2.68×10^4	1.33×10^{-1}	6.03×10^4	5.90×10^{-2}
275	1.452×10^6		28.113	23.73	2567	1.888×10^5	5.68×10^{-8}	2.68×10^{-11}	1.06×10^{-14}	4.46×10^{-12}	3.96×10^{12}	3.70×10^3	5.87×10^4	6.30×10^{-2}	1.32×10^5	2.80×10^{-2}
300	1.584×10^6		27.782	23.56	2728	2.070×10^5	2.93×10^{-8}	1.38×10^{-11}	5.09×10^{-15}	2.14×10^{-12}	1.91×10^{12}	3.83×10^3	1.22×10^5	3.15×10^{-2}	2.74×10^5	1.40×10^{-2}
325	1.716×10^6		27.457	23.40	2887	2.226×10^5	1.46×10^{-8}	6.90×10^{-12}	2.04×10^{-15}	8.58×10^{-13}	7.87×10^{11}	3.95×10^3	2.95×10^5	1.34×10^{-2}	6.65×10^5	5.94×10^{-3}
350	1.848×10^6		27.138	23.23	3045	2.399×10^5	8.96×10^{-9}	4.23×10^{-12}	1.37×10^{-15}	5.77×10^{-13}	5.23×10^{11}	4.07×10^3	4.44×10^5	9.16×10^{-3}	1.00×10^6	4.07×10^{-3}
375	1.980×10^6		26.824	23.07	3201	2.570×10^5	5.46×10^{-9}	2.58×10^{-12}	7.64×10^{-16}	3.21×10^{-13}	2.95×10^{11}	4.19×10^3	7.88×10^5	5.32×10^{-3}	1.77×10^6	2.36×10^{-3}
391	2.064×10^6	0.000	26.626	22.92	3299	2.685×10^5	3.82×10^{-9}	1.81×10^{-12}	5.34×10^{-16}	2.25×10^{-13}	2.06×10^{11}	4.27×10^3	1.13×10^6	3.78×10^{-3}	2.54×10^6	1.68×10^{-3}
400	2.112×10^6	1.204×10^6	26.517	22.92	3299	2.697×10^5	3.23×10^{-9}	1.53×10^{-12}	4.52×10^{-16}	1.90×10^{-13}	1.75×10^{11}	4.27×10^3	1.33×10^6	3.21×10^{-3}	2.99×10^6	1.43×10^{-3}
450	2.376×10^6	8.129×10^6	25.919	22.92	3299	2.759×10^5	1.23×10^{-9}	5.81×10^{-13}	1.72×10^{-16}	7.24×10^{-14}	6.64×10^{10}	4.27×10^3	3.21×10^6	1.33×10^{-3}	7.22×10^6	5.91×10^{-4}
475	2.508×10^6	1.153×10^7	25.628	22.92	3299	2.790×10^5	7.62×10^{-10}	3.60×10^{-13}	1.07×10^{-16}	4.51×10^{-14}	4.13×10^{10}	4.27×10^3	5.63×10^6	7.59×10^{-4}	1.27×10^7	3.37×10^{-4}
500	2.640×10^6	1.489×10^7	25.342	22.92	3299	2.822×10^5	4.76×10^{-10}	2.25×10^{-13}	6.66×10^{-17}	2.80×10^{-14}	2.57×10^{10}	4.27×10^3	9.05×10^6	4.72×10^{-4}	2.04×10^7	2.10×10^{-4}
550	2.904×10^6	2.151×10^7	24.783	22.92	3299	2.885×10^5	1.89×10^{-10}	8.93×10^{-14}	2.64×10^{-17}	1.11×10^{-14}	1.02×10^{10}	4.27×10^3	2.28×10^7	2.87×10^{-4}	5.13×10^7	1.28×10^{-4}
600	3.168×10^6	2.798×10^7	24.243	22.92	3299	2.945×10^5	7.63×10^{-11}	3.61×10^{-14}	1.07×10^{-17}	4.51×10^{-15}	4.13×10^9	4.27×10^3	5.63×10^7	7.59×10^{-5}	1.27×10^8	3.37×10^{-5}
700	3.696×10^6	4.051×10^7	23.215	22.92	3299	3.076×10^5	1.32×10^{-11}	6.24×10^{-15}	1.85×10^{-18}	7.79×10^{-16}	7.14×10^8	4.27×10^3	3.26×10^8	1.31×10^{-5}	7.33×10^8	5.83×10^{-6}
800	4.224×10^6	5.251×10^7	22.250	22.92	3299	3.214×10^5	2.47×10^{-12}	1.17×10^{-15}	3.45×10^{-19}	1.45×10^{-16}	1.33×10^8	4.27×10^3	1.75×10^9	2.44×10^{-6}	3.93×10^9	1.09×10^{-6}
900	4.752×10^6	6.401×10^7	21.345	22.92	3299	3.350×10^5	4.95×10^{-13}	2.34×10^{-16}	6.92×10^{-20}	2.91×10^{-17}	2.67×10^7	4.27×10^3	8.71×10^9	4.90×10^{-7}	1.96×10^{10}	2.18×10^{-7}
1000	5.280×10^6	7.505×10^7	20.493	22.92	3299	3.489×10^5	1.05×10^{-13}	4.96×10^{-17}	1.47×10^{-20}	6.19×10^{-18}	5.68×10^6	4.27×10^3	4.09×10^{10}	1.04×10^{-7}	9.21×10^{10}	4.64×10^{-8}
1200	6.336×10^6	9.586×10^7	18.223	22.92	3299	3.924×10^5	5.75×10^{-15}	2.72×10^{-18}	8.04×10^{-22}	3.39×10^{-19}	3.10×10^5	4.27×10^3	7.50×10^{11}	5.69×10^{-9}	1.69×10^{12}	2.53×10^{-9}
1400	7.392×10^6	1.151×10^8	17.551	22.92	3299	4.074×10^5	3.90×10^{-16}	1.84×10^{-19}	5.45×10^{-23}	2.29×10^{-20}	2.10×10^4	4.27×10^3	1.11×10^{12}	3.86×10^{-10}	2.49×10^{13}	1.71×10^{-10}
1500	7.920×10^6	1.242×10^8	16.914	22.92	3299	4.227×10^5	1.09×10^{-16}	5.15×10^{-20}	1.52×10^{-23}	6.40×10^{-21}	5.87×10^3	4.27×10^3	3.96×10^{12}	1.08×10^{-10}	8.91×10^{13}	4.79×10^{-11}
1750	9.240×10^6	1.456×10^8	15.466	22.92	3299	4.623×10^5	5.48×10^{-18}	2.59×10^{-21}	7.66×10^{-25}	3.23×10^{-22}	2.96×10^3	4.27×10^3	7.85×10^{14}	5.44×10^{-12}	1.77×10^{15}	2.42×10^{-12}
2000	1.056×10^7	1.651×10^8	14.197	22.92	3299	5.037×10^5	3.58×10^{-19}	1.69×10^{-22}	5.01×10^{-26}	2.11×10^{-23}	1.93 × 10	4.27×10^3	1.20×10^{16}	3.55×10^{-13}	2.71×10^{16}	1.58×10^{-13}
2500	1.320×10^7	1.997×10^8	12.085	22.92	3299	5.917×10^5	2.84×10^{-21}	1.34×10^{-24}	3.97×10^{-28}	1.67×10^{-25}	1.53×10^{-1}	4.27×10^3	1.52×10^{18}	2.81×10^{-15}	3.42×10^{18}	1.25×10^{-15}
3000	1.584×10^7	2.293×10^8	10.412	22.92	3299	6.867×10^5	4.52×10^{-23}	2.14×10^{-26}	6.32×10^{-30}	2.66×10^{-27}	2.44×10^{-3}	4.27×10^3	9.53×10^{19}	4.48×10^{-17}	2.14×10^{20}	1.99×10^{-17}
3500	1.848×10^7	2.550×10^8	9.064	22.92	3299	7.889×10^5	1.24×10^{-24}	5.86×10^{-28}	1.73×10^{-31}	7.28×10^{-29}	6.68×10^{-5}	4.27×10^3	3.48×10^{21}	1.23×10^{-18}	7.83×10^{21}	5.45×10^{-18}
4000	2.112×10^7	2.774×10^8	7.961	22.92	3299	8.981×10^5	5.41×10^{-26}	2.56×10^{-29}	7.57×10^{-33}	3.19×10^{-30}	2.92×10^{-6}	4.27×10^3	7.96×10^{22}	5.36×10^{-19}	1.79×10^{23}	2.38×10^{-19}
4500	2.376×10^7	2.972×10^8	7.049	22.92	3299	1.014×10^6	3.39×10^{-27}	1.60×10^{-30}	4.74×10^{-34}	2.00×10^{-31}	1.83×10^{-7}	4.27×10^3	1.27×10^{24}	3.36×10^{-21}	2.86×10^{24}	1.49×10^{-21}
5000	2.640×10^7	3.147×10^8	6.284	22.92	3299	1.138×10^6	2.94×10^{-28}	1.39×10^{-31}	4.11×10^{-35}	1.73×10^{-32}	1.59×10^{-8}	4.27×10^3	1.46×10^{25}	2.92×10^{-22}	3.29×10^{25}	1.30×10^{-22}
5500	2.904×10^7	3.304×10^8	5.638	22.92	3299	1.268×10^6	3.27×10^{-29}	1.55×10^{-32}	4.57×10^{-36}	1.92×10^{-33}	1.76×10^{-9}	4.27×10^3	1.32×10^{26}	3.23×10^{-23}	2.97×10^{26}	1.44×10^{-23}

1 lb/ft² = 0.3591 mm of Hg

Table 37

ATMOSPHERIC MODEL II.- VALUES OF TEMPERATURE, PRESSURE, AND DENSITY ABOVE THE F_2 LAYER

Latitude 45° Metric Units. p_a = 1014 mb, $\rho_a = 1.223 \times 10^{-3}$ gm/cm³

Height h km	Height h mi	Potential ϕ ergs	Apparent Gravity g'	Mol Wt M	Temp T °K	Scale Height H km	Pressure p millibars	Pressure Ratio p/p_a	Density ρ gm/cm³	Density Ratio σ ρ/ρ_a	Number Density n particles/cm³	Mean Particle Speed v cm/sec	$d = 3 \times 10^{-8}$cm Mean Free Path L cm	$d = 3 \times 10^{-8}$cm Mean Collision Freq ν 1/sec	$d = 2 \times 10^{-8}$cm Mean Free Path L cm	$d = 2 \times 10^{-8}$cm Mean Collision Freq ν 1/sec
300	186.41		894.09	24.35	1100	4.197×10	4.84×10^{-7}	4.77×10^{-10}	1.29×10^{-13}	1.05×10^{-10}	3.21×10^{9}	9.78×10^{4}	7.79×10^{4}	1.26	1.75×10^{5}	5.58×10^{-1}
322	200		888.23	24.25	1151	4.439×10	2.91×10^{-7}	2.87×10^{-10}	7.36×10^{-14}	6.02×10^{-11}	1.84×10^{9}	1.00×10^{5}	1.36×10^{5}	7.39×10^{-1}	3.05×10^{5}	3.28×10^{-1}
362	225		877.60	24.07	1244	4.890×10	1.23×10^{-7}	1.21×10^{-10}	2.85×10^{-14}	2.33×10^{-11}	7.20×10^{8}	1.05×10^{5}	3.47×10^{5}	3.01×10^{-1}	7.81×10^{5}	1.34×10^{-1}
402	250		867.15	23.89	1336	5.353×10	5.60×10^{-8}	5.53×10^{-11}	1.21×10^{-14}	9.85×10^{-12}	3.06×10^{9}	1.09×10^{5}	8.17×10^{5}	1.33×10^{-1}	1.84×10^{6}	5.90×10^{-2}
443	275		856.89	23.71	1426	5.755×10	2.72×10^{-8}	2.68×10^{-11}	5.46×10^{-15}	4.46×10^{-12}	1.40×10^{9}	1.13×10^{5}	1.79×10^{5}	6.30×10^{-2}	4.03×10^{6}	2.80×10^{-2}
483	300		846.81	23.54	1516	6.311×10	1.40×10^{-8}	1.38×10^{-11}	2.62×10^{-15}	2.14×10^{-12}	6.75×10^{7}	1.17×10^{5}	3.71×10^{6}	3.15×10^{-2}	8.35×10^{6}	1.40×10^{-2}
523	325		836.90	23.38	1604	6.786×10	7.00×10^{-9}	6.90×10^{-12}	1.05×10^{-15}	8.58×10^{-13}	2.78×10^{7}	1.21×10^{5}	9.00×10^{6}	1.34×10^{-2}	2.03×10^{7}	5.94×10^{-3}
563	350		827.17	23.20	1692	7.313×10	4.29×10^{-9}	4.23×10^{-12}	7.06×10^{-16}	5.77×10^{-13}	1.85×10^{7}	1.24×10^{5}	1.35×10^{7}	9.16×10^{-3}	3.05×10^{7}	4.07×10^{-3}
604	375		817.60	23.04	1779	7.832×10	2.61×10^{-9}	2.58×10^{-12}	3.93×10^{-16}	3.21×10^{-13}	1.04×10^{7}	1.28×10^{5}	2.40×10^{7}	5.32×10^{-3}	5.40×10^{7}	2.36×10^{-3}
630	391	0.000	811.57	22.92	1833	8.185×10	1.83×10^{-9}	1.81×10^{-12}	2.75×10^{-16}	2.25×10^{-13}	7.27×10^{6}	1.30×10^{5}	3.44×10^{7}	3.78×10^{-3}	7.74×10^{7}	1.68×10^{-3}
644	400	1.633×10^{13}	808.22	22.92	1833	8.219×10	1.55×10^{-9}	1.53×10^{-12}	2.33×10^{-16}	1.90×10^{-13}	6.18×10^{6}	1.30×10^{5}	4.05×10^{7}	3.21×10^{-3}	9.11×10^{7}	1.43×10^{-3}
724	450	1.102×10^{14}	790.01	22.92	1833	8.409×10	5.89×10^{-10}	5.81×10^{-13}	8.86×10^{-17}	7.24×10^{-14}	2.34×10^{6}	1.30×10^{5}	9.79×10^{7}	1.33×10^{-3}	2.20×10^{8}	5.91×10^{-4}
765	475	1.563×10^{14}	781.14	22.92	1833	8.504×10	3.65×10^{-10}	3.60×10^{-13}	5.51×10^{-17}	4.51×10^{-14}	1.46×10^{6}	1.30×10^{5}	1.72×10^{8}	7.59×10^{-4}	3.86×10^{8}	3.37×10^{-4}
805	500	2.019×10^{14}	772.42	22.92	1833	8.600×10	2.28×10^{-10}	2.25×10^{-13}	3.43×10^{-17}	2.80×10^{-14}	9.08×10^{5}	1.30×10^{5}	2.76×10^{8}	4.72×10^{-4}	6.20×10^{8}	2.10×10^{-4}
885	550	2.917×10^{14}	755.40	22.92	1833	8.794×10	9.05×10^{-11}	8.93×10^{-14}	1.36×10^{-17}	1.11×10^{-14}	3.60×10^{5}	1.30×10^{5}	6.95×10^{8}	2.87×10^{-4}	1.56×10^{9}	1.28×10^{-4}
966	600	3.794×10^{14}	738.94	22.92	1833	8.975×10	3.65×10^{-11}	3.61×10^{-14}	5.51×10^{-18}	4.51×10^{-15}	1.46×10^{5}	1.30×10^{5}	1.72×10^{9}	7.59×10^{-5}	3.86×10^{9}	3.37×10^{-5}
1127	700	5.493×10^{14}	707.59	22.92	1833	9.375×10	6.32×10^{-12}	6.24×10^{-15}	9.53×10^{-19}	7.79×10^{-16}	2.52×10^{4}	1.30×10^{5}	9.92×10^{9}	1.31×10^{-5}	2.23×10^{10}	5.83×10^{-6}
1288	800	7.120×10^{14}	678.19	22.92	1833	9.795×10	1.18×10^{-12}	1.17×10^{-15}	1.78×10^{-19}	1.45×10^{-16}	4.70×10^{3}	1.30×10^{5}	5.33×10^{10}	2.44×10^{-6}	1.19×10^{11}	1.09×10^{-6}
1448	900	8.680×10^{14}	650.59	22.92	1833	1.021×10^{2}	2.37×10^{-13}	2.34×10^{-16}	3.56×10^{-20}	2.91×10^{-17}	9.43×10^{2}	1.30×10^{5}	2.65×10^{11}	4.90×10^{-7}	5.93×10^{11}	2.18×10^{-7}
1609	1000	1.018×10^{15}	624.64	22.92	1833	1.063×10^{2}	5.03×10^{-14}	4.96×10^{-17}	7.57×10^{-21}	6.19×10^{-18}	2.01×10^{2}	1.30×10^{5}	1.25×10^{12}	1.04×10^{-7}	2.79×10^{12}	4.64×10^{-8}
1931	1200	1.300×10^{15}	555.43	22.92	1833	1.196×10^{2}	2.75×10^{-15}	2.72×10^{-18}	4.14×10^{-22}	3.39×10^{-19}	1.09×10	1.30×10^{5}	2.29×10^{13}	5.69×10^{-8}	5.11×10^{13}	2.53×10^{-8}
2253	1400	1.561×10^{15}	534.95	22.92	1833	1.242×10^{2}	1.87×10^{-16}	1.84×10^{-19}	2.81×10^{-23}	2.29×10^{-20}	7.42×10^{-1}	1.30×10^{5}	3.37×10^{14}	3.86×10^{-10}	7.54×10^{14}	1.71×10^{-10}
2414	1500	1.684×10^{15}	515.54	22.92	1833	1.289×10^{2}	5.22×10^{-17}	5.15×10^{-20}	7.83×10^{-24}	6.40×10^{-21}	2.07×10^{-1}	1.30×10^{5}	1.21×10^{15}	1.08×10^{-10}	2.70×10^{15}	4.79×10^{-11}
2816	1750	1.974×10^{15}	471.41	22.92	1833	1.409×10^{2}	2.62×10^{-18}	2.59×10^{-21}	3.94×10^{-25}	3.23×10^{-22}	1.05×10^{-2}	1.30×10^{5}	2.39×10^{16}	5.44×10^{-12}	5.35×10^{16}	2.42×10^{-12}
3219	2000	2.239×10^{15}	432.72	22.92	1833	1.535×10^{2}	1.71×10^{-19}	1.69×10^{-22}	2.58×10^{-26}	2.11×10^{-23}	6.82×10^{-4}	1.30×10^{5}	3.67×10^{17}	3.55×10^{-13}	8.20×10^{17}	1.58×10^{-13}
4023	2500	2.708×10^{15}	368.36	22.92	1833	1.803×10^{2}	1.36×10^{-21}	1.34×10^{-24}	2.04×10^{-28}	1.67×10^{-25}	5.40×10^{-6}	1.30×10^{5}	4.63×10^{19}	2.81×10^{-15}	1.03×10^{20}	1.25×10^{-15}
4828	3000	3.109×10^{15}	317.36	22.92	1833	2.093×10^{2}	2.16×10^{-23}	2.14×10^{-26}	3.25×10^{-30}	2.66×10^{-27}	8.62×10^{-8}	1.30×10^{5}	2.90×10^{21}	4.48×10^{-17}	6.49×10^{21}	1.99×10^{-17}
5633	3500	3.458×10^{15}	276.27	22.92	1833	2.404×10^{2}	5.94×10^{-25}	5.86×10^{-28}	8.91×10^{-32}	7.28×10^{-29}	2.36×10^{-9}	1.30×10^{5}	1.06×10^{23}	1.23×10^{-19}	2.37×10^{23}	5.45×10^{-19}
6438	4000	3.762×10^{15}	242.66	22.92	1833	2.737×10^{2}	2.59×10^{-26}	2.56×10^{-29}	3.90×10^{-33}	3.19×10^{-30}	1.03×10^{-10}	1.30×10^{5}	2.43×10^{24}	5.36×10^{-19}	5.42×10^{24}	2.38×10^{-19}
7242	4500	4.030×10^{15}	214.84	22.92	1833	3.092×10^{2}	1.62×10^{-27}	1.60×10^{-30}	2.44×10^{-34}	2.00×10^{-31}	6.46×10^{-12}	1.30×10^{5}	3.87×10^{25}	3.36×10^{-21}	8.65×10^{25}	1.49×10^{-21}
8047	5000	4.267×10^{15}	191.54	22.92	1833	3.468×10^{2}	1.41×10^{-28}	1.39×10^{-31}	2.12×10^{-35}	1.73×10^{-32}	5.62×10^{-13}	1.30×10^{5}	4.46×10^{26}	2.92×10^{-22}	9.95×10^{26}	1.30×10^{-22}
8851	5500	4.480×10^{15}	171.83	22.92	1833	3.866×10^{2}	1.57×10^{-29}	1.55×10^{-32}	2.35×10^{-36}	1.92×10^{-33}	6.22×10^{-14}	1.30×10^{5}	4.03×10^{27}	3.23×10^{-23}	8.99×10^{27}	1.44×10^{-23}

1 millibar (mb) = 10^3 dynes/cm² = 0.750 mm of Hg

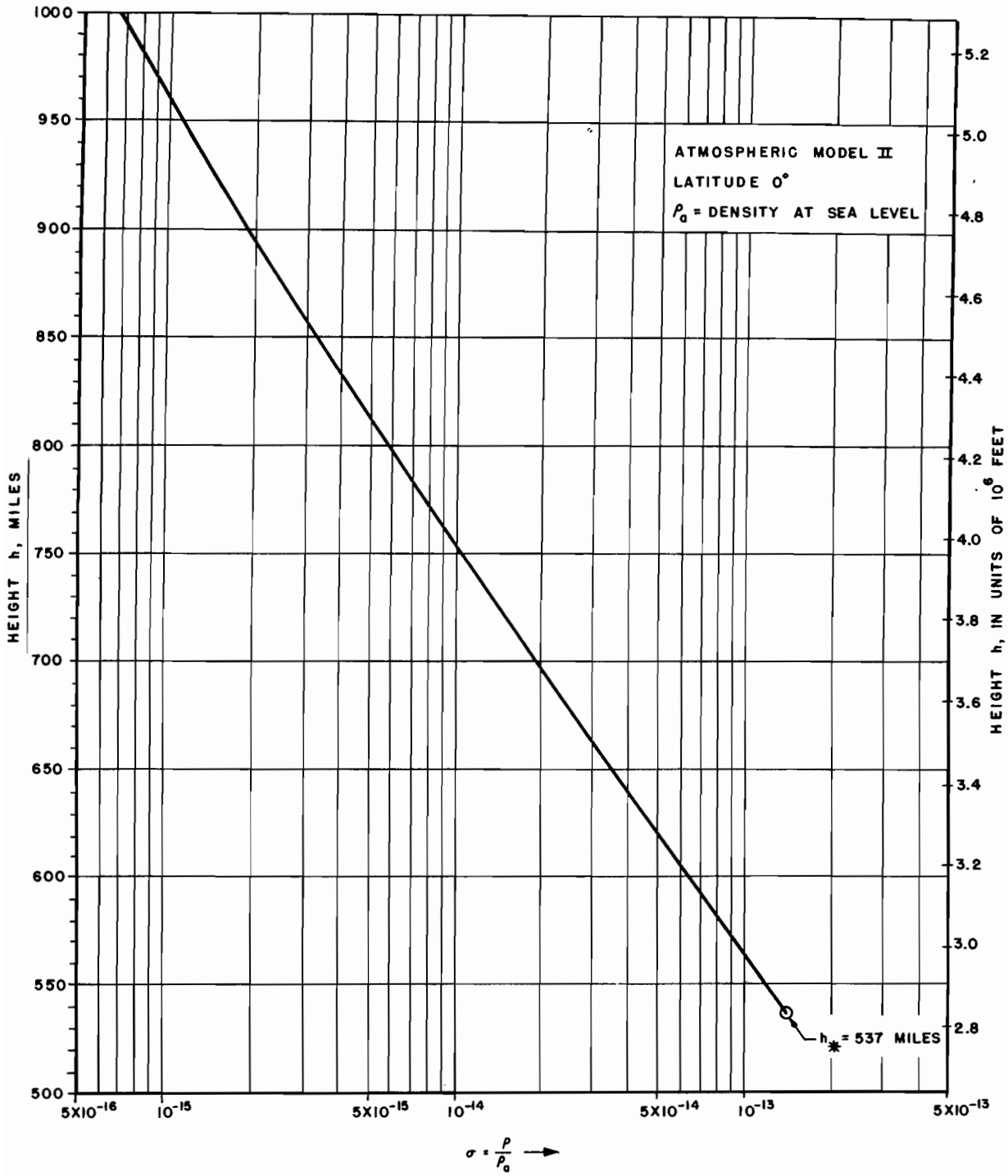

ADOPTED VALUES OF THE DENSITY RATIO σ FOR ATMOSPHERIC MODEL II FROM h_* UP TO 1000 MILES. LATITUDE 0°. ENGINEERING UNITS.

FIG. 29

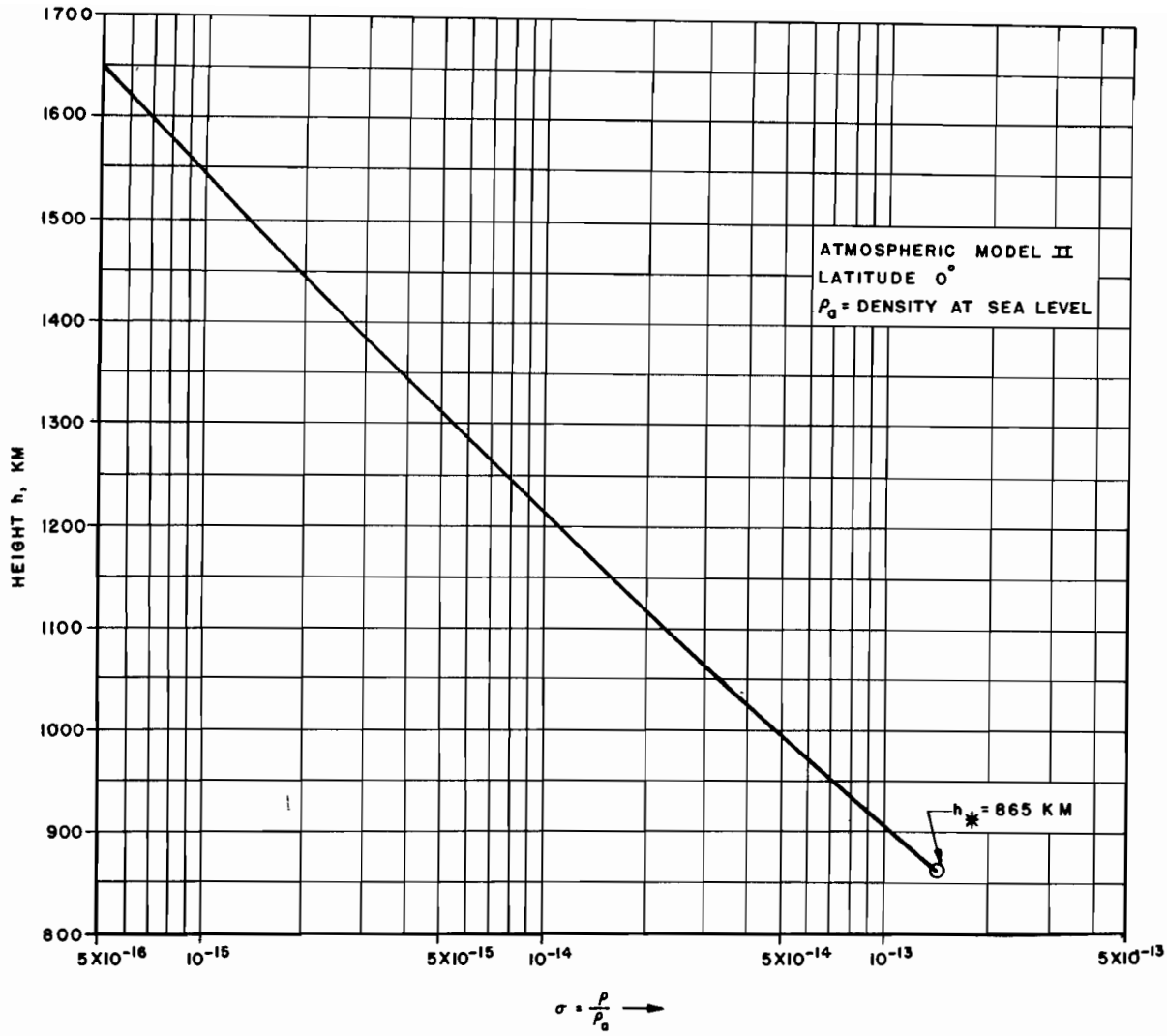

ADOPTED VALUES OF THE DENSITY RATIO σ FOR ATMOSPHERIC MODEL II FROM h_* UP TO 1000 MILES. LATITUDE 0°. METRIC UNITS.

FIG. 30

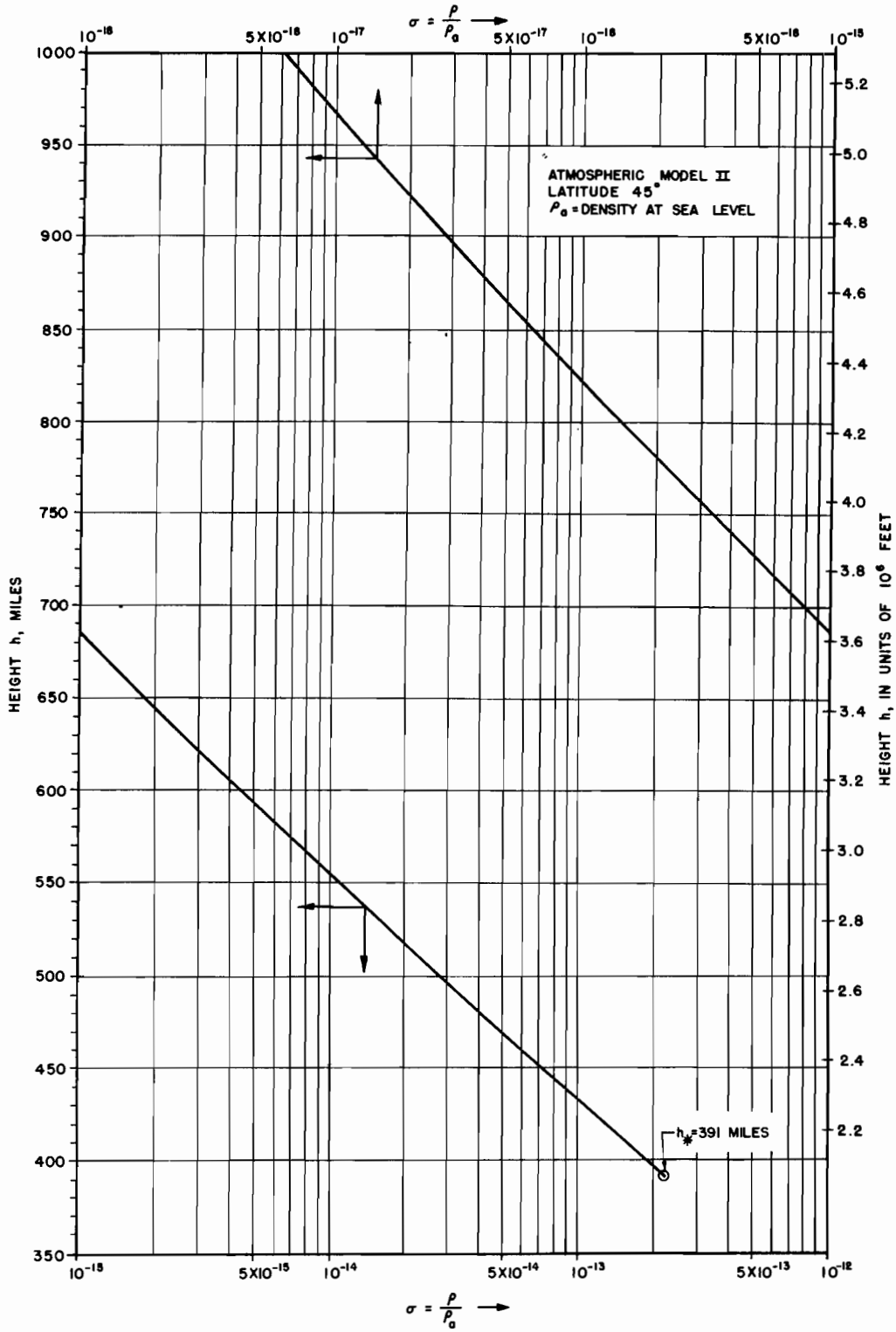

ADOPTED VALUES OF THE DENSITY RATIO σ FOR ATMOSPHERIC MODEL II FROM h_* UP TO 1000 MILES. LATITUDE 45°. ENGINEERING UNITS.

FIG. 31

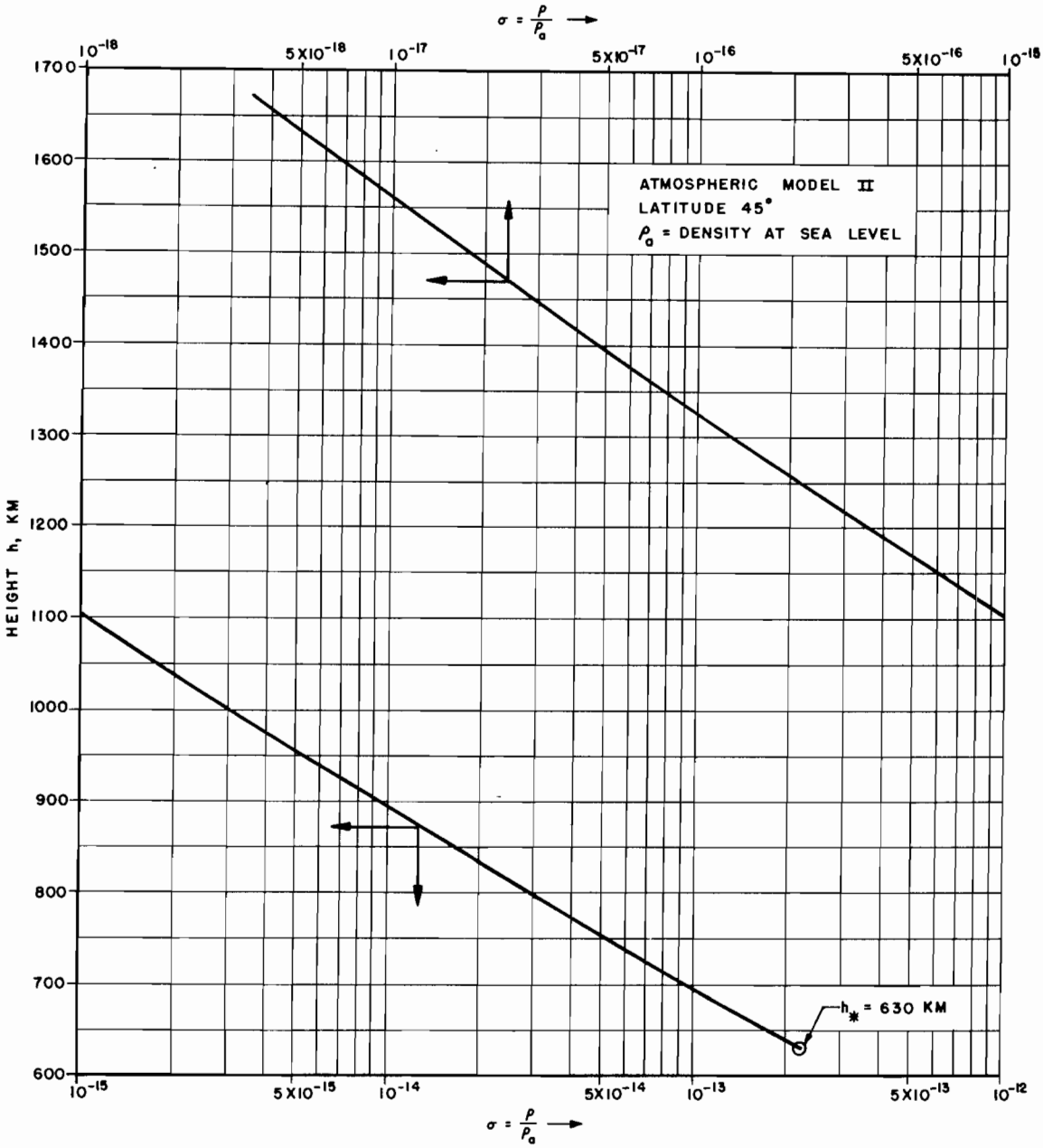

ADOPTED VALUES OF THE DENSITY RATIO σ FOR ATMOSPHERIC MODEL II FROM h_* UP TO 1000 MILES. LATITUDE 45°. METRIC UNITS.

FIG. 32

III. THE ATMOSPHERE ABOVE THE F_2 LAYER – ATMOSPHERIC MODEL III

In atmospheric model I the atmospheric gas was treated as a continuum with no account taken of the motion of the individual particles, even though at sufficiently great heights the gas becomes attenuated to a degree comparable to that of the interstellar gas. In this model the degree of diffusion equilibrium was automatically specified by the assumed law of variation of M with height (Eq.36) and by the value used for the constant M_L (see Section II-E). The vertical temperature distribution was specified by the assumption of thermal equilibrium with the interstellar gas (at 10,000°K) at the "limit" of the atmosphere, where both gases have the same pressure.

In model II it is recognized that above the F_2 layer, beginning at some height h_*, the mean free path becomes so large that the atmospheric gas particles begin to move over paths which are essentially dynamical orbits in a gravitational field, subject to the dynamical condition of constant angular momentum. Thus, model II is characterized by the concept of a dynamical orbit region above the height h_* where individual particles are rising and falling over large vertical distances, and where any particle having a sufficiently high velocity — the escape velocity, Eq.(38) — would have a probability of escaping from the earth entirely. Using the particle velocity 4.5×10^5 cm/sec mentioned on p.89, it is found that the time of vertical flight of such a particle in a gravitational field is of the order of 15 minutes. Since this time interval can be shown to be negligibly small compared with that required for ionization by solar radiation, it is permissible to assume that the total energy of each particle remains unchanged during its flight in the dynamical orbit region. It then follows from the discussion on p.63 that the atmosphere above the height h_* will be isothermal, will have a Maxwellian velocity distribution, and will have a vertical density distribution given by the Boltzmann law — Eq.(41). If, in addition, there is no appreciable increase in the degree of ionization of the atmosphere between the F_2 layer and the height h_*, it follows that the particles situated above h_* will also be predominantly neutral. In model II no account was taken of diffusion equilibrium (composition and temperature were assumed constant), and the temperatures used in establishing the height h_* were taken from model I.

In model III an attempt will be made to combine the idea of an isothermal dynamical orbit region — used in model II — with the effects of diffusion equilibrium, treating the latter on a more rational basis than was employed for model I. Further consideration will be given to the temperature above the F_2 layer and, in particular, to the temperature T_* of the dynamical orbit region and the height h_* where it may be considered to begin.

The atmosphere above 300 km has been studied recently by L. Spitzer, Jr.[61], who uses the term "exosphere" to denote the free-flight dynamical orbit region above the height h_*. Among other things, Spitzer has derived certain theoretical results concerning the height h_* and the temperature T_*, and these results will be used in connection with model III. In view of the rather complete lack of information and theoretical results concerning the temperatures which might exist above the F_2 layer, Spitzer's analysis will be presented below in detail[5a].

III-A. THE MAXIMUM TEMPERATURE OF THE UPPER ATMOSPHERE (EXOSPHERE)

It will be recalled that in model II the highest temperature attained in the upper atmosphere was the constant value T_* at and above the height h_*, and that this temperature was derived from the temperature distribution of model I. Spitzer[61] has considered the maximum possible temperature that might be expected throughout the atmosphere at and above the level h_* on the basis of a simplified analysis of the ionizing absorption of ultra-violet radiation by oxygen atoms and the electron excitation of neutral oxygen atoms. His analysis is based upon a consideration of the oxygen atom, and in particular upon the fact that the oxygen atom has an excited $^1D_2$ state corresponding to an excitation potential of 1.96 electron volts (ev) above the ground state[62],[63]. Thus an electron with more than 1.96 ev of kinetic energy can, by collision, excite an oxygen atom to the $^1D_2$ state.

That excited states of the oxygen atom are present in the upper atmosphere is fully attested by the analysis of the spectrum of the light of the night sky[64],[64a],[64b],[64c]. Why the temperature analysis is based on the excited $^1D_2$ state of the oxygen atom rather than on some other excited state of oxygen, or on an excited state of nitrogen, is explained by Spitzer[67] in the following remarks:

- "Since the overwhelming majority of atoms in the upper atmosphere will be in the ground level, collisional excitations from the ground level will have the largest effect on the temperature. Most excited states have such high energy that no electrons in the upper atmosphere would be moving fast enough to excite them; hence it is the lowest excited state, or level, which has the greatest influence. For example, the lowest excited level of the oxygen atom is the $^1D_2$ state, which lies 1.96 volts above the ground level. An electron can excite an atom to this level only if it has an energy greater than 1.96 volts. The existence of this level reduces the temperature until the number of electrons with energies above this critical value will be fairly small. The next higher excited level is the $^1S_0$ level; this level lies 4.17 volts above the ground level and the number of

[5a] The results presented here for the temperature T_* of the exosphere are based on a preliminary analysis which has been revised to some extent in Ref.(61).

electrons capable of exciting to this state an atom originally in the ground level will be negligibly small at any temperature which seems likely for the upper atmosphere.

"Nitrogen atoms should also be considered in this connection, of course. The first excited state of nitrogen lies 2.37 volts above the ground level. Since the number of electrons with energies greater than 2.37 volts is much less than the corresponding number with energies greater than 1.96 volts, nitrogen atoms will not be so effective in depressing the temperature as oxygen atoms will be.

"Two other mechanisms should also be considered in this connection. The excited levels of the nitrogen molecule lie considerably closer to the ground level than do the excited atomic states. If there is any appreciable number of nitrogen molecules at great heights, these may have an important effect on the temperature. Also, the oxygen negative ion should be considered. Detachment of an electron from such an ion, resulting from absorption of a quantum of radiation, will tend to increase the temperature, while detachment of an electron by collision with another electron will tend to decrease the temperature. Preliminary calculations show that neither of these effects can change appreciably the conclusions reached[61] on the basis of the neutral oxygen atom."

The analysis is based upon the consideration that the loss in free electron kinetic energy resulting from the excitation collision process is replenished in equal amount by the process of photo-ionization. In order to proceed with the analysis, it is necessary to know the collision cross section corresponding to the excitation process. This collision cross section may be expressed as a fraction q of the geometrical cross section $\pi d^2/4$ of a rigid sphere of diameter d. For this purpose Spitzer uses the value $q = 1/5$ based on the results of Hebb and Menzel[65] for the O III ion (i.e., the doubly ionized oxygen atom, O^{++}). The energy density of the excitation collision process will be proportional to the collision frequency of the electrons with the oxygen atoms, and to the free electron kinetic energy given up in the excitational collisions producing the excited $^1D_2$ state of the oxygen atoms. The general theory of the motion of electrons in a gas when inelastic (excitation) collisions are possible is very complicated[65a], and since Spitzer's analysis is intended only as a rough, first approximation, several simplifying assumptions are used. If $E_i = m_e v_i^2/2$ (v_i = electron velocity corresponding to kinetic energy E_i) denotes the energy level of the excited $^1D_2$ state of the oxygen atom, all electrons with kinetic energy E greater than E_i (velocity greater than v_i) can, by collision, excite the atom to the $^1D_2$ level. It is therefore necessary, first of all, to estimate the number of electron-oxygen collisions per cm^3 per sec for the electrons with velocity greater than v_i. Letting ν_{eO} denote the electron-oxygen collision frequency considering only the electrons with velocity greater than v_i, and assuming a Maxwellian distribution for both gases, it is found (Ref. 65a, p.92) that

$$\nu_{eO} = \sqrt{\frac{2}{\pi}}\; n_e n_O S_{eO} \left(\frac{m_e}{kT}\right)^{\frac{3}{2}} \int_{v_i}^{\infty} e^{-m_e v^2/2kT}\, dv \;, \tag{64}$$

where

n_e = number of free electrons per cm^3

n_O = number of oxygen atoms per cm^3

m_e = mass of electron

m_O = mass of oxygen atom

S_{eO} = collision cross section for electron and oxygen atom = $q \times \frac{\pi d^2}{4}$

k = Boltzmann's constant

v = electron velocity.

Owing to the small mass of the electron, it is assumed in deriving (64) that the ratio m_e/m_O is negligible compared to 1, and also that the velocity of the atoms is negligible relative to the electron velocity.

Eq. (64) can be integrated (Ref. 65a, p.92) yielding the result

$$\nu_{eO} = \frac{2}{\sqrt{\pi}} n_e n_O S_{eO} \left(\frac{2kT}{m_e}\right)^{\frac{1}{2}} \left[\left(\frac{m_e}{2kT}\right)^2 + 1\right] e^{-\frac{E_i}{kT}}, \tag{64a}$$

where $E_i = m_e v_i^2/2$. The term $(m_e/2kT)^2$ is very small compared to 1 and may be neglected. Using the relation[65b] between the temperature and the average electron velocity v_e, the term $(2kT/m_e)^{1/2}$ may be replaced by $\sqrt{\pi}\, v_e/2$, and the collision frequency equation becomes

$$\nu_{eO} = n_e n_O S_{eO} v_e \, e^{-\frac{E_i}{kT}} \tag{64b}$$

It is assumed as a rough approximation that every collision of an electron having kinetic energy greater than E_i is an excitation collision, although actually there exists only a certain probability that these collisions will be excitational[65c]. On the basis of this assumption, each electron-oxygen collision, (64b), represents a loss E_i (= 1.96 electron volts for the $^1D_2$ state) of free electron kinetic energy. Replacing the collision cross section by $S_{eO} = 1/5 \times \pi d^2/4$, where d is the diameter of the oxygen atom, and letting $P = \exp(-E_i/kT)$, the total loss in free electron kinetic energy is $1.96\, n_e n_O \pi d^2 v_e P/20$ electron volts per cm^3 per sec. The quantity P may be written

$$P = e^{-\frac{E_i}{kT}} = 10^{-1.96 \times \frac{5040}{T}} = 10^{-1.96\theta}, \tag{65}$$

where $\theta = 5040/T$ with T in degrees Kelvin.

For thermodynamic equilibrium the loss in free electron kinetic energy resulting from the excitational collision process with the neutral oxygen atoms must be balanced by a gain in free electron kinetic energy brought about by photo-ionization resulting from the absorption of ultra-violet solar radiation. The photo-ionization of the atoms is governed by the photoelectric equation[66]

$$\frac{1}{2} m_e v_e^2 = h\nu - eV_i \ , \tag{66}$$

where

$\frac{1}{2} m_e v_e^2$ = the kinetic energy with which the photoelectron is ejected

h = Planck's constant

ν = the frequency of the ionizing radiation

e = the electronic charge

V_i = the ionization potential.

Thus the excess kinetic energy of the photoelectron depends upon the frequency of the photo-ionizing radiation. A knowledge of this excess energy is essential for the analysis. Spitzer obtains an average value of one electron volt for the excess photoelectron kinetic energy on the basis of the following argument[67].

> "Although the excess kinetic energy depends on the frequencies of the photo-ionizing radiation, the average energy carried off by photoelectrons tends to be proportional to the temperature of the surface which produces the ionizing radiation, quite independently of how weak this radiation may be. An analysis of this effect has been given by Eddington†. The color temperature radiation from the sun at the high frequencies of interest is somewhat uncertain. Radiation from a black body at 5000°K would yield photoelectrons with an average kinetic energy of about 0.3 of an electron volt. The actual energy will depend on the detailed slope shown by the curve of radiation intensity as a function of frequency. On the assumption that the radiation in the ultra-violet corresponds to a higher temperature than in the visible region of the spectrum, one volt is taken as the average kinetic energy of the photoelectrons. A more precise estimate would be difficult to obtain, and would depend both on the variation of the photoelectric absorption of oxygen with increasing frequency, and also on the detailed radiation from the sun in the ultra-violet[6]. Similar considerations would also apply to the nitrogen atom. If the ionizing radiation from the sun at the appropriate frequencies corresponds to that of a black body at about 10,000°K, the excess kinetic energy of the photoelectron will again be about 1 volt. It should be noted that this excess kinetic energy depends not upon the absolute intensity of the radiation but upon the variation of this intensity with frequency. As long as this frequency variation corresponds to that of a black body at temperature T, the ejected electrons will tend to have an average kinetic energy corresponding to a kinetic temperature 2/3 T."

If μ is the probability of ionization per unit time, the number of photoelectrons released per cm^3 per second is μn_0; and since each electron is released in the ionization process with a kinetic energy of about 1 electron volt, μn_0 also gives the gain in energy per cm^3 per second. For equilibrium conditions this gain in energy

---

† Eddington, Sir A.S., *The Internal Constitution of the Stars*, Cambridge: University Press, pp.376-377, 1926.

[6] The appropriate equations governing this effect have been given by Spitzer in a paper to appear in the *Astrophys. J.*, Vol.107.

from ionization must be balanced by the loss in free electron kinetic energy which occurs in the excitational collision process with the oxygen atoms. The energy balance is therefore represented by

$$\mu n_O = 1.96 \frac{\pi d^2}{20} n_e n_O v_e P = 1.96 \frac{\pi d^2}{20} n_e n_O v_e 10^{-1.96\theta} \text{ , or}$$

$$10^{1.96\theta} = 1.96 \frac{\pi d^2}{20} \frac{n_e}{\mu} v_e \text{ .} \tag{67}$$

Since 1 electron volt = 1.6×10^{-12} ergs, v_e has a value of about 6×10^7 cm/sec. Using $d = 2 \times 10^{-8}$ cm for the diameter of the neutral oxygen atom, Eq. (67) may be written

$$10^{1.96\theta} = 7.4 \times 10^{-9} \frac{n_e}{\mu} \tag{68}$$

Since, for steady state conditions, the electron density n_e is related to the recombination coefficient α and the ionization probability μ by the equation (Ref. 59, p.98)

$$n_e = \left(\frac{n_O \mu}{\alpha}\right)^{1/2} , \tag{69}$$

the energy balance equation, (68), may be written

$$10^{1.96\theta} = 7.4 \times 10^{-9} \left(\frac{n_O}{\alpha \mu}\right)^{1/2} . \tag{70}$$

It now remains to evaluate α and μ. In the absence of any information concerning these quantities in the atmosphere above the F_2 layer, Spitzer assumes the values are approximately the same as in the F_2 layer. The values of n_e and α for the F_2 layer as given by Bates and Massey[68] are:

maximum electron density $n_e = 1.0 \times 10^6$ per cm^3 (day), 2.5×10^5 per cm^3 (night).

recombination coefficient $\alpha = 8 \times 10^{-11}$ cm^3/sec (day), 3×10^{-10} cm^3/sec (night).

On the basis of these figures the mean values $n_e = 6 \times 10^5$ per cm^3 and $\alpha = 2 \times 10^{-10}$ cm^3/sec will be used. The corresponding value for μ may be obtained from (69),

$$\mu = \alpha \frac{n_e^2}{n_O} . \tag{71}$$

Using $n = 3 \times 10^9$ per cm^3 for the total number density in the F_2 layer (i.e., per latitude 45°, Table 14), and assuming that the composition in this layer is 22% O by mass (corresponding to 33% O and 67% N_2 by volume), it is found that for the F_2 layer

$$n_O = \frac{0.22 \times 3 \times 10^9 \times m_1 \times 24}{m_1 \times 16} = 1 \times 10^9 \text{ per cm}^3 , \tag{71a}$$

where m_1 is the mass of an atom of unit atomic weight ($m_1 = 1.6489 \times 10^{-24}$ gram) and where $M = 24$ is used as the mean molecular weight in the F_2 layer. On the basis of the values above it is found from (71) that

$$\mu = 2 \times 10^{-10} \frac{36 \times 10^{10}}{1 \times 10^{9}} = 7 \times 10^{-8} \text{ per second,}$$

and Eq. (70) becomes $10^{1.96\theta} = 2\, n_O^{1/2}$, or

$$T = \frac{9878}{0.301 + 0.5 \log_{10} n_O}, \ ^\circ\text{K}. \tag{72}$$

This is the expression which results for the temperature of the isothermal exosphere, or free flight region, when the value $d = 2 \times 10^{-8}$ cm is used[7].

If the percentage composition by mass is the same at the height of the base of the exosphere, h_*, as in the F_2 layer — i.e., $n_O = 0.22\, n_*, M_* = 24$ — the temperature T_* at the base of the exosphere is determined by

$$T_* = \frac{9878}{0.5 \log_{10} 0.22\, n_* + 0.301} = \frac{19756}{\log_{10} n_* - 0.056}. \tag{73}$$

Replacing n_* in terms of T_* by means of relation (79) derived below, this may be written

$$T_* = \frac{19756}{\log_{10} \dfrac{M_* g'_*}{\sqrt{2}\, \pi\, d^2\, R_u T_*} - 0.056}, \tag{74}$$

where g'_* is the apparent gravity at the height h_*. For the purposes of this equation it is assumed that the atmosphere rotates with the earth as a solid out to the distance $r_* = a + h_*$, and therefore that Eq. (11) is applicable. If it should be assumed that the composition at h_* is 100% O ($M_* = 16$), then $n_O = n_*$ and the temperature equation is[7]

$$T_* = \frac{19756}{\log_{10} \dfrac{M_* g'_*}{\sqrt{2}\, \pi\, d^2\, R_u T_*} + 0.602}. \tag{75}$$

---

[7] When $d = 3 \times 10^{-8}$ cm is used, Eq. (72) becomes

$$T = \frac{9878}{0.653 + 0.5 \log n_O}, \tag{72a}$$

and Eqs. (74) and (75) become respectively

$$T_* = \frac{19756}{\log_{10} \dfrac{M_* g'_*}{\sqrt{2}\, \pi\, d^2\, R_u T_*} + 0.648} \quad (74a), \qquad T_* = \frac{19756}{\log_{10} \dfrac{M_* g'_*}{\sqrt{2}\, \pi\, d^2\, R_u T_*} + 1.306} \quad (75a).$$

These equations may be solved for T_*, provided M_* and g'_* are known. The apparent gravity g'_* is a quantity which varies very slowly with altitude and need be specified only very roughly. For this purpose, advantage may be taken of the results of model II — Tables 29-33 — which indicate that as far as order of magnitude is concerned the height h_* may be expected to lie somewhere within the limits of 500 and 1000 km. It is also reasonable to suppose that the relative amount of atomic oxygen present at the base of the exosphere lies between the limits given by $16 \leqq M_* \leqq 24$. On this basis, Table 38 has been prepared to show the possible values of T_*. Since there is some uncertainty concerning the exact value which should be used for d, the calculation was made for the two values $d = 2 \times 10^{-8}$ cm and $d = 3 \times 10^{-8}$ cm. No account is taken here of any possible variation of T_* with latitude, although this could have been done by using the appropriate value for n_0 in the F_2 layer at the equator — Eq. (71a).

It is seen from Table 38 that the value of T_* is fairly insensitive to the rather wide range of conditions imposed. For this reason an average value $T_* = 2500°K$ will be adopted.

Table 38

POSSIBLE VALUES FOR THE TEMPERATURE T_* IN THE EXOSPHERE

M_*	g'_* cm/sec^2	d cm	T_*
24	840.272~(500 km)	2×10^{-8}	2581
24	840.272~(500 km)	3×10^{-8}	2457
24	730.655~(1000 km)	2×10^{-8}	2598
24	730.655~(1000 km)	3×10^{-8}	2477
16	840.272~(500 km)	2×10^{-8}	2420
16	840.272~(500 km)	3×10^{-8}	2311
16	730.655~(1000 km)	2×10^{-8}	2435
16	730.655~(1000 km)	3×10^{-8}	2328

III-B. THE HEIGHT OF THE BASE OF THE EXOSPHERE (DYNAMICAL ORBIT REGION)

The height h_* of the base of the exosphere has already been discussed to some extent in Section II-F in connection with model II. The treatment given there was slightly ambiguous, inasmuch as the collision probability of a particle escaping to infinity was not specified as definitely as could be desired. The concept of the exosphere — or dynamical orbit region — is that there will exist a certain height h_* (actually a transition layer), situated somewhere above the F_2 layer, where the mean free path of neutral gas particles becomes so large and the collision frequency so small that particles moving upward from this height begin to behave more or less as

free bodies moving in a gravitational field. A particle moving upward from the height h_* will travel over large distances before it collides with another particle, the total number of collisions experienced depending upon the starting height h_* and the vertical distance travelled.

The probability of collision P of an atmospheric particle in travelling upward through a vertical distance L has already been discussed in Section II-F, where it was shown, Eq. (52), that $P = 2\pi d^2 \int_0^L n\, dh$. The height h_* of the base of the exosphere may be conveniently defined as the height at which the mean free path L of an upward-moving gas particle becomes infinite. Thus the height h_* is defined by the condition that the gas particle is certain to undergo a collision ($P = 1$) only when the mean free path is infinite ($L = \infty$). Or, stated in a slightly different manner, a particle moving upward from h_* would, if it had sufficient velocity (i.e., the escape velocity), travel to infinity experiencing only a single collision with another particle. On this basis, the relation which defines h_* is†

$$1 = \sqrt{2}\,\pi\, d^2 \int_{h_*}^{\infty} n\, dh \ . \tag{76}$$

From the hydrostatic equation $\left(dp/p = -Mg'dh/R_uT = -dh/H_1\right.$, see (53a)$\left.\right)$ and the equation of state ($p = nkT$), the vertical distribution of the particle density (number density) above a height h_* may be expressed by

$$n = n_* \frac{T_*}{T} e^{-\int_{h_*}^{h} \frac{Mg'}{R_uT} dh} = n_* \frac{T_*}{T} e^{-\int_{h_*}^{h} \frac{dh}{H}} , \tag{77}$$

where $H = kT/mg' = R_uT/Mg'$ is the scale height. Since in model III the region above h_* is considered to be isothermal, $T = T_*$ is to be used in the region $h > h_*$. Consider now a particle moving vertically upward from h_* out to infinity. As far as the collision probability of this particle is concerned, this depends only upon the total number of particles it passes through above h_* and not upon how these particles are distributed in the vertical. Therefore it is not necessary to know the actual distribution of M (i.e., n) but only the total number of particles N_* above h_* contained in a column of unit cross section. The total number of particles N_* may be obtained from the simple concepts of the scale height.

Although the scale height was discussed previously in Section II-F, it is instructive to examine this quantity from a slightly different point of view. Consider the pressure p_* at a given (but arbitrary) height h_* in the atmosphere. This pressure is simply the weight of the total atmosphere above h_* contained in a column of unit cross section, and is therefore expressed by $p_* = \int_{h_*}^{\infty} \rho g'\, dh$. Suppose now that the actual atmosphere *above* h_* is imagined to be replaced by an equivalent atmosphere having the constant density ρ_* and the constant temperature T_*, and that this equivalent atmospheric layer has exactly the correct thickness to give the same

† The value $P = 1$ used here is considered the correct value to use in order to define the height h_*. The value $P = 1/10$ used in connection with model II is somewhat ambiguous and is unnecessarily small.

pressure p_* as before. Also, as a further property specified in the definition of the equivalent layer, assume that gravity is constant with the value g'_* throughout this layer. Denoting this thickness by the quantity H_*, we have the relation

$$p_* = \int_{h_*}^{\infty} \rho g' dh = \int_{h_*}^{h_*+H_*} \rho_* g'_* dh = \rho_* g'_* \int_{h_*}^{h_*+H_*} dh = \rho_* g'_* H_* \ , \tag{77a}$$

which defines H_*. It is evident that the equivalent layer has the properties of an incompressible fluid and therefore does not satisfy the equation of state. At the level h_*, however, the equation of state $p_*/\rho_* = R_u T_*/M_*$ is still valid and, when combined with (77a), yields the relation $H_* = R_u T_*/M_* g'_*$. This gives the thickness of the equivalent isothermal incompressible (i.e., homogeneous) layer and is called the scale height. Since, in deriving relation (77a), there were no restrictions concerning the amount of dissociation or of diffusion equilibrium which might be present above h_* in the actual atmosphere, the value of the scale height is unaffected by the presence of these processes. Since $\rho = \rho_*$ is constant in the homogeneous layer, it follows from (18) that neither n nor M are necessarily constant in this layer, but only that the product Mn = constant = $M_* n_*$. It does not appear that this concept of the scale height, (77a), is capable of yielding any information concerning the value of N_*.

Suppose now that the actual atmosphere *above* h_* is imagined to be replaced by a second hypothetical atmosphere having the same mass and therefore giving the same pressure p_* as the actual atmosphere, but for which the temperature, composition, and gravity are assumed constant, with the values T_*, M_*, and g'_* respectively. Unlike the first case, in which that atmosphere above h_* was considered as an incompressible fluid, in this second case the atmosphere behaves as a gas (is compressible) and obeys the equation of state. Theoretically, this atmosphere will extend to infinity. It is evident that even though diffusion equilibrium may exist in the actual atmosphere, this second hypothetical atmosphere will give the correct value for the total number of particles N_* provided no dissociation occurs above h_* [8]. It is also evident that the scale height has the same value as before — i.e., $H = H_* = R_u T_*/M_* g'_*$. Using this value for H, the number density equation, (77), becomes simply

$$n = n_* \, e^{-\frac{(h - h_*)}{H_*}} \ . \tag{78}$$

The total number of particles N_* is therefore obtained by the integration

$$N_* = \int_{h_*}^{\infty} n \, dh = n_* H_* \equiv n_* \frac{R_u T_*}{M_* g'_*} \ . \tag{78a}$$

[8] The simple procedure used here for obtaining N_* is valid, since, in model III, all dissociation processes which occur are assumed to have taken place below h_*. In particular, all dissociation is assumed to take place below the level of diffusion equilibrium, h_d — see Section III-D. If dissociation should be present at levels above h_*, it is evident that it would not be possible to replace the atmosphere above h_* by an equivalent (same mass) atmosphere of constant composition M_* and still obtain the correct value for N_*. Since dissociation requires that H change with height, in order to calculate the correct value of N_* in this case it would be necessary to have information concerning the variation of H with height.

In this second concept H_* is simply interpreted, (78), as the increase in height necessary for n to decrease to $1/e$ of its value at n_*. (Also, see Chapman, Ref. 15, pp. 489-492.)

Using the result contained in (78a), it follows from (76) that

$$n_* = \frac{1}{\sqrt{2}\,\pi\, d^2\, H_*} \equiv \frac{M_* g'_*}{\sqrt{2}\,\pi\, d^2\, R_u T_*} \,. \tag{79}$$

This is essentially the equation which defines the height h_* of the base of the exosphere.

The height h_* may now be obtained by applying Eq. (77) between the level h_0 (the height of the F_2 layer) and the level h_* (the height of the base of the exosphere). In this interval it will be assumed that the temperature variation is linear, such that $T = T_0 + \alpha(h - h_0)$, where $\alpha = (T_* - T_0)/(h_* - h_0)$. Since in model III the atmosphere will be treated on the basis that complete diffusion equilibrium exists beginning at about 100 km above the F_2 layer, it follows that the molecular weight M_* will be less than M_0. For the purpose of determining h_* it will be assumed that the variation of M may be approximated by the linear relation $M = M_0 - \beta\,(h - h_0)$, where $\beta = (M_0 - M_*)/(h_* - h_0)$.

It follows from Eq. (77) that

$$n_* = \frac{M_* g'_*}{\sqrt{2}\,\pi\, d^2\, R_u T_*} = n_0 \frac{T_0}{T_*} \exp - \left[\frac{\bar{g}'}{R_u} \int_{h_0}^{h_*} \frac{M_0 - \beta(h - h_0)}{T_0 + \alpha(h - h_0)}\, dh \right]$$

$$= n_0 \frac{T_0}{T_*} \exp - \left[\frac{\bar{g}'}{R_u} \int_{r_0}^{r_*} \frac{M_0 - \beta(r - r_0)}{T_0 - \alpha(r - r_0)}\, dr \right] \tag{80}$$

where $r = a + h$, and $g' = g_a(a/r)^2 - r\,\Omega^2 \cos\theta$ is the apparent gravity. In comparison with the uncertainty involved in the molecular weight and temperature, the variation in gravity may be neglected in the interval $(h_* - h_0)$ and it is sufficiently accurate here to use a mean value $\bar{g}'$. Performing the integration, Eq. (80) may be written

$$n_* = \frac{M_* g'_*}{\sqrt{2}\,\pi\, d^2\, R_u T_*} = n_0 \frac{T}{T_*} \exp - \left\{ \frac{\bar{g}'}{R_u} \left[\frac{M_0}{\alpha} \left(\log\,[\alpha(r_* - r_0) + T_0] - \log T_0 \right) \right.\right.$$

$$\left.\left. - \beta \left(\frac{r_* - r_0}{\alpha} - \frac{T_0}{\alpha^2} \log\,[\alpha(r_* - r_0) + T_0] + \frac{T_0}{\alpha^2} \log T_0 \right) \right] \right\} \,. \tag{81}$$

Inserting $\alpha = (T_* - T_o)/(r_* - r_o)$ and $\beta = (M_o - M_*)/(r_* - r_o)$, this gives the relation

$$\frac{M_* g'_*}{\sqrt{2}\,\pi\, d^2\, R_u T_*} = n_o \frac{T_o}{T_*} \exp - \left\{ \frac{\bar{g}'}{R_u} \left[M_o \left(\frac{r_* - r_o}{T_* - T_o} \right) \log \frac{T_*}{T_o} \right.\right.$$

$$\left.\left. - \frac{M_* - M_o}{T_* - T_o} \left(\left[r_* - r_o \right] \left[1 - \frac{T_o}{T_* - T_o} \log \frac{T_*}{T_o} \right] \right) \right] \right\} . \qquad (82)$$

The height h_* of the exosphere $(h_* = r_* - a)$ is found by numerical solution of this equation for r_*, using $T_* = 2500°K$ and the following values for the F_2 layer:

Latitude 0°: h_o = 400 km, T_o = 1800°K, M_o = 24, a = 6378.4 km

Latitude 45°: h_o = 300 km, T_o = 1100°K, M_o = 24.35, a = 6367.5 km

Although the exact value of M_* is as yet unknown (since this depends upon the results of a diffusion equilibrium calculation), it appears safe to assume that the composition must lie between the limits $24 > M_* > 12$. The particle diameter d may likewise be taken to lie within the limits 2×10^{-8} cm $< d < 3 \times 10^{-8}$ cm. On the basis of these limits, a range of values for h_* is obtained as shown in Table 39. From these results it is believed satisfactory to adopt the average values h_* = 750 km at lat. 0°, and h_* = 650 km at lat. 45°. These values are not greatly different from those obtained for model II.

Table 39

POSSIBLE VALUES FOR THE HEIGHT h_* OF THE BASE OF THE EXOSPHERE

(Calculated From Eq.(82))

Latitude, θ	Molecular Weight, M_*	Particle Diameter, d	Calculated Height, h_*
0°	24	2×10^{-8} cm	614 km
0°	24	3×10^{-8} cm	691 km
0°	16	2×10^{-8} cm	617 km
0°	16	3×10^{-8} cm	682 km
0°	12	2×10^{-8} cm	790 km
0°	12	3×10^{-8} cm	900 km
45°	24.35	2×10^{-8} cm	517 km
45°	24.35	3×10^{-8} cm	576 km
45°	16	2×10^{-8} cm	514 km
45°	16	3×10^{-8} cm	565 km
45°	12	2×10^{-8} cm	685 km
45°	12	3×10^{-8} cm	772 km

III-C. DIFFUSION EQUILIBRIUM

It seems reasonable to suppose that at sufficiently great heights above the earth's surface, the processes, such as convection and turbulence, which cause mixing of the atmosphere (and therefore constant composition) will become inoperative, and that the constituent gases of the atmosphere will then become distributed in the vertical according to their molecular weights, with a greater concentration of heavy gases below and of light gases above. Thus, when the particle densities of the gases are distributed in the vertical in such a way that each constituent is in gravity equilibrium with its own partial pressure (Dalton's law) at all heights above a certain lower level, the atmosphere above this level is said to be in diffusion equilibrium. The minimum height above which this state of affairs exists will be referred to as the level of diffusion equilibrium.

An analysis of the diffusion or settling-out process in an atmospheric gas mixture has been given by Maris[69] and Epstein[70]. Calculations of the composition of the upper atmosphere at various heights on the basis of diffusion equilibrium have been made by Chapman and Milne[71] (1920), and by Maris[69] (1928-1929). Chapman and Milne assumed that diffusion equilibrium would exist beginning in the stratosphere at heights of the order of 20 to 50 km; and, since their analysis was made before the high ionosphere temperatures were known, they assumed the remainder of the upper atmosphere above 50 km to be at the constant low temperature 219°C (492°K). Maris concluded that diffusion equilibrium must exist above 100 km and assumed that the temperature of the upper atmosphere never exceeds 360°C (633°K). In view of the high ionosphere temperatures which are now believed to exist above 100 km, the results of these two investigations are no longer applicable, and it is therefore necessary to consider anew the effects of diffusion equilibrium on the basis of the ionosphere temperatures which have been presented.

For this purpose advantage may be taken of the results of Mitra and Rakshit[35] (1938) who — realizing the implications of the high ionosphere temperatures in this connection — investigated diffusion equilibrium in the upper atmosphere on the basis of the high F region temperatures. They assumed in their calculations a temperature of 300°K at 100 km, increasing linearly to 1100°K at 300 km — the same temperature distribution as used in the present study for the atmosphere at lat. 45° (Fig. 7). Since the results of their calculations show that complete diffusion equilibrium will certainly exist above 400 km at lat. 45°, this figure will be adopted as the height of the diffusion equilibrium level at lat. 45°. Similar results are not available corresponding to the vertical temperature distribution used at the equator (Fig. 5), and in view of the fact that these temperatures are higher than those at lat. 45°, 500 km will be adopted as the height of the diffusion equilibrium level at lat. 0°.

III-D. DENSITY CALCULATION FOR THE REGION BETWEEN THE F_2 LAYER AND THE LEVEL OF DIFFUSION EQUILIBRIUM

In order to carry out the calculation of the vertical distribution of density above the F_2 layer, the atmosphere above this level must be treated as three separate regions — the region between the F_2 layer and the level of diffusion equilibrium,

the region between the level of diffusion equilibrium and the base of the exosphere, and the region of the isothermal exosphere extending outward into space. As pointed out above — Section III-B — the temperature is assumed to increase linearly between the F_2 layer at distance r_o from the center of the earth ($r_o = a + h_o$) and the base of the exosphere at distance r_* ($r_* = a + h_*$). The temperature at any level r in the region $r_o \leqq r \leqq r_*$ is determined by

$$\left.\begin{aligned} T &= T_o + \alpha\,(r - r_o), \\ \alpha &= \frac{T_* - T_o}{r_* - r_o}\,. \end{aligned}\right\} \qquad (83)$$

At the equator, $\alpha = 2 \times 10^{-5}$ °K/cm; at lat. 45°, $\alpha = 4 \times 10^{-5}$ °K/cm. If the subscript d is used to denote the level of diffusion equilibrium, then since r_d is less than r_* it follows that (83) also gives the temperature distribution in the first region to be considered — $r_o \leqq r \leqq r_d$. Consideration must next be given to the distribution of the mean molecular weight M in this region.

Recent observational evidence from ionospheric radio reflections in the tropics[72], together with theoretical considerations of physical processes in the upper atmosphere, strongly suggest the existence, above the F_2 layer, of an additional ionized layer called the G layer, which is situated at heights of the order of 400 to 700 km[73]. The existence of a G layer is interpreted as indicating that the nitrogen must be dissociated at these levels, since otherwise the number density would not be great enough to produce, by ionization, a sufficiently large electron density to account for the reflection of radio waves. In the absence of any further, more precise, information concerning the dissociation of nitrogen, it seems permissible — and is at the same time convenient — to assume, as an average condition, that complete dissociation of nitrogen exists beginning at the level of diffusion equilibrium. Accordingly, all nitrogen will be assumed to exist in the atomic state beginning at the height h_d, and the composition at this level will be that corresponding to complete dissociation of a mixture originally composed of O_2 and N_2 in the proportions shown at 83 km in Tables 7 and 8. We thus have the following conditions upon which the calculations will be based:

Latitude, 0°

F_2 layer: h_o = 400 km, composition = 33% O + 67% N_2 by volume, M_o = 24.00, T_o = 1800°K
Level of diffusion equilibrium: h_d = 500 km, composition = 20% O + 80% N by volume, M_d = 14.40, T_d = 2000°K

Latitude, 45°

F_2 layer: h_o = 300 km, composition = 30.5% O + 69.5% N_2 by volume, M_o = 24.35, T_o = 1100°K
Level of diffusion equilibrium: h_d = 400 km, composition = 20% O + 80% N by volume, M_d = 14.40, T_d = 1500°K

Although the composition at 83 km at lat. 45° — 30.5% O + 69.5% N_2 — would lead to the value M_d = 14.33 (for 18% O + 82% N), it will be noted that the value M_d = 14.40 (20% O + 80% N) has been used instead. This has but negligible effect on the calculations and allows the convenience of having the same composition at the diffusion level at both latitudes.

Between the heights h_o and h_d a linear variation of the molecular weight will be assumed, as given by the relation

$$M = M_o - \beta\,(r - r_o) \text{ and } \beta = \frac{M_o - M_d}{r_d - r_o}, \text{ for } r_o \leqq r \leqq r_d\,. \tag{84}$$

At the equator, $\beta = 9.60 \times 10^{-7}$ 1/cm; at lat. 45°, $\beta = 9.95 \times 10^{-7}$ 1/cm. From Eqs.(9) and (10) the pressure p in the region $r_o \leqq r \leqq r_d$ is given by[9]

$$\log \frac{p}{p_o} = -\frac{1}{R_u} \int_{r_o}^{r} \frac{Mg'}{T}\, dr\,.$$

---

[9] Introducing (83) and (84) and the relation (11) for g', the pressure equation may be written

$$\log \frac{p}{p_o} = -\frac{1}{R_u} \int_{r_o}^{r} \frac{(M - \beta r)\left[g_a\left(\frac{a}{r}\right)^2 - r\Omega^2 \cos\theta\right]}{T_o + \alpha\,(r - r_o)}\, dr$$

$$- \frac{(M_o + \beta r_o)}{R_u} \int_{r_o}^{r} \frac{\left[g_a\left(\frac{a}{r}\right)^2 - r\Omega^2 \cos^2\theta\right]}{T_o + \alpha\,(r - r_o)}\, dr\,. \tag{84a}$$

The second integral has already been evaluated and is given as Eq.(14b). The first integration is readily carried out yielding

$$- \frac{1}{R_u} \int_{r_o}^{r} \frac{(M - \beta r)\left[g_a\left(\frac{a}{r}\right)^2 - r\Omega^2 \cos^2\theta\right]}{T_o + \alpha\,(r - r_o)}\, dr$$

$$= -\frac{1}{R_u}\,[M_o\alpha + \beta\,(T_o - \alpha r_o)]\left\{\left[\frac{g_a a^2}{(T_o - \alpha r_o)^2} + \frac{\Omega^2\,(T_o - \alpha r_o)}{\alpha^3}\right] \log \frac{T_o + \alpha\,(r_* - r_o)}{T_o}\right.$$

$$\left. - \frac{g_a a^2}{(T_o - \alpha r_o)^2} \log \frac{r_*}{r_o} - \frac{\Omega^2 \cos^2\theta}{\alpha^2}\,(r_* - r_o)\right\} + (r_* - r_o)\left[\frac{M_o g_a a^2}{r_o r_*\,(T_o - \alpha r_o)}\right.$$

$$\left. + \frac{\beta}{2\alpha}\,\Omega^2 \cos^2\theta\,(r_* + r_o)\right]\,. \tag{84b}$$

By combining (14b) and (84b) it is therefore possible to calculate $\log p/p_o$ exactly, for the case with M, T, and g' variable. However, these expressions are so involved that it is preferable to use small intervals with the simpler expression (86).

As in model II, it is assumed that the atmosphere rotates with the earth as a solid up to the base of the exosphere. Introducing (83) and (84), and assuming that the integration will be carried out step-wise for individual intervals $\Delta r = r_{i+1} - r_i$ which are sufficiently small that an average value $\bar{g}_i'$ may be used in each interval, the formula used for calculating the pressure becomes

$$\frac{p_{i+1}}{p_i} = \exp - \left[\frac{\bar{g}_i'}{R_u} \int_{r_i}^{r_{i+1}} \frac{[M_i - \beta(r - r_i)]}{[T_i + \alpha(r - r_i)]} \, dr \right]. \tag{85}$$

Performing the integration — see (81) — this gives the pressure formula

$$\frac{p_{i+1}}{p_i} = \exp - \left\{ \frac{\bar{g}_i'}{R_u} \left[\frac{M_i}{\alpha} \left\{ \log \left[\alpha(r_{i+1} - r_i) + T_i\right] - \log T_i \right\} - \beta \left\{ \frac{r_{i+1} - r_i}{\alpha} - \frac{T_i}{\alpha^2} \log \left[\alpha(r_{i+1} - r_i) + T_i\right] + \frac{T_i}{\alpha^2} \log T_i \right\} \right] \right\}. \tag{86}$$

Having the pressure, temperature, and mean molecular weight, the density is calculated as usual from the equation of state, Eq.(16).

III-E. DENSITY CALCULATION FOR THE REGION BETWEEN THE LEVEL OF DIFFUSION EQUILIBRIUM AND THE BASE OF THE EXOSPHERE

Above the level h_d of diffusion equilibrium the gases begin to separate according to their individual molecular weights, and it is necessary to determine the density distribution separately for each constituent gas. Let the subscript x denote a constituent gas. According to Dalton's law of partial pressures, each constituent x of the mixture behaves as though it alone were present, and we have

$$dp_x = - \rho_x g' dr \ , \ p_x = \rho_x \frac{R_u}{M_x} T \ , \text{ and}$$

$$\frac{p_x}{p_{xd}} = \exp \left[- \frac{M_x}{R_u} \int_{r_d}^{r} \frac{g'}{T} \, dr \right]. \tag{87}$$

Making use of the equation of state and introducing $g' = g_a(a/r)^2 - r\,\Omega^2 \cos^2\theta$ and $T = T_d + \alpha(r - r_d)$, Eq.(87) yields the density relation

$$\frac{\rho_x}{\rho_{xd}} = \frac{T_d}{T_d + \alpha\,(r - r_d)} \exp - \frac{M}{R_u} \left\{ (r - r_d) \left[\frac{g_a a^2}{r r_d (T_d - \alpha r_d)} - \frac{\Omega^2 \cos^2\theta}{\alpha} \right] \right.$$

$$\left. - \left[\frac{\alpha g_a a^2}{(T_d - \alpha r_d)^2} + \frac{(T_d - \alpha r_d)\Omega^2 \cos^2\theta}{\alpha^2} \right] \log \frac{T_d}{T_d + \alpha(r - r_d)} - \frac{\alpha}{(T_d - \alpha r_d)^2}\, g_a a^2 \log \frac{r}{r_d} \right\}, \quad (88)$$

see Eq.(14b). This formula is used to calculate the partial densities from h_d up to the level of the base of the exosphere h_*. It is noted that since there are no approximations involved in this equation, it is not necessary to carry out the calculations step-wise by means of small height intervals.

Since the lighter gases become important in the diffusion equilibrium region above h_d, it is necessary in this region to consider hydrogen and helium as possible constituents of the atmosphere. No attempt will be made here to enter into a discussion of the controversial question regarding the existence of hydrogen and helium in the upper atmosphere[15],[46],[74],[75]. Since the existence of these elements has not been disproved, it will be assumed that hydrogen and helium are present and that at the level h_d of diffusion equilibrium the relative amounts present are approximately the same as in the troposphere (Table 6, p.16). Since all oxygen is dissociated at the level h_d, and since hydrogen has a lower dissociation potential than oxygen, it is not considered unreasonable to expect that all hydrogen will be dissociated at and above h_d, and it will be assumed that this is the case. The composition used at the level h_d for starting the calculations in the diffusion equilibrium region is given in Table 40†. The percentages of helium and especially of hydrogen are not exactly the same as those given in Table 6, but have been rounded off to an even number. In view of the order of accuracy of the analysis as a whole, this approximation seems entirely justified. Other atmospheric constituents which occur in the troposphere, such as Ar, CO_2, and H_2O are probably relatively unimportant in this region of the atmosphere and have been neglected.

Knowing the total density ρ_d at the level h_d (from the calculations of Section III-D), the partial densities ρ_{xd} at this level are determined from the relation

$$\rho_{xd} = n_{xd}\, m_{xd} = C_{xd}\, \rho_d\,, \quad (89)$$

---

† For Tables 40 through 45 see pages 125 through 130.

where n_{xd} is the partial number density and C_{xd} is the percentage composition by mass of the constituent x at the level of diffusion equilibrium ($h = h_d$). Using these values of ρ_{xd} (Table 40), the partial gas densities in the region from h_d to h_* are calculated according to Eq.(88). The total gas density ρ at any level is obtained as the sum of the partial densities, $\rho = \Sigma \rho_x$. The mean molecular weight M is determined from the relation[10] (Ref.(71), p.365)

$$M = \frac{1}{\sum \frac{\rho_x}{\rho} \frac{1}{M_x}}, \tag{90}$$

and the total pressure is then obtained from the equation of state, $p = \rho \frac{R_u}{M} T$. The percentage composition by mass, C_x, is determined by the ratios $C_x = \rho_x/\rho$. Since $\rho_x = m_x n_x = \rho C_x$, the partial number densities may be calculated from the relation

$$n_x = \frac{\rho_x}{M_x m_1} = \frac{\rho C_x}{M_x m_1}, \tag{91}$$

where m_1 is the mass of unit atomic weight ($m_1 = 1.6489 \times 10^{-24}$ gram). On the basis of the calculations described, the conditions obtaining at the base of the exosphere h_* are as shown in Table 41.

III-F. DENSITY CALCULATION FOR THE EXOSPHERE

In the free-flight region, or exosphere, above h_* it is no longer permissible to assume that the atmospheric particles rotate with the earth as a solid, and in this region, since the particles move in individual orbits, their motion will be governed by the condition of constant angular momentum as described in Section II-F. Since this condition requires that $\omega = (r_*/r)^2\Omega$, Eq.(61), the expression for the apparent gravity becomes

$$g' = g_a \left(\frac{a}{r}\right)^2 - r\omega^2 \cos^2\theta = g_a \left(\frac{a}{r}\right)^2 - \frac{r_*^4\Omega^2}{r^3} \cos^2\theta \cdot \tag{92}$$

---

[10] This may be shown as follows: The mean molecular weight M is defined by $M = \rho/nm_1$, where ρ is total density, n is total number density, and m_1 is the mass of a particle of unit atomic weight - see Eq.(18). This may also be written $M = \rho/m_1\Sigma n_x$. Eq.(18) also holds for the partial densities and we have $n_x = \rho_x/m_1 M_x$. Using this expression for n_x, it follows that

$$M = \frac{\rho}{m_1 \Sigma n_x} = \frac{\rho}{m_1 \sum \frac{\rho_x}{m_1 M_x}} = \frac{\rho}{\sum \frac{\rho_x}{M_x}} = \frac{1}{\sum \frac{\rho_x}{\rho} \frac{1}{M_x}}$$

Owing to the isothermal property of the exosphere, the density formula becomes relatively simple. Thus for the exosphere where $T = T_* = \text{const.}$, the variation in density is given by

$$\frac{\rho_x}{\rho_{x_*}} = \exp\left\{-\frac{M_{x_*}}{R_u T_*}\int_{r_*}^{r}\left[g_a\left(\frac{a}{r}\right)^2 - \frac{r_*^4\Omega^2}{r^3}\cos^2\theta\right]dr\right\}, \text{ or} \tag{93}$$

$$\frac{\rho_x}{\rho_{x_*}} = \exp\left\{-\frac{M_{x_*}}{R_u T_*}\left[g_a\frac{a^2}{r_*}\left(1-\frac{r_*}{r}\right) - \frac{1}{2}r_*^2\Omega^2\left(1-\frac{r_*^2}{r^2}\right)\cos^2\theta\right]\right\}. \tag{94}$$

The total density, mean molecular weight, and total pressure are calculated as explained in Section III-E.

The basic characteristics of atmospheric model III together with the methods employed in its calculation have now been completely described. The results of the calculations are given in Tables 42-45. The vertical distribution of the density ratio σ from the F_2 layer up to 1000 miles is plotted in Figs.33-36†. The corresponding vertical temperature distribution is shown in Figs.37 and 38.

IV. CONCLUSIONS

Three different atmospheric models have been treated, which, while exactly the same below the F_2 layer, have different properties and characteristics above this level.

As far as the atmosphere below the F_2 layer is concerned, the results derived here up to 120 km may be compared with those given by Warfield[13] — both studies were carried out independently and appeared at about the same time. To make this comparison, a plot of the density ratio and the mean molecular weight used (for lat. 45°) is shown in Figs. 39 and 40. Both calculations were based upon exactly the same vertical distribution of temperature, Table 3 and Fig. 3. It is seen from Fig. 39 that the density distribution is practically the same for both calculations, particularly up to about 80 km, where the dissociation of oxygen begins to take place. The slight differences shown are due mainly to the differences in the values used for the vertical distribution of composition (Fig. 40) and possibly, to some extent, to differences in the manner in which gravity has been treated.

---

† For Figs.33 through 44 see pages 131 through 142.

Above the F_2 layer a comparison may be made between the three atmospheric models considered here by using, for example, the values derived for lat. 45°; these are plotted in Fig. 41 (temperature), Fig. 42 (composition), and Fig. 43 (density ratio). Above 1000 km there is little doubt that model II, based on constant M, gives values for density which are much too low, and either model I or model III is much to be preferred in this region. Except for the uncertainties in the determination of T_* — which could have a considerable effect if the value used for T_* is much too high — it is believed that model III is the most acceptable of the three models considered.

An outstanding feature of Fig. 42 is the large vertical distance above h_d over which the composition for model III remains practically constant. This is the result of the fact that the atomic weights of nitrogen and oxygen are nearly equal and the circumstance that the atmosphere is composed almost entirely of these two elements at the level h_d. It is only above 3000 km that the presence of helium and hydrogen begins to have any appreciable effect in determining the composition. Above 10,000 km atomic hydrogen is the predominant element, and the composition again remains constant.

It was pointed out in connection with model I (Section II-E) that the vertical distribution of density obtained did not seem to be much affected by the particular value — 0.5, 7.0, 14.0 — used for M_L. This result is shown in Fig. 44, where it is seen that the three curves lie very close together. It is on the basis of this result that it is considered satisfactory to use adopted values for model I, as calculated for the single average value $M_L = 7.0$.

In view of the concepts leading to models I, II, and III, it appears unlikely that it would be necessary to consider as a possibility the condition $dT/dh < 0$ at any level above the F_2 layer. That is, the temperature above the F_2 layer may be expected to increase or at least to reach an isothermal condition, but not to decrease. However, it is realized that the atmosphere has been considered herein from a rather broad point of view, and it has not been possible in the time available to analyze all the various implications of the concepts used. In particular, the extremely high temperatures associated with model I, and even the considerably lower temperatures associated with the exosphere of models II and III, might imply such a large amount of escape of the atmospheric gas particles that the possibility of the occurrence of such high temperatures would have to be abandoned. In this connection the following remarks by Spitzer[67] are of particular interest.

> "It is difficult to reconcile the high temperatures found for the upper atmosphere of the earth with what is known about the atmosphere of Mars. It is well established that Mars has a considerable atmosphere, and Kuiper (Yerkes Observatory) has shown recently from infrared spectra that this atmosphere contains about as much carbon dioxide as does that of the earth. On the other hand, it is also well established that the velocity of escape from Mars is about ½ the velocity of escape from the earth. Since theoretical analysis shows that the shape of the radiation intensity-frequency curve is more important than the absolute intensity of the radiation, one would suppose that the temperature of the upper atmosphere of Mars would be about the same as for the earth. At such a high temperature the carbon and oxygen atoms would have left Mars long ago, in contradiction to the observed presence of these elements. The answer to this

dilemma is certainly not clear, since the various lines of evidence pointing to a high temperature for the upper atmosphere of the earth seem rather strong. However, one cannot wholly exclude the possibility that the temperature of the earth's upper atmosphere may be considerably less than that which we have been led to assume."

Although the implications of the high temperature as regards the escape of atmosphere present a problem of very real concern and one which must certainly be investigated, it must be pointed out again — as mentioned in Section II-B in connection with model I — that the escape process is greatly hindered by the presence of the earth's magnetic field if the gas is more or less completely ionized. Thus it appears that the escape process cannot be adequately discussed until more is known concerning the degree of ionization of the upper atmosphere above the F_2 layer. Model I, for example, although having a very high temperature at its limit, was assumed to be completely ionized there. Models II and III, on the other hand, although having a lower temperature, were assumed to consist mainly of neutral particles.

It was pointed out in Section I-A that the temperature (or more exactly, the quantity T/M in the F region may be deduced in two different ways from radio wave measurements: (1) by evaluating the scale height H in the reflecting layer from measurements of virtual height vs. reflected frequency, and (2) by evaluating the electron collision frequency ν_e in the reflecting layer from measurements of change in amplitude of the reflected wave. Although the presence of high kinetic temperatures in the F region seems to be fairly well established, it would be extremely valuable — and of fundamental importance — to have further theoretical investigations of the relation between the radio wave properties of the ionized layers and the quantities H and ν_e. Since it is the ratio T/M only which is determined by these methods — Eqs. (1) and (2) — the determination of the temperature itself is no more accurate than the value M used for the composition, which must be known or determined by independent means. Thus, there is a great need for more accurate information concerning the composition of the F region, and, in particular, the level at which the dissociation of nitrogen begins and the level at which the dissociation becomes complete.

Also, as pointed out in footnote [3], it would be a valuable contribution to the knowledge of the upper atmosphere if the extensive world-wide ionosphere data were analyzed and a deduction made of the corresponding temperature-height relationships. These results could then be analyzed to determine mean values for the diurnal, seasonal, and geographical variations in the height and temperature of the ionized layers. Work along these lines — based on the CRPL data published by the National Bureau of Standards — has been initiated at RAND. This will give, for example, information concerning the temperature characteristics of the polar atmosphere, information which is entirely lacking at present. It should also give values for the temperature of the ionosphere in the equatorial region which are more accurate than those which have been used here.

In conclusion, it may be pointed out that the results which have been presented here, especially those pertaining to the region above the F_2 layer, must be considered in the nature of a first attempt at the deduction of the vertical distribution of density up to extreme altitudes. It is to be expected that these values will have to be changed, more or less, as more theoretical results and experimental data become available.

Table 40

COMPOSITION ASSUMED AT THE BEGINNING OF THE REGION OF DIFFUSION EQUILIBRIUM, $h = h_d$

Lat. 0°: h_d = 500 km
= 310.7 mi

$\rho_d = 6.500 \times 10^{-15}$ gr/cm^3
$= 1.262 \times 10^{-14}$ slug/ft^3

Lat. 45°: h_d = 400 km
= 248.5 mi

$\rho_d = 1.120 \times 10^{-14}$ gr/cm^3
$= 2.174 \times 10^{-14}$ slug/ft^3

Element	O	N	He	H
% composition by volume	19.9994	80.0000	5×10^{-4}	1×10^{-4}
% composition by mass, C_{xd}	22.221-	77.778-	1.39×10^{-4}	6.0×10^{-6}
Lat. 0°: partial density ρ_{xd}, gr/cm^3	1.444×10^{-15}	5.056×10^{-15}	9.035×10^{-21}	3.90×10^{-22}
Lat. 0°: partial density ρ_{xd}, slug/ft^3	2.804×10^{-15}	9.817×10^{-15}	1.754×10^{-20}	7.57×10^{-22}
Lat. 45°: partial density ρ_{xd}, gr/cm^3	2.489×10^{-15}	8.960×10^{-15}	1.557×10^{-20}	6.72×10^{-22}
Lat. 45°: partial density ρ_{xd}, slug/ft^3	4.833×10^{-15}	1.740×10^{-14}	3.023×10^{-20}	1.30×10^{-21}

Table 41

CONDITIONS AT THE BASE OF THE EXOSPHERE, $h = h_*$

LATITUDE 0°

$h_* = 750$ km, $T_* = 2500°K$, $p_* = 1.57 \times 10^{-8}$ mb, $\rho_* = 1.083 \times 10^{-15}$ gr/cm^3, $n_* = 4.58 \times 10^7 \frac{1}{cm^3}$,

$= 466.0$ mi $= 4500°R$ $= 3.28 \times 10^{-8}$ lb/ft^2 $= 2.103 \times 10^{-15}$ slug/ft^3 $= 1.30 \times 10^{12} \frac{1}{ft^3}$

Element	O	N	He	H
Molecular weight	16.000	14.000	4.000	1.008
Partial density ρ_{x*}, gr/cm^3	2.022×10^{-16}	8.805×10^{-16}	4.675×10^{-21}	2.796×10^{-22}
Partial density ρ_{x*}, slug/ft^3	3.926×10^{-16}	1.710×10^{-15}	9.078×10^{-21}	5.429×10^{-22}
% composition by mass, C_{x*}	18.68	81.32	4.32×10^{-4}	2.58×10^{-5}

LATITUDE 45°

$h_* = 650$ km, $T_* = 2500°K$, $p_* = 1.53 \times 10^{-8}$ mb, $\rho_* = 1.055 \times 10^{-15}$ gr/cm^3, $n_* = 4.46 \times 10^7 \frac{1}{cm^3}$

$= 403.9$ mi $= 4500°R$ $= 3.20 \times 10^{-8}$ lb/ft^2 $= 2.049 \times 10^{-15}$ slug/ft^3 $= 1.26 \times 10^{12} \frac{1}{ft^3}$

Element	O	N	He	H
Molecular weight	16.000	14.000	4.000	1.008
Partial density ρ_{x*}, gr/cm^3	1.908×10^{-16}	8.636×10^{-16}	5.639×10^{-21}	3.542×10^{-22}
Partial density ρ_{x*}, lb/ft^3	3.705×10^{-16}	1.677×10^{-15}	1.095×10^{-20}	6.878×10^{-22}
% composition by mass C_{x*}	18.10	81.90	5.35×10^{-4}	3.36×10^{-5}

Table 42

ATMOSPHERIC MODEL III - VALUES OF TEMPERATURE, PRESSURE, AND DENSITY ABOVE THE F_2 LAYER

Latitude 0°. Engineering Units. p_a = 2115 lb/ft², ρ_a = 2.286 × 10⁻³ slug/ft³

Height h mi	Height h ft	Apparent Gravity g' ft/sec²	Temp T °R	Percentage Composition by Mass C_x: Atomic Oxygen	Atomic Nitrogen	Atomic Helium	Atomic Hydrogen	Mean Mol Wt M	Scale Height H ft	Pressure p lb/ft²	Pressure Ratio p/p_a	Density ρ slugs/ft³	Density Ratio σ ρ/ρ_a	Number Density n particles/ft³	Mean Particle Speed v ft/sec	$d = 2 \times 10^{-8}$ cm: Mean Free Path L ft	Mean Collision Freq ν 1/sec	$d = 3 \times 10^{-8}$ cm: Mean Free Path L ft	Mean Collision Freq ν 1/sec
248.5	1.312×10^6	28.393	3240	33% O	67% N_2	--	--	24.00	2.364×10^5	4.33×10^{-7}	2.04×10^{-10}	6.43×10^{-14}	2.82×10^{-11}	2.37×10^{13}	4.13×10^3	2.21×10^4	1.87×10^{-1}	9.81×10^3	4.22×10^{-1}
264.1	1.394×10^6	28.183	3330	--	--	--	--	21.60	2.720×10^5	3.12×10^{-7}	1.47×10^{-10}	4.08×10^{-14}	1.79×10^{-11}	1.67×10^{12}	4.43×10^3	3.14×10^4	1.41×10^{-1}	1.39×10^4	3.17×10^{-1}
279.6	1.476×10^6	27.976	3420	--	--	--	--	19.20	3.166×10^5	2.36×10^{-7}	1.11×10^{-10}	2.66×10^{-14}	1.17×10^{-11}	1.23×10^{12}	4.76×10^3	4.26×10^4	1.11×10^{-1}	1.89×10^4	2.51×10^{-1}
295.1	1.558×10^6	27.771	3510	--	--	--	--	16.80	3.740×10^5	1.86×10^{-7}	8.77×10^{-11}	1.79×10^{-14}	7.85×10^{-12}	9.43×10^{12}	5.15×10^3	5.58×10^4	9.24×10^{-2}	2.47×10^4	2.08×10^{-1}
310.7	1.640×10^6	27.568	3600	22.21	77.78	1.39×10^{-4}	6.00×10^{-6}	14.40	4.509×10^5	1.57×10^{-7}	7.41×10^{-11}	1.26×10^{-14}	5.54×10^{-12}	7.76×10^{12}	5.64×10^3	6.76×10^4	8.32×10^{-2}	3.00×10^4	1.88×10^{-1}
326.2	1.722×10^6	27.367	3690	21.79	78.21	1.58×10^{-4}	7.09×10^{-6}	14.39	4.659×10^5	1.31×10^{-7}	6.20×10^{-11}	1.03×10^{-14}	4.51×10^{-12}	6.31×10^{12}	5.71×10^3	8.30×10^4	6.87×10^{-2}	3.67×10^4	1.55×10^{-1}
341.8	1.804×10^6	27.169	3780	21.41	78.59	1.80×10^{-4}	8.34×10^{-6}	14.38	4.810×10^5	1.10×10^{-7}	5.20×10^{-11}	8.43×10^{-15}	3.69×10^{-12}	5.18×10^{12}	5.77×10^3	1.01×10^5	5.70×10^{-2}	4.49×10^4	1.29×10^{-1}
357.3	1.886×10^6	26.972	3870	20.99	79.01	2.03×10^{-4}	9.75×10^{-6}	14.38	4.961×10^5	9.32×10^{-8}	4.40×10^{-11}	6.97×10^{-15}	3.05×10^{-12}	4.28×10^{12}	5.84×10^3	1.22×10^5	4.77×10^{-2}	5.41×10^4	1.08×10^{-1}
372.8	1.968×10^6	26.778	3960	20.62	79.38	2.28×10^{-4}	1.13×10^{-6}	14.37	5.118×10^5	7.92×10^{-8}	3.74×10^{-11}	5.79×10^{-15}	2.53×10^{-12}	3.57×10^{12}	5.91×10^3	1.47×10^5	4.01×10^{-2}	6.53×10^4	9.04×10^{-2}
388.4	2.050×10^6	26.590	4050	20.26	79.74	2.56×10^{-4}	1.21×10^{-6}	14.36	5.272×10^5	6.76×10^{-8}	3.20×10^{-11}	4.83×10^{-15}	2.11×10^{-12}	2.97×10^{12}	5.97×10^3	1.77×10^5	3.39×10^{-2}	7.81×10^4	7.64×10^{-2}
403.9	2.133×10^6	26.396	4140	19.92	80.08	2.86×10^{-4}	1.53×10^{-6}	14.36	5.433×10^5	5.80×10^{-8}	2.74×10^{-11}	4.06×10^{-15}	1.77×10^{-12}	2.49×10^{12}	6.04×10^3	2.10×10^5	2.88×10^{-2}	9.32×10^4	6.49×10^{-2}
419.4	2.215×10^6	26.208	4230	19.59	80.41	3.18×10^{-4}	1.74×10^{-6}	14.35	5.590×10^5	5.00×10^{-8}	2.36×10^{-11}	3.42×10^{-15}	1.50×10^{-12}	2.10×10^{12}	6.10×10^3	2.49×10^5	2.45×10^{-2}	1.11×10^5	5.53×10^{-2}
435.0	2.297×10^6	26.012	4320	19.27	80.73	3.53×10^{-4}	1.99×10^{-6}	14.35	5.758×10^5	4.33×10^{-8}	2.04×10^{-11}	2.89×10^{-15}	1.27×10^{-12}	1.78×10^{12}	6.17×10^3	2.94×10^5	2.10×10^{-2}	1.30×10^5	4.74×10^{-2}
450.5	2.379×10^6	25.838	4410	18.95	81.05	3.94×10^{-4}	2.29×10^{-6}	14.34	5.919×10^5	3.72×10^{-8}	1.76×10^{-11}	2.45×10^{-15}	1.07×10^{-12}	1.50×10^{12}	6.23×10^3	3.48×10^5	1.79×10^{-2}	1.54×10^5	4.04×10^{-2}
466.0	2.461×10^6	25.656	4500	18.68	81.32	4.32×10^{-4}	2.58×10^{-6}	14.33	6.083×10^5	3.28×10^{-8}	1.55×10^{-11}	2.10×10^{-15}	9.21×10^{-13}	1.30×10^{12}	6.30×10^3	4.04×10^5	1.56×10^{-2}	1.79×10^5	3.52×10^{-2}
497.1	2.625×10^6	25.300	4500	18.12	81.88	5.24×10^{-4}	3.31×10^{-6}	14.32	6.174×10^5	2.51×10^{-8}	1.18×10^{-11}	1.61×10^{-15}	7.04×10^{-13}	9.91×10^{11}	6.30×10^3	5.28×10^5	1.20×10^{-2}	2.34×10^5	2.69×10^{-2}
528.2	2.789×10^6	24.952	4500	17.58	82.42	6.34×10^{-4}	4.24×10^{-6}	14.31	6.265×10^5	1.93×10^{-8}	9.11×10^{-12}	1.23×10^{-15}	5.40×10^{-13}	7.62×10^{11}	6.30×10^3	6.86×10^5	9.20×10^{-3}	3.05×10^5	2.07×10^{-2}
559.2	2.953×10^6	24.612	4500	17.06	82.94	7.65×10^{-4}	5.40×10^{-6}	14.30	6.355×10^5	1.49×10^{-8}	7.02×10^{-12}	9.51×10^{-16}	4.16×10^{-13}	5.89×10^{11}	6.31×10^3	8.89×10^5	7.10×10^{-3}	3.94×10^5	1.60×10^{-2}
590.3	3.117×10^6	24.278	4500	16.56	83.44	9.21×10^{-4}	6.86×10^{-6}	14.30	6.447×10^5	1.15×10^{-8}	5.44×10^{-12}	7.36×10^{-16}	3.22×10^{-13}	4.56×10^{11}	6.31×10^3	1.15×10^6	5.49×10^{-3}	5.12×10^5	1.24×10^{-2}
621.4	3.281×10^6	23.950	4500	16.07	83.92	1.11×10^{-3}	8.68×10^{-6}	14.29	6.539×10^5	8.94×10^{-9}	4.22×10^{-12}	5.71×10^{-16}	2.50×10^{-13}	3.54×10^{11}	6.32×10^3	1.48×10^6	4.27×10^{-3}	6.56×10^5	9.61×10^{-3}
683.5	3.609×10^6	23.316	4500	15.16	84.84	1.58×10^{-3}	1.38×10^{-4}	14.27	6.725×10^5	5.45×10^{-9}	2.57×10^{-12}	3.48×10^{-16}	1.52×10^{-13}	2.15×10^{11}	6.33×10^3	2.42×10^6	2.60×10^{-3}	1.08×10^6	5.86×10^{-3}
745.6	3.937×10^6	22.706	4500	14.31	85.68	2.24×10^{-3}	2.15×10^{-4}	14.25	6.913×10^5	3.36×10^{-9}	1.59×10^{-12}	2.16×10^{-16}	9.40×10^{-14}	1.33×10^{11}	6.33×10^3	3.94×10^6	1.61×10^{-3}	1.75×10^6	3.62×10^{-3}
807.8	4.265×10^6	22.119	4500	13.53	86.47	3.14×10^{-3}	3.33×10^{-4}	14.24	7.104×10^5	2.11×10^{-9}	9.96×10^{-13}	1.34×10^{-16}	5.88×10^{-14}	8.35×10^{10}	6.33×10^3	6.27×10^6	1.01×10^{-3}	2.79×10^6	2.23×10^{-3}
869.9	4.593×10^6	21.556	4500	12.79	87.20	4.36×10^{-3}	5.09×10^{-4}	14.22	7.297×10^5	1.34×10^{-9}	6.31×10^{-13}	8.50×10^{-17}	3.72×10^{-14}	5.30×10^{10}	6.33×10^3	9.88×10^6	6.40×10^{-4}	4.40×10^6	1.44×10^{-3}
932.0	4.921×10^6	21.013	4500	12.11	87.88	6.00×10^{-3}	7.70×10^{-4}	14.21	7.492×10^5	8.58×10^{-10}	4.05×10^{-13}	5.46×10^{-17}	2.39×10^{-14}	3.40×10^{10}	6.33×10^3	1.54×10^7	4.11×10^{-4}	6.86×10^6	9.25×10^{-4}
994.2	5.249×10^6	20.491	4500	11.48	88.51	8.19×10^{-3}	1.15×10^{-3}	14.20	7.690×10^5	5.58×10^{-10}	2.63×10^{-13}	3.53×10^{-17}	1.55×10^{-14}	2.20×10^{10}	6.33×10^3	2.38×10^7	2.67×10^{-4}	1.06×10^7	6.00×10^{-4}
1056	5.577×10^6	19.988	4500	10.89	89.09	1.11×10^{-2}	1.70×10^{-3}	14.18	7.892×10^5	3.65×10^{-10}	1.73×10^{-13}	2.31×10^{-17}	1.02×10^{-14}	1.44×10^{10}	6.34×10^3	3.61×10^7	1.75×10^{-4}	1.61×10^7	3.94×10^{-4}
1118	5.905×10^6	19.503	4500	10.34	89.64	1.49×10^{-2}	2.50×10^{-3}	14.17	8.095×10^5	2.42×10^{-10}	1.14×10^{-13}	1.54×10^{-17}	6.73×10^{-15}	9.60×10^9	6.34×10^3	5.45×10^7	1.16×10^{-4}	2.42×10^7	2.62×10^{-4}
1181	6.234×10^6	19.035	4500	9.814	90.16	1.97×10^{-2}	3.62×10^{-3}	14.16	8.301×10^5	1.63×10^{-10}	7.69×10^{-14}	1.03×10^{-17}	4.51×10^{-15}	6.43×10^9	6.34×10^3	8.14×10^7	7.80×10^{-5}	3.61×10^7	1.76×10^{-4}
1243	6.562×10^6	18.584	4500	9.350	90.62	2.63×10^{-2}	5.21×10^{-3}	14.15	8.511×10^5	1.10×10^{-10}	5.19×10^{-14}	6.95×10^{-18}	3.05×10^{-15}	4.36×10^9	6.35×10^3	1.20×10^8	5.28×10^{-5}	5.35×10^7	1.19×10^{-4}
1553	8.202×10^6	16.554	4500	7.379	92.50	9.72×10^{-2}	2.83×10^{-2}	14.04	9.624×10^5	1.79×10^{-11}	8.46×10^{-15}	1.13×10^{-18}	4.93×10^{-16}	7.08×10^8	6.36×10^3	7.38×10^8	8.64×10^{-5}	3.28×10^8	1.94×10^{-5}
1864	9.842×10^6	14.839	4500	5.936	93.62	.3105	.1274	13.77	1.095×10^6	3.61×10^{-12}	1.71×10^{-15}	2.23×10^{-19}	9.75×10^{-17}	1.43×10^8	6.43×10^3	3.64×10^9	1.76×10^{-6}	1.62×10^8	3.96×10^{-6}
2175	1.148×10^7	13.377	4500	4.836	93.80	.8740	.4885	12.98	1.289×10^6	9.02×10^{-13}	4.26×10^{-16}	5.24×10^{-20}	2.29×10^{-17}	3.57×10^7	6.63×10^3	1.47×10^{10}	4.52×10^{-7}	6.53×10^9	1.02×10^{-6}
2485	1.312×10^7	12.122	4500	3.947	92.25	2.186	1.616	11.13	1.659×10^6	2.90×10^{-13}	1.37×10^{-16}	1.44×10^{-20}	6.31×10^{-18}	1.14×10^7	7.15×10^3	4.56×10^{10}	1.57×10^{-7}	2.03×10^{10}	3.52×10^{-7}
2796	1.476×10^7	11.035	4500	3.156	87.40	4.836	4.606	8.18	2.478×10^6	1.27×10^{-13}	5.99×10^{-17}	4.64×10^{-21}	2.03×10^{-18}	5.01×10^6	8.33×10^3	1.04×10^{11}	8.00×10^{-8}	4.63×10^{10}	1.80×10^{-7}
3107	1.640×10^7	10.087	4500	2.389	77.22	9.272	11.12	5.26	4.217×10^6	7.56×10^{-14}	3.57×10^{-17}	1.78×10^{-21}	7.78×10^{-19}	3.00×10^6	1.04×10^4	1.75×10^{11}	5.95×10^{-8}	7.78×10^{10}	1.34×10^{-7}
3728	1.968×10^7	8.525	4500	1.010	42.86	20.02	36.10	2.28	1.153×10^7	4.70×10^{-14}	2.22×10^{-17}	4.78×10^{-22}	2.09×10^{-19}	1.85×10^6	1.58×10^4	2.82×10^{11}	5.61×10^{-8}	1.25×10^{11}	1.26×10^{-7}
4350	2.297×10^7	7.300	4500	.2973	15.90	23.62	60.19	1.50	2.046×10^7	3.80×10^{-14}	1.80×10^{-17}	2.54×10^{-22}	1.12×10^{-19}	1.50×10^6	1.95×10^4	3.48×10^{11}	5.61×10^{-8}	1.55×10^{11}	1.26×10^{-7}
4971	2.625×10^7	6.321	4500	8.13×10^{-3}	5.306	21.34	72.69	1.28	2.775×10^7	3.32×10^{-14}	1.57×10^{-17}	1.89×10^{-22}	8.29×10^{-20}	1.31×10^6	2.11×10^4	3.97×10^{11}	5.31×10^{-8}	1.77×10^{11}	1.19×10^{-7}
5592	2.953×10^7	5.527	4500	2.42×10^{-3}	1.881	18.00	80.10	1.19	3.405×10^7	2.99×10^{-14}	1.41×10^{-17}	1.59×10^{-22}	6.95×10^{-20}	1.18×10^6	2.19×10^4	4.43×10^{11}	4.94×10^{-8}	1.97×10^{11}	1.11×10^{-7}
6214	3.281×10^7	4.873	4500	8.14×10^{-3}	.7357	15.07	84.19	1.14	4.010×10^7	2.74×10^{-14}	1.29×10^{-17}	1.40×10^{-22}	6.12×10^{-20}	1.08×10^6	2.23×10^4	4.86×10^{11}	4.61×10^{-8}	2.15×10^{11}	1.04×10^{-7}
9320	4.921×10^7	2.862	4500	1.48×10^{-4}	2.31×10^{-2}	7.310	92.67	1.06	7.331×10^7	2.02×10^{-14}	9.54×10^{-18}	9.63×10^{-23}	4.22×10^{-20}	7.99×10^5	2.31×10^4	6.53×10^{11}	3.53×10^{-8}	2.91×10^{11}	7.95×10^{-8}
12427	6.562×10^7	1.880	4500	1.19×10^{-5}	2.61×10^{-3}	4.528	95.47	1.04	1.141×10^8	1.69×10^{-14}	7.98×10^{-18}	7.88×10^{-23}	3.45×10^{-20}	6.68×10^5	2.34×10^4	7.84×10^{11}	2.99×10^{-8}	3.48×10^{11}	6.72×10^{-8}
15534	8.202×10^7	1.329	4500	2.12×10^{-6}	5.87×10^{-4}	3.244	96.76	1.03	1.630×10^8	1.50×10^{-14}	7.07×10^{-18}	6.91×10^{-23}	3.03×10^{-20}	5.92×10^5	2.35×10^4	8.83×10^{11}	2.66×10^{-8}	3.94×10^{11}	5.99×10^{-8}
18641	9.842×10^7	0.989	4500	6.06×10^{-7}	1.99×10^{-4}	2.541	97.46	1.03	2.202×10^8	1.37×10^{-14}	6.49×10^{-18}	6.31×10^{-23}	2.76×10^{-20}	5.44×10^5	2.36×10^4	9.61×10^{11}	2.45×10^{-8}	4.26×10^{11}	5.51×10^{-8}
21748	1.148×10^8	0.764	4500	2.34×10^{-7}	8.71×10^{-5}	2.109	97.89	1.02	2.858×10^8	1.29×10^{-14}	6.08×10^{-18}	5.88×10^{-23}	2.58×10^{-20}	5.10×10^5	2.36×10^4	1.03×10^{12}	2.30×10^{-8}	4.56×10^{11}	5.17×10^{-8}
24855	1.312×10^8	0.609	4500	1.11×10^{-7}	4.56×10^{-5}	1.822	98.18	1.02	3.598×10^8	1.22×10^{-14}	5.77×10^{-18}	5.59×10^{-23}	2.45×10^{-20}	4.84×10^5	2.36×10^4	1.08×10^{12}	2.18×10^{-8}	4.79×10^{11}	4.91×10^{-8}
27961	1.476×10^8	0.496	4500	6.08×10^{-8}	2.71×10^{-5}	1.618	98.38	1.02	4.422×10^8	1.17×10^{-14}	5.54×10^{-18}	5.36×10^{-23}	2.34×10^{-20}	4.64×10^5	2.36×10^4	1.13×10^{12}	2.10×10^{-8}	5.02×10^{11}	4.72×10^{-8}
31068	1.640×10^8	0.412	4500	3.71×10^{-8}	1.76×10^{-5}	1.468	98.53	1.02	5.330×10^8	1.13×10^{-14}	5.36×10^{-18}	5.16×10^{-23}	2.26×10^{-20}	4.47×10^5	2.37×10^4	1.16×10^{12}	2.03×10^{-8}	5.18×10^{11}	4.56×10^{-8}
34175	1.804×10^8	0.347	4500	2.45×10^{-8}	1.23×10^{-5}	1.352	98.65	1.02	6.322×10^8	1.10×10^{-14}	5.21×10^{-18}	5.03×10^{-23}	2.20×10^{-20}	4.36×10^5	2.37×10^4	1.20×10^{12}	1.97×10^{-8}	5.31×10^{11}	4.44×10^{-8}
37282	1.968×10^8	0.297	4500	1.72×10^{-8}	9.08×10^{-6}	1.261	98.74	1.02	7.400×10^8	1.08×10^{-14}	5.08×10^{-18}	4.89×10^{-23}	2.15×10^{-20}	4.25×10^5	2.37×10^4	1.23×10^{12}	1.93×10^{-8}	5.45×10^{11}	4.34×10^{-8}

Table 43

ATMOSPHERIC MODEL III - VALUES OF TEMPERATURE, PRESSURE, AND DENSITY ABOVE THE F_2 LAYER

Latitude 0°. Metric Units. p_a = 1013 mb, $\rho_a = 1.177 \times 10^{-3}$ gm/cm³

Height h km	Height h mi	Apparent Gravity g' cm/sec²	Temp T °K	Percentage Composition by Mass C_x: Atomic Oxygen	Atomic Nitrogen	Atomic Helium	Atomic Hydrogen	Mean Mol Wt M	Scale Height H km	Pressure p millibars	Pressure Ratio p/p_a	Density ρ gram/cm³	Density Ratio σ ρ/ρ_a	Number Density n particles/cm³	Mean Particle Speed v cm/sec	$d = 2 \times 10^{-8}$ cm: Mean Free Path L cm	$d = 2 \times 10^{-8}$ cm: Mean Collision Freq ν 1/sec	$d = 3 \times 10^{-8}$ cm: Mean Free Path L cm	$d = 3 \times 10^{-8}$ cm: Mean Collision Freq ν 1/sec
400	248.5	865.42	1800	33%O	67%N_2			24.00	7.21×10	2.07×10^{-7}	2.04×10^{-10}	3.31×10^{-14}	2.82×10^{-11}	8.37×10^{8}	1.26×10^{5}	6.74×10^{6}	1.87×10^{-1}	2.99×10^{5}	4.22×10^{-1}
425	264.1	859.02	1850					21.60	8.29×10	1.49×10^{-7}	1.47×10^{-10}	2.10×10^{-14}	1.79×10^{-11}	5.89×10^{8}	1.35×10^{5}	9.58×10^{6}	1.41×10^{-1}	4.24×10^{5}	3.17×10^{-1}
450	279.6	852.70	1900					19.20	9.65×10	1.13×10^{-7}	1.11×10^{-10}	1.37×10^{-14}	1.17×10^{-11}	4.33×10^{8}	1.45×10^{5}	1.30×10^{7}	1.11×10^{-1}	5.77×10^{5}	2.51×10^{-1}
475	295.1	846.45	1950					16.80	1.14×10^{2}	8.89×10^{-8}	8.77×10^{-11}	9.21×10^{-15}	7.85×10^{-12}	3.33×10^{8}	1.57×10^{5}	1.70×10^{7}	9.24×10^{-2}	7.52×10^{5}	2.08×10^{-1}
500	310.7	840.27	2000	22.21	77.78	1.39×10^{-4}	6.00×10^{-6}	14.40	1.37×10^{2}	7.51×10^{-8}	7.41×10^{-11}	6.50×10^{-15}	5.54×10^{-12}	2.74×10^{8}	1.72×10^{5}	2.06×10^{7}	8.32×10^{-2}	9.13×10^{5}	1.88×10^{-1}
525	326.2	834.16	2050	21.79	78.21	1.58×10^{-4}	7.09×10^{-6}	14.39	1.42×10^{2}	6.28×10^{-8}	6.20×10^{-11}	5.30×10^{-15}	4.51×10^{-12}	2.23×10^{8}	1.74×10^{5}	2.53×10^{7}	6.87×10^{-2}	1.12×10^{6}	1.55×10^{-1}
550	341.8	828.11	2100	21.41	78.59	1.80×10^{-4}	8.34×10^{-6}	14.38	1.47×10^{2}	5.27×10^{-8}	5.20×10^{-11}	4.34×10^{-15}	3.69×10^{-12}	1.83×10^{8}	1.76×10^{5}	3.08×10^{7}	5.70×10^{-2}	1.37×10^{6}	1.29×10^{-1}
575	357.3	822.12	2150	20.99	79.01	2.03×10^{-4}	9.75×10^{-6}	14.38	1.51×10^{2}	4.46×10^{-8}	4.40×10^{-11}	3.59×10^{-15}	3.05×10^{-12}	1.51×10^{8}	1.78×10^{5}	3.73×10^{7}	4.77×10^{-2}	1.65×10^{6}	1.08×10^{-1}
600	372.8	816.20	2200	20.62	79.38	2.28×10^{-4}	1.13×10^{-5}	14.37	1.56×10^{2}	3.79×10^{-8}	3.74×10^{-11}	2.98×10^{-15}	2.53×10^{-12}	1.26×10^{8}	1.80×10^{5}	4.49×10^{7}	4.01×10^{-2}	1.99×10^{6}	9.04×10^{-2}
625	388.4	810.45	2250	20.26	79.74	2.56×10^{-4}	1.21×10^{-5}	14.36	1.61×10^{2}	3.24×10^{-8}	3.20×10^{-11}	2.49×10^{-15}	2.11×10^{-12}	1.05×10^{8}	1.82×10^{5}	5.38×10^{7}	3.39×10^{-2}	2.38×10^{6}	7.64×10^{-2}
650	403.9	804.56	2300	19.92	80.08	2.86×10^{-4}	1.53×10^{-5}	14.36	1.66×10^{2}	2.78×10^{-8}	2.74×10^{-11}	2.09×10^{-15}	1.77×10^{-12}	8.81×10^{7}	1.84×10^{5}	6.41×10^{7}	2.88×10^{-2}	2.84×10^{6}	6.49×10^{-2}
675	419.4	798.82	2350	19.59	80.41	3.18×10^{-4}	1.74×10^{-5}	14.35	1.70×10^{2}	2.39×10^{-8}	2.36×10^{-11}	1.76×10^{-15}	1.50×10^{-12}	7.43×10^{7}	1.86×10^{5}	7.60×10^{7}	2.45×10^{-2}	3.37×10^{6}	5.53×10^{-2}
700	435.0	792.85	2400	19.27	80.73	3.53×10^{-4}	1.99×10^{-5}	14.35	1.75×10^{2}	2.07×10^{-8}	2.04×10^{-11}	1.49×10^{-15}	1.27×10^{-12}	6.30×10^{7}	1.88×10^{5}	8.97×10^{7}	2.10×10^{-2}	3.97×10^{6}	4.74×10^{-2}
725	450.5	787.54	2450	18.95	81.05	3.94×10^{-4}	2.29×10^{-5}	14.34	1.80×10^{2}	1.78×10^{-8}	1.76×10^{-11}	1.26×10^{-15}	1.07×10^{-12}	5.31×10^{7}	1.90×10^{5}	1.06×10^{7}	1.79×10^{-2}	4.71×10^{6}	4.04×10^{-2}
750	466.0	781.98	2500	18.68	81.32	4.32×10^{-4}	2.58×10^{-5}	14.33	1.85×10^{2}	1.57×10^{-8}	1.55×10^{-11}	1.08×10^{-15}	9.21×10^{-13}	4.58×10^{7}	1.92×10^{5}	1.23×10^{7}	1.56×10^{-2}	5.46×10^{6}	3.52×10^{-2}
800	497.1	771.15	2500	18.12	81.88	5.24×10^{-4}	3.31×10^{-5}	14.32	1.88×10^{2}	1.20×10^{-8}	1.18×10^{-11}	8.28×10^{-16}	7.04×10^{-13}	3.50×10^{7}	1.92×10^{5}	1.61×10^{7}	1.20×10^{-2}	7.14×10^{6}	2.69×10^{-2}
850	528.2	760.55	2500	17.58	82.42	6.34×10^{-4}	4.24×10^{-5}	14.31	1.91×10^{2}	9.23×10^{-9}	9.11×10^{-12}	6.36×10^{-16}	5.40×10^{-13}	2.69×10^{7}	1.92×10^{5}	2.09×10^{7}	9.20×10^{-3}	9.29×10^{6}	2.07×10^{-2}
900	559.2	750.16	2500	17.06	82.94	7.65×10^{-4}	5.40×10^{-5}	14.30	1.94×10^{2}	7.12×10^{-9}	7.02×10^{-12}	4.90×10^{-16}	4.16×10^{-13}	2.08×10^{7}	1.92×10^{5}	2.71×10^{7}	7.10×10^{-3}	1.20×10^{7}	1.60×10^{-2}
950	590.3	739.98	2500	16.56	83.44	9.21×10^{-4}	6.86×10^{-5}	14.30	1.97×10^{2}	5.51×10^{-9}	5.44×10^{-12}	3.79×10^{-16}	3.22×10^{-13}	1.61×10^{7}	1.92×10^{5}	3.50×10^{7}	5.49×10^{-3}	1.56×10^{7}	1.24×10^{-2}
1000	621.4	730.01	2500	16.07	83.92	1.11×10^{-3}	8.68×10^{-5}	14.29	1.99×10^{2}	4.28×10^{-9}	4.22×10^{-12}	2.94×10^{-16}	2.50×10^{-13}	1.25×10^{7}	1.92×10^{5}	4.51×10^{7}	4.27×10^{-3}	2.00×10^{7}	9.61×10^{-3}
1100	683.5	710.66	2500	15.16	84.84	1.58×10^{-3}	1.38×10^{-4}	14.27	2.05×10^{2}	2.61×10^{-9}	2.57×10^{-12}	1.79×10^{-16}	1.52×10^{-13}	7.61×10^{6}	1.93×10^{5}	7.39×10^{7}	2.60×10^{-3}	3.29×10^{7}	5.86×10^{-3}
1200	745.6	692.07	2500	14.31	85.68	2.24×10^{-3}	2.15×10^{-4}	14.25	2.11×10^{2}	1.61×10^{-9}	1.59×10^{-12}	1.11×10^{-16}	9.40×10^{-14}	4.70×10^{6}	1.93×10^{5}	1.20×10^{8}	1.61×10^{-3}	5.32×10^{7}	3.62×10^{-3}
1300	807.8	674.20	2500	13.53	86.47	3.14×10^{-3}	3.33×10^{-4}	14.24	2.17×10^{2}	1.01×10^{-9}	9.96×10^{-13}	6.91×10^{-17}	5.88×10^{-14}	2.95×10^{6}	1.93×10^{5}	1.91×10^{8}	1.01×10^{-3}	8.49×10^{7}	2.23×10^{-3}
1400	869.9	657.02	2500	12.79	87.20	4.36×10^{-3}	5.09×10^{-4}	14.22	2.22×10^{2}	6.40×10^{-10}	6.31×10^{-13}	4.38×10^{-17}	3.72×10^{-14}	1.87×10^{6}	1.93×10^{5}	3.01×10^{8}	6.40×10^{-4}	1.34×10^{8}	1.44×10^{-3}
1500	932.0	640.48	2500	12.11	87.88	6.00×10^{-3}	7.70×10^{-4}	14.21	2.28×10^{2}	4.11×10^{-10}	4.05×10^{-13}	2.81×10^{-17}	2.39×10^{-14}	1.20×10^{6}	1.93×10^{5}	4.70×10^{8}	4.11×10^{-4}	2.09×10^{8}	9.25×10^{-4}
1600	994.2	624.56	2500	11.48	88.51	8.19×10^{-3}	1.15×10^{-3}	14.20	2.34×10^{2}	2.67×10^{-10}	2.63×10^{-13}	1.82×10^{-17}	1.55×10^{-14}	7.78×10^{5}	1.93×10^{5}	7.24×10^{8}	2.67×10^{-4}	3.22×10^{8}	6.00×10^{-4}
1700	1056	609.23	2500	10.89	89.09	1.11×10^{-2}	1.70×10^{-3}	14.18	2.41×10^{2}	1.75×10^{-10}	1.73×10^{-13}	1.19×10^{-17}	1.02×10^{-14}	5.10×10^{5}	1.93×10^{5}	1.10×10^{9}	1.75×10^{-4}	4.90×10^{8}	3.94×10^{-4}
1800	1118	594.45	2500	10.34	89.64	1.49×10^{-2}	2.50×10^{-3}	14.17	2.47×10^{2}	1.16×10^{-10}	1.14×10^{-13}	7.91×10^{-18}	6.73×10^{-15}	3.39×10^{5}	1.93×10^{5}	1.66×10^{9}	1.16×10^{-4}	7.39×10^{8}	2.62×10^{-4}
1900	1181	580.20	2500	9.814	90.16	1.97×10^{-2}	3.62×10^{-3}	14.16	2.53×10^{2}	7.79×10^{-11}	7.69×10^{-14}	5.30×10^{-18}	4.51×10^{-15}	2.27×10^{5}	1.93×10^{5}	2.48×10^{9}	7.80×10^{-5}	1.10×10^{9}	1.76×10^{-4}
2000	1243	566.46	2500	9.350	90.62	2.63×10^{-2}	5.21×10^{-3}	14.15	2.59×10^{2}	5.26×10^{-11}	5.19×10^{-14}	3.58×10^{-18}	3.05×10^{-15}	1.54×10^{5}	1.93×10^{5}	3.66×10^{9}	5.28×10^{-5}	1.63×10^{9}	1.19×10^{-4}
2500	1553	504.58	2500	7.379	92.50	9.72×10^{-2}	2.83×10^{-2}	14.04	2.93×10^{2}	8.58×10^{-12}	8.46×10^{-15}	5.80×10^{-19}	4.93×10^{-16}	2.50×10^{4}	1.94×10^{5}	2.25×10^{10}	8.64×10^{-5}	9.99×10^{9}	1.94×10^{-5}
3000	1864	452.30	2500	5.936	93.62	.3105	.1274	13.77	3.34×10^{2}	1.73×10^{-12}	1.71×10^{-15}	1.15×10^{-19}	9.75×10^{-17}	5.05×10^{3}	1.96×10^{5}	1.11×10^{11}	1.76×10^{-6}	4.95×10^{10}	3.96×10^{-6}
3500	2175	407.75	2500	4.836	93.80	.8740	.4885	12.98	3.93×10^{2}	4.32×10^{-13}	4.26×10^{-16}	2.70×10^{-20}	2.29×10^{-17}	1.26×10^{3}	2.02×10^{5}	4.47×10^{11}	4.52×10^{-7}	1.99×10^{11}	1.02×10^{-6}
4000	2485	369.47	2500	3.947	92.25	2.186	1.616	11.13	5.06×10^{2}	1.39×10^{-13}	1.37×10^{-16}	7.42×10^{-21}	6.31×10^{-18}	4.04×10^{2}	2.18×10^{5}	1.39×10^{12}	1.57×10^{-7}	6.19×10^{11}	3.52×10^{-7}
4500	2796	336.34	2500	3.156	87.40	4.836	4.606	8.18	7.55×10^{2}	6.07×10^{-14}	5.99×10^{-17}	2.39×10^{-21}	2.03×10^{-18}	1.77×10^{2}	2.54×10^{5}	3.18×10^{12}	8.00×10^{-8}	1.41×10^{12}	1.80×10^{-7}
5000	3107	307.47	2500	2.389	77.22	9.272	11.12	5.26	1.29×10^{3}	3.62×10^{-14}	3.57×10^{-17}	9.15×10^{-22}	7.78×10^{-19}	1.06×10^{2}	3.17×10^{5}	5.33×10^{12}	5.95×10^{-8}	2.37×10^{12}	1.34×10^{-7}
6000	3728	259.86	2500	1.010	42.86	20.02	36.10	2.28	3.52×10^{3}	2.25×10^{-14}	2.22×10^{-17}	2.46×10^{-22}	2.09×10^{-19}	6.55×10	4.82×10^{5}	8.59×10^{12}	5.61×10^{-8}	3.82×10^{12}	1.26×10^{-7}
7000	4350	222.51	2500	.2973	15.90	23.62	60.19	1.50	6.24×10^{3}	1.82×10^{-14}	1.80×10^{-17}	1.31×10^{-22}	1.12×10^{-19}	5.31×10	5.94×10^{5}	1.06×10^{13}	5.61×10^{-8}	4.71×10^{12}	1.26×10^{-7}
8000	4971	192.67	2500	8.13×10^{-2}	5.306	21.34	72.69	1.28	8.46×10^{3}	1.59×10^{-14}	1.57×10^{-17}	9.75×10^{-23}	8.29×10^{-20}	4.64×10	6.44×10^{5}	1.21×10^{13}	5.31×10^{-8}	5.40×10^{12}	1.19×10^{-7}
9000	5592	168.46	2500	2.42×10^{-2}	1.881	18.00	80.10	1.19	1.04×10^{4}	1.43×10^{-14}	1.41×10^{-17}	8.17×10^{-23}	6.95×10^{-20}	4.17×10	6.67×10^{5}	1.35×10^{13}	4.94×10^{-8}	6.00×10^{12}	1.11×10^{-7}
10,000	6214	148.53	2500	8.14×10^{-3}	.7357	15.07	84.19	1.14	1.22×10^{4}	1.31×10^{-14}	1.29×10^{-17}	7.20×10^{-23}	6.12×10^{-20}	3.81×10	6.80×10^{5}	1.48×10^{13}	4.61×10^{-8}	6.56×10^{12}	1.04×10^{-7}
15,000	9320	87.22	2500	1.48×10^{-4}	2.31×10^{-2}	7.310	92.67	1.06	2.23×10^{4}	9.67×10^{-15}	9.54×10^{-18}	4.96×10^{-23}	4.22×10^{-20}	2.82×10	7.04×10^{5}	1.99×10^{13}	3.53×10^{-8}	8.86×10^{12}	7.95×10^{-8}
20,000	12,427	57.31	2500	1.19×10^{-5}	2.61×10^{-3}	4.528	95.47	1.04	3.48×10^{4}	8.09×10^{-15}	7.98×10^{-18}	4.06×10^{-23}	3.45×10^{-20}	2.36×10	7.12×10^{5}	2.39×10^{13}	2.99×10^{-8}	1.06×10^{13}	6.72×10^{-8}
25,000	15,534	40.51	2500	2.12×10^{-6}	5.87×10^{-4}	3.244	96.76	1.03	4.97×10^{4}	7.17×10^{-15}	7.07×10^{-18}	3.56×10^{-23}	3.03×10^{-20}	2.09×10	7.16×10^{5}	2.69×10^{13}	2.66×10^{-8}	1.20×10^{13}	5.99×10^{-8}
30,000	18,641	30.14	2500	6.06×10^{-7}	1.99×10^{-4}	2.541	97.46	1.03	6.71×10^{4}	6.58×10^{-15}	6.49×10^{-18}	3.25×10^{-23}	2.76×10^{-20}	1.92×10	7.18×10^{5}	2.93×10^{13}	2.45×10^{-8}	1.30×10^{13}	5.51×10^{-8}
35,000	21,748	23.30	2500	2.34×10^{-7}	8.71×10^{-5}	2.109	97.89	1.02	8.71×10^{4}	6.16×10^{-15}	6.08×10^{-18}	3.03×10^{-23}	2.58×10^{-20}	1.80×10	7.19×10^{5}	3.13×10^{13}	2.30×10^{-8}	1.39×10^{13}	5.17×10^{-8}
40,000	24,855	18.55	2500	1.11×10^{-7}	4.56×10^{-5}	1.822	98.18	1.02	1.10×10^{5}	5.85×10^{-15}	5.77×10^{-18}	2.88×10^{-23}	2.45×10^{-20}	1.71×10	7.20×10^{5}	3.30×10^{13}	2.18×10^{-8}	1.46×10^{13}	4.91×10^{-8}
45,000	27,961	15.12	2500	6.08×10^{-8}	2.71×10^{-5}	1.618	98.38	1.02	1.35×10^{5}	5.62×10^{-15}	5.54×10^{-18}	2.76×10^{-23}	2.34×10^{-20}	1.64×10	7.20×10^{5}	3.43×10^{13}	2.10×10^{-8}	1.53×10^{13}	4.72×10^{-8}
50,000	31,068	12.55	2500	3.71×10^{-8}	1.76×10^{-5}	1.468	98.53	1.02	1.62×10^{5}	5.43×10^{-15}	5.36×10^{-18}	2.66×10^{-23}	2.26×10^{-20}	1.58×10	7.21×10^{5}	3.55×10^{13}	2.03×10^{-8}	1.58×10^{13}	4.56×10^{-8}
55,000	34,175	10.59	2500	2.45×10^{-8}	1.23×10^{-5}	1.352	98.65	1.02	1.93×10^{5}	5.28×10^{-15}	5.21×10^{-18}	2.59×10^{-23}	2.20×10^{-20}	1.54×10	7.21×10^{5}	3.65×10^{13}	1.97×10^{-8}	1.62×10^{13}	4.44×10^{-8}
60,000	37,282	9.06	2500	1.72×10^{-8}	9.08×10^{-6}	1.261	98.74	1.02	2.26×10^{5}	5.15×10^{-15}	5.08×10^{-18}	2.52×10^{-23}	2.15×10^{-20}	1.50×10	7.21×10^{5}	3.74×10^{13}	1.93×10^{-8}	1.66×10^{13}	4.34×10^{-8}

1 millibar = 10^3 dynes/cm² = 0.750 mm of Hg

Table 44

ATMOSPHERIC MODEL III - VALUES OF TEMPERATURE, PRESSURE, AND DENSITY ABOVE THE F_2 LAYER

Latitude 45°. Engineering Units. p_a = 2116 lb/ft², ρ_a = 2.286 × 10⁻³ slug/ft³

Height h mi	Height h ft	Apparent Gravity g' ft/sec²	Temp T °K	Percentage Composition by Mass C_x: Atomic Oxygen	Atomic Nitrogen	Atomic Helium	Atomic Hydrogen	Mean Mol Wt M	Scale Height H ft	Pressure p lb/ft²	Pressure Ratio p/p_a	Density ρ slug/ft³	Density Ratio σ ρ/ρ_a	Number Density n particles/ft³	Mean Particle Speed v ft/sec	$d = 2 \times 10^{-8}$ cm: Mean Free Path L ft	Mean Collision Freq ν 1/sec	$d = 3 \times 10^{-8}$ cm: Mean Free Path L ft	Mean Collision Freq ν 1/sec
186.4	9.842×10^5	29.334	1980	30.5% O	69.5% N_2	--	--	24.35	1.370×10^5	1.01×10^{-6}	4.78×10^{-10}	2.50×10^{-13}	1.05×10^{-10}	9.09×10^{12}	3.21×10^3	5.77×10^3	5.56×10^{-1}	2.56×10^3	1.26
201.9	1.066×10^6	29.114	2160	--	--	--	--	21.86	1.687×10^5	5.94×10^{-7}	2.81×10^{-10}	1.21×10^{-13}	5.09×10^{-11}	4.90×10^{12}	3.54×10^3	1.07×10^4	3.30×10^{-1}	4.76×10^3	7.46×10^{-1}
217.5	1.148×10^6	28.897	2340	--	--	--	--	19.38	2.078×10^5	3.83×10^{-7}	1.82×10^{-10}	6.39×10^{-14}	2.68×10^{-11}	2.92×10^{12}	3.90×10^3	1.80×10^4	2.18×10^{-1}	7.97×10^3	4.91×10^{-1}
233.0	1.230×10^6	28.682	2520	--	--	--	--	16.89	2.586×10^5	2.69×10^{-7}	1.27×10^{-10}	3.63×10^{-14}	1.52×10^{-11}	1.90×10^{12}	4.33×10^3	2.76×10^4	1.57×10^{-1}	1.22×10^4	3.55×10^{-1}
248.5	1.312×10^6	28.469	2700	22.22	77.78	1.39×10^{-4}	6.00×10^{-6}	14.40	3.275×10^5	2.03×10^{-7}	8.57×10^{-11}	2.17×10^{-14}	9.14×10^{-12}	1.34×10^{12}	4.86×10^3	3.94×10^4	1.24×10^{-1}	1.74×10^4	2.80×10^{-1}
264.1	1.394×10^6	28.260	2880	21.64	78.36	1.66×10^{-4}	7.51×10^{-6}	14.39	3.520×10^5	1.59×10^{-7}	7.52×10^{-11}	1.60×10^{-14}	6.74×10^{-12}	9.85×10^{11}	5.02×10^3	5.31×10^4	9.45×10^{-2}	2.36×10^4	2.13×10^{-1}
279.6	1.476×10^6	28.052	3060	21.13	78.87	1.95×10^{-4}	9.26×10^{-6}	14.38	3.786×10^5	1.27×10^{-7}	6.01×10^{-11}	1.20×10^{-14}	5.07×10^{-12}	7.39×10^{11}	5.18×10^3	7.09×10^4	7.32×10^{-2}	3.14×10^4	1.65×10^{-1}
295.1	1.558×10^6	27.846	3240	20.64	79.36	2.27×10^{-4}	1.13×10^{-5}	14.37	4.026×10^5	1.03×10^{-7}	4.87×10^{-11}	9.20×10^{-15}	3.88×10^{-12}	5.66×10^{11}	5.35×10^3	9.25×10^4	5.78×10^{-2}	4.10×10^4	1.30×10^{-1}
310.7	1.640×10^6	27.649	3420	20.20	79.80	2.62×10^{-4}	1.35×10^{-5}	14.36	4.281×10^5	8.47×10^{-8}	4.01×10^{-11}	7.16×10^{-15}	3.01×10^{-12}	4.42×10^{11}	5.48×10^3	1.19×10^5	4.62×10^{-2}	5.28×10^4	1.04×10^{-1}
326.2	1.722×10^6	27.442	3600	19.78	80.22	2.99×10^{-4}	1.61×10^{-5}	14.35	4.544×10^5	7.03×10^{-8}	3.32×10^{-11}	5.65×10^{-15}	2.38×10^{-12}	3.48×10^{11}	5.64×10^3	1.51×10^5	3.74×10^{-2}	6.69×10^4	8.43×10^{-2}
341.8	1.804×10^6	27.242	3780	19.40	80.60	3.40×10^{-4}	1.89×10^{-5}	14.35	4.810×10^5	5.90×10^{-8}	2.79×10^{-11}	4.50×10^{-15}	1.90×10^{-12}	2.78×10^{11}	5.77×10^3	1.89×10^5	3.06×10^{-2}	8.37×10^4	6.91×10^{-2}
357.3	1.886×10^6	27.046	3960	19.04	80.96	3.83×10^{-4}	2.21×10^{-5}	14.34	5.075×10^5	5.00×10^{-8}	2.37×10^{-11}	3.65×10^{-15}	1.54×10^{-12}	2.25×10^{11}	5.91×10^3	2.33×10^5	2.54×10^{-2}	1.03×10^5	5.72×10^{-2}
372.8	1.968×10^6	26.884	4140	18.70	81.30	4.29×10^{-4}	2.56×10^{-5}	14.33	5.341×10^5	4.28×10^{-8}	2.02×10^{-11}	2.99×10^{-15}	1.26×10^{-12}	1.84×10^{11}	6.04×10^3	2.85×10^5	2.12×10^{-2}	1.26×10^5	4.79×10^{-2}
388.4	2.050×10^6	26.659	4320	18.39	81.61	4.78×10^{-4}	2.94×10^{-5}	14.33	5.623×10^5	3.68×10^{-8}	1.74×10^{-11}	2.47×10^{-15}	1.04×10^{-12}	1.52×10^{11}	6.17×10^3	3.44×10^5	1.79×10^{-2}	1.53×10^5	4.04×10^{-2}
403.9	2.133×10^6	26.468	4500	18.10	81.90	5.35×10^{-4}	3.36×10^{-5}	14.32	5.902×10^5	3.20×10^{-8}	1.51×10^{-11}	2.04×10^{-15}	8.62×10^{-13}	1.26×10^{11}	6.30×10^3	4.13×10^5	1.52×10^{-2}	1.84×10^5	3.43×10^{-2}
435.0	2.297×10^6	26.096	4500	17.53	82.47	6.53×10^{-4}	4.34×10^{-5}	14.31	5.991×10^5	2.42×10^{-8}	1.14×10^{-11}	1.55×10^{-15}	6.54×10^{-13}	9.60×10^{11}	6.30×10^3	5.45×10^5	1.16×10^{-2}	2.42×10^5	2.60×10^{-2}
466.0	2.461×10^6	25.731	4500	16.99	83.01	7.95×10^{-4}	5.60×10^{-5}	14.30	6.079×10^5	1.85×10^{-8}	8.73×10^{-12}	1.18×10^{-15}	4.98×10^{-13}	7.31×10^{11}	6.30×10^3	7.15×10^5	8.83×10^{-3}	3.18×10^5	1.99×10^{-2}
497.1	2.625×10^6	25.374	4500	16.47	83.53	9.64×10^{-4}	7.18×10^{-5}	14.29	6.168×10^5	1.41×10^{-8}	6.68×10^{-12}	9.05×10^{-16}	3.81×10^{-13}	5.61×10^{11}	6.31×10^3	9.35×10^5	6.75×10^{-3}	4.17×10^5	1.52×10^{-2}
528.2	2.789×10^6	25.024	4500	15.96	84.03	1.17×10^{-3}	9.19×10^{-5}	14.28	6.260×10^5	1.09×10^{-8}	5.13×10^{-12}	6.93×10^{-16}	2.92×10^{-13}	4.30×10^{11}	6.32×10^3	1.22×10^6	5.19×10^{-3}	5.41×10^5	1.17×10^{-2}
559.2	2.953×10^6	24.681	4500	15.48	84.52	1.41×10^{-3}	1.17×10^{-4}	14.28	6.352×10^5	8.37×10^{-9}	3.96×10^{-12}	5.34×10^{-16}	2.25×10^{-13}	3.31×10^{11}	6.33×10^3	1.58×10^6	4.00×10^{-3}	7.02×10^5	9.01×10^{-3}
590.3	3.117×10^6	24.346	4500	15.02	84.98	1.69×10^{-3}	1.49×10^{-4}	14.27	6.440×10^5	6.47×10^{-9}	3.06×10^{-12}	4.14×10^{-16}	1.74×10^{-13}	2.56×10^{11}	6.33×10^3	2.04×10^6	3.10×10^{-3}	9.06×10^5	6.97×10^{-3}
621.4	3.281×10^6	24.017	4500	14.57	85.43	2.03×10^{-3}	1.88×10^{-4}	14.26	6.535×10^5	5.03×10^{-9}	2.38×10^{-12}	3.20×10^{-16}	1.35×10^{-13}	1.99×10^{11}	6.33×10^3	2.63×10^6	2.41×10^{-3}	1.17×10^6	5.42×10^{-3}
683.5	3.609×10^6	23.379	4500	13.73	86.27	2.91×10^{-3}	2.98×10^{-4}	14.24	6.719×10^5	3.07×10^{-9}	1.45×10^{-12}	1.96×10^{-16}	8.22×10^{-14}	1.21×10^{11}	6.33×10^3	4.30×10^6	1.47×10^{-3}	1.92×10^6	3.30×10^{-3}
745.6	3.937×10^6	22.766	4500	12.94	87.05	4.11×10^{-3}	4.67×10^{-4}	14.23	6.906×10^5	1.89×10^{-9}	8.95×10^{-13}	1.21×10^{-16}	5.08×10^{-14}	7.50×10^{10}	6.33×10^3	6.99×10^6	9.07×10^{-4}	3.10×10^6	2.04×10^{-3}
807.8	4.265×10^6	22.308	4500	12.22	87.78	5.77×10^{-3}	7.23×10^{-4}	14.21	7.100×10^5	1.19×10^{-9}	5.60×10^{-13}	7.53×10^{-17}	3.17×10^{-14}	4.70×10^{10}	6.33×10^3	1.12×10^7	5.68×10^{-4}	4.95×10^6	1.28×10^{-3}
869.9	4.593×10^6	21.611	4500	11.55	88.44	8.01×10^{-3}	1.11×10^{-3}	14.20	7.290×10^5	7.52×10^{-10}	3.55×10^{-13}	4.78×10^{-17}	2.01×10^{-14}	2.97×10^{10}	6.33×10^3	1.76×10^7	3.60×10^{-4}	7.81×10^6	8.11×10^{-4}
932.0	4.921×10^6	21.065	4500	10.92	89.06	1.10×10^{-2}	1.67×10^{-3}	14.19	7.487×10^5	4.82×10^{-10}	2.28×10^{-13}	3.07×10^{-17}	1.29×10^{-14}	1.91×10^{10}	6.34×10^3	2.74×10^7	2.31×10^{-4}	1.22×10^7	5.20×10^{-4}
994.2	5.249×10^6	20.541	4500	10.34	89.64	1.51×10^{-2}	2.50×10^{-3}	14.17	7.687×10^5	3.13×10^{-10}	1.48×10^{-13}	1.98×10^{-17}	8.35×10^{-15}	1.24×10^{10}	6.34×10^3	4.23×10^7	1.50×10^{-4}	1.88×10^7	3.38×10^{-4}
1056	5.577×10^6	20.034	4500	9.804	90.17	2.04×10^{-2}	3.70×10^{-3}	14.16	7.887×10^5	2.05×10^{-10}	9.70×10^{-14}	1.30×10^{-17}	5.47×10^{-15}	8.13×10^9	6.35×10^3	6.43×10^7	9.85×10^{-5}	2.86×10^7	2.22×10^{-4}
1243	6.562×10^6	18.626	4500	8.397	91.54	4.84×10^{-2}	1.13×10^{-2}	14.11	8.514×10^5	6.18×10^{-11}	2.92×10^{-14}	3.90×10^{-18}	1.64×10^{-15}	2.44×10^9	6.36×10^3	2.14×10^8	2.97×10^{-5}	9.51×10^7	6.68×10^{-5}
1553	8.202×10^6	16.588	4500	6.604	93.16	.1788	6.15×10^{-2}	13.94	9.675×10^5	1.01×10^{-11}	4.78×10^{-15}	6.31×10^{-19}	2.65×10^{-16}	3.99×10^9	6.40×10^3	1.31×10^9	4.89×10^{-6}	5.81×10^8	1.10×10^{-5}
1864	9.842×10^6	14.866	4500	5.286	93.87	.5699	.2767	13.42	1.122×10^6	2.08×10^{-12}	9.83×10^{-16}	1.25×10^{-19}	5.26×10^{-17}	8.21×10^7	6.53×10^3	6.36×10^9	1.02×10^{-6}	2.82×10^9	2.31×10^{-6}
2175	1.148×10^7	13.399	4500	4.262	93.10	1.591	1.052	11.96	1.396×10^6	5.51×10^{-13}	2.60×10^{-16}	2.95×10^{-20}	1.24×10^{-17}	2.19×10^7	6.89×10^3	2.39×10^{10}	2.88×10^{-7}	1.06×10^{10}	6.49×10^{-7}
2485	1.312×10^7	12.139	4500	3.392	89.32	3.887	3.402	9.14	2.016×10^6	2.04×10^{-13}	9.62×10^{-17}	8.33×10^{-21}	3.50×10^{-18}	8.04×10^6	7.91×10^3	6.50×10^{10}	1.22×10^{-7}	2.89×10^{10}	2.74×10^{-7}
2796	1.476×10^7	11.049	4500	2.566	80.10	8.148	9.194	5.87	3.451×10^6	1.08×10^{-13}	5.09×10^{-17}	2.83×10^{-21}	1.19×10^{-18}	4.25×10^6	9.84×10^3	1.23×10^{11}	8.03×10^{-8}	5.45×10^{10}	1.81×10^{-7}
3107	1.640×10^7	10.100	4500	1.757	64.02	14.13	20.10	3.55	6.237×10^6	7.52×10^{-14}	3.55×10^{-17}	1.20×10^{-21}	5.04×10^{-19}	2.97×10^6	1.27×10^4	1.76×10^{11}	7.21×10^{-8}	7.81×10^{10}	1.62×10^{-7}
728	1.968×10^7	8.534	4500	.5616	26.86	23.13	49.44	1.76	1.489×10^7	5.39×10^{-14}	2.55×10^{-17}	4.23×10^{-22}	1.78×10^{-19}	2.13×10^6	1.80×10^4	2.46×10^{11}	7.32×10^{-8}	1.09×10^{11}	1.65×10^{-7}
4350	2.297×10^7	7.306	4500	.1378	8.306	22.76	68.80	1.35	2.267×10^7	4.49×10^{-14}	2.12×10^{-17}	2.72×10^{-22}	1.14×10^{-19}	1.78×10^6	2.05×10^4	2.95×10^{11}	6.97×10^{-8}	1.31×10^{11}	1.57×10^{-7}
4971	2.625×10^7	6.322	4500	3.51×10^{-3}	2.584	19.18	78.20	1.21	2.922×10^7	3.99×10^{-14}	1.88×10^{-17}	2.16×10^{-22}	9.09×10^{-20}	1.58×10^6	2.17×10^4	3.31×10^{11}	6.54×10^{-8}	1.47×10^{11}	1.47×10^{-7}
5592	2.953×10^7	5.529	4500	1.02×10^{-2}	.8932	15.78	83.32	1.15	3.507×10^7	3.59×10^{-14}	1.70×10^{-17}	1.85×10^{-22}	7.81×10^{-20}	1.42×10^6	2.22×10^4	3.67×10^{11}	6.04×10^{-8}	1.63×10^{11}	1.36×10^{-7}
6214	3.281×10^7	4.875	4500	3.38×10^{-2}	.3451	13.12	86.53	1.12	4.091×10^7	3.30×10^{-14}	1.56×10^{-17}	1.65×10^{-22}	6.96×10^{-20}	1.31×10^6	2.25×10^4	4.00×10^{11}	5.62×10^{-8}	1.78×10^{11}	1.26×10^{-7}
9320	4.921×10^7	2.861	4500	6.05×10^{-5}	1.07×10^{-2}	6.234	93.76	1.06	7.395×10^7	2.44×10^{-14}	1.15×10^{-17}	1.16×10^{-22}	4.88×10^{-20}	9.68×10^5	2.32×10^4	5.38×10^{11}	4.30×10^{-8}	2.40×10^{11}	9.68×10^{-8}
12427	6.562×10^7	1.879	4500	4.85×10^{-6}	1.20×10^{-2}	3.847	96.23	1.04	1.148×10^8	2.05×10^{-14}	9.69×10^{-18}	9.51×10^{-23}	4.00×10^{-20}	8.10×10^5	2.34×10^4	6.43×10^{11}	3.64×10^{-8}	2.86×10^{11}	8.18×10^{-8}
15534	8.202×10^7	1.328	4500	8.64×10^{-7}	2.70×10^{-4}	2.749	97.25	1.03	1.637×10^8	1.82×10^{-14}	8.59×10^{-18}	8.37×10^{-23}	3.53×10^{-20}	7.19×10^5	2.35×10^4	7.25×10^{11}	3.24×10^{-8}	3.23×10^{11}	7.29×10^{-8}
18641	9.842×10^7	.988	4500	2.47×10^{-7}	9.12×10^{-5}	2.152	97.85	1.02	2.210×10^8	1.65×10^{-14}	7.79×10^{-18}	7.65×10^{-23}	3.22×10^{-20}	6.60×10^5	2.36×10^4	7.91×10^{11}	2.98×10^{-8}	3.51×10^{11}	6.70×10^{-8}
21748	1.148×10^8	.764	4500	9.54×10^{-8}	4.00×10^{-5}	1.785	98.21	1.02	2.867×10^8	1.56×10^{-14}	7.39×10^{-18}	7.15×10^{-23}	3.01×10^{-20}	6.17×10^5	2.36×10^4	8.46×10^{11}	2.79×10^{-8}	3.77×10^{11}	6.28×10^{-8}
24855	1.312×10^8	.608	4500	4.52×10^{-8}	2.10×10^{-5}	1.541	98.46	1.02	3.609×10^8	1.48×10^{-14}	7.01×10^{-18}	6.78×10^{-23}	2.85×10^{-20}	5.89×10^5	2.36×10^4	8.89×10^{11}	2.66×10^{-8}	3.97×10^{11}	5.98×10^{-8}
27961	1.476×10^8	.495	4500	2.48×10^{-8}	1.24×10^{-5}	1.369	98.63	1.02	4.436×10^8	1.43×10^{-14}	6.74×10^{-18}	6.49×10^{-23}	2.73×10^{-20}	5.64×10^5	2.37×10^4	9.25×10^{11}	2.55×10^{-8}	4.13×10^{11}	5.74×10^{-8}
31068	1.640×10^8	.411	4500	1.51×10^{-8}	8.11×10^{-6}	1.241	98.76	1.02	5.344×10^8	1.38×10^{-14}	6.51×10^{-18}	6.27×10^{-23}	2.64×10^{-20}	5.47×10^5	2.37×10^4	9.58×10^{11}	2.47×10^{-8}	4.26×10^{11}	5.56×10^{-8}
34175	1.804×10^8	.347	4500	9.98×10^{-9}	5.66×10^{-6}	1.144	98.86	1.02	6.338×10^8	1.34×10^{-14}	6.33×10^{-18}	6.10×10^{-23}	2.57×10^{-20}	5.30×10^5	2.37×10^4	9.88×10^{11}	2.40×10^{-8}	4.40×10^{11}	5.40×10^{-8}
37282	1.968×10^8	.297	4500	7.02×10^{-9}	3.92×10^{-6}	1.067	98.93	1.02	7.421×10^8	1.31×10^{-14}	6.19×10^{-18}	5.94×10^{-23}	2.50×10^{-20}	5.18×10^5	2.37×10^4	1.01×10^{12}	2.34×10^{-8}	4.49×10^{11}	5.28×10^{-8}
43496	2.297×10^8	.224	4500	3.99×10^{-9}	2.56×10^{-6}	.9536	99.05	1.02	9.833×10^8	1.26×10^{-14}	5.95×10^{-18}	5.71×10^{-23}	2.41×10^{-20}	4.98×10^5	2.37×10^4	1.05×10^{12}	2.26×10^{-8}	4.66×10^{11}	5.08×10^{-8}

Table 45

ATMOSPHERIC MODEL III - VALUES OF TEMPERATURE, PRESSURE, AND DENSITY ABOVE THE F_2 LAYER

Latitude, 45°. Metric Units. p_a = 1014 mb, ρ_a = 1.223 × 10^{-3} gm/cm³

Height h km	Height h mi	Apparent Gravity g' cm/sec²	Temp T °K	Percentage Composition by Mass C_x: Atomic Oxygen	Atomic Nitrogen	Atomic Helium	Atomic Hydrogen	Mean Mol Wt M	Scale Height H	Pressure p millibars	Pressure Ratio p/p_a	Density ρ gram/cm³	Density Ratio σ ρ/ρ_a	Number Density n particles/cm³	Mean Particle Speed v cm/sec	d = 2 × 10^{-8}cm: Mean Free Path L cm	Mean Collision Freq ν 1/sec	d = 3 × 10^{-8}cm: Mean Free Path L cm	Mean Collision Freq ν 1/sec
300	186.4	894.09	1100	30.5%O	69.5%N_2			24.35	4.20 × 10	4.84 × 10^{-7}	4.78 × 10^{-10}	1.29 × 10^{-13}	1.05 × 10^{-10}	3.21 × 10^{9}	9.78 × 10^{4}	1.76 × 10^{8}	5.56 × 10^{-1}	7.79 × 10^{6}	1.26
325	201.9	887.39	1200					21.86	5.14 × 10	2.85 × 10^{-7}	2.81 × 10^{-10}	6.24 × 10^{-14}	5.09 × 10^{-11}	1.73 × 10^{9}	1.08 × 10^{5}	3.26 × 10^{6}	3.30 × 10^{-1}	1.45 × 10^{6}	7.46 × 10^{-1}
350	217.5	880.77	1300					19.38	6.33 × 10	1.84 × 10^{-7}	1.82 × 10^{-10}	3.29 × 10^{-14}	2.68 × 10^{-11}	1.03 × 10^{9}	1.19 × 10^{5}	5.48 × 10^{5}	2.18 × 10^{-1}	2.43 × 10^{5}	4.91 × 10^{-1}
375	233.0	874.22	1400					16.89	7.88 × 10	1.29 × 10^{-7}	1.27 × 10^{-10}	1.87 × 10^{-14}	1.52 × 10^{-11}	6.70 × 10^{8}	1.32 × 10^{5}	8.42 × 10^{5}	1.57 × 10^{-1}	3.73 × 10^{5}	3.55 × 10^{-1}
400	248.5	867.75	1500	22.22	77.78	1.39 × 10^{-4}	6.00 × 10^{-6}	14.40	9.98 × 10	9.70 × 10^{-8}	8.57 × 10^{-11}	1.12 × 10^{-14}	9.14 × 10^{-12}	4.72 × 10^{8}	1.48 × 10^{5}	1.20 × 10^{6}	1.24 × 10^{-1}	5.30 × 10^{5}	2.80 × 10^{-1}
425	264.1	861.35	1600	21.64	78.36	1.66 × 10^{-4}	7.51 × 10^{-6}	14.39	1.07 × 10^{2}	7.62 × 10^{-8}	7.52 × 10^{-11}	8.24 × 10^{-15}	6.74 × 10^{-12}	3.48 × 10^{8}	1.53 × 10^{5}	1.62 × 10^{6}	9.45 × 10^{-2}	7.20 × 10^{5}	2.13 × 10^{-1}
450	279.6	855.01	1700	21.13	78.87	1.95 × 10^{-4}	9.26 × 10^{-6}	14.38	1.15 × 10^{2}	6.09 × 10^{-8}	6.01 × 10^{-11}	6.20 × 10^{-15}	5.07 × 10^{-12}	2.61 × 10^{8}	1.58 × 10^{5}	2.16 × 10^{6}	7.32 × 10^{-2}	9.57 × 10^{5}	1.65 × 10^{-1}
475	295.1	848.75	1800	20.64	79.36	2.27 × 10^{-4}	1.13 × 10^{-5}	14.37	1.23 × 10^{2}	4.94 × 10^{-8}	4.87 × 10^{-11}	4.74 × 10^{-15}	3.88 × 10^{-12}	2.00 × 10^{8}	1.63 × 10^{5}	2.82 × 10^{6}	5.78 × 10^{-2}	1.25 × 10^{6}	1.30 × 10^{-1}
500	310.7	842.75	1900	20.20	79.80	2.62 × 10^{-4}	1.35 × 10^{-5}	14.36	1.30 × 10^{2}	4.06 × 10^{-8}	4.01 × 10^{-11}	3.69 × 10^{-15}	3.01 × 10^{-12}	1.56 × 10^{8}	1.67 × 10^{5}	3.63 × 10^{6}	4.62 × 10^{-2}	1.61 × 10^{6}	1.04 × 10^{-1}
525	326.2	836.42	2000	19.78	80.22	2.99 × 10^{-4}	1.61 × 10^{-5}	14.35	1.38 × 10^{2}	3.37 × 10^{-8}	3.32 × 10^{-11}	2.91 × 10^{-15}	2.38 × 10^{-12}	1.23 × 10^{8}	1.72 × 10^{5}	4.60 × 10^{6}	3.74 × 10^{-2}	2.04 × 10^{6}	8.43 × 10^{-2}
550	341.8	830.36	2100	19.40	80.60	3.40 × 10^{-4}	1.89 × 10^{-5}	14.35	1.47 × 10^{2}	2.83 × 10^{-8}	2.79 × 10^{-11}	2.32 × 10^{-15}	1.90 × 10^{-12}	9.82 × 10^{7}	1.76 × 10^{5}	5.75 × 10^{6}	3.06 × 10^{-2}	2.55 × 10^{6}	6.91 × 10^{-2}
575	357.3	824.36	2200	19.04	80.96	3.83 × 10^{-4}	2.21 × 10^{-5}	14.34	1.55 × 10^{2}	2.40 × 10^{-8}	2.37 × 10^{-11}	1.88 × 10^{-15}	1.54 × 10^{-12}	7.94 × 10^{7}	1.80 × 10^{5}	7.11 × 10^{6}	2.54 × 10^{-2}	3.15 × 10^{6}	5.72 × 10^{-2}
600	372.8	819.43	2300	18.70	81.30	4.29 × 10^{-4}	2.56 × 10^{-5}	14.33	1.63 × 10^{2}	2.05 × 10^{-8}	2.02 × 10^{-11}	1.54 × 10^{-15}	1.26 × 10^{-12}	6.49 × 10^{7}	1.84 × 10^{5}	8.69 × 10^{6}	2.12 × 10^{-2}	3.85 × 10^{6}	4.79 × 10^{-2}
625	388.4	812.56	2400	18.39	81.61	4.78 × 10^{-4}	2.94 × 10^{-5}	14.33	1.71 × 10^{2}	1.76 × 10^{-8}	1.74 × 10^{-11}	1.27 × 10^{-15}	1.04 × 10^{-12}	5.36 × 10^{7}	1.88 × 10^{5}	1.05 × 10^{7}	1.79 × 10^{-2}	4.66 × 10^{6}	4.04 × 10^{-2}
650	403.9	806.75	2500	18.10	81.90	5.35 × 10^{-4}	3.36 × 10^{-5}	14.32	1.80 × 10^{2}	1.53 × 10^{-8}	1.51 × 10^{-11}	1.05 × 10^{-15}	8.62 × 10^{-13}	4.46 × 10^{7}	1.92 × 10^{5}	1.26 × 10^{7}	1.52 × 10^{-2}	5.60 × 10^{6}	3.43 × 10^{-2}
700	435.0	795.40	2500	17.53	82.47	6.53 × 10^{-4}	4.34 × 10^{-5}	14.31	1.83 × 10^{2}	1.16 × 10^{-8}	1.14 × 10^{-11}	8.00 × 10^{-16}	6.54 × 10^{-13}	3.39 × 10^{7}	1.92 × 10^{5}	1.66 × 10^{7}	1.16 × 10^{-2}	7.38 × 10^{6}	2.60 × 10^{-2}
750	466.0	784.28	2500	16.99	83.01	7.95 × 10^{-4}	5.60 × 10^{-5}	14.30	1.85 × 10^{2}	8.85 × 10^{-9}	8.73 × 10^{-12}	6.09 × 10^{-16}	4.98 × 10^{-13}	2.58 × 10^{7}	1.92 × 10^{5}	2.18 × 10^{7}	8.83 × 10^{-3}	9.69 × 10^{6}	1.99 × 10^{-2}
800	497.1	773.39	2500	16.47	83.53	9.64 × 10^{-4}	7.18 × 10^{-5}	14.29	1.88 × 10^{2}	6.77 × 10^{-9}	6.68 × 10^{-12}	4.66 × 10^{-16}	3.81 × 10^{-13}	1.98 × 10^{7}	1.92 × 10^{5}	2.85 × 10^{7}	6.75 × 10^{-3}	1.27 × 10^{7}	1.52 × 10^{-2}
850	528.2	762.73	2500	15.96	84.03	1.17 × 10^{-3}	9.19 × 10^{-5}	14.28	1.91 × 10^{2}	5.20 × 10^{-9}	5.13 × 10^{-12}	3.57 × 10^{-16}	2.92 × 10^{-13}	1.52 × 10^{7}	1.92 × 10^{5}	3.71 × 10^{7}	5.19 × 10^{-3}	1.65 × 10^{7}	1.17 × 10^{-2}
900	559.2	752.29	2500	15.48	84.52	1.41 × 10^{-3}	1.17 × 10^{-4}	14.28	1.94 × 10^{2}	4.01 × 10^{-9}	3.96 × 10^{-12}	2.75 × 10^{-16}	2.25 × 10^{-13}	1.17 × 10^{7}	1.93 × 10^{5}	4.81 × 10^{7}	4.00 × 10^{-3}	2.14 × 10^{7}	9.01 × 10^{-3}
950	590.3	742.06	2500	15.02	84.98	1.69 × 10^{-3}	1.49 × 10^{-4}	14.27	1.96 × 10^{2}	3.10 × 10^{-9}	3.06 × 10^{-12}	2.13 × 10^{-16}	1.74 × 10^{-13}	9.05 × 10^{6}	1.93 × 10^{5}	6.22 × 10^{7}	3.10 × 10^{-3}	2.76 × 10^{7}	6.97 × 10^{-3}
1000	621.4	732.04	2500	14.57	85.43	2.03 × 10^{-3}	1.88 × 10^{-4}	14.26	1.99 × 10^{2}	2.41 × 10^{-9}	2.38 × 10^{-12}	1.65 × 10^{-16}	1.35 × 10^{-13}	7.03 × 10^{6}	1.93 × 10^{5}	8.01 × 10^{7}	2.41 × 10^{-3}	3.56 × 10^{7}	5.42 × 10^{-3}
1100	683.5	712.59	2500	13.73	86.27	2.91 × 10^{-3}	2.98 × 10^{-4}	14.24	2.05 × 10^{2}	1.47 × 10^{-9}	1.45 × 10^{-12}	1.01 × 10^{-16}	8.22 × 10^{-14}	4.28 × 10^{6}	1.93 × 10^{5}	1.31 × 10^{8}	1.47 × 10^{-3}	5.84 × 10^{7}	3.30 × 10^{-3}
1200	745.6	693.91	2500	12.94	87.05	4.11 × 10^{-3}	4.67 × 10^{-4}	14.23	2.10 × 10^{2}	9.07 × 10^{-10}	8.95 × 10^{-13}	6.21 × 10^{-17}	5.08 × 10^{-14}	2.65 × 10^{6}	1.93 × 10^{5}	2.13 × 10^{8}	9.07 × 10^{-4}	9.45 × 10^{7}	2.04 × 10^{-3}
1300	807.8	679.96	2500	12.22	87.78	5.77 × 10^{-3}	7.23 × 10^{-4}	14.21	2.16 × 10^{2}	5.68 × 10^{-10}	5.60 × 10^{-13}	3.88 × 10^{-17}	3.17 × 10^{-14}	1.66 × 10^{6}	1.93 × 10^{5}	3.40 × 10^{8}	5.68 × 10^{-4}	1.51 × 10^{8}	1.28 × 10^{-3}
1400	869.9	658.69	2500	11.55	88.44	8.01 × 10^{-3}	1.11 × 10^{-3}	14.20	2.22 × 10^{2}	3.60 × 10^{-10}	3.55 × 10^{-13}	2.46 × 10^{-17}	2.01 × 10^{-14}	1.05 × 10^{6}	1.93 × 10^{5}	5.36 × 10^{8}	3.60 × 10^{-4}	2.38 × 10^{8}	8.11 × 10^{-4}
1500	932.0	642.07	2500	10.92	89.06	1.10 × 10^{-2}	1.67 × 10^{-3}	14.19	2.28 × 10^{2}	2.31 × 10^{-10}	2.28 × 10^{-13}	1.58 × 10^{-17}	1.29 × 10^{-14}	6.73 × 10^{5}	1.93 × 10^{5}	8.36 × 10^{8}	2.31 × 10^{-4}	3.71 × 10^{8}	5.20 × 10^{-4}
1600	994.2	626.08	2500	10.34	89.64	1.51 × 10^{-2}	2.50 × 10^{-3}	14.17	2.34 × 10^{2}	1.50 × 10^{-10}	1.48 × 10^{-13}	1.02 × 10^{-17}	8.35 × 10^{-15}	4.37 × 10^{5}	1.93 × 10^{5}	1.29 × 10^{9}	1.50 × 10^{-4}	5.72 × 10^{8}	3.38 × 10^{-4}
1700	1056	610.64	2500	9.804	90.17	2.04 × 10^{-2}	3.70 × 10^{-3}	14.16	2.40 × 10^{2}	9.83 × 10^{-11}	9.70 × 10^{-14}	6.69 × 10^{-18}	5.47 × 10^{-15}	2.87 × 10^{5}	1.93 × 10^{5}	1.96 × 10^{9}	9.85 × 10^{-5}	8.72 × 10^{8}	2.22 × 10^{-4}
2000	1243	567.73	2500	8.397	91.54	4.84 × 10^{-2}	1.13 × 10^{-2}	14.11	2.60 × 10^{2}	2.96 × 10^{-11}	2.92 × 10^{-14}	2.01 × 10^{-18}	1.64 × 10^{-15}	8.62 × 10^{4}	1.94 × 10^{5}	6.52 × 10^{9}	2.97 × 10^{-5}	2.90 × 10^{9}	6.68 × 10^{-5}
2500	1553	505.59	2500	6.604	93.16	.1788	6.15 × 10^{-2}	13.94	2.95 × 10^{2}	4.84 × 10^{-12}	4.78 × 10^{-15}	3.25 × 10^{-19}	2.65 × 10^{-16}	1.41 × 10^{4}	1.95 × 10^{5}	3.99 × 10^{10}	4.89 × 10^{-6}	1.77 × 10^{10}	1.10 × 10^{-5}
3000	1864	453.12	2500	5.286	93.87	.5699	.2767	13.42	3.42 × 10^{2}	9.96 × 10^{-13}	9.83 × 10^{-16}	6.43 × 10^{-20}	5.26 × 10^{-17}	2.90 × 10^{3}	1.99 × 10^{5}	1.94 × 10^{11}	1.02 × 10^{-6}	8.61 × 10^{10}	2.31 × 10^{-6}
3500	2175	408.41	2500	4.262	93.10	1.591	1.052	11.96	4.25 × 10^{2}	2.64 × 10^{-13}	2.60 × 10^{-16}	1.52 × 10^{-20}	1.24 × 10^{-17}	7.72 × 10^{2}	2.10 × 10^{5}	7.29 × 10^{11}	2.88 × 10^{-7}	3.24 × 10^{11}	6.49 × 10^{-7}
4000	2485	370.01	2500	3.392	89.32	3.887	3.402	9.14	6.14 × 10^{2}	9.75 × 10^{-14}	9.62 × 10^{-17}	4.29 × 10^{-21}	3.50 × 10^{-18}	2.84 × 10^{2}	2.41 × 10^{5}	1.98 × 10^{12}	1.22 × 10^{-7}	8.80 × 10^{11}	2.74 × 10^{-7}
4500	2796	336.78	2500	2.566	80.10	8.148	9.194	5.87	1.05 × 10^{3}	5.16 × 10^{-14}	5.09 × 10^{-17}	1.46 × 10^{-21}	1.19 × 10^{-18}	1.50 × 10^{2}	3.00 × 10^{5}	3.74 × 10^{12}	8.03 × 10^{-8}	1.66 × 10^{12}	1.81 × 10^{-7}
5000	3107	307.84	2500	1.757	64.02	14.13	20.10	3.55	1.90 × 10^{3}	3.60 × 10^{-14}	3.55 × 10^{-17}	6.16 × 10^{-22}	5.04 × 10^{-19}	1.05 × 10^{2}	3.86 × 10^{5}	5.35 × 10^{12}	7.21 × 10^{-8}	2.38 × 10^{12}	1.62 × 10^{-7}
6000	3728	260.11	2500	.5616	26.86	23.13	49.44	1.76	4.54 × 10^{3}	2.58 × 10^{-14}	2.55 × 10^{-17}	2.18 × 10^{-22}	1.78 × 10^{-19}	7.52 × 10	5.48 × 10^{5}	7.49 × 10^{12}	7.32 × 10^{-8}	3.33 × 10^{12}	1.65 × 10^{-7}
7000	4350	222.68	2500	.1378	8.306	22.76	68.80	1.35	6.91 × 10^{3}	2.15 × 10^{-14}	2.12 × 10^{-17}	1.40 × 10^{-22}	1.14 × 10^{-19}	6.27 × 10	6.26 × 10^{5}	8.98 × 10^{12}	6.97 × 10^{-8}	3.99 × 10^{12}	1.57 × 10^{-7}
8000	4971	192.68	2500	3.51 × 10^{-3}	2.584	19.18	78.20	1.21	8.91 × 10^{3}	1.91 × 10^{-14}	1.88 × 10^{-17}	1.11 × 10^{-22}	9.09 × 10^{-20}	5.57 × 10	6.61 × 10^{5}	1.01 × 10^{13}	6.54 × 10^{-8}	4.49 × 10^{12}	1.47 × 10^{-7}
9000	5592	168.53	2500	1.02 × 10^{-2}	.8932	15.78	83.32	1.15	1.07 × 10^{4}	1.72 × 10^{-14}	1.70 × 10^{-17}	9.55 × 10^{-23}	7.81 × 10^{-20}	5.02 × 10	6.77 × 10^{5}	1.12 × 10^{13}	6.04 × 10^{-8}	4.98 × 10^{12}	1.36 × 10^{-7}
10,000	6214	148.58	2500	3.38 × 10^{-3}	.3451	13.12	86.53	1.12	1.25 × 10^{4}	1.58 × 10^{-14}	1.56 × 10^{-17}	8.52 × 10^{-23}	6.96 × 10^{-20}	4.61 × 10	6.87 × 10^{5}	1.22 × 10^{13}	5.62 × 10^{-8}	5.43 × 10^{12}	1.26 × 10^{-7}
15,000	9320	87.21	2500	6.05 × 10^{-3}	1.07 × 10^{-2}	6.234	93.76	1.06	2.25 × 10^{4}	1.17 × 10^{-14}	1.15 × 10^{-17}	5.97 × 10^{-23}	4.88 × 10^{-20}	3.42 × 10	7.08 × 10^{5}	1.64 × 10^{13}	4.30 × 10^{-8}	7.31 × 10^{12}	9.68 × 10^{-8}
20,000	12,427	57.28	2500	4.85 × 10^{-6}	1.20 × 10^{-3}	3.847	96.23	1.04	3.50 × 10^{4}	9.82 × 10^{-15}	9.69 × 10^{-18}	4.90 × 10^{-23}	4.00 × 10^{-20}	2.86 × 10	7.14 × 10^{5}	1.96 × 10^{13}	3.64 × 10^{-8}	8.73 × 10^{12}	8.18 × 10^{-8}
25,000	15,534	40.48	2500	8.64 × 10^{-7}	2.70 × 10^{-4}	2.749	97.25	1.03	4.99 × 10^{4}	8.71 × 10^{-15}	8.59 × 10^{-18}	4.31 × 10^{-23}	3.53 × 10^{-20}	2.54 × 10	7.17 × 10^{5}	2.21 × 10^{13}	3.24 × 10^{-8}	9.84 × 10^{12}	7.29 × 10^{-8}
30,000	18,641	30.12	2500	2.47 × 10^{-7}	9.12 × 10^{-5}	2.152	97.85	1.02	6.74 × 10^{4}	7.90 × 10^{-15}	7.79 × 10^{-18}	3.94 × 10^{-23}	3.22 × 10^{-20}	2.33 × 10	7.19 × 10^{5}	2.41 × 10^{13}	2.98 × 10^{-8}	1.07 × 10^{13}	6.70 × 10^{-8}
35,000	21,748	23.28	2500	9.54 × 10^{-8}	4.00 × 10^{-5}	1.785	98.21	1.02	8.74 × 10^{4}	7.49 × 10^{-15}	7.39 × 10^{-18}	3.68 × 10^{-23}	3.01 × 10^{-20}	2.18 × 10	7.20 × 10^{5}	2.58 × 10^{13}	2.79 × 10^{-8}	1.15 × 10^{13}	6.28 × 10^{-8}
40,000	24,855	18.53	2500	4.52 × 10^{-8}	2.10 × 10^{-5}	1.541	98.46	1.02	1.10 × 10^{5}	7.11 × 10^{-15}	7.01 × 10^{-18}	3.49 × 10^{-23}	2.85 × 10^{-20}	2.08 × 10	7.20 × 10^{5}	2.71 × 10^{13}	2.66 × 10^{-8}	1.21 × 10^{13}	5.98 × 10^{-8}
45,000	27,961	15.10	2500	2.48 × 10^{-8}	1.24 × 10^{-5}	1.369	98.63	1.02	1.35 × 10^{5}	6.83 × 10^{-15}	6.74 × 10^{-18}	3.34 × 10^{-23}	2.73 × 10^{-20}	1.99 × 10	7.21 × 10^{5}	2.82 × 10^{13}	2.55 × 10^{-8}	1.26 × 10^{13}	5.74 × 10^{-8}
50,000	31,068	12.54	2500	1.51 × 10^{-8}	8.11 × 10^{-6}	1.241	98.76	1.02	1.63 × 10^{5}	6.60 × 10^{-15}	6.51 × 10^{-18}	3.23 × 10^{-23}	2.64 × 10^{-20}	1.93 × 10	7.21 × 10^{5}	2.92 × 10^{13}	2.47 × 10^{-8}	1.30 × 10^{13}	5.56 × 10^{-8}
55,000	34,175	10.58	2500	9.98 × 10^{-9}	5.66 × 10^{-6}	1.144	98.86	1.02	1.93 × 10^{5}	6.42 × 10^{-15}	6.33 × 10^{-18}	3.14 × 10^{-23}	2.57 × 10^{-20}	1.87 × 10	7.22 × 10^{5}	3.01 × 10^{13}	2.40 × 10^{-8}	1.34 × 10^{13}	5.40 × 10^{-8}
60,000	37,282	9.05	2500	7.02 × 10^{-9}	3.92 × 10^{-6}	1.067	98.93	1.02	2.26 × 10^{5}	6.27 × 10^{-15}	6.19 × 10^{-18}	3.06 × 10^{-23}	2.50 × 10^{-20}	1.83 × 10	7.22 × 10^{5}	3.08 × 10^{13}	2.34 × 10^{-8}	1.37 × 10^{13}	5.28 × 10^{-8}
70,000	43,496	6.83	2500	3.99 × 10^{-9}	2.56 × 10^{-6}	.9536	99.05	1.02	3.00 × 10^{5}	6.03 × 10^{-15}	5.95 × 10^{-18}	2.94 × 10^{-23}	2.41 × 10^{-20}	1.76 × 10	7.22 × 10^{5}	3.20 × 10^{13}	2.26 × 10^{-8}	1.42 × 10^{13}	5.08 × 10^{-8}

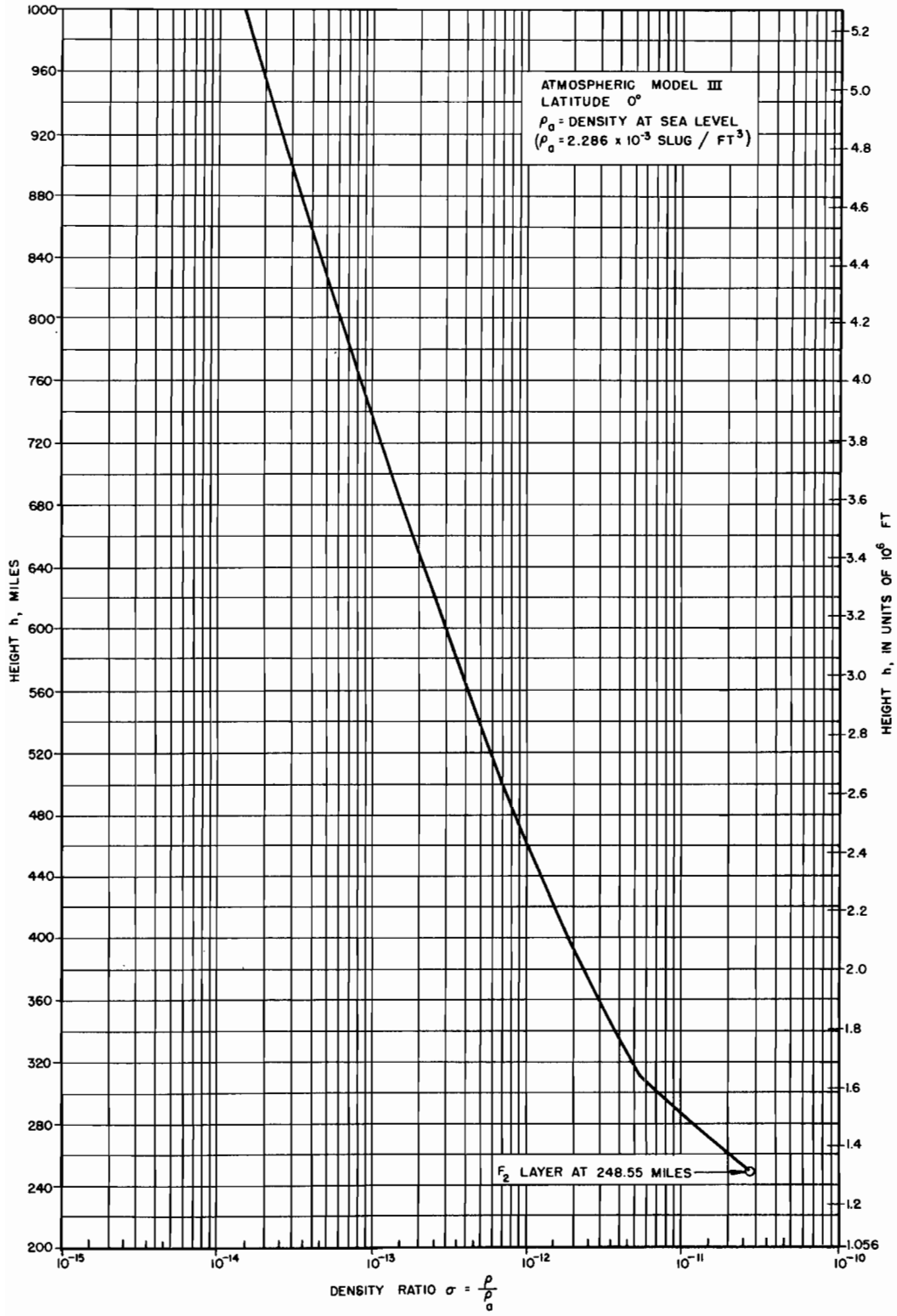

ATMOSPHERIC MODEL III - VERTICAL DISTRIBUTION OF THE DENSITY RATIO σ FROM THE F_2 LAYER UP TO 1000 MILES AT LATITUDE 0°. ENGINEERING UNITS.

FIG. 33

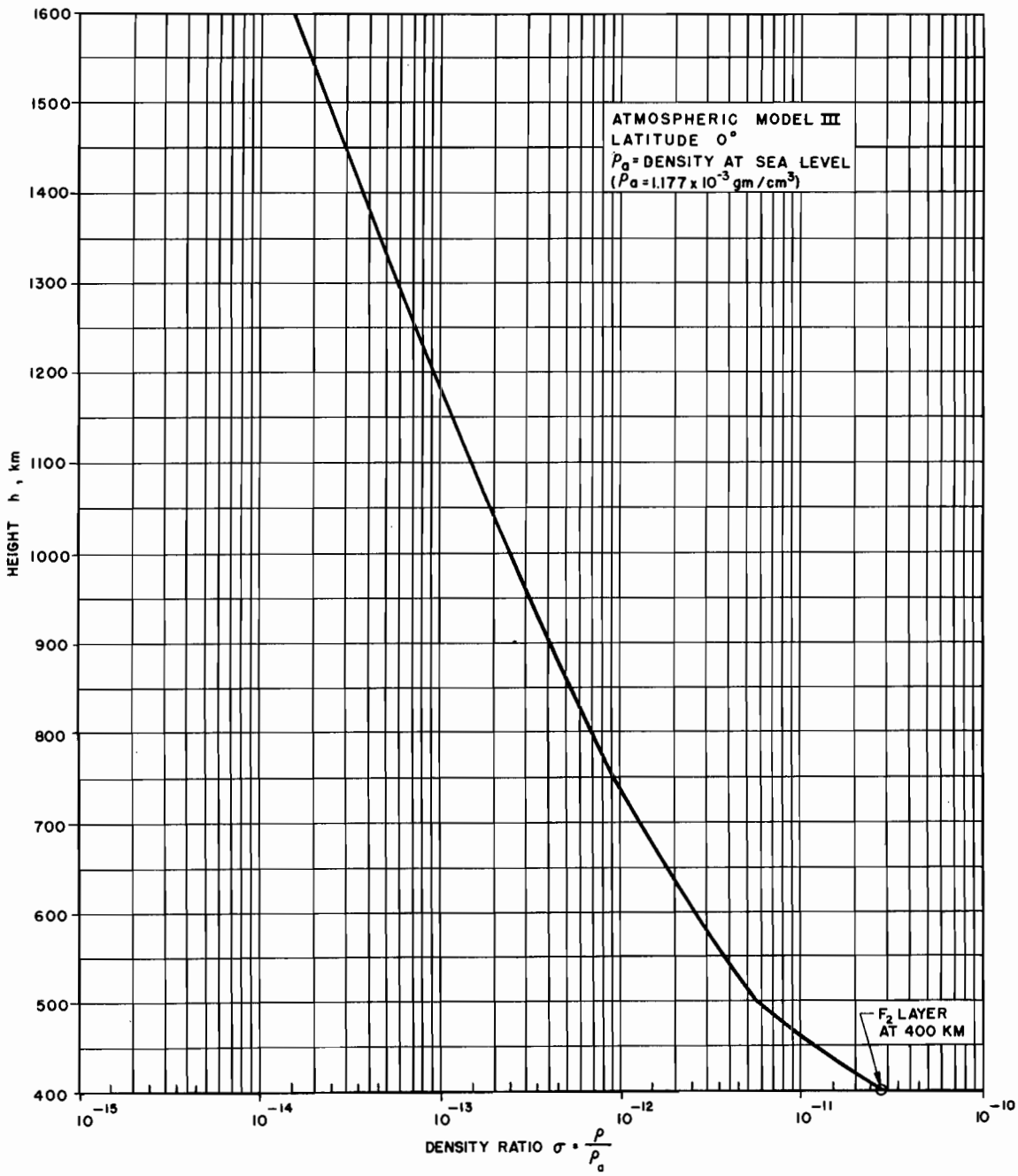

ATMOSPHERIC MODEL III - VERTICAL DISTRIBUTION OF THE DENSITY RATIO σ FROM THE F_2 LAYER UP TO 1600 KM AT LATITUDE 0°. METRIC UNITS.

FIG. 34

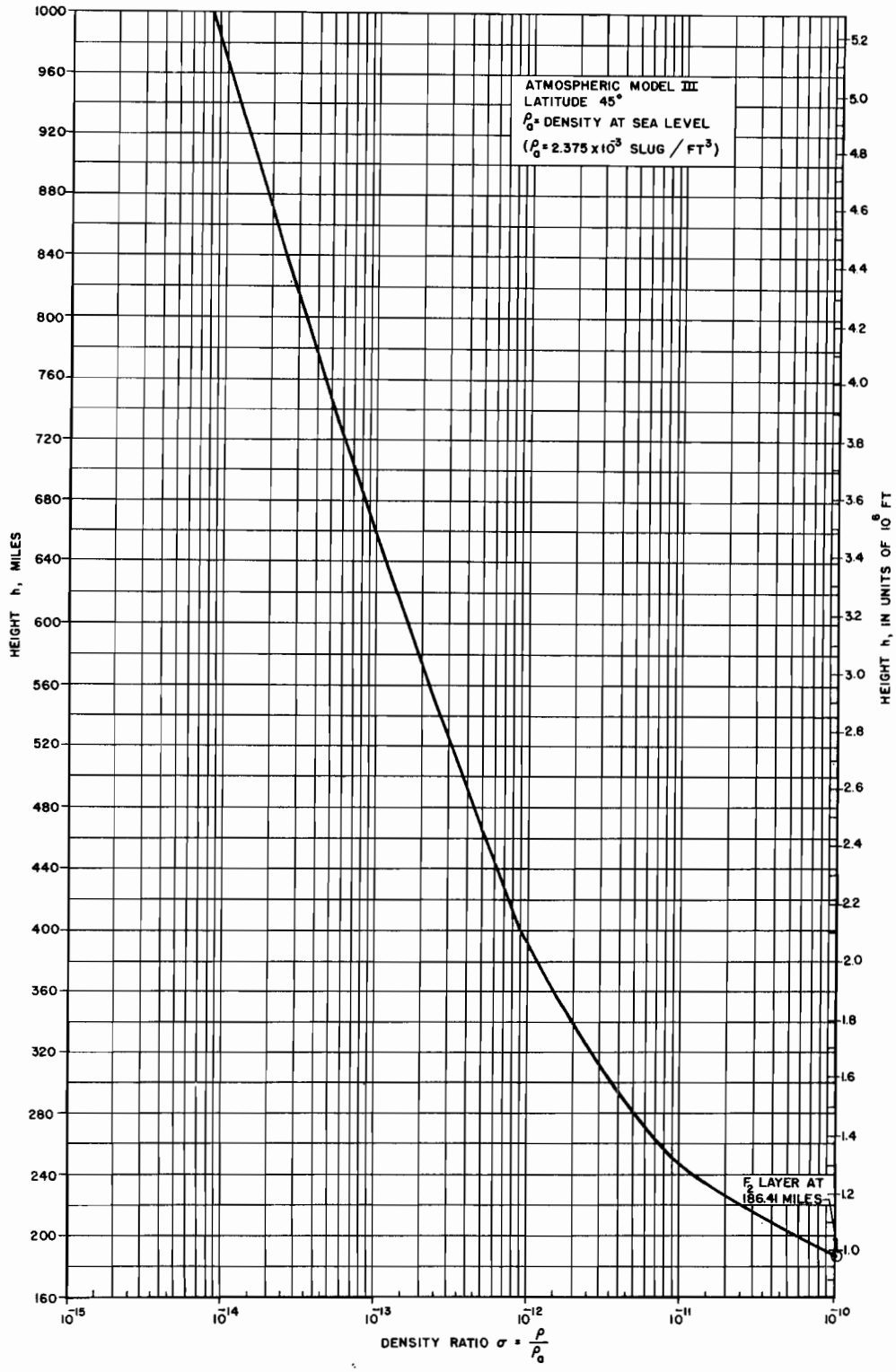

ATMOSPHERIC MODEL III-VERTICAL DISTRIBUTION OF THE DENSITY RATIO σ FROM THE F_2 LAYER UP TO 1000 MILES AT LATITUDE 45° ENGINEERING UNITS.

FIG. 35

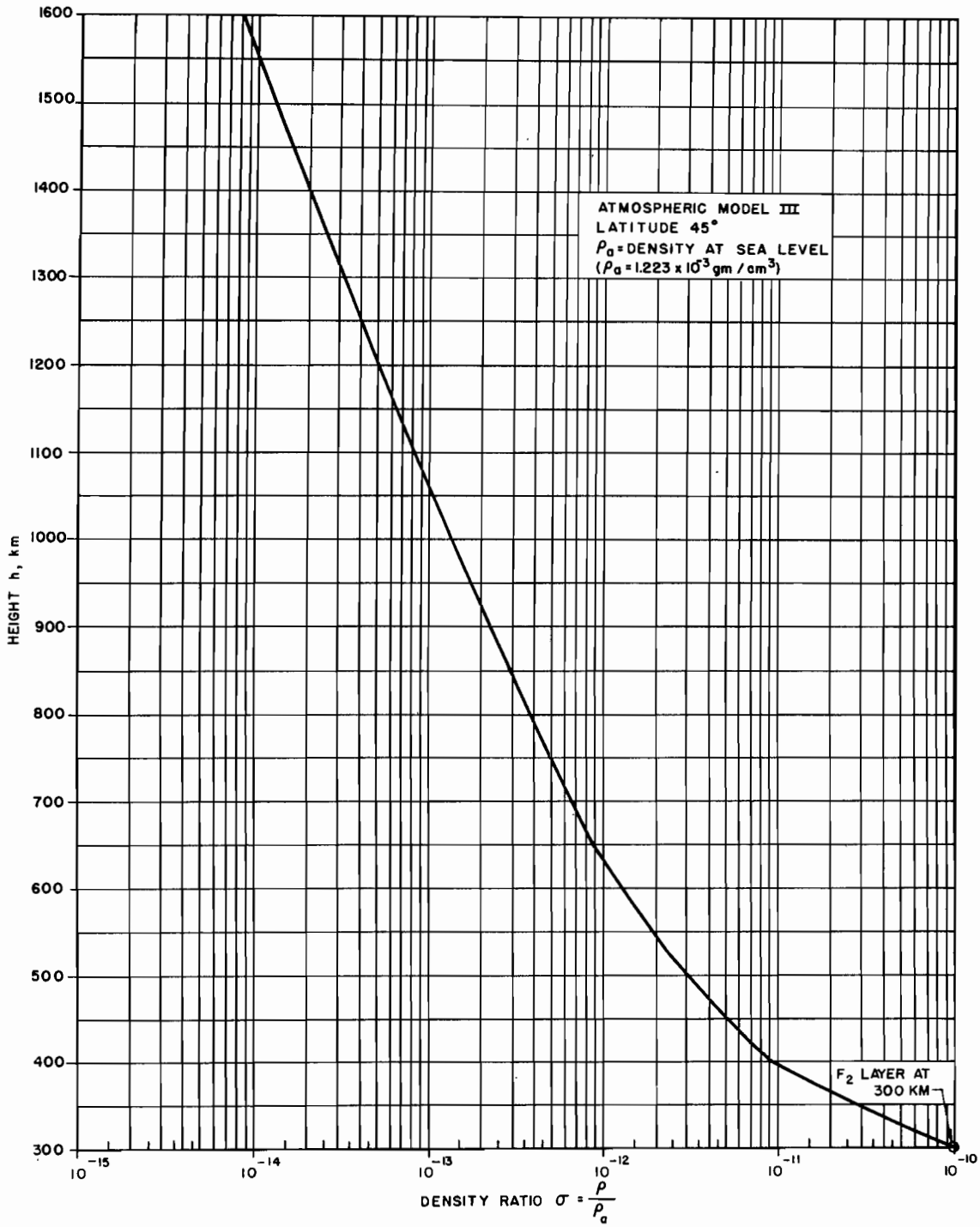

ATMOSPHERIC MODEL III-VERTICAL DISTRIBUTION OF THE DENSITY RATIO σ FROM THE F_2 LAYER UP TO 1600 KM AT LATITUDE 45° METRIC UNITS.

FIG. 36

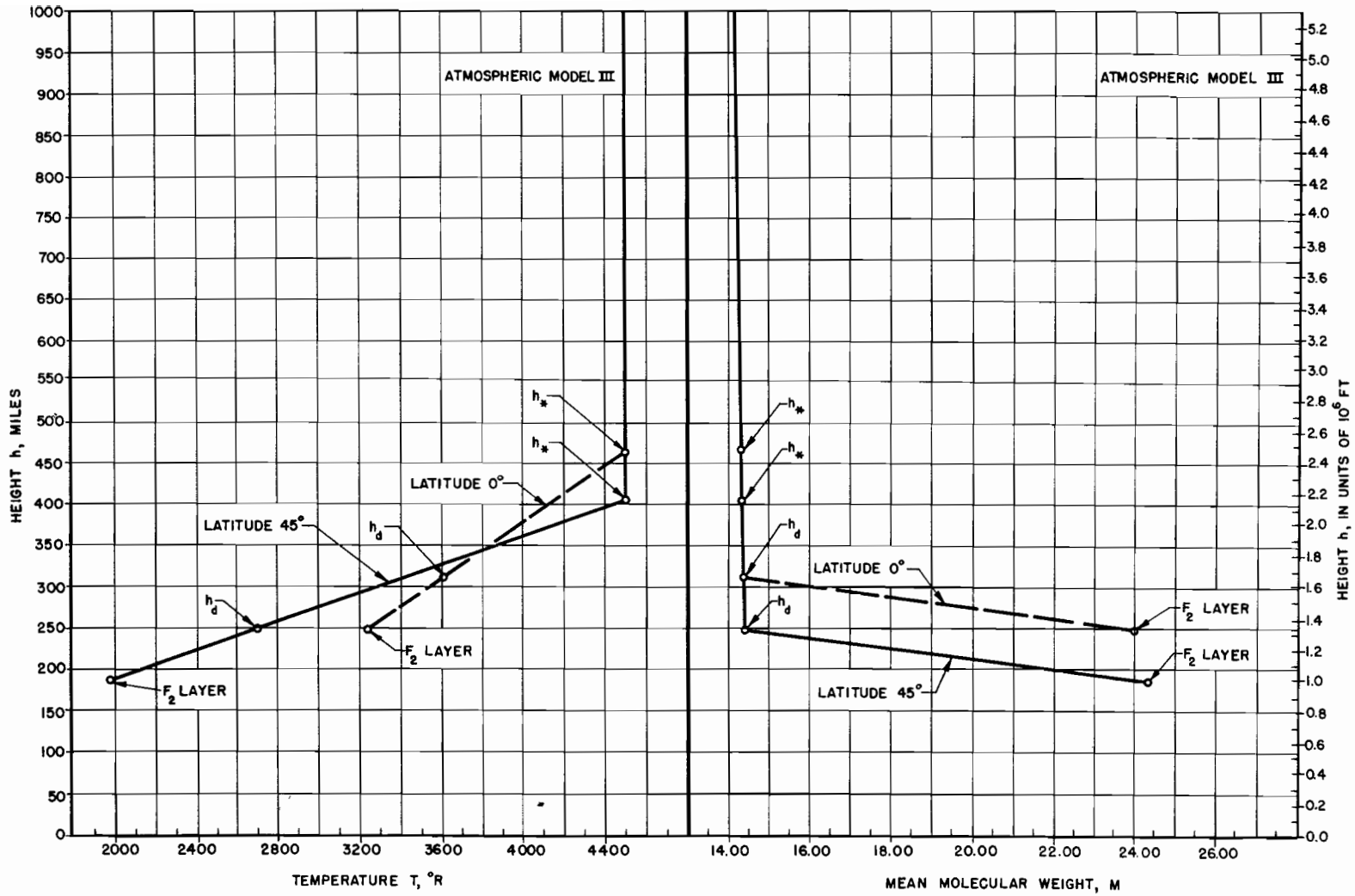

ATMOSPHERIC MODEL III-VERTICAL DISTRIBUTION OF THE TEMPERATURE AND COMPOSITION FROM THE F_2 LAYER UP TO 1000 MILES. ENGINEERING UNITS.

FIG. 37

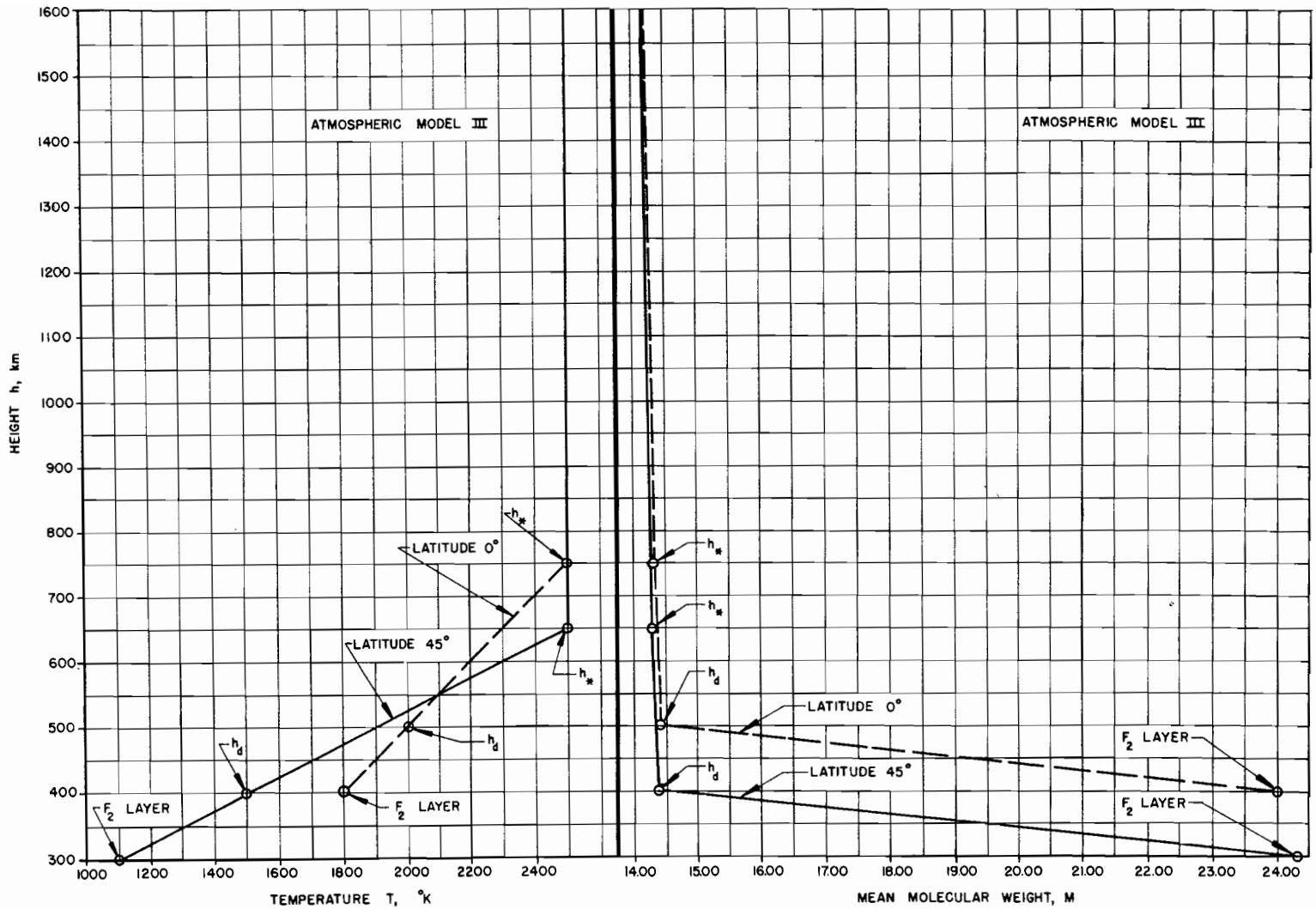

ATMOSPHERIC MODEL III – VERTICAL DISTRIBUTION OF THE TEMPERATURE AND COMPOSITION FROM THE F_2 LAYER UP TO 1600 KM. METRIC UNITS.

FIG. 38

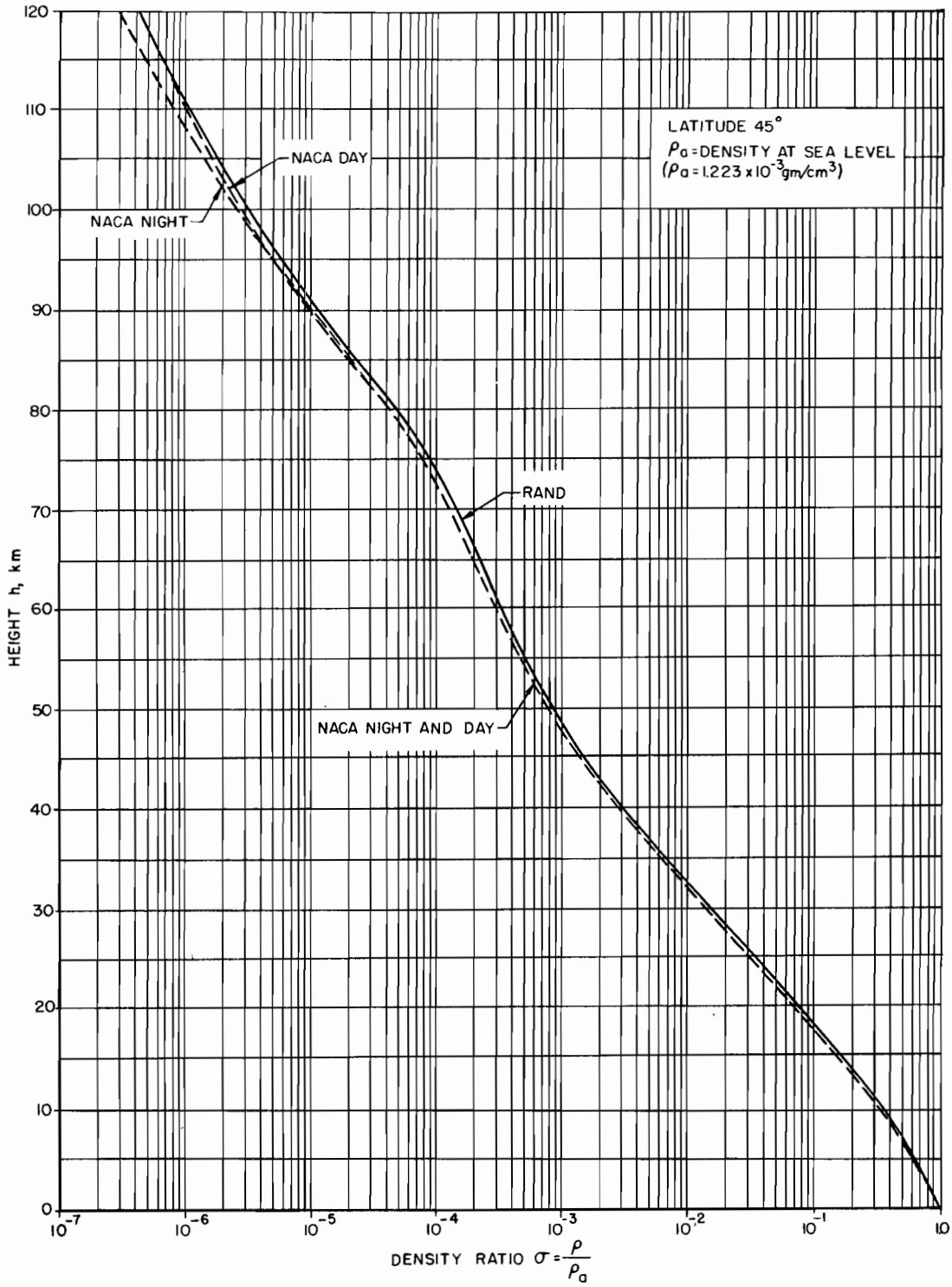

VERTICAL DISTRIBUTION OF THE DENSITY RATIO σ
FROM SEA LEVEL UP TO 120 KM. LATITUDE 45°.

FIG. 39

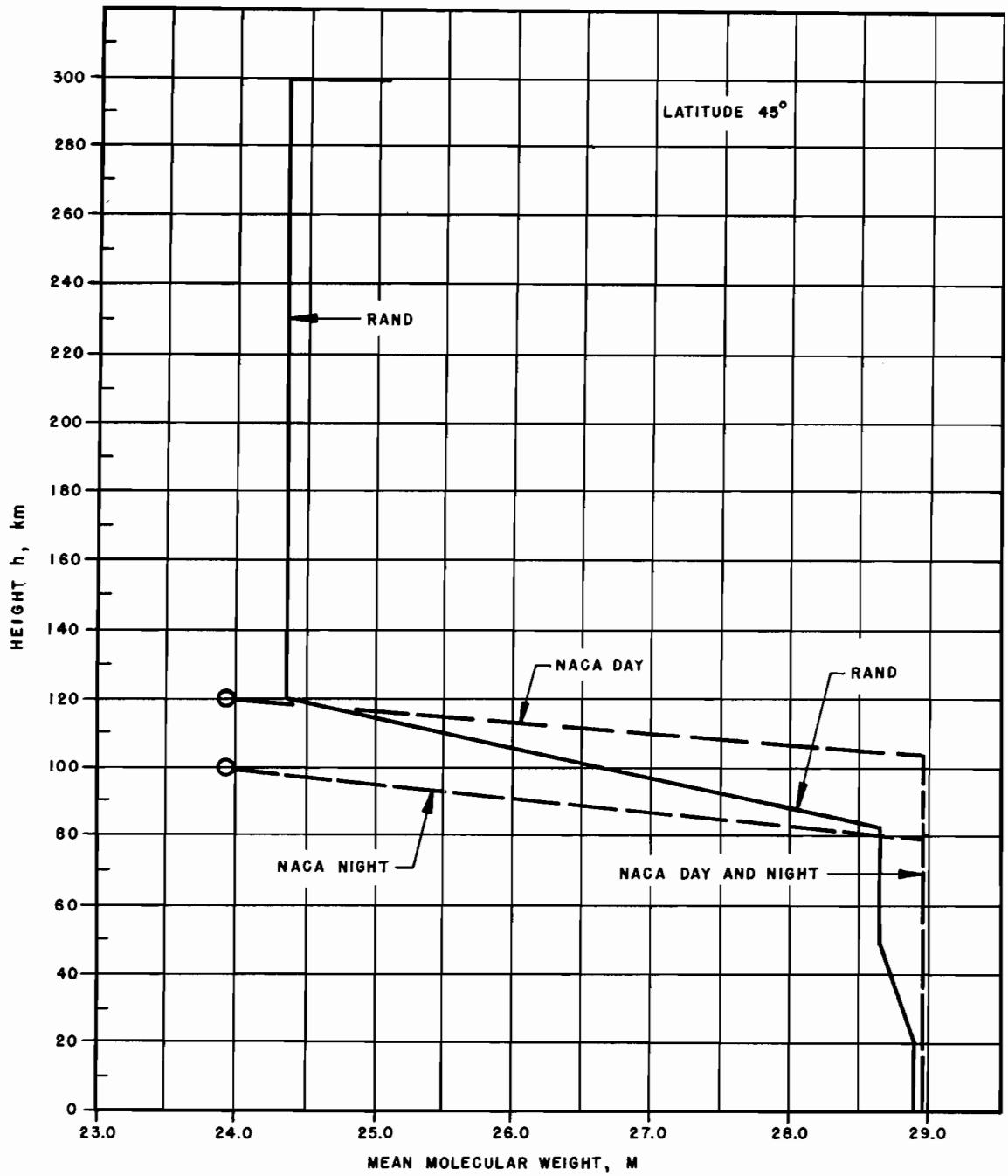

VERTICAL DISTRIBUTION OF MEAN MOLECULAR WEIGHT FROM SEA LEVEL UP TO THE F_2 LAYER. LATITUDE 45°

FIG. 40

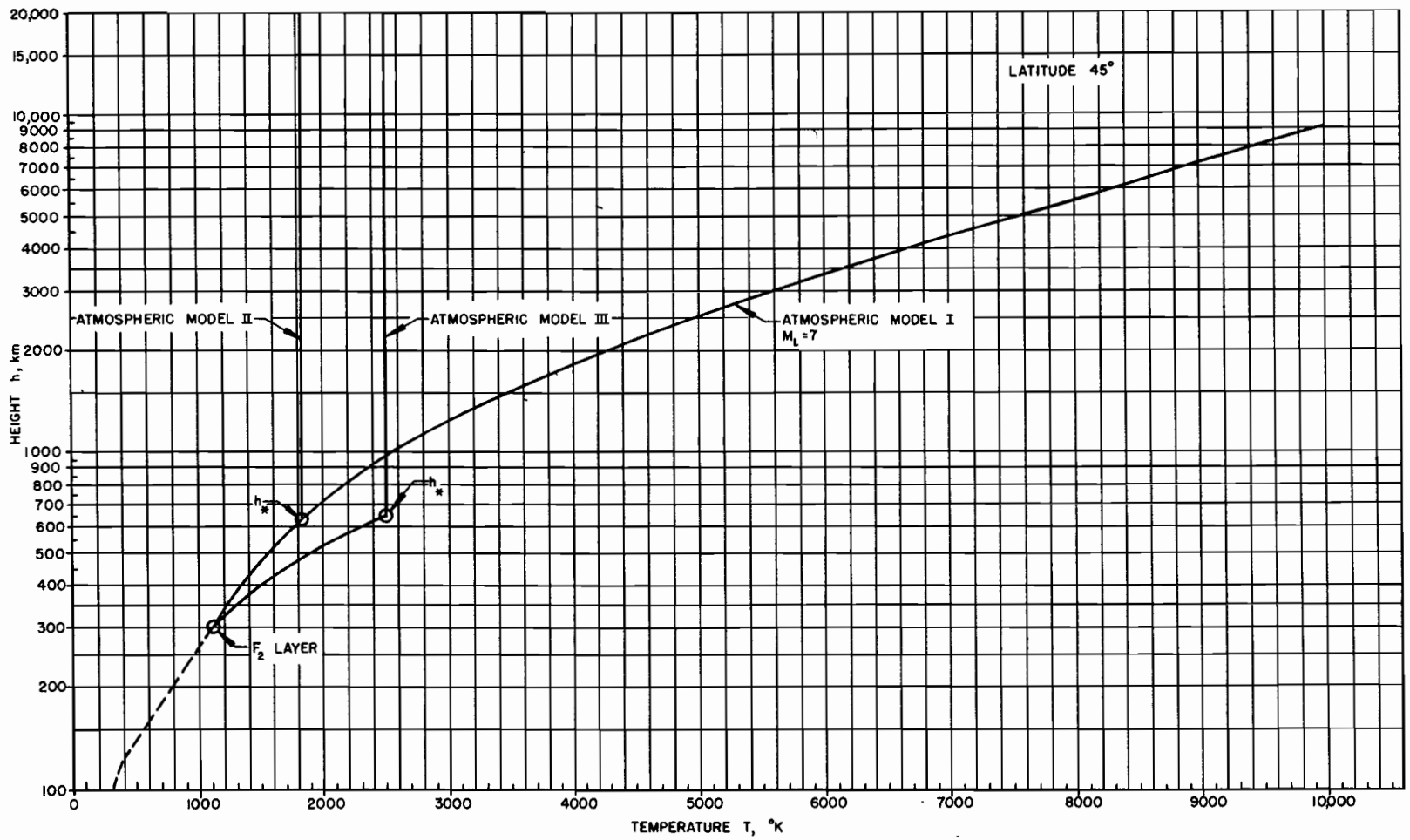

VERTICAL DISTRIBUTION OF TEMPERATURE ABOVE THE F_2 LAYER FOR MODELS I, II, AND III AT LATITUDE 45.° METRIC UNITS

FIG. 41

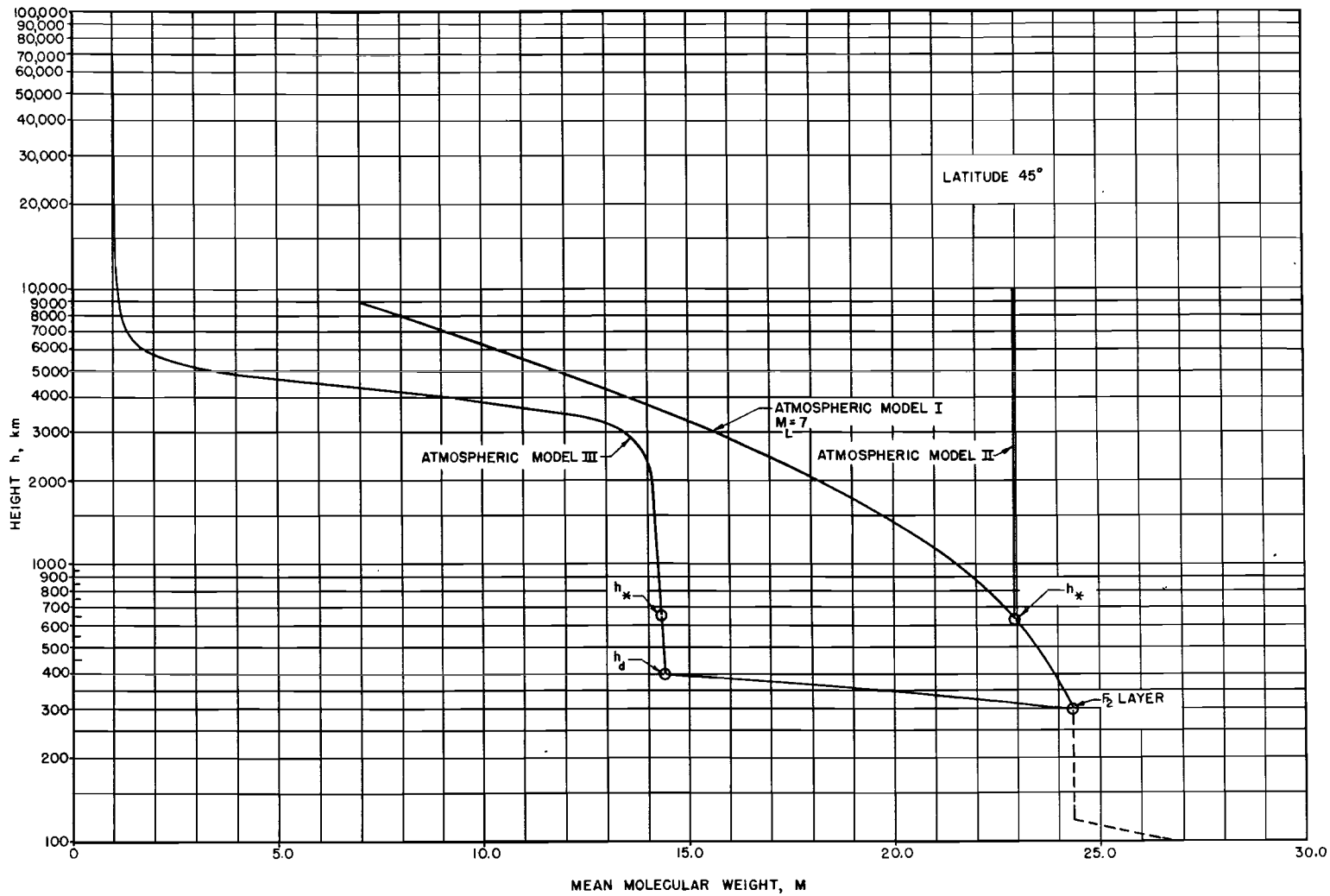

VERTICAL DISTRIBUTION OF MEAN MOLECULAR WEIGHT ABOVE THE F_2 LAYER FOR MODELS I, II, AND III AT LATITUDE 45°.

FIG. 42

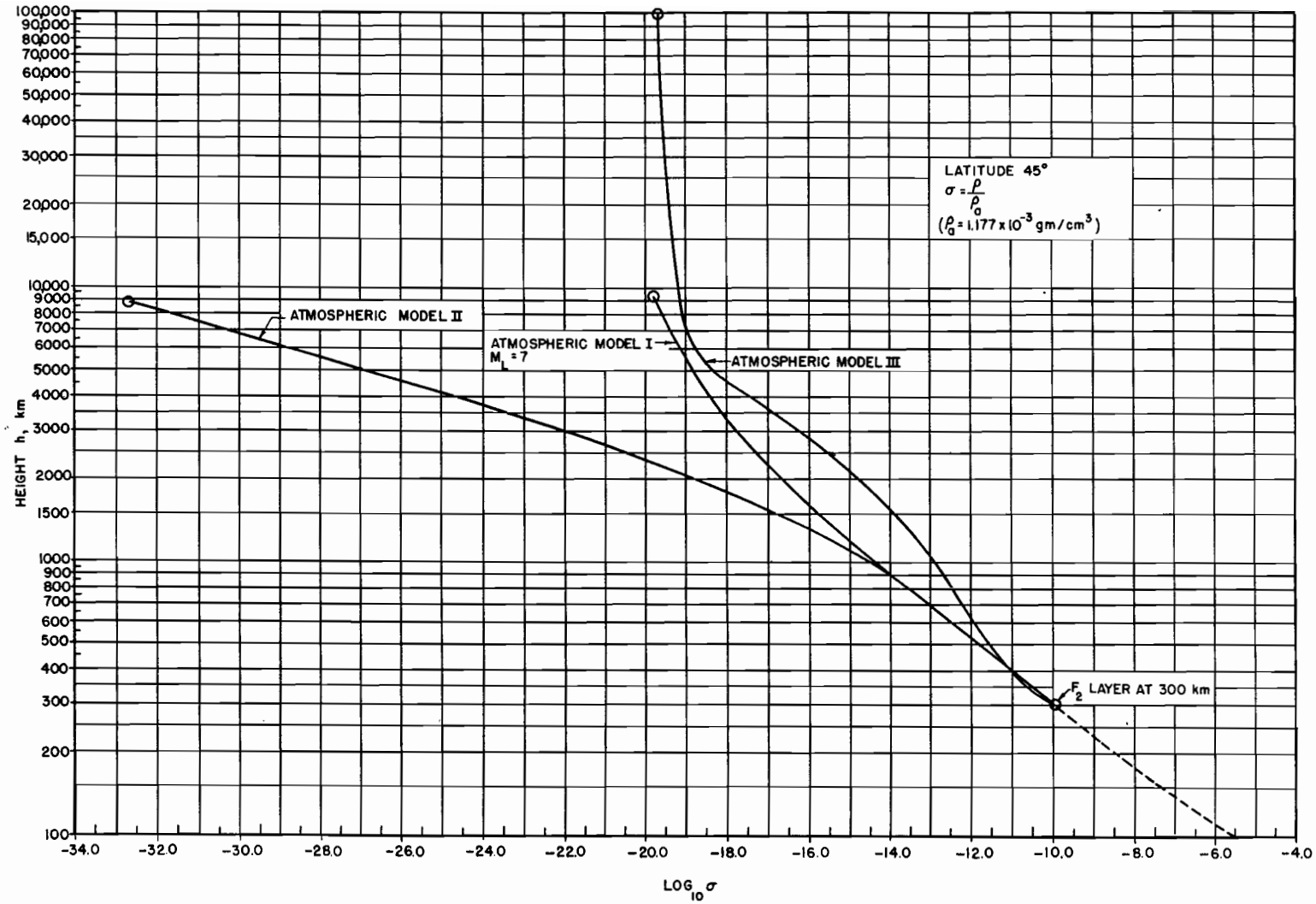

VERTICAL DISTRIBUTION OF THE DENSITY RATIO σ ABOVE THE F_2 LAYER FOR MODELS I, II, AND III AT LATITUDE 45°

FIG. 43

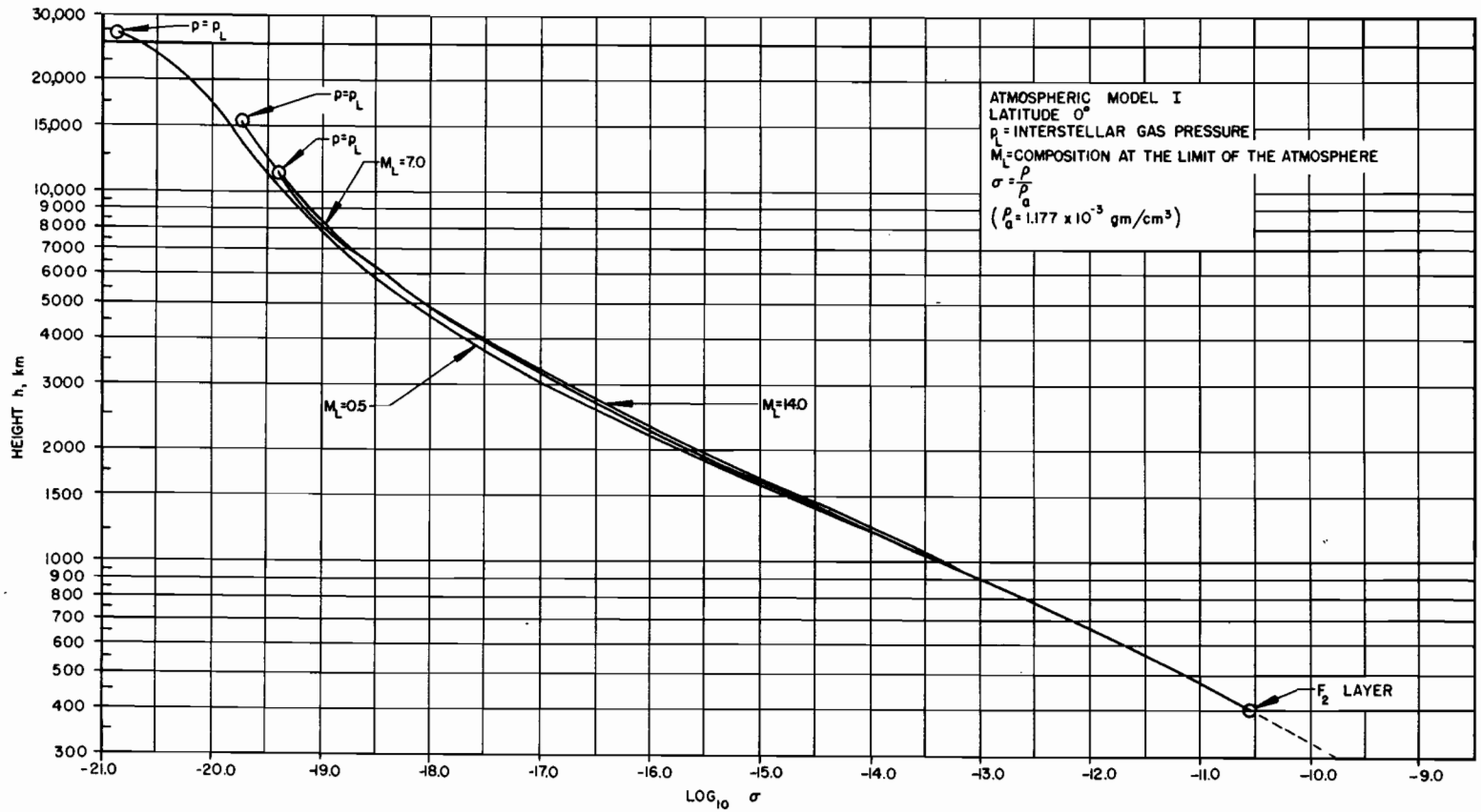

PLOT SHOWING THE SMALL EFFECT OF THE VALUE USED FOR M_L IN DETERMINING THE VERTICAL DENSITY DISTRIBUTION FOR MODEL I. LATITUDE 0.°

FIG. 44

REFERENCES

(1) Sänger, E., *Gaskinetik sehr hoher Fluggeschwindigkeiten,* Deutsche Luftfahrtforschung, Forschungs Bericht 972, Berlin, 1938, Douglas Aircraft Company, Inc., Translation F.R. 369.

(1a) Sänger, E., and Bredt, J., *A Rocket Drive for Long Range Bombers,* Deutsche Luftfahrtforschung, Untersuchengen u. Mitteilunger Nr. 3538, 1944, Bureau of Aeronautics, Navy Department, Washington, D.C., Translation CGD-32.

(2) Tsien, H.S., "Superaerodynamics, Mechanics of Rarefied Gases," *Journal of the Aeronautical Sciences,* Vol.13, p.653, No.12, December, 1946.

(3) Berkner, L.V., *Terrestrial Magnetism and Electricity, in* Fleming, J.A., editor, *Physics of the Earth* - VIII, New York: McGraw-Hill Book Company, Inc., Chap.9, 1939.

(4) Hulburt, E.O., *Terrestrial Magnetism and Electricity, in* Fleming, J.A., editor, *Physics of the Earth* - VIII, New York: McGraw-Hill Book Company, Inc., Chap.10, 1939.

(5) Mitra, S.K., "Report on the Present State of Our Knowledge of the Ionosphere," *Proc. of the National Institute of Sciences of India,* Vol.1, No.3, Calcutta, 1935.

(6) Millington, G., *Fundamental Principles of Ionospheric Transmission,* Part I, Baddow Report 990, British Admiralty, September, 1943.

(7) Diehl, W.S., *Standard Atmosphere--Tables and Data,* NACA Technical Report No.218, 1925 and 1940.

(8) Bjerknes, V., *et al.,* "Hydrodynamique Physique," Les Presses Universitaires de France, Paris, Vol.3, pp.684-687, 1934.

(9) Haurwitz, B., "The Physical State of the Upper Atmosphere," *Reprinted from the Journal of the Royal Astronomical Society of Canada,* Toronto, 1941.

(10) Penndorf, R., "The Temperature of the Upper Atmosphere," *Bulletin of the American Meteorological Society,* Vol.27, p.331, June, 1946.

(11) Penndorf, R., *The Constitution of the Stratosphere,* Bulletin of the American Meteorological Society, Vol.27, p.343, June 1946.

(12) Gutenberg, B., "Physical Properties of the Atmosphere up to 100 km," *Journal of Meteorology,* Vol.3, p.27, June, 1946.

(13) Warfield, C.N., *Tentative Tables for the Properties of the Upper Atmosphere,* NACA Technical Note No.1200, January, 1947.

(14) Appleton, E.V., "The Upper Atmosphere--The Structure of the Atmosphere as Deduced From Ionosphere Observations," *Quart. Jour. Roy. Met. Soc.,* Vol.65, pp.324-328, 1939.

(15) Chapman, S., and Bartels, J., *Geomagnetism,* Oxford: Clarendon Press, Vol.1, Chap.15, 1940.

(16) Appleton, E.V., "A Method of Measuring the Collisional Frequency of Electrons in the Ionosphere," *Nature,* Vol.135, 1935.

(17) Eckersley, T.L., "Collision Frequency and Molecular Density in the F_1 layer of the Ionosphere," *Nature*, Vol.135, p.435, 1935.

(18) Farmer, F.T., and Ratcliffe, J.A., "Measurements of the Absorption of Wireless Waves in the Ionosphere," *Proc. Roy. Soc.*, Vol.A151, pp.370-383, 1935.

(19) Farmer, F.T., and Ratcliffe, J.A., "Frequency Collision of Electrons in the Ionosphere," *Nature*, Vol.135, p.585, 1935.

(20) Fuchs, J., Eine Radio-Methode zur Bestimmung der Absoluttemperatur der Ionosphäre. Meteorologische Zeitschrift, Band 53, p.41, February, 1936.

(21) Martyn, D.F., and Pulley, O.O., "The Temperatures and Constituents of the Upper Atmosphere," *Proc. Roy. Soc.*, Vol.A154, p.482, 1936.

(22) Godfrey, G.H., and Price, W.L., "Thermal Radiation and Absorption in the Upper Atmosphere," *Proc. Roy. Soc.*, Vol.A163, p.228, 1937.

(23) Das, A.K., "On the Temperature of the Earth's Outer Atmosphere and the Forbidden OI Lines of the Night-Sky Spectrum," *Gerlands Beiträge zur Geophysik*, Vol.47, p.136, 1936.

(24) Senda, K., "Über die Temperatur der ultrahohen Atmosphäre nach der Dissoziationstheorie," *Jour. Shanghai Science Institute*, Section I, Vol.1, p.163, 1938.

(25) Bhar, J.N., "Stratification of the Ionosphere and the Origin of the E_1 Layer," *Indian Jour. of Physics*, Vol.12, p.364, 1938.

(26) Penndorf, R., "Die Ionosphärentemperaturen," *Die Naturwissenschaften*, Band 28, p.751, 1940.

(27) Berkner, L.V., and Wells, H.W., "*F*-Region Ionosphere Investigations at Low Latitudes," *Terr. Mag.*, Vol.39, p.215, 1934.

(28) Zenneck, J., *Physik der hohen Atmosphäre--Ergebnisse der kosmischen Physik*, Band III, Leipzig: Akademische Verlagsgesellschaft, M.B.H., p.32, 1938.

(29) Joos, G., *Theoretical Physics*, New York: G.E. Stechert & Company, Chap.34, 1934.

(30) Paneth, F.A., "Composition of the Upper Atmosphere--Direct Chemical Investigation," *Quart. Jour. Roy. Met. Soc.*, Vol.65, pp.304-310, 1939.

(31) Chapman, S., "The Upper Atmosphere--Spectroscopic and Other Evidence as to Chemical Composition and Dissociation," *Quart. Jour. Roy. Met. Soc.*, Vol.65, pp.310-319, 1939.

(32) Penndorf, R., "Die Zusammensetzung der Luft in der hohen Atmosphäre," *Meteorologische Zeitschrift*, Vol.55, p.30, 1938.

(33) Wulf, O.R., and Deming, L.S., "On the Production of the Ionospheric Regions *E* and *F* and the Lower Altitude Ionization Causing Radio Fade-Outs," *Terr. Mag.*, Vol.43, pp.283-298, 1938.

(34) Cowling, T.G., "The Electrical Conductivity of an Ionized Gas in a Magnetic Field With Applications to the Solar Atmosphere and the Ionosphere," *Proc. Roy. Soc.*, Vol.A183, pp.470-474, 1945.

(35) Mitra, S.K., and Rakshit, H., "Distribution of the Constituent Gases and Their Pressures in the Upper Atmosphere," *Indian Journal of Physics*, Vol.12, p.6, 1938.

(36) Regener, E., *The Structure and Composition of the Stratosphere*, AAF Translation No.509, Wright Field, Dayton, Ohio, 1946.

(37) Pekeris, C.L., "The Vertical Distribution of Ionization in the Upper Atmosphere," *Terr. Mag.*, Vol.45, p.205, 1940.

(38) Tsien, H.S., and Schamberg, R., "Propagation of Plane Sound Waves in Rarefied Gases," *Jour. of Acoustical Soc. of America*, Vol.18, No.2, p.334, October, 1946.

(39) Goldberg, L., and Aller, L.H., *Atoms, Stars, and Nebulae*, Philadelphia: The Balkiston Company, p.197, 1943.

(40) Ledoux, P., "A Summary of the Symposium on Interstellar Lines at the Yerkes Observatory," *Popular Astronomy*, No.490, p.513, December, 1941.

(41) Struve, O., "The Physical State of the Interstellar Gas Clouds," *Proc. Nat'l. Acad. Sci.*, Vol.25, p.36, 1939.

(42) Spitzer, L., Jr., "The Dynamics of the Interstellar Medium II," *Astrophys. J.*, Vol.95, No.3, p.329, 1942.

(43) Swings, P., "Considerations Regarding Cometary and Interstellar Molecules," *Astrophys. J.*, Vol.95, p.270, 1942.

(44) Eddington, A., *Internal Constitution of the Stars*, Cambridge: University Press, pp.373-377, 1926.

(45) Jeans, J.H., "On Radiative Equilibrium and the Rotation of Astronomical Masses," *Monthly Notices of the Roy. Astr. Soc.*, Vol.86, p.328, 1926.

(46) Lindemann, F.A., "Discussion on the Constitution of the Upper Atmosphere," *Quart. Jour. Roy. Met. Soc.*, Vol.65, p.332, 1939.

(47) Ferraro, V.C.A., "Diffusion of Ions in the Ionosphere," *Terr. Mag.*, Vol.50, No.3, p.215, September, 1945.

(48) Jones, H. Spencer, "The Atmospheres of the Planets," *Quart. Jour. Roy. Met. Soc.*, Vol.68, p.121, April, 1942.

(49) Saha and Srivastava, *Treatise on Heat*, Calcutta: The Indian Press, Ltd., p.695, 1935.

(50) Saha, M.N., and Saha, N.K., *A Treatise on Modern Physics*, Calcutta: The Indian Press, Ltd., Vol.1, p.628, 1934.

(51) Hewson, E.W., "A Survey of the Facts and Theories of the Aurora," *Reviews of Modern Physics*, Vol.9, p.422, October, 1937.

(52) Langer, R.M., *Physical Review*, Vol.55, p.423, 1939.

(53) Jeans, J.R., *The Dynamical Theory of Gases*, Cambridge: University Press, Chap.15, 1925.

(54) Bjerknes, V., "On the Dynamics of the Circular Vortex With Applications to the Atmosphere and Atmospheric Vortex and Wave Motions," *Geofysiske Publicationer*, Vol.2, No.4, *Kristiania*, Vol.2, No.4, 1921.

(55) Bryan, G.H., "The Kinetic Theory of Planetary Atmospheres," *Phil. Trans. of the Roy. Soc. of London,* Series A, Vol.196, p.1, 1901.

(56) Milne, E.A., "The Escape of Molecules From an Atmosphere, With Special Reference to the Boundary of a Gaseous Star," *Transactions of the Cambridge Philosophical Society,* Cambridge: University Press, Vol.22, No.26, pp.483-517, 1923.

(57) Kennard, E.H., *Kinetic Theory of Gases,* New York: McGraw-Hill Book Company, Inc., 1931.

(58) Loeb, L.B., *The Kinetic Theory of Gases,* New York: McGraw-Hill Book Company, Inc., p.220, 1934.

(59) Cobine, J.D., *Gaseous Conductors,* New York: McGraw-Hill Book Company, Inc., p.22, 1941.

(60) Vassy, A., and Vassy, M.E., "La Temperature de la Haute Atmosphere," *Le Journal de Physique et le Radium,* Serie VIII, Tome III, pp.14-15, January, 1942.

(61) Spitzer, L., Jr., *The Terrestrial Atmosphere Above 400 Kilometers,* Symposium on Planetary Atmospheres held at Yerkes Observatory, 1947.
To appear in a centennial volume of the Yerkes Observatory.

(62) Herzberg, G., *Atomic Spectra and Atomic Structure,* Dover Publications, 1944.

(63) Bacher, R., and Goudsmit, S., *Atomic Energy States,* New York: McGraw-Hill Book Company, Inc., 1932.

(64) Elvey, C.T., Swings, P., and Linke, W., "The Spectrum of the Night Sky," *Astrophys. J.,* Vol.93, p.337, 1941.

(64a) Elvey, C.T., and Farnsworth, A.H., "Spectrophotometric Observations of the Light of the Night Sky," *Astrophys. J.,* Vol.96, p.451, November, 1942.

(64b) Elvey, C.T., "The Light of the Night Sky," *Reviews of Modern Physics,* Vol.14, Nos.2-3, p.140, 1942.

(64c) Massey, H.S.W., and Bates, D.R., *The Properties of Neutral and Ionized Atomic Oxygen and Their Influence on the Upper Atmosphere,* The Physical Society, London, *Reports on Progress in Physics,* Vol.9, 1942-43.

(65) Hebb, M.J., and Menzel, D.H., "Physical Processes in Gaseous Nebulae X - Collisional Excitation of Nebulium," *Astrophys. J.,* Vol.92, p.408, 1940.

(65a) Chapman, S., and Cowling, T.G., *The Mathematical Theory of Non-Uniform Gases,* Cambridge: University Press, p.352, 1939.

(65b) Loeb, L.B., *Fundamental Processes of Electrical Discharge in Gases,* New York: John Wiley & Sons, p.652, 1939.

(65c) Taylor, H.S., and Glasstone, S., *A Treatise on Physical Chemistry,* New York: D. Van Nostrand Company, Inc., Vol.1, p.380, 1941.

(66) Richtmeyer, F.K., and Kennard, E.H., *Introduction to Modern Physics,* New York: McGraw-Hill Book Company, Inc., p.248, 1942.

(67) Spitzer, L., Jr., *Private Communication,* November, 1947.

(68) Bates, D.R., and Massey, H.S.W., "The Basic Reactions in the Upper Atmosphere - I, "*Proc. Roy. Soc.*, London, Vol.187, No.1010, November, 1946; Part II, "The Theory of Recombination in the Ionized Layers," Vol.192, No.1028, December, 1947.

(69) Maris, H.B., "The Upper Atmosphere," *Terr. Mag.*, Vol.33, p.233, 1928, and Vol.34, No.1, p.45, 1929.

(70) Epstein, P.S., "Über Gasentmischung in der Atmosphäre," *Gerlands Beiträge zur Geophysik*, Band 35, Heft 1, 1932.

(71) Chapman, S., and Milne, E.A., "The Composition, Ionization and Viscosity of the Atmosphere at Great Heights," *Quart. Jour. Roy. Met. Soc.*, Vol.46, No.196, 1920.

(72) Report on Japanese Research on Radio Wave Propagation, General Headquarters, U.S. Army Forces, Pacific, Tokyo, Vol.1, p.18, 1946. See also the Central Radio Propagation Laboratory publications of the National Bureau of Standards.

(73) Bailey, D.K., and Menzel, D.H., *The G Layer of the Ionosphere*, Project RAND, Douglas Aircraft Company, Inc., Report RA-15057, August, 1947
Also to appear as a paper in the publication of the International Scientific Radio Union Congress - 1947.

(74) Deb, A.C., "Temperature of the Upper Atmosphere," *Science and Culture*, Calcutta, Vol.6, p.502, 1941.

(75) Kaplan, J., "Hydrogen in the Upper Atmosphere," *Nature*, Vol.136, p.549, 1935.

ADDITIONAL REFERENCES OF INTEREST

(76) Woolley, R.v.d.R., "The Mechanism of Ionospheric Ionization," *Proc. Roy. Soc.*, London, Vol.A187, p.403, December, 1946.

(77) Woolley, R.v.d.R., "Radiative Equilibrium in the Ionosphere," *Proc. Roy. Soc.*, London, Vol.A189, p.218, April, 1947.

(78) Pande, A., "Critical Survey of Recent Theoretical Work on the Ionosphere," *Terr. Mag.*, Vol.52, No.3, September, 1947.

(79) Manning, L.A., *A Survey of the Literature of the Ionosphere*, Department of Electrical Engineering, Stanford University, Palo Alto, Calif., Report No.1-F1, August, 1947.
Prepared under Army Air Forces Contract. This contains a very complete bibliography together with brief abstracts.

(80) Whipple, F.L., "Meteors and the Earth's Upper Atmosphere," *Reviews of Modern Physics*, Vol.15, No.1, October, 1943.

(81) Hulburt, E.O., "Terrestrial Magnetic Variations and Aurorae," *Reviews of Modern Physics*, Vol.9, January, 1937.

(82) George, E.F., "Electronic Collision Frequency in the Upper Atmosphere," *Proceedings of the I.R.E.*, p.249, 1947.

(83) Gosh, S.N., "A Note on 'Effective Recombination Coefficient' in the Ionospheric Regions," *Proceedings of the National Institute of Sciences of India,* Vol.10, No.3, pp.333-342, 1944.

(84) Appleton, E.V., "On Two Methods of Ionospheric Investigation," *Proceedings of the Physical Society,* London, Vol.45, p.673, 1933.

(85) Mitra, S.K., *The Upper Atmosphere,* Calcutta: Royal Asiatic Society of Bengal, January, 1947.
Although this book has not yet been available for examination, the advance notices indicate that it contains a complete account of the present state of knowledge of the upper atmosphere, including the ionosphere, the aurora, the light of the night sky, etc.

(86) Wu, Ta-You, "On the Existence of Atomic Nitrogen in the Upper Atmosphere of the Earth," *Physical Review,* Vol.66, Nos.3-4, p.65, August, 1944.

(87) Hulburt, E.O., "The Upper Atmosphere of the Earth," *Jour. of Optical Soc. of America,* Vol.37, No.6, June, 1947.

(88) Mimno, H.R., "The Physics of the Ionosphere," *Reviews of Modern Physics,* Vol.9, No.1, January, 1937.

(89) Spitzer, Lyman, Jr., "The Temperature of Interstellar Matter - I," *Astrophys. J.,* Vol. 107, No.1, January 1948.

(90) Hulbert, E.O., "Ionization in the Upper Atmosphere of the Earth," *Phys. Rev.,* Vol.31, No.6, p.1018, June 1928.

(91) Chapman, S., "The Absorption and Dissociative or Ionizing Effect of Monochromatic Radiation in an Atmosphere on a Rotating Earth," *Proc. Phys. Soc.,* London, Vol.43, p.26, Part I, January 1931.

(92) *Ibid.,* "Part II, Grazing Incidence," Part 5, p.483, September.

(93) Barbier, Daniel, and Chalonge, Daniel, *De La Stratosphère A L'Ionosphère,* Paris: Presses Universitaires De France, 1942.

(94) Ratner, Benjamin, "Upper Air Values of Temperature, Pressure, and Relative Humidity over the United States and Alaska," *Climate and Crop Weather Division, Weather Bureau,* U.S. Department of Commerce, May 1945.

(95) Ratner, Benjamin, "Temperature Frequencies in the Upper Air," *Climate and Crop Weather Division, Weather Bureau,* U.S. Department of Commerce, January 1946.

(96) Petrie, William, "Excitation Conditions in the Upper Atmosphere As Determined From A Study of Atomic Emission Lines in the Auroral Spectrum," *Can. J. Research,* A, 25, p.293, September 1947.

(97) Seaton, S.L., "Temperature and Recombination Coefficient in the Ionosphere," *J. Meteorol.,* Vol.4, No.6, December 1947.

(98) Appleton, E.V., "Temperature Changes in the Higher Atmosphere," *Nature,* Vol.136, p.52, July 1935.

(99) Gauzit, J., "The Composition of the Upper Atmoshpere According to the Dissociation of Oxygen and Nitrogen Molecules," *Bulletin American Meteorological Society,* Vol.25, No.6, p.245, June 1944.

(100) Vegard, L., "Resultats Recents concernant le spectre auroral et l'etat de la Haute Atmosphère," *La Météorologie*, Nos.16 and 17, May - June, July - August 1938.

(101) Herzberg, G., and Herzberg, L., "Production of Nitrogen Atoms In The Upper Atmosphere," *Nature*, Vol.161, p.283, February 21, 1948.

(102) Woodward, R.H., "A Model of The Ionosphere," *Terr. Mag.* Vol.53, No.1, p.1-25, March 1948.

(103) Bannon, J., and Wood, F.W., "Cause and Effect in Region F_2 of the Ionosphere," *Terr. Mag.* Vol.51, No.1, March 1946.

(104) Wulf, O.R., "Light Absorption in The Atmosphere and Its Photochemistry," *Jour. of Optical Soc. of America*, Vol.25, p.231, August 1935.

(105) Rakshit, H., "Distribution of Molecular and Atomic Oxygen in the Upper Atmosphere," *Indian Phys.*, Vol.21, No.2, pp.57-68, April 1947.

(106) Gowan, E.H., "Ozonosphere Temperatures Under Radiative Equilibrium," *Proc. Roy. Soc.*, London, Vol.190A, No.1021, July 1947.

(107) *Ibid.*, "Night Cooling of the Ozonosphere."

(108) Dobson, G.M.B., Brewer, A.W., and Cutlong, B.M., "Meteorology of the Lower Stratosphere," *Proc. Roy. Soc.*, London, No.1001, Vol.185, February 1946.